Characterisation of guanylin and uroguanylin in the digestive system

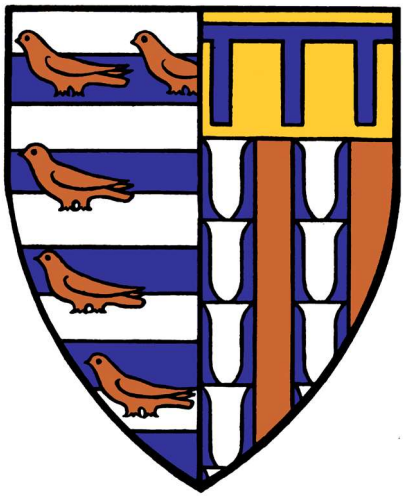

Florent Serge Dyé

Pembroke College, University of Cambridge

This dissertation is submitted for the degree of Doctor of Philosophy

November 2018

Abstract

Characterisation of guanylin and uroguanylin in the digestive system

Florent Dyé

Guanylin and uroguanylin are closely related peptides originating from the intestinal mucosa with established roles in salt and water homeostasis and the regulation of gut physiology. These hormones are secreted as the propeptides, ProGuanylin and ProUroguanylin, and post-translationally processed into active peptides in the intestinal lumen. Those active peptides activate the guanylyl cyclase C (GC-C) receptor from the lumen and catalyse the production of the intracellular secondary messenger cGMP. Subsequently cGMP stimulates both cGMP-dependent protein kinase II (PKGII) and protein kinase A (PKA). Both PKGII and PKA phosphorylate the cystic fibrosis transmembrane conductance regulator (CFTR), leading to an efflux of chloride in the lumen, resulting in fluid secretion into the intestine. The importance of this hormone-receptor system in human gastrointestinal physiology is epitomised by GC-C being the receptor for diarrheagenic bacterial enterotoxins. Observed human mutations in the receptor cause its hyperactivation or inactivation, leading to familial syndromes of diarrhoea and meconium ileus, respectively. The function of guanylin and uroguanylin is not restricted to intestinal physiology, as several other studies demonstrated their role on water and salt homeostasis in the kidney as well as a potential hypothalamic satiety effect. Therefore, the control of the guanylin peptides' secretion may serve to regulate food intake through endocrine regulation.

Understanding the role of guanylin peptides in healthy & disease states, the regulation of their secretion and their localisation in the digestive system has been limited by the lack of specific antibodies against the active human peptides and their prohormone precursors. The aim of this project was to address these deficiencies.

In this thesis, specific antibodies were generated and utilised in immunoassays, which provided the ability to quantify accurately the circulating levels of proforms in human samples. Furthermore, liquid chromatography–mass spectrometry (LC-MS) analysis on human and mouse biological samples challenged the current knowledge of the bioactive peptides. The newly developed immunoassays provided opportunities to investigate pharmacological mediators that modulate guanylin and uroguanylin secretion from intestinal epithelium into the gut lumen and bloodstream. Finally, using newly generated transgenic mice expressing a fluorescent protein under the control of the guanylin promoter, the localisation of guanylin-expressing cells was examined in the gastrointestinal tract.

Whilst several models used in this study did not draw a consensus on the specific stimuli resulting in proforms' secretion, the tools developed advanced the knowledge on the localisation of guanylin-expressing cells. Understanding the mechanisms of expression will provide novel insights into the physiological roles of these peptides and their possible involvement in pathophysiological states.

Declaration

I hereby declare that this dissertation is the result of my own work and includes nothing which is the outcome of work done in collaboration with others except as specified in the text.

It is not substantially the same as any that I have submitted, or, is being concurrently submitted for a degree or diploma or other qualification at the University of Cambridge or any other University or similar institution. I further state that no substantial part of my dissertation has already been submitted, or, is being concurrently submitted for any such degree, diploma or other qualification at the University of Cambridge or any other University or similar institution.

This dissertation does not exceed 60,000 words, excluding figures, tables, appendices and bibliography.

Florent S. Dyé, November 2018

Table of Contents

Acknowledgements

First of all, I would like to thank my supervisors, past and present, Ben Challis, Fiona Gribble, Frank Reimann and Stephen O'Rahilly at the University of Cambridge and my industrial supervisor Maria Groves at MedImmune for their guidance, encouragement and support over the past few years. I would also like to acknowledge the funding bodies BBSRC and Medimmune for providing my studentship.

At MedImmune, I had the incredible opportunity to learn from brilliant scientists across the Antibody Discovery and Protein Engineering department as well as the Cardiovascular and Metabolic diseases department. I am particularly grateful to Jenny Percival-Alwyn for her support and assistance, Kate Goode, Jacqui Naylor and Franco Ferraro for sharing their knowledge and teaching me new techniques.

I was also privileged to work alongside the friendly Gribble/Reimann research group and I would like to thank all members of the lab for their help and feedback and I am particularly obliged to Debbie Goldspink, Richard Kay and Pierre Larraufie for their time and expertise. I would like to thank Geoff Roberts, Claire Meek, and Juraj Rievaj as well for sharing with me some of their samples they harvested during their own studies.

I would like to thank Debbie, Pierre, Jenny, Van and Jacqui who, in addition to my supervisors, had a critical eye on this thesis.

Additionally, I would like to express my gratitude to my friends back home, my friends in Pembroke and in town as well as my little French family in Cambridge, who provided me some welfare, support, and distraction when needed. Finally, my upmost gratitude goes to my family, my mum, dad and sister for their life-long encouragement and support. Merci.

I dedicate this work to my grandad, Papi André, who was always a source of inspiration.

List of abbreviations

5-HT	serotonin (5-hydroxy-tryptamine)
ACN	Acetonitrile
acTub	Acetylated-α-tubulin
AKT	v-akt murine thymoma viral oncogene homolog 1 or protein kinase B
ANOVA	Analysis of variance
ANP	Atrial natriuretic peptide
APC	Adenomatous polyposis coli
AWERB	Animal Welfare and Ethical Review Body
BAC	Bacterial artificial chromosome
BAT	Brown adipose tissue
Biotinylated-Guanylin	Guanylin-AEEAc-Lys(biotinyl) amide (human) trifluoroacetate salt
Biotinylated-Uroguanylin	Uroguanylin-AEEAc-Lys(biotinyl) amide (human) trifluoroacetate salt
BiP	Binding immunoglobulin protein
BME	Basement Membrane Extract
BNP	Brain natriuretic peptide
bp	Base pair
BSA	Bovine serum albumin
cAMP	Cyclic adenosine monophosphate
CCK	cholecystokin
cDNA	Complementary DNA
CDR	Complementary determining region
CFM	Continuous Flow Microspotter
CFTR	Cystic fibrosis transmembrane conductance regulator
cGMP	Cyclic guanosine-3',5' monophosphate
CHOP	CCAAT/-enhancer-binding protein homologous
CIC	Chronic idiopatic constipation
CNG	Cyclic nucleotide-gated channel
CNP	C-type natriuretic peptide
CRIP	Cysteine-rich intestinal polypeptide
CSD	Congenital sodium diarrhoea
DAPI	4',6-diamidino-2-phenylindole
DCLK1	Doublecortin-like kinase 1
DIO	Diet-induced obesity
DMEM	Dulbecco's modified Eagle's medium
DMSO	Dimethyl sulfoxide
DNA	Deoxyribonucleic acid
DTT	1,4-Dithiothreitol
dU-ssDNA	Uracil containing single stranded DNA
EC	Enterochromaffin cells
ECL	Enterochromaffin-like cells
EDTA	Ethylenediamine tetraacetic acid

EEC	Enteroendocrine cells
EGF	Epidermal growth factor
ELISA	Enzyme-linked immunosorbent assay
EMA	European Medicines Agency
ER	Endoplasmic reticulum
ETEC	Enterotoxigenic *E. coli*
EYFP	Enhanced yellow fluorescent protein
FA	Formic acid
FACS	Fluorescence-activated cell sorting
FAE	follicle-associated epithelium
Fcgbp	Fc-γ-binding protein
FDA	Food and Drug Administration
FRET	Förster resonance energy transfer
GC-C	Guanylyl cyclase C
GFR	Glomerular filtration rate
GI	Gastrointestinal
GIP	Glucose-dependent insulinotropic polypeptide
GLP	Glucagon-like peptides
GO	Gene ontology
GP2	Glycoprotein 2
GST	Glutathione S-transferase
Guanylin-KLH	Acetyl-Guanylin-AEEAc-Lys(succinyl-KLH) amide (human)
HB	Heparin Buffer
HBSS	Hanks' buffered salt solution
HCDR	Heavy chain complementary determining region
HEPES	2-[4-(2-hydroxyethyl)-1-piperazin-1-yl]ethanesulfonic acid
HES	Hairy/Enhancer of Split
HF	High fat
hr	Hour
HRP	Horseradish peroxidase
HTRF	Homogenous Time Resoled Fluorescence
IBMX	3-isobutyl-1-methylxanthine
IBS	Irritable bowel syndrome
IgG	Immunoglobulin G
IMAC	Immobilized metal affinity chromatography
Insl5	Insulin-like 5 peptide
IPTG	Isopropyl β-D-1-thiogalactopyranoside
IV	Intravenous
KLH	Keyhole Limpet Hemocyanin
KO	Knock out
L-15	Leibovitz-15
LC	Liquid Chromatography
LCDR	Light chain complementary determining region
LDH	Lactate dehydrogenase

LPS	Lipopolysaccharides
MBP	Maltose-binding protein
MMP7	Metalloproteinase 7
MOI	Multiplicity of infection
MOPC	Mouse Plasmacytoma Cells
mRNA	Messenger ribonucleic acid
MS	Mass spectrometry
MS/MS	Tandem mass spectrometry
MW	Molecular weight
NHE2	Sodium/hydrogen exchanger
NICD	Notch intracellular domain
OD	Optical density
ON	Overnight
PBS	Phosphate-buffered saline
PCR	Polymerase chain reaction
PDEIII	Phosphodiesterase III
PEI	Polyethylenimine
Pen/Strep	Penicillin/Streptomycin
PKA	Protein kinase A
PKAII	cAMP-dependent protein kinase II
PKC	Protein kinase C
PKGII	cGMP-dependent protein kinase II
PLCβ2	Phospholipase Cβ2
PMA	Phorbol-12-myristate-13-acetate
ProGN	ProGuanylin
ProUGN	ProUroguanylin
PTEN	Phosphatase and tensin homolog
PYY	Peptide YY
RAAS	Renin-Angiotensin-Aldosterone System
RELMβ	Resistin-like molecule β
RIA	Radioimmunoassay
RNA	Ribonucleic acid
ROCK	Rho-associated protein kinase
ROMK	Renal outer Medullary Potassium Channel
RP-HPLC	Reversed-Phase High-Performance Liquid Chromatography
rpm	Rotation per minute
RSPO1	R-spondin-1
RT	Room temperature
RT	Reverse transcription
RT-PCR	Real time polymerase chain reaction
RU	Response unit
SA	Streptavidin
SCFA	Short-chain fatty acid
scFv	Single-chain variable fragment

SDS-PAGE	Sodium dodecyl sulfate–polyacrylamide gel electrophoresis
SEC	Size-exclusion chromatography
SMT	Standardised meal test
SPE	Solid phase extraction
SPR	Surface Plasmon Resonance
ss	Single stranded
ST	Heat-stable enterotoxins
TA	Transit amplifying
TDCA	Taurodeoxycholic acid
TMB	Tetramethylbenzidine
TNF-α	Tumor necrosis factor-α
tRNA	Transfer RNA
trp	Trypsin
TRPM5	Transient receptor potential cation channel subfamily M member 5
TRX	Thioredoxin
TYAG	TY media, 100 µg/ml ampicillin, 2% (w/v) glucose
TYAGC	TYAG media, 10 µg/ml chloramphenicol
TYAK	TY media, 100 µg/ml ampicillin, 50 µg/ml kanamycin
TYAKU	TYAK media, 0.25 µg/ml uridine
TYG	TY media, 2% (w/v) glucose
Uroguanylin-KLH	Acetyl-Uroguanylin-AEEAc-Lys(succinyl-KLH) amide (human)
WAT	White adipose tissue
Wnt	Wingless/Integrated
WT	Wild-type
YAC	Yeast artificial chromosome

Chapter 1: Introduction

1.1 The digestive system

The digestive system is composed of the gastrointestinal tract as well as accessory organs of digestion such as liver, gall bladder and pancreas. The gastrointestinal tract is composed of all structures between mouth and anus, encompassing the oesophagus, stomach, small and large intestine. The digestive system has three important roles: breakdown food extracts, absorb the nutrients and, finally, expel metabolic waste products.

In brief, the stomach stores food temporarily and initialises digestion mechanically by movement of the stomach, and chemically through secretion of pepsins and hydrochloric acid. The digestion process continues in the small intestine, the primary site of nutrient absorption (Boron and Boulpaep, 2016). The large intestine reabsorbs electrolytes and fluids and stores undigested material before expulsion from the body. Accessory glands and organs help the digestive process: the pancreas secretes digestive enzymes into the duodenum as well as bicarbonate (HCO_3^-) to neutralise acids from stomach. Bile is secreted by the liver and stored in the gallbladder before being secreted in the duodenum where it plays an important role in the digestion of fat (Boron and Boulpaep, 2016).

1.1.1 Structure of the small and large intestine

The intestine includes the small intestine encompassing the duodenum, jejunum and ileum and the large intestine or colon subdivided into ascending, transverse, descending, sigmoid colon and rectum. While the basic anatomical organisation of the gastrointestinal tract can vary along its length, a similar organisation can be found in the tissue structure from surface to lumen: a serosa, muscle layers (muscularis externa), a submucosa, and a mucosa (figure 1.1). The serosa is a layer of connective tissue covered with squamous epithelial cells that envelops the muscularis externa. This muscle layer is composed of 2 layers of smooth muscle with the outer layer being longitudinal and the inner layer being circular muscle (Lowe and Anderson, 2015). The submucosal layer contains loose connective tissue with collagen and elastin fibrils, large blood vessels and glands that secrete intestinal fluid into the lumen. The mucosa is the inner layer of the gastrointestinal tract in contact with the lumen. It entails a muscularis mucosae, which is the last layer of smooth muscle, and contains the lamina propria and the epithelium (Lowe and Anderson, 2015; Boron and Boulpaep, 2016). The lamina

propria is a layer of loose connective tissue containing blood capillaries, enteric neurons (Furness, 2000), and immune cells such as lymphocytes and mast cells (Mowat and Agace, 2014). The intestinal epithelium is a single layer of cells in close contact with the lumen of the gastrointestinal tract within which the nature of cells varies along the GI tract. In the small intestine the epithelial surface area is amplified by a monolayer of cells that evaginate into structures called villi and other structures called crypts (figure 1.1). In contrast, the colon only presents crypts or invagination, and has a surface epithelium. Therefore, crypts and villi allow for an enormous extension of the surface area in contact with the lumen, believed to be greater than 200m^2 in humans (Vereecke, Beyaert and van Loo, 2011).

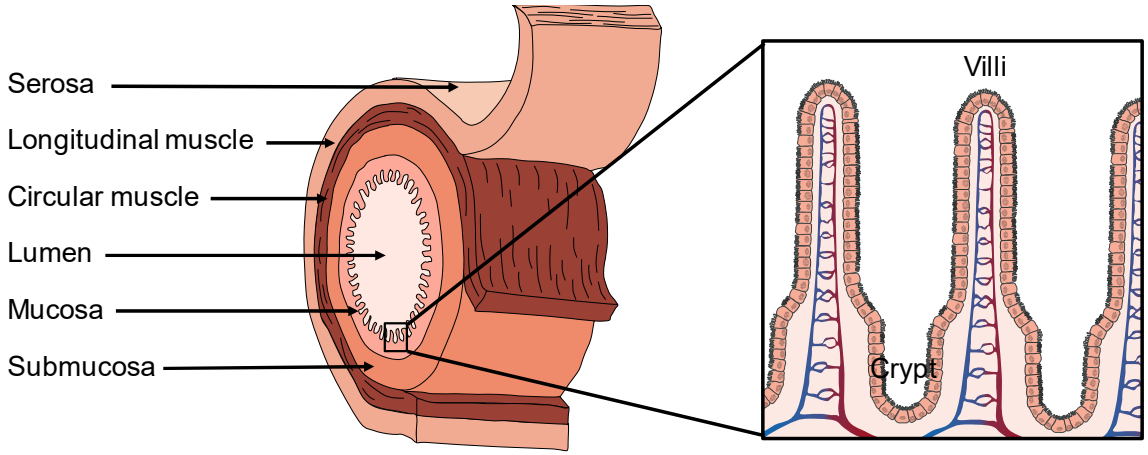

Figure 1.1: Schematic illustration of the mammalian small intestinal. Figure adapted from Husvéth, 2011.

1.1.2 Epithelial cells of the small and large intestine

Small and large intestine epithelium regenerates rapidly with a complete cell renewal of 4-5 days (Heath, 1996) and is composed of diverse cell populations. Enterocytes are the predominant cell type in the intestine and represent 80-95% of intestinal epithelial cells (Cheng and Leblond, 1974a; van der Flier and Clevers, 2009). Goblet cells represent 4-16% of the cellular population with their abundance increasing along the gastrointestinal tract (Hazel Cheng, 1974; Karam, 1999). Enteroendocrine and tuft cells represent 1% and 0.4% of the cell population, respectively (Cheng and Leblond, 1974b; Gerbe *et al.*, 2011). Paneth cells are located at the bottom of the crypt in the small intestine. While the colon does not possess Paneth cells at the bottom of the crypts, Paneth-like cells were discovered in response to mucosal inflammation (Cunliffe *et al.*, 2001; Fahlgren *et al.*, 2003). Finally, M-cells, were described in the 1970s but are still a poorly defined cell lineage within the intestinal epithelium (Bockman and Cooper, 1973; Owen and Jones, 1974a). These cells are thought to take up

antigens (pinocytosis) and deliver/present these to underlying lymphocyte (Miller *et al.*, 2007; Ohno, 2016).

All cells from the large and small intestine are derived from stem cells. Stem cells are located at the niche of the crypt with an approximate ratio of 15 cells per crypt (Bjerknes and Cheng, 1999; Clevers and Bevins, 2013), and are discernible by their *Lgr5+* biomarker (Barker *et al.*, 2007). These stem cells proliferate to generate a pool of undifferentiated cells forming the transit amplifying (TA) zone which can replenish the stem cell pool following damage to the epithelial cell layer(Potten, Booth and Pritchard, 1997; Yan *et al.*, 2012) as well as differentiate into non-multipotent epithelial cells from the secretory (goblet, Paneth and enteroendocrine cells) or absorptive (enterocytes) lineages (Barker and Clevers, 2010) (figure 1.2). The proliferative activity of the stem cells is Wnt-dependent, with evidence suggesting Wnt secretion by neighbouring Paneth cells and/or subepithelial telocytes (Sato *et al.*, 2011; Shoshkes-Carmel *et al.*, 2018).

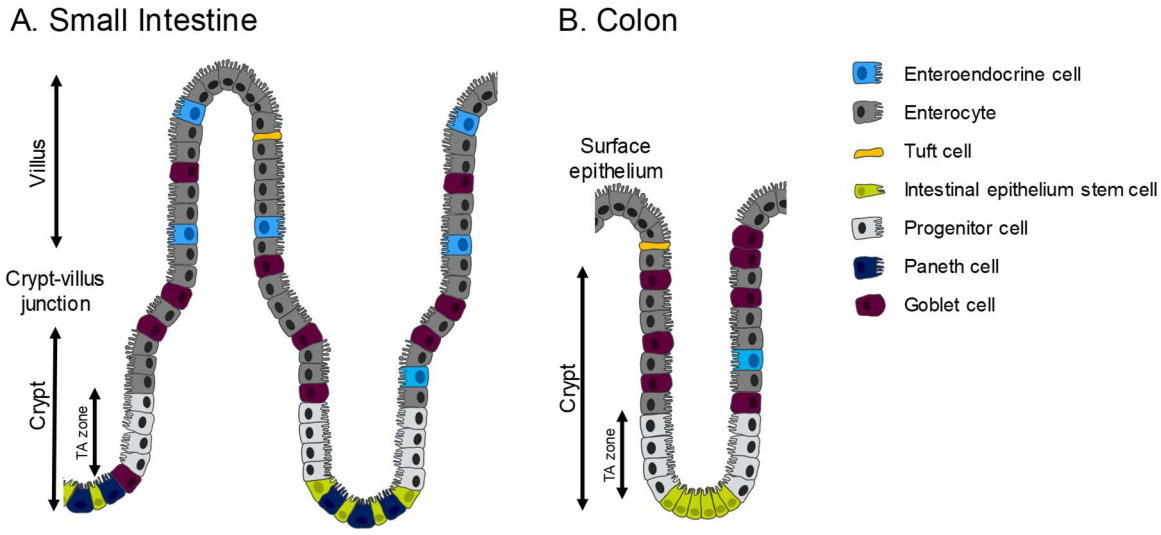

Figure 1.2: Schematic illustration of the structure of the intestinal structures from the small intestine and colon. The small intestine presents both crypts and villi whereas the colon presents crypts that end at the surface epithelium. In the intestine, enterocytes are the major type of cells, with other cell types such as enteroendocrine cells, goblet cells and tuft cells are distributed among the enterocytes. Intestinal epithelial stem cells, are present at the bottom of the crypt interspaced by Paneth cells. TA zone represents the transit amplifying zone. Figure adapted from Mowat and Agace, 2014.

The cell differentiation process is regulated by the Notch signalling pathway (figure 1.3). Briefly, Notch receptors and ligands play a key role in cell allocation. When any of the 5 Notch ligands bind any of the 4 Notch receptors, the Notch receptor is cleaved. The free Notch intracellular domain (NICD) is translocated into the nucleus, which in turn promotes the

transcription of the Hairy/Enhancer of Split (HES). HES can inhibit the transcription factor Math1 (van der Flier and Clevers, 2009; May and Kaestner, 2010), allowing the cell to become an enterocyte. When the Notch signalling pathway is not active, expression of Math1 leads cells to a secretory fate (Yang *et al.*, 2001). An important aspect of the Notch signalling pathway is its lateral inhibition of neighbouring cells that will, as a consequence, adopt a different fate (Artavanis-Tsakonas, Rand and Lake, 1999). Other specialisations in the secretory lineage occur to differentiate cells between Paneth cells, goblet cells and enteroendocrine cells with the transcription factors Ngn3 being essential for differentiation into enteroendocrine cells (Mellitzer *et al.*, 2010). The inhibitory effect of Gfi1 on Ngn3 was proven necessary for the differentiation of cells into either Paneth or goblet cells (Shroyer *et al.*, 2005). Klf4 was confirmed as essential for the differentiation of goblet cells (Katz *et al.*, 2002) and Sox9 crucial for the differentiation of Paneth cells (Mori-Akiyama *et al.*, 2007). While also expressed in Tuft cells, Sox9 was not indispensable to their differentiation (Gerbe *et al.*, 2016). It was demonstrated that the Wnt pathway also impacted the cell differentiation of cells from the secretory lineage (Pinto *et al.*, 2003).

Cells from the TA zone migrate to the villi (or toward the surface epithelium in the case of the colon) except for Paneth cells and rare enteroendocrine cells which migrate to the niche of the crypt (Crosnier, Stamataki and Lewis, 2006; Barker, van de Wetering and Clevers, 2008).

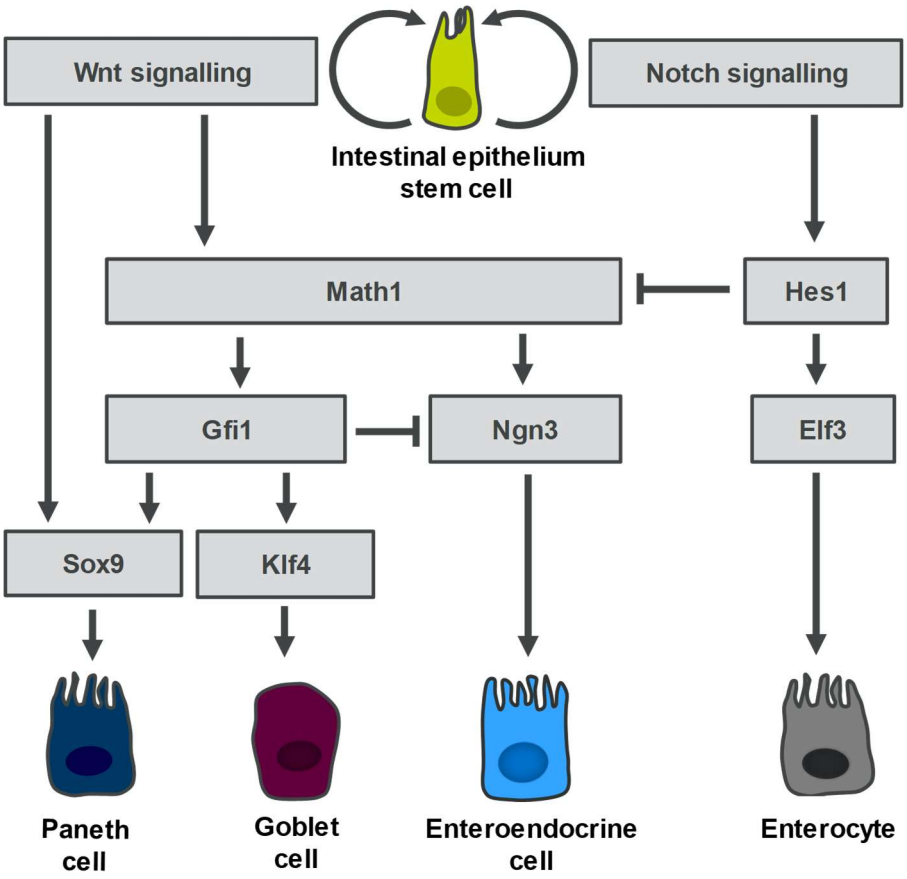

Figure 1.3: Simplified overview of the epithelial cell lineage differentiation in the intestine. Wnt and Notch pathways are acting on both the proliferation of the intestinal stem cells as well as the differentiation into the different cell types present in the epithelium. Figure adapted from (van der Flier and Clevers, 2009).

Enteroendocrine cells

Pear-shaped enteroendocrine cells (EEC) are located in the epithelium of the GI tract and represent 1% of the total epithelial cells in the small and large intestines. The apical surface presents microvilli directly into the GI lumen, while the basolateral surface releases hormone-containing vesicles (Pearse *et al.*, 1970; Schonhoff, Giel-Moloney and Leiter, 2004; Crosnier, Stamataki and Lewis, 2006). More than 10 subclasses of EECs have been identified and classified according to the principal peptide hormone that is produced within each cell. For instance, D-cells secrete somatostatin (Van Op den bosch *et al.*, 2009), G-cells secrete gastrin (Dockray, Dimaline and Varro, 2005), I-cells secrete cholecystokinin (CCK) (Liddle, 1997), K-cells secrete glucose-dependent insulinotropic polypeptide (GIP) (Baggio and Drucker, 2007), L cells produce glucagon-like peptides GLP1 and GLP2 as well as peptide YY (PYY) and insulin-like 5 peptide (Insl5) (Sjölund *et al.*, 1983; Habib *et al.*, 2012; Drucker and Yusta, 2014; Billing *et al.*, 2018). Although it was first believed that each subcategory of EECs only secreted hormones from a single peptide precursor (except in the case of PYY and GLP-1), new evidence

highlights the co-expression of hormones from individual cells (Habib *et al.*, 2012; Fothergill *et al.*, 2017).

While some hormones such as serotonin (5-HT) and somatostatin are secreted by EECs throughout the entire gastrointestinal tract, subclasses of EECs are distributed to varying degrees along the small and large intestines (figure 1.4). Enterochromaffin cells (EC), enterochromaffin-like cells (ECL), D-cells, G-cells and P/D1 cells are present within the stomach. In the duodenum, K-cells, I-cells and S-cells are the major cell types found. N-cells are present in duodenum as well as jejunum and ileum. Finally, L-cells are produced throughout the whole intestine with a different secretion gradient between GLP, PYY and Insl5 (Gribble and Reimann, 2016). The EEC lifecycle is estimated to 3-10 days in the duodenum and jejunum, and 60 days in ileum and colon (Tsubouchi and Leblond, 1979).

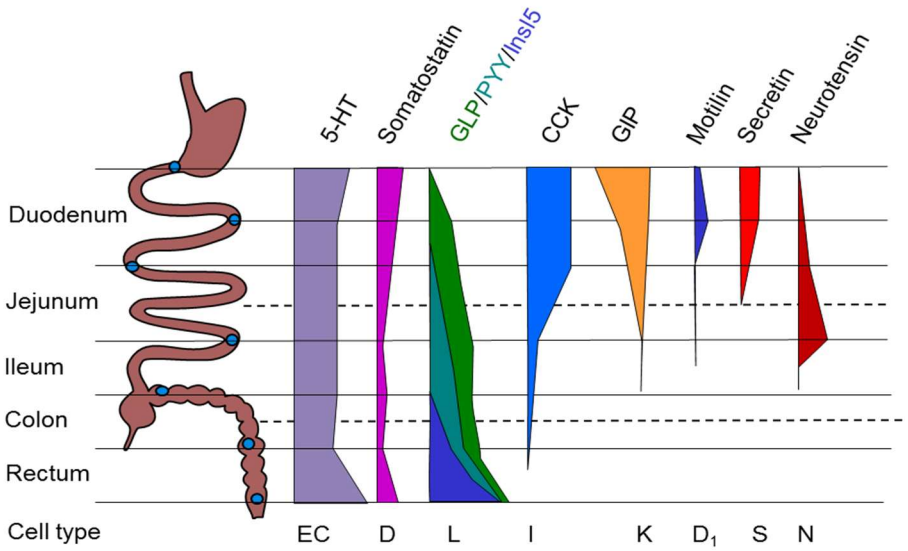

Figure 1.4: Schematic representation of enteroendocrine hormone distribution and cell-type along the small and large intestine. Enteroendocrine hormones are secreted from specialised cell-types, with varying densities along the intestine as indicated. Figure adapted by F. Reimann, based on an immunohistochemical study by Sjölund *et al.*, 1983 and updated to include Insl5 using data from Grosse *et al.*, 2014.

The main role of the EECs is to respond to nutrients passing through the GI tract and to transform the received information into gut hormone signals (Engelstoft *et al.*, 2008). These signals can act locally to regulate gut motility, absorption, secretion of digestive enzymes as well as acting outside the gastrointestinal tract to regulate satiety, energy expenditure, energy homeostasis, and glucose homeostasis (Murphy and Bloom, 2006; Engelstoft *et al.*, 2008; Woods, 2009; Field, Chaudhri and Bloom, 2010; Parker, Gribble and Reimann, 2014).

Goblet cells

Goblet cells were so-named due to their cup-like appearance. Goblet cells are highly polarised with the nucleus confined to the basolateral side and secretory granules at the apical side of the cell. Granules distend the cell's theca resulting in the goblet cell shape (Guyton and Hall, 2016). The apical side of the cell presents microvilli increasing the surface area of the cell for secretion. They are the most abundant cells from the secretory lineage within the intestinal epithelium with up to 10-15% of the small intestine epithelium composed of goblet cells, while the colon epithelium may contain up to 50% of goblet cells (Noah, Donahue and Shroyer, 2011).

Goblet cells secrete mucins, in particular MUC2 which is the main structural molecule of the intestinal mucous. The assembly of this large and complex molecule is a major task for the goblet cell (Karlsson *et al.*, 1996). It is assumed that the mucus secreted by goblet cells is the first line of defence against physical and chemical injury and therefore the main role of goblet cells is to function in the innate immune response and the protection from pathogens (Kim and Ho, 2010; Johansson and Hansson, 2014; Pelaseyed *et al.*, 2014). As well as mucins, goblet cells secrete components of the mucus layer such as the Fc-γ-binding protein (Fcgbp) which stabilises the mucous layer (Johansson, Thomsson and Hansson, 2009), resistin-like molecule β (RELMβ) inhibiting intestinal worm infection (Herbert *et al.*, 2009), and trefoil peptides promoting the epithelial growth and repair (Taupin and Podolsky, 2003; Rodríguez-Piñeiro *et al.*, 2013).

Enterocytes

Enterocytes (or colonocytes in the large intestine) are the most abundant cell type from duodenum to colon and usually represent more than 80% of all intestinal epithelial cells (Cheng and Leblond, 1974a). Their main role is the absorption of nutrients from the luminal surface and transfer to the basolateral side of the cell. Enterocytes are highly polarised cells that present rigid and closely positioned microvilli on the apical side. These microvilli, described as a brush border, increase the cell surface area in the intestinal lumen (Mooseker, 1985). The enterocytes on the apical surface form a continuous, filamentous and negatively charged glycocalyx formed by acidic mucopolysaccharides and glycoproteins (Maury *et al.*, 1995). This glycocalyx layer contains glycoproteins and dissacharidases that facilitate terminal digestion (Semenza, 1986). The glycocalyx presence is also considered to serve as a protective

barrier for the epithelium as it prevents macromolecular aggregates, bacteria, and viruses to come in contact with the epithelium (Frey *et al.*, 1996).

As mentioned previously, enterocytes principle function is to absorb nutrient macromolecules across the epithelium to the basolateral side. Nutrients such as sugars, amino acids and ions are absorbed via epithelial transporters. Enterocytes, which are unable to perform phagocytosis, absorb macromolecules via pinocytosis: clathrin-mediated endocytosis and caveolae-mediated endocytosis mechanisms (Snoeck, Goddeeris and Cox, 2005). Enterocytes undergo continuous maturation throughout their movement towards the tip of the villus. When reaching the tip of the villus, the mature enterocyte's life terminates by the cell's expulsion in the lumen concomitantly to its apoptosis. It is suggested that cells are shed away by concerted contraction from neighbouring cells and cytoplasmic elongation underneath the detaching cell to preserve the epithelial barrier function and integrity during enterocyte death (Rosenblatt, Raff and Cramer, 2001; Vereecke, Beyaert and van Loo, 2011).

Paneth cells

In comparison with other cell lineages, the Paneth cell lineage is quite different. Paneth cells reside at the basis of the crypt of Lieberkühn in the small intestine only. They are the few rare cells, that when differentiating, migrate towards the crypt niche (H Cheng, 1974) where their differentiation is completed and the most matured cells can be identified (Bjerknes and Cheng, 1981). Each crypt contains around 10 mature Paneth cells that have a life span of 30 days (Bjerknes and Cheng, 1981; Garabedian *et al.*, 1997; Clevers and Bevins, 2013).

Paneth cells contain large secretory granules that are present on the apical surface. These granules contain proteins that are involved in the innate immune response including α-defensins, lysozyme, secretory phospholipase A2, lipopolysaccharide (LPS)-binding protein, RegIII-g, and xanthine oxidase, matrix metalloproteinase 7 (MMP7), CD95 ligand, IgA, CD1d, cysteine-rich intestinal polypeptide (CRIP), CD15, and metallothionein, as well as proinflammatory mediators (interleukin17A, tumour necrosis factor-α (TNF-α), IL-1b, and lipokines) (Ouellette, no date; Takahashi *et al.*, 2008; Stappenbeck, 2009). Antimicrobial peptides and proteins are discharged via exocytosis in the lumen playing a key role to defend the crypt from microbial invasion in the crypt. The antimicrobial peptides defence extends to the mucosal epithelium via their diffusion through the mucus layer (Meyer-Hoffert *et al.*, 2008). The defence provided by the antimicrobial peptides also contribute to the microbiota

composition (Forte, 1999; Peterson *et al.*, 2007; Hapfelmeier *et al.*, 2010; Salzman *et al.*, 2010).

A final important role of the Paneth cells is their implication in the stem cell niche and on the stem cells. It was shown that the Paneth cells support the stem cells in "minigut" organoid cultures by secreting EGF, Wnt3 and Notch ligand Dll4 (Sato *et al.*, 2011). Paneth cells could play as nutritional sensors and adjust the stem cell response to calorie restriction through the mTORC1 signalling pathway (Yilmaz *et al.*, 2012).

Tuft cells

Tuft cells (or brush cells) are a rare type of epithelial cells that account for 0.4-1% of the total intestinal epithelial cell population (Gerbe, Legraverend and Jay, 2012; Howitt *et al.*, 2016). Their characteristic shape consists of brush-like microvilli on the apical side with the presence of lateral microvilli (von Moltke, 2018). The role of the apical brush-like process has not been defined as their characterisation has been limited by the lack of cell-specific markers. However, more recently, doublecortin-like kinase 1 (DCLK1) has recently been identified as a putative specific marker for tuft cells (Gerbe *et al.*, 2016; Howitt *et al.*, 2016; von Moltke *et al.*, 2016).

It has been suggested that tuft cells may serve as taste chemosensory cells. Evidence showed that tuft cells express taste-related GPCRs such as the taste receptor type1 members 1 and 3 (Bezencon, le Coutre and Damak, 2007; Hass, Schwarzenbacher and Breer, 2010) as well as taste-related proteins: transient receptor potential cation channel subfamily M member 5 (Trpm5) and Phospholipase Cβ2 (PLCβ2) (Bezencon, le Coutre and Damak, 2007; Bezençon *et al.*, 2008; Liu *et al.*, 2011) which convert bitter, sweet and umami tastes into signals.

M cells

M cells (or Microfold cells) are a poorly characterised cell type found in the follicle-associated epithelium (FAE) of Peyer's patches and lymphoid follicles and account for 5-10% of epithelial cells in those areas (Owen and Jones, 1974b). M cells display fold-like structures (that gave the name microfold cells) on the apical side instead of microvilli, and the basolateral side is invaginated. These invaginations accommodate dendritic cells, macrophages or lymphocytes, and facilitate the presentation of microbes to those antigen-presenting cells (Brandtzaeg *et al.*, 2008). For instance, glycoprotein 2 (GP2) is an M cell specific marker working as a bacterial

receptor (Hase *et al.*, 2009). Therefore, it is suggested that the role of M cells is to sample the lumen and transfer the detected pathogens to the immune system (Ohno, 2016).

1.1.3 Microbiota and cross-talk with the gut epithelium

In addition to containing food and nutrients, the intestinal lumen also comprises a diverse and dynamic microorganism population that inhabits or passes by the gastrointestinal tract, called gut microbiota. The number of microorganisms is estimated to be above 10^{14} with a combined genome containing at least 100 times as many genes as the human genome (Bäckhed *et al.*, 2005; Gill *et al.*, 2006). The microbiota is not only comprised of bacteria, but also archaea, fungi, viruses and parasites can also be present and play a role in a mutually beneficial relationship with the host (Neish, 2009; Scarpellini *et al.*, 2015).

It is now assumed that the microbiota offers benefits to the host and acts in multiple physiological roles such as housekeeping the intestinal epithelium integrity (Natividad and Verdu, 2013), immunity (Gerritsen *et al.*, 2011; Bäumler and Sperandio, 2016) and nutrition (den Besten *et al.*, 2013). Digestive metabolic pathways of anaerobic microbiota leads to the release of vitamin K, folate or short-chain fatty acids (SCFAs). SCFAs, a fermentation end product of dietary fibre constitutes an important source of energy to the host and a key metabolic mediator (Tolhurst *et al.*, 2012; Larraufie *et al.*, 2018; Lu, Gribble and Reimann, 2018). It was also suggested that SCFAs have an effect on host immunity (Biagi *et al.*, 2013).

As described previously, the intestinal epithelium offers a strong physical and chemical barrier to detrimental enteric microorganisms. It is suspected that the enterocyte closely packed villi structure, as well as the presence of glycoprotein enzymes, brush border glycocalyx and secretion of antibacterial mucins and defensins in the mucus, are all measures employed by the host to defend itself. The microbiota provides another important protective line of resistance against exogenous bacteria and prevents potential invasion. The microbiota can prevent pathogen attachment to the epithelial cells using antimicrobial activity (Klaenhammer, 1993; Ramare *et al.*, 1993; Riley and Wertz, 2002; Servin, 2004) as well as competing for nutrient availability (Hooper *et al.*, 1999; Nicholson and Wilson, 2003; Srikanth and McCormick, 2008).

Even though microbiota and host work cooperatively to protect the integrity of the intestinal epithelial, exogenous microbiota-fashioned counter strategies can be used to take-over

signalling pathways and cellular mechanisms, with some pathogenic microbes targeting specific epithelial structures (Schauer, 1997). For instance, it was shown that human enterotoxigenic *E. coli* (ETEC) strains bind via their pili to epithelial cells before starting a colonisation process associated with acute diarrheal disease (Deneke *et al.*, 1983). These ETEC can then deregulate fluid secretion and provoke secretory diarrhoea via their enterotoxin peptides such as the heat stable peptides variants (STa) acting via the endogenous guanylate cyclase C (GC-C) receptor present on enterocytes (Carey, 1978; Field *et al.*, 1978; Hughes *et al.*, 1978).

1.2 Guanylin peptides

1.2.1 The guanylate cyclase C receptor and its activation

The guanylate cyclase C (GC-C) receptor is a type I transmembrane receptor that belongs to a large natriuretic peptide receptor family: the guanylate cyclase receptors. The guanylate cyclase family responds to a diverse range of signals that catalyse the conversion of guanosine triphosphate to cyclic guanosine-3',5' monophosphate (cGMP). (Schulz *et al.*, 1990).

The GC-C is a 1050 amino acid protein consisting of an extracellular receptor domain and a transmembrane domain, as well as kinase and catalytic domains (Vaandrager, 2002). The receptor is mainly expressed in the intestine on the brush border membrane of epithelial cells (de Jonge, 1975) and is distributed throughout the small intestine along the crypt-villus axis. In the colon, the receptor is mainly restricted to the crypts (Basu and Visweswariah, 2010). Orthologue GC-C receptors were identified in birds and fish substantiating its evolutionary conservation and probable importance (Biswas *et al.*, 2009). The GC-C was discovered in the 1970s as the intestinal receptor for exogenous diarrhoeagenic bacterial heat-stable enterotoxins (STs) (Field *et al.*, 1978; Hughes *et al.*, 1978). When investigating the cause of bacterial diarrhoea, boiling diarrhoea-inducing substances was demonstrated insufficient to eliminate the diarrheal effect, thus concluding that heat-stable toxins were activating the receptor as well as heat-labile toxins (Forte, 2004b). GC-C was found to be the principal receptor for heat-stable enterotoxins (STa), a major causative factor in ETEC-induced secretory diarrhoea, causing the commonly experienced "traveller's diarrhoea" as well as significantly contributing towards increased infant mortality in developing countries (Field *et al.*, 1978; Hughes *et al.*, 1978; Okoh and Osode, 2008). To date, only two endogenous ligands have been found in humans, namely guanylin and uroguanylin.

1.2.2 Discovery of the guanylin peptides

Identification of STa as an exogenous ligand for the GC-C receptor in the small and large intestines did not initially prompt the search for potential endogenous ligands. Fifteen years after the discovery of the receptor, the endogenous counterparts to STa, guanylin and uroguanylin, were discovered in 1992 and 1993, respectively (Mark G Currie *et al.*, 1992; Hamra *et al.*, 1993). Guanylin was initially purified from rat jejunum and demonstrated to increase cGMP levels in T84 human colon carcinoma cells. The protein sequence was assessed using an automated Edman degradation chemistry which allowed the determination of protein sequence after extracting the peptides by boiling the tissue samples in acid (Mark G Currie *et al.*, 1992).

When extracts of rat kidney showed cGMP-stimulating activity in T84 cells such as STa or guanylin (M G Currie *et al.*, 1992; Schulz, Chrisman and Garbers, 1992), a renal source of guanylin was investigated. Hamra *et al.*, anticipating the isolation of guanylin from opossum's urine, were surprised to isolate two peptides that activated the human intestinal T84 cell GC-C. The first was guanylin while the second was a closely related 16 amino-acid peptide containing 53% homology with guanylin. Due to the location of its discovery and having a similar activity to guanylin, this new peptide was named uroguanylin (Hamra *et al.*, 1993). Guanylin peptides is the common idiom used when referring to both peptides.

Both guanylin and uroguanylin are the active peptide domains of longer proforms (ProGuanylin and ProUroguanylin) which present little or undetectable biological activity on the GC-C receptor (de Sauvage *et al.*, 1992; Hamra *et al.*, 1996). Uroguanylin and guanylin affinities to the GC-C were evaluated to be 10 and 100-fold lower, respectively, in comparison to the ST enterotoxin (Forte *et al.*, 1993; Hamra *et al.*, 1993). Recent studies showed that guanylin and uroguanylin peptides are able to bind to another guanylate cyclase receptor, GC-D, that is expressed in olfactory bulb epithelium (Leinders-Zufall *et al.*, 2007; Cockerham *et al.*, 2009; Duda and Sharma, 2009).

1.3 Structure, expression and secretion of the guanylin peptides

1.3.1 Structure of guanylin-related peptides

To date, four known guanylin-related peptides have been identified. Guanylin and uroguanylin were found in multiple species ranging from rodents (Wiegand, Kato and Currie, 1992) to

humans (Wiegand *et al.*, 1992; Kita *et al.*, 1994). The two other closely related peptides, called lymphoguanylin and renoguanylin have not yet be identified in humans. Lymphoguanylin was isolated from opposum's spleen through transcript analysis and presents 40% and 80% homology with guanylin and uroguanylin, respectively. Lymphoguanylin is able to activate GC-C in a similar fashion to guanylin and uroguanylin (Forte *et al.*, 1999). Renoguanylin was shown to be expressed exclusively in the intestine and kidney of eels (Yuge *et al.*, 2003). It presents 75% and 88% homology with guanylin and uroguanylin, respectively. In conclusion, guanylin and uroguanylin are closely related peptides, and peptide orthologues are highly conserved across vertebrates (figure 1.5) suggesting an evolutionary conserved role for these peptides.

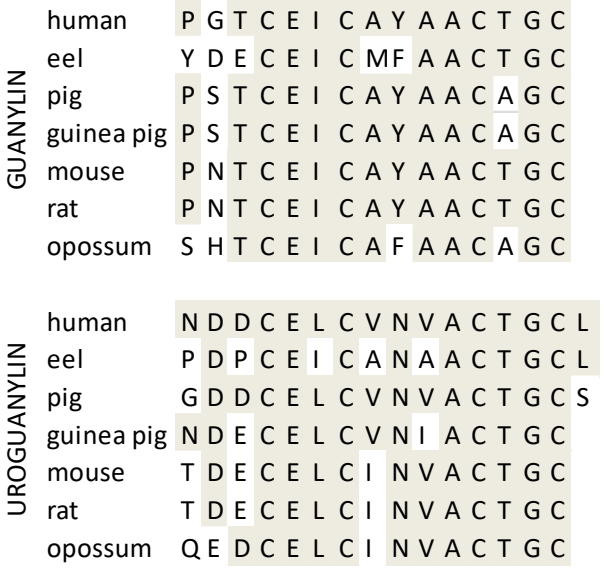

Figure 1.5: Amino Acid sequences of active guanylin and uroguanylin in different species. Amino acid residues identical to the human sequence are highlighted.

The human genes encoding for guanylin and uroguanylin are located on chromosome 1 (1p34-35 and 1p33-34, respectively) (Hill *et al.*, 1995; Magert *et al.*, 1998) and, the mouse genes are found on chromosome 4 (Sciaky, Kosiba and Cohen, 1994; Whitaker, Steinbrecher, *et al.*, 1997). Interestingly, guanylin and uroguanylin loci are in close proximity to genes that encode other natriuretic peptides. Indeed, the human atrial natriuretic peptide (ANP) gene is present on chromosome 1 in position 1p36.2 (Yang-Feng *et al.*, 1985), as well as the brain natriuretic peptide (BNP) gene (Steinhelper, 1993; Arden *et al.*, 1995). The C-type natriuretic peptide gene is however localised on chromosome 2 in humans (Ogawa *et al.*, 1994). ANP and BNP activate receptors from the guanylate cyclase receptor family and like guanylin and uroguanylin, generate intracellular cGMP (Schulz, 1999).

The genes encoding guanylin and uroguanylin possess similar genomic structures with 3 exons and 2 introns. Both peptides are synthesised as preprohormones and post-translationally processed by prohormone convertases of uncertain identity to remove the signal peptide and produce further prohormone intermediates and, eventually, the bioactive peptide (de Sauvage *et al.*, 1992; Kita *et al.*, 1994) (figure 1.6). The preprohormone pre-ProGuanylin, consists of 115 amino acids and is processed to give a 94 amino acid prohormone (ProGuanylin) with further processing resulting in the putative bioactive guanylin protein consisting of a 15 amino acids (de Sauvage *et al.*, 1992). Similarly, pre-ProUroguanylin consists of 112 amino acids and is processed to give an 86 amino acid intermediate with the believed active version of uroguanylin, consisting of a 16 amino acid peptide (Kita *et al.*, 1994).

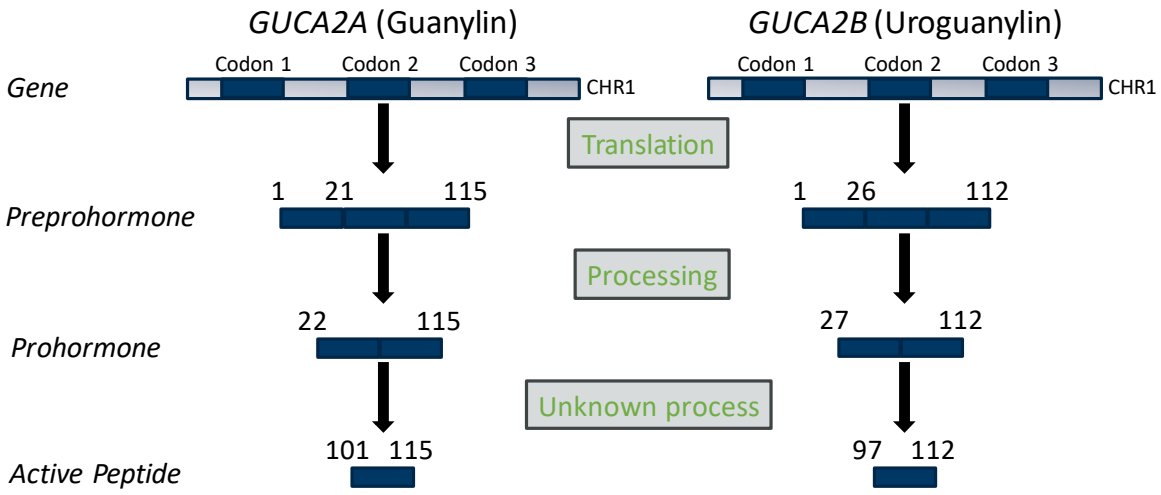

Figure 1.6: Schematic overview of the assumed synthesis and processing of guanylin and uroguanylin peptides. Guanylin and uroguanylin have 3 exons and 2 introns. Once translated into pre-ProGuanylin and pro-ProUroguanylin, the signal peptide is cleaved giving a 94 amino acids ProGuanylin, and a 86 amino acids ProUroguanylin. Prohormone convertases are believed to cleave the proforms resulting in a 15 amino acids guanylin and a 16 amino acids uroguanylin. Figure adapted from Sindic *et al.*, 2013.

Both active peptides adopt similar tertiary structures owing to the presence of two disulfide bonds, with the configuration Cys4–Cys12 and Cys7–Cys15 for both guanylin and uroguanylin. These disulphide bonds were revealed to be essential for peptide function (Nokihara *et al.*, 1997). Furthermore, guanylin and uroguanylin share a highly conserved five amino acid C-terminal motif (Ala-Cys-Thr-Gly-Cys) which is assumed to be required for GC-C receptor activation as it is the common motif between the guanylin peptides and the ST peptide (Forte, 2004a).

The structural difference between guanylin and uroguanylin distinguishes them in their sensitivity towards proteases and pH dependency. Uroguanylin is highly resistant to

proteolytic attack and inactivation by endoproteases, such as chymotrypsin, due to the presence of a critical asparagine residue. In contrast, guanylin has a tyrosine residue rather than asparagine in the same position, rendering the peptide sensitive to degradation by chymotrypsin with further degradation occurring within urine (Hamra *et al.*, 1996). Moreover, the affinity of guanylin peptides to their cognate receptor, GC-C, is pH dependent. Hamra *et al.* showed that the N-termini of both peptides affects their pH dependence. Uroguanylin was more potent at pH 5 whereas guanylin exhibited increased potency in more basic conditions (pH 8) (Hamra *et al.*, 1997). It is established that the surface of the intestinal epithelium presents a different microenvironment with variable pH, with the colonic lumen becoming more acidic due to the release of SCFAs by the microbiota (Bown *et al.*, 1974; Daniel *et al.*, 1985; Chu and Montrose, 1995). Hamra *et al.* concluded that guanylin was potent in pH conditions rendering uroguanylin's potency low and vice versa.

1.3.2 Tissue distribution

The predominant location of guanylin and uroguanylin expression is the intestine. Uroguanylin expression is higher in the proximal intestine and decreases distally along the axis of the small intestine and colon. In contrast, guanylin expression in the gut is highest distally (Whitaker, Witte, *et al.*, 1997). Transcripts levels of mRNA were also found in the kidney. Uroguanylin was expressed abundantly in comparison with guanylin, and patterns of expression also differed. Isolation of proximal tubules and collecting duct allowed Potthast and colleagues to perform qPCR on uroguanylin and guanylin (Potthast *et al.*, 2001). The investigators found that uroguanylin expression was highest in the proximal tubules and lowest in the other segments tested (glomeruli, thick ascending limbs of Henle's loop and collecting ducts). Guanylin mRNA expression was detectable in the collecting duct and followed an opposite distribution when compared with uroguanylin expression (Potthast *et al.*, 2001).

Renewed research interest in the localisation of guanylin peptides occurred during the 1990s and early 2000s, however during this period the available reagents and utilised detection methods did not generate reliable and reproducible data. Uroguanylin was detected in lung, pancreas, stomach, salivary glands, pancreatic islet β cells in rats (Miyazato *et al.*, 1996; Nakazato *et al.*, 1998; Kulaksiz, Rausch, *et al.*, 2001; Kulaksiz, Schmid, *et al.*, 2001; Kulaksiz *et al.*, 2004). Guanylin expression was detected in opossum's brain and reproductive organs, liver

and gallbladder (Fan *et al.*, 1997; Jaleel *et al.*, 2002; Schwabe and Cetin, 2012). Details of their localisation and used methods will be discussed further in chapter 7.

The GC-C receptor is primarily localised on the apical brush border membrane of intestinal and colonic epithelium (Krause' *et al.*, 1994; Nandi, Bhandari and Visweswariah, 1997; Qian *et al.*, 2000). Qian *et al.* found that GC-C mRNA levels were relatively uniform in all regions of the intestine. However, Krause *et al*. showed that the distribution of GC-C expression decreased distally along the axis of the small intestine and colon using both binding of radiolabelled ST to GC-C receptor and a cGMP accumulation bioassay of intestinal mucosa. Interestingly, GC-C expression was shown to be high in neonates which may explain an apparent increased sensitivity of this population to the effects of the heat stable *E. coli* enterotoxin STa (Cohen *et al.*, 1988; Al-Majali *et al.*, 2007).

The GC-C receptor is also expressed in a number of extra-intestinal tissues. In opossum, high levels of GC-C mRNA have been measured in the renal cortex (London *et al.*, 1999) and recent studies in rodents have identified GC-C mRNA expression in the mediobasal hypothalamus (Valentino *et al.*, 2011). The GC-C was also identified in midbrain dopamine neurons (Gong *et al.*, 2011) as well as in the hypothalamus and, more specifically, arcuate nucleus in mice (Kim *et al.*, 2016). Subsequent studies have suggested an integral role for this receptor in the regulation of food intake and energy homeostasis (Valentino *et al.*, 2011; Cintia Folgueira *et al.*, 2016).

1.3.3 Site-directed secretion of ProGuanylin and ProUroguanylin

After the discovery of the guanylin peptides and their role in intestinal water and electrolyte homeostasis, research focused mainly on the possible roles for these peptides in the kidney. Such studies focused on the mechanisms by which guanylin peptides access the kidney and the factors that regulate their secretion from intestinal epithelial cells. In order for these peptides to activate distant targets expressed in the kidney or the brain, they must be secreted into the circulation. Using immunoassays and Reversed-Phase High-Performance Liquid Chromatography (RP-HPLC), Kinoshita *et al.* found that uroguanylin and ProUroguanylin circulate in the bloodstream with ProUroguanylin identified as the predominant circulating form (Kinoshita, Fujimoto, *et al.*, 1997; Kinoshita *et al.*, 1999). Through the use of Ussing chambers, subsequent studies found that both ProGuanylin and guanylin were detected on the basolateral side of the membrane upon stimulation with several different stimulants

including bombesin, bethanechol, 8-Br-cGMP and carbachol (Martin *et al.*, 1999). To date, this study is the only one to provide experimental evidence supporting bidirectional secretion of guanylin peptides from intestinal epithelial cells. Secretion from the luminal side would affect the water and salt homeostasis locally, and basal secretion may exert an endocrine effect on distant organs (such as kidney and brain). Martin *et al.* suggested that guanylin was mainly secreted from the luminal side with the concentration of guanylin 6-fold higher than levels measured from the basolateral membrane of the Ussing chambers. To date, the sole source of circulating guanylin peptides is believed to be the intestine.

1.4 Physiology of guanylin peptides

1.4.1 Guanylin and uroguanylin as intestinal natriuretic peptides

The role of the guanylin peptides in the gastrointestinal tract became of interest when intraluminal guanylin and uroguanylin were shown to activate the GC-C receptor localised in the brush border membrane of enterocytes. Both guanylin and uroguanylin were shown to stimulate transepithelial chloride secretion in a T84 assay model (Hamra *et al.*, 1993; Kita *et al.*, 1994; Nokihara *et al.*, 1997). An early study by Carrithers *et al.* supported natriuretic roles of the guanylin peptides by demonstrating that sodium chloride intake increased *Guca2a* mRNA expression in rat intestine (Carrithers *et al.*, 2002). Human data corroborated these findings with uroguanylin plasma levels and urinary secretion higher in healthy participants on a high-salt diet compared to those on a low salt diet (Kinoshita, Fujimoto, *et al.*, 1997).

In the intestine, the binding of uroguanylin to the GC-C receptor leads to the secretion of Cl^-, HCO_3^- and Na^+ as well as water in the lumen (figure 1.7) via activation of the cystic fibrosis transmembrane regulator anion channel (CFTR) (Cuthbert *et al.*, 1994).

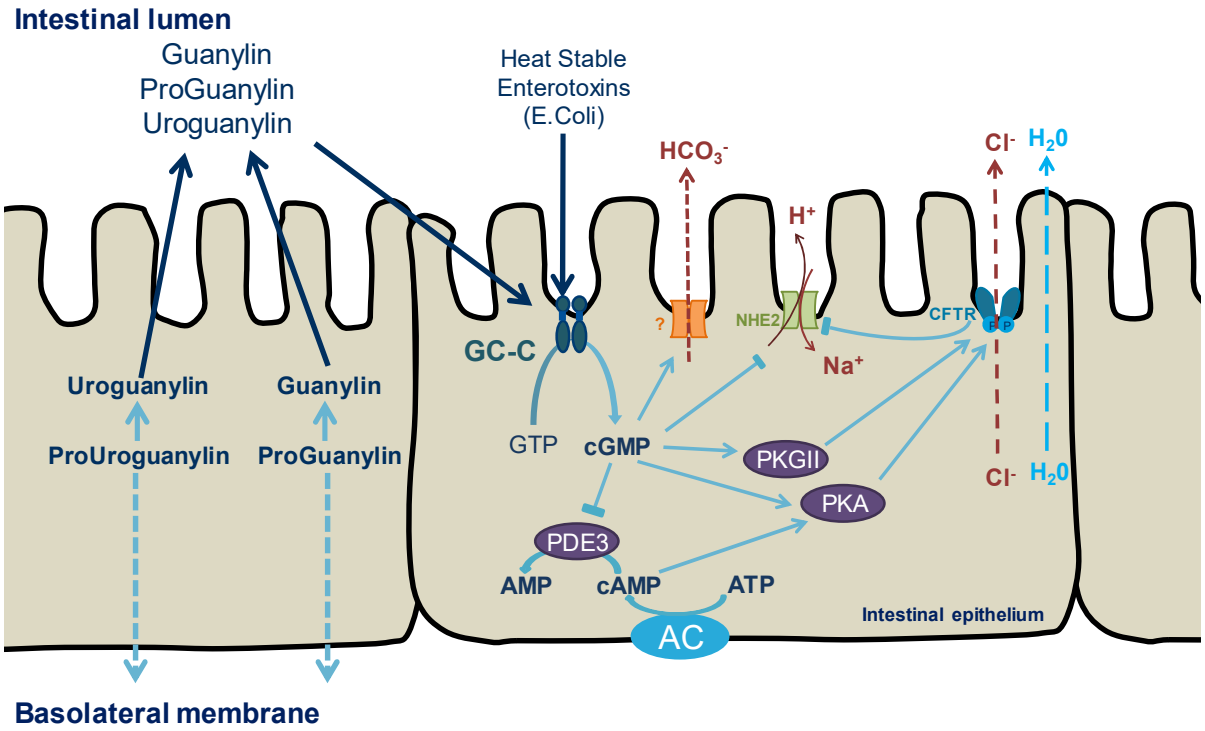

Figure 1.7: Proposed signalling pathways of the guanylin peptides in the intestine. Guanylin peptides activate the GC-C receptor on the luminal side leading to the generation of cGMP. Intracellular cGMP subsequently binds and activates 3 downstream effectors: cGMP-dependent protein kinases (PKGs), phosphodiesterases (PDEs) and cAMP-dependent protein kinases (PKAs). The increasing concentration of cGMP inhibits the Na^+/H^+ exchanger type 2 (NHE2) and activates the protein Kinase G type II (PKG2). Activation of the cGMP also stimulates the Protein Kinase A (PKA) in two different ways. Firstly, it can activate PKA directly. Secondly it can activate PKA indirectly by the inhibiting the phosphodiesterase III (PDE3). This inhibition will lead to an increase in cAMP which will in turn activate PKA. Finally, PKA and PKGII will both phosphorylate the CFTR leading to an efflux of Cl^- in the lumen. This extracellular Cl^- secretion will stimulate the $Cl^-/HCO3^-$exchanger. The amount of electrolyte will increase in the intestinal lumen and the increased osmolarity will reduce the water absorption from the lumen to the blood. Figure adapted from Rahbi *et al.*, 2012.

The GC-C receptor is activated following binding of either the STa toxin or the cognate ligands guanylin or uroguanylin to the extracellular domain of the GC-C. The guanylate cyclase catalytic domain leads to an increased intracellular concentration of cGMP. cGMP, in turn, stimulates the opening of the CFTR resulting in an increased secretion of chloride and bicarbonate via two different mechanisms; the first is phosphorylation by cGMP-dependent protein kinase II (PKGII) (French *et al.*, 1995; Vaandrager, Bot and De Jonge, 1997) or by cAMP-dependent protein kinase II (PKAII) (Forte *et al.*, 1992; Chao *et al.*, 1994). cGMP inhibits phosphodiesterase III (PDEIII), which hydrolyses cAMP into AMP, increasing intracellular cAMP which consequently activates PKAII (Vaandrager *et al.*, 2000). Activity of cGMP activity does not only stimulate chloride and bicarbonate secretion in the lumen, but also acts as an inhibitor of the sodium/hydrogen exchanger (NHE2) (Toriano *et al.*, 2011). The increased luminal osmolarity drives the movement of water into the intestinal lumen.

1.4.2 Uroguanylin a new satiety hormone

Guanylyl cyclase and its signalling product cGMP are involved in the control of food intake and satiety in two invertebrates; *Drosophila* (Kaun *et al.*, 2007) and *C. elegans* (You *et al.*, 2008). A role for uroguanylin in the regulation of energy homeostasis and as a novel regulator of the gut-brain axis has been suggested (Valentino *et al.*, 2011). Mice lacking GC-C (GC-C$^{-/-}$) were found to be hyperphagic and heavier compared with wild-type (WT) mice. Furthermore, GC-C$^{-/-}$ mice exhibited cardiac hypertrophy, hyperleptinemia, hyperinsulinemia and impaired glucose tolerance. Systemic administration of a GC-C ligand STa induced satiety in WT but not GC-C$^{-/-}$ mice. These findings coupled with the detection of RNA expression of the GC-C receptor in the mediobasal hypothalamus supported GC-C activation as a mechanism to induce satiety. Intestinal secretion of ProUroguanylin was stimulated upon food consumption which subsequently induced satiety. As no endogenous ligand for the GC-C receptor was found in the hypothalamus, the authors concluded that food consumption induced secretion of ProUroguanylin from intestinal epithelial cells into the systemic circulation followed by proteolytic cleavage within the hypothalamus, by an unknown proteolytic enzyme, into the active peptide uroguanylin.

Data published in 2015 found similar results for uroguanylin and contributed towards its potential role in energy homeostasis. The chronic central infusion of uroguanylin decreased adiposity and body weight in diet-induced obesity (DIO) mice without causing a change in food intake. Centrally administered uroguanylin induced browning of the white adipose tissue (WAT) to promote brown adipose tissue (BAT) thermogenesis. Finally faecal output was increased through the parasympathetic nervous system when uroguanylin was centrally infused and compared in mice that received a surgical vagotomy (Cintia Folgueira *et al.*, 2016). The same lab found that mice fasted for 48hrs showed significantly reduced levels of uroguanylin in plasma compared to mice fed *ad libitum*. Plasma levels of uroguanylin returned to baseline when the animals were fed again or following leptin challenge (C. Folgueira *et al.*, 2016). In leptin deficient ob/ob mice, uroguanylin levels were unchanged after fasting but leptin treatment increased the uroguanylin levels to levels observed in WT mice fed *ad libitum*. The authors concluded that ProUroguanylin was a nutritional status regulator but that it was leptin dependent (C. Folgueira *et al.*, 2016).

In humans, recent clinical studies have found decreased uroguanylin levels in obese adolescent and adult subjects when compared to healthy participants (A. Rodríguez *et al.*, 2016; Di Guglielmo, Perdue, *et al.*, 2018; Di Guglielmo, Tonb, *et al.*, 2018). However transcript levels of both *GUCA2A* and *GUCA2B* were significantly higher in the jejunal division site of patients following Roux-en-Y gastric bypass surgery when compared to levels before the operation (Fernandez-Cachon *et al.*, 2018).

However, results from Begg *et al.* have questioned the link between central administration of uroguanylin and food intake or body weight change in lean mice. GC-C$^{-/-}$ mice were not hyperphagic and heavier compared with wild-type animals. Mice lacking the *Guca2b* gene (*Guca2b*$^{-/-}$) were found to have a slight increase in adiposity and body weight, in addition to glucose intolerance. The methodology of this work was different to the previously described studies, which could explain the different results obtained. For example, the use of lean rats for GC-C agonist studies, feeding regime, and animal sex all differed from the original protocol (Begg *et al.*, 2014).

1.4.3 Guanylin peptides and crypt-villous proliferation

As mentioned previously in 1.1.2, the intestinal epithelium undergoes continuous regeneration via stem cells at the base of the crypt-villus axis following a cycle of proliferation, differentiation and metabolic maturation before apoptosis (Bjerknes and Cheng, 1999; Barker, van de Wetering and Clevers, 2008; Clevers, 2013). There is an increasing number of publications recognising a relationship between GC-C receptor expression and a potential anti-proliferative action in the intestine. For instance, in GC-C$^{-/-}$ mice, the length of the crypts from duodenum to colon were considered longer when compared to WT mice (Li, Lin, *et al.*, 2007). Hyperplasia caused by proliferating cells was associated with an increase in cell migration and apoptosis in GC-C$^{-/-}$ mouse colon. Enterocyte proliferation was also observed when compared with cells from the secretory lineage (Li, Lin, *et al.*, 2007). In a subsequent study, deletion of GC-C in mice carrying an adenomatous polyposis coli (APC) mutation, a tumour suppressor gene, increased the incidence of tumours within the colon as well as altering the genomic integrity of the tumour (Yang *et al.*, 1997; Fodde and Smits, 2001). However in the small intestine, GC-C deficiency increased tumorigenesis through enhanced proliferation without modification of genomic integrity (Li, Schulz, *et al.*, 2007). Additional observations suggest that cGMP production increases expression and activity of the tumour

suppressor PTEN (Phosphatase and tensin homolog) and therefore inhibits the v-akt murine thymoma viral oncogene homolog 1 (AKT) signalling (Lin *et al.*, 2010a; Gibbons *et al.*, 2013). AKT inhibition would reverse the tumorigenic Warburg metabolic phenotype in human and murine colon cancer cells through coordinated regulation of cell cycle, metabolism, chromosomal instability and/or cell death (Robey and Hay, 2009; Ward and Thompson, 2012).

Therefore, reduced GC-C receptor signalling is assumed to have impaired epithelial cell function that increases the susceptibility to intestinal tumorigenesis and colorectal cancer. These data suggest that the GC-C receptor may serve as a tumour repressor, but surprisingly its expression is conserved and over-expressed in some colorectal tumours (Schulz *et al.*, 2006). A plethora of publications highlight the fact that the expression of guanylin and uroguanylin are commonly absent in colorectal cancer. The loss of gene transcripts happens early on in the transformation process and could play a role at an early stage of carcinogenesis (Zhang, 1997; Cohen, Hawkins and Witte, 1998; Steinbrecher *et al.*, 2000, 2002; Notterman *et al.*, 2001; Glebov *et al.*, 2006). Guanylin peptide loss was subsequently defined in adenomas, as well as in adenocarcinomas. In a cohort of more than 280 volunteers with stage I–III colorectal cancer, guanylin mRNA and protein expression were lost or significantly lower (100-1000 fold lower) in cancerous tissues compared to healthy adjacent tissues for more than 85% of the volunteers (Wilson *et al.*, 2014). The deficiency of guanylin and uroguanylin expression may silence the GC-C, which would normally act as a tumour suppressor and interrupt the homeostatic mechanisms that regulate the colorectal epithelium. In conclusion, the guanylin peptides may impact crypt-villous proliferation through activation and maintenance of the GC-C receptor.

1.4.4 Uroguanylin, a controversial role in the gastrointestinal-renal natriuretic signalling axis

In 1975, it was demonstrated that human kidney presented a greater natriuretic response to an oral load of sodium compared with an equivalent amount of sodium delivered intravenously (Lennane *et al.*, 1975; Carey, 1978). This led to the hypothesis that the gastrointestinal tract complements the action of the Renin-Angiotensin-Aldosterone System and the Atrial Natriuretic Peptide (ANP) in the monitoring of a natriuretic response to postprandial salt absorption. Renewed interest in the role of the gastrointestinal tract in the maintenance of salt and water homeostasis increased following the discovery of the action of guanylin peptides in the intestine.

It was established that guanylin peptides promote natriuretic, kaliuretic and diuretic effects in mice in a dose and time dependent manner. Using a sealed-urethra mouse model, it was shown that the injection of uroguanylin or guanylin increased renal sodium excretion while glomerular filtration rate (GFR), plasma creatinine concentration, urine osmolarity, heart rate, and blood pressure remained constant (Carrithers *et al.*, 1999). In another study, uroguanylin knockout mice were found to have an impaired salt excretion (Lorenz *et al.*, 2003).

While researchers largely agree on the natriuretic effect of guanylin peptides in kidney, the mode of action and origin of the peptides are more controversial topics. Researchers have proposed both a similar mechanism to the one found in the intestine, and an alternate GC-C independent pathway. Corroborating the first hypothesis, highly expressed GC-C receptor was observed in opposum's kidney (London *et al.*, 1999) and there is a strong correlation between urinary excretion of uroguanylin and the cGMP response to high-salt diet (Kinoshita, Fujimoto, *et al.*, 1997). However, GC-C$^{-/-}$ mice presented a uroguanylin-induced natriuretic renal effect (Carrithers *et al.*, 1999, 2004) and GC-C transcript expression was undetectable in rat kidney ((Qian *et al.*, 2011).

Furthermore, the source of guanylin peptides that would mediate renal action has been subject to debate. The fact that uroguanylin transcript levels are undetectable in the kidney (Forte, Fan and Hamra, 1996; Li *et al.*, 1997) and the presence of proforms in plasma (Moss *et al.*, 2008) with indication that ProUroguanylin was processed as the active peptide in the kidney (Qian *et al.*, 2008) has substantiated this theory. However rats and mice fed a high-salt diet did not exhibit significant differences in uroguanylin or ProUroguanylin plasma despite having higher levels of uroguanylin in urine, therefore supporting a renal origin of uroguanylin (Fukae *et al.*, 2002; Elitsur *et al.*, 2006).

In 2012, a study by Preston and colleagues suggested that a gastrointestinal-renal axis that controls renal natriuresis may not exist in humans. The authors found no difference in the cumulative or hourly natriuretic response to oral versus intravenous sodium administration (Preston *et al.*, 2012). Whilst no difference in intestinal salt secretion was detected, this study did provide some indication that guanylin peptides may be produced within the kidneys and act locally.

1.5 Pathology

1.5.1 Molecular genetics of familial diarrhoea and meconium ileus syndromes

The intestinal natriuretic action of the guanylin peptides and the role they play in water and electrolyte homeostasis might be of crucial importance to gut transit. Indeed, studies have reported that genetic mutations in the GC-C receptor alter gastrointestinal transit, resulting in syndromes characterised by either diarrhoea or meconium ileus.

Fiskerstrand *et al.* studied 32 members of a Norwegian family that were affected by chronic diarrhoea and compared them to 14 family members that were not affected. After performing exome sequencing, a heterozygous missense mutation (c.2519G→T) was found in the GC-C receptor of all affected family members. Functional studies of the mutant GC-C were performed using transfected HEK293T cell lines and a cGMP functional assay. This mutation caused an overproduction of cGMP which likely triggers hyperactivation of CFTR resulting in increased chloride and water secretion from enterocytes to the gut lumen leading to chronic diarrhoea. For the same guanylin or uroguanylin concentration, the mutant GC-C was more active and resulted in abnormal levels of cGMP in the intestinal cells. Family members affected by the mutation appeared to have predispositions to small bowel obstruction or oesophageal hernia (Fiskerstrand *et al.*, 2012).

In a study of four unrelated volunteers suffering from congenital sodium diarrhoea (CSD) syndromes, missense mutations in the GC-C sequence were detected by whole-exome sequencing and chromosomal microarray analyses (Müller *et al.*, 2015). All mutations were functionally studied in transfected HEK293T cells. All mutations enhanced intracellular cGMP to endogenous and exogenous ligands; this was not a consequence of increased ligand-receptor binding, but rather was due to hyperactivation of the mutant receptors (Müller *et al.*, 2015).

Finally, meconium ileus is a condition where the content of infant distal ileum and cecum is extremely sticky and causes the bowel to be blocked at birth. More than 80% of cases are caused by mutations of the CFTR (Rosenstein and Langbaum, 1980) and 15-20% of infants with cystic fibrosis develop meconium ileus (Eggermont, 1996). However, 20% of new-borns suffering meconium ileus had no clinical evidence of cystic fibrosis (Fakhoury *et al.*, 1992). Two independent studies identified loss of function mutations in *GUCY2C* (GC-C gene) in two

unrelated Bedouin and one Lebanese family, with infants presenting with meconium ileus but no other features suggestive of cystic fibrosis (Romi, Cohen, Landau, Alkrinawi, Yerushalmi, Hershkovitz, Newman-Heiman, Garry R. Cutting, *et al.*, 2012; Smith *et al.*, 2015). In the Bedouin kindred, a homozygous missense mutation in the extracellular domain of the GC-C receptor led to reduced synthesis of cGMP and a reduction of the CFTR activity (Romi, Cohen, Landau, Alkrinawi, Yerushalmi, Hershkovitz, Newman-Heiman, Garry R. Cutting, *et al.*, 2012). In the Lebanese kindred, a homozygous truncating mutation cleaved the guanylate cyclase catalytic domain and abrogated the production of cGMP and therefore CFTR activity (Smith *et al.*, 2015).

1.5.2 Role of guanylin in colorectal cancer

Intestinal epithelium is a remarkable dynamic structure experiencing a nearly complete cell renewal every 4-5 days (Heath, 1996). This epithelial homeostasis and continuous regeneration are controlled by important processes such as proliferation, differentiation, metabolic reprogramming and genomic integrity (Barker, 2014). Defective differentiation along the secretory lineage of epithelial cells, accelerated cell cycle and hyper proliferation, genomic instability in intestinal epithelial cells (increasing DNA double strand breaks, loss of heterozygosity, and point mutations on genes central to tumorigenesis including APC and β-catenin), are all factors that increase dysregulation of cell metabolism and are the foundation of the Warburg phenotype (Bertram, 2000; Hanahan and Weinberg, 2000, 2011; Ward and Thompson, 2012). The Warburg phenotype is based on the observed change that cancer cells change their more efficient oxidative phosphorylation metabolism to anaerobic glycolysis pathway (Warburg, 1956).

As mentioned in 1.4.3, guanylin and uroguanylin gene expression is commonly lost in colorectal tumours (Wilson *et al.*, 2014) while their receptor GC-C is over-expressed (Schulz *et al.*, 2006) and the loss of cognate ligands would silence the receptor. It is hypothesised that the GC-C and its ligand signalling axis plays a role in the regulation of the regenerative processes, and could function as a tumour suppressor to maintain the integrity of the intestinal epithelium (Li, Lin, *et al.*, 2007; Li, Schulz, *et al.*, 2007; Lin *et al.*, 2010b). The loss of guanylin and uroguanylin could act at an early stage of the carcinogenesis (Zhang, 1997; Cohen, Hawkins and Witte, 1998; Steinbrecher *et al.*, 2000, 2002; Notterman *et al.*, 2001; Glebov *et al.*, 2006). It has been previously shown that STa and uroguanylin have

antiproliferative actions on the adenocarcinoma cell line T84 (Kunwar Shailubhai *et al.*, 2000; Pitari *et al.*, 2001, 2003). Additionally, supplementation of uroguanylin in food and water has been shown to decrease intestinal tumorigenesis in a mice carrying the APC mutation (Kunwar Shailubhai *et al.*, 2000).

Today, epidemiological evidence suggests an association between obesity and an increased risk of several cancer types, and high prediagnosis BMI was associated with increased mortality (Campbell *et al.*, 2015; Renehan, Zwahlen and Egger, 2015). The emerging role of the GC-C receptor on energy homeostasis and food intake as well as its role on crypt-villous proliferation might suggest that this receptor is at the intersection between obesity and colorectal cancer. One of the first studies to suggest such a role was published by Lin *et al.* who showed that guanylin mRNA in human colon was inversely correlated with BMI in morbidly obese participants (BMI over 35) showing a 80% decrease in *GUCA2A* transcripts. Furthermore, they observed that mice on a high fat (HF) or high calorie (HC) diet did lose guanylin expression in the colon. The loss of the GC-C signalling pathway (via the loss of guanylin expression) resulted in abnormal intestinal epithelium with increased β-catenin expression mirroring a result observed in GC-$C^{-/-}$ mice. Interestingly, *GUCA2A* levels were restored after 4 weeks of replacing the HF or HC diet to a lean diet. The hypercaloric diets increased the endoplasmic reticulum (ER) stress markers Binding immunoglobulin protein (BiP) (Lee, 2005) and the CCAAT/-enhancer-binding protein homologous (CHOP) protein (Wang *et al.*, 1996) in the intestinal epithelium. Lin *et al.* suggest that the reversible calorie-dependent loss of guanylin is induced by ER stress and the unfolded protein response in colonic epithelium (Lin *et al.*, 2016). However, in this study, the researchers only focused on guanylin and omitted to discuss the expression of uroguanylin, the second endogenous ligand of the GC-C receptor. Silencing of the GC-C would only be concluded if both ligands are downregulated or lost.

1.5.3 Role of uroguanylin in kidney disease and hypertension

Due to the potential natriuretic role of guanylin peptides in the kidney, few studies have been performed on participants presenting kidney diseases. Kinoshita *et al.* found that blood pressure and plasma uroguanylin levels were higher in the case of chronic glomerulonephritis patients as well as in patients suffering from chronic renal failure (Kinoshita, Fujimoto, *et al.*, 1997; Kinoshita *et al.*, 1999). These studies found that there was a strong correlation between

of guanylin and creatine levels in plasma, with creatine being a marker used for routine analysis of kidney function (Gowda *et al.*, 2010).

A study in uroguanylin knock out (KO) mice showed that animals lacking uroguanylin had an impaired ability to excrete an enteral load of NaCl. KO mice were also hypertensive and this increase in blood pressure was independent of the degree of oral salt intake (Lorenz *et al.*, 2003).

1.5.4 Therapeutic targeting of the GC-C receptor

The gut motility function of the GC-C signalling axis has instigated the development of drugs by pharmaceutical companies to treat chronic digestive diseases. Analogues of guanylin peptides and the enterotoxin STa are being developed and are currently in clinical trials as potential drug therapies to treat chronic constipation conditions. For instance, irritable bowel syndrome (IBS) associated with constipation and chronic idiopathic constipation (CIC) can have a detrimental impact on quality of life (Koloski, Talley and Boyce, 2000; El-Serag, Olden and Bjorkman, 2002; Sun *et al.*, 2011) with more than 15% of the general population affected by such disorders in Western countries (Lovell and Ford, 2012). Abdominal and stomach pain as well as bloating are common side effects of constipation associated with IBS (Heidelbaugh *et al.*, 2015). Linaclotide, a poorly absorbed GC-C agonist, is the first drug to be approved by both the Food and Drug Administration (FDA) and the European Medicines Agency (EMA) in 2012, and is distributed by Allergan under the licensed name Linzess to treat IBS with constipation and chronic constipation with no known cause (Corsetti and Tack, 2013). Plecanatide is the second GC-C agonist drug on the market that was approved by the FDA in 2017. The drug is manufactured by Synergy Pharmaceuticals, Inc and is sold under the name Trulance for the treatment of CIC and IBS (Brenner *et al.*, 2018). A second product in development from Synergy Pharmaceuticals is dolcanatide, which has higher stability in the intestinal proteolytic milieu, and is currently in development to treat ulcerative colitis. Both linaclotide and plecanatide were shown to reduce visceral and abdominal pain but precipitated diarrhoea as a side effect in 10% of the patients (Shah, Kim and Schoenfeld, 2018).

Association of chronic constipation with the development of colorectal cancer has been a subject of controversy. However a meta-analysis performed on 9 previously published studies highlighted an increased risk of colorectal cancer linked to constipation with an odds ratio of 1.48 and a 95% confidence intervals of 1.32-1.66 (Sonnenberg and Müller, 1993). Since the

role of GC-C on colorectal cancer has been studied, linaclotide and plecanatide have been proposed as a preventive strategy to the development of colorectal cancer (Scarpignato and Blandizzi, 2014). The first human study on the bioactivity of linaclotide was performed with the purpose to use it for colorectal cancer chemoprevention (Weinberg *et al.*, 2017). Observations were made that in patients responding to linaclotide with a cGMP pharmacodynamic response, there was a reduced crypt proliferation in the small and large intestine when measured by Ki67 immunohistochemistry assessment (Hoos *et al.*, 2001; Li *et al.*, 2015; Weinberg *et al.*, 2017).

1.6 Aims of thesis

Guanylin and uroguanylin are peptides produced by the intestinal epithelium with proposed roles in salt and water homeostasis. While the downstream signalling pathway has been elucidated in the intestine, understanding the role of guanylin peptides in healthy and disease states, the regulation of their secretion and their localisation in the digestive system has been limited by the lack of specific antibodies against the active human peptides and their prohormone precursors. The aim of this project was to address these deficiencies.

With this in mind, in the first part of my thesis, I established and validated novel high throughput monoclonal antibody-based immunoassays to enable the quantification of guanylin peptide proforms ProGuanylin and ProUroguanylin (Chapter 3). I produced antibodies against the historically defined active versions of the peptides and used these to investigate their presence in human biological samples and redefined their sequence (Chapter 4). Subsequently, the specificity of these immunoassays was assessed on human plasma samples and reference ranges of guanylin peptides in healthy volunteers in fasting and post-prandial states, as well as in healthy and disease states (Chapter 5). *In vitro* cell based assays and *ex vivo* experimental systems combined with these immunoassays were used to investigate the effects of salt, gut and vagal stimuli on the secretion of the guanylin and uroguanylin (Chapter 6). Finally, I generated a transgenic reporter mouse model expressing a fluorescent protein under the control of the guanylin promoter to examine the localisation of guanylin-expressing cells in the gastrointestinal tract (Chapter 7).

Overall, this work has shed new light on the secretion and localisation of the guanylin peptides in mouse and human in the digestive system.

Chapter 2: Materials and Methods

2.1 Production of the hormone proforms: ProGuanylin and ProUroguanylin

2.1.1 Construction of the propeptide expression vectors

Recombinant propeptides were expressed as thioredoxin fusion proteins with the following configuration: Propeptide - AviTag – PreScission protease cleavage site – linker – His6 Tag – Thioredoxin. The AviTag peptide (GLNDIFEAQKIEWHE) allows site-specific biotinylation on the lysine residue by BirA and the PreScission protease cleavage site (LEVLFQVGP) allows the removal of the His6 tag and Thioredoxin after affinity purification.

DNA constructs encoding the human propeptides -either ProGuanylin (accession number Q02747) or ProUroguanylin (accession number Q16661)- Avi Tag and protease site were commercially synthesized (GeneArt, ThermoFisher) with restriction sites NcoI on the 5' and BglII on the 3' end for cloning into a T7 RNA polymerase-based expression vector pET-32a (Novagen, Madison, WI). Double restriction digestion with BglII (NEB, #R0144S) and NcoI enzymes (NEB, #R0193S) were performed according to the manufacturer's instructions followed by T4 DNA ligation (NEB, #M0202S) and transformation into DH5α *E. coli* strain (in house). Refer to appendix 1 for schematic of the pET-32a constructs.

2.1.2 Expression of ProGuanylin and ProUroguanylin

The production of soluble ProGuanylin in *E. coli* was described in Lauber *et al.*, 2003. This method was used to produce 25mg of ProGuanylin for the hybridoma generation, screening and assay development.

The expression vector for ProGuanylin was transformed into Origami2 (DE3) (Novagen Merck Millipore #71408-3) followed by selection on a 2xTYAG plate at 37˚C overnight (ON). One colony was used to inoculate a 5mL LB starter culture containing 200µg/mL ampicillin followed by ON incubation at 280rpm at 37˚C. The starter culture was subsequently used to inoculate a 400mL culture flask at an optical density (OD) of 0.1. The culture was grown to an OD of 0.8, followed by addition of 1mM isopropyl β-D-1-thiogalactopyranoside (IPTG) and incubation at 30˚C for 4hrs. Cells were harvested by centrifugation at 4000rpm at 4˚C for 15 minutes.

The above method was optimised for ProUroguanylin as the protein was largely insoluble in *E. coli*. Variables including duration of expression, temperature, IPTG concentration and bacterial strains were assessed by SDS-PAGE. The optimised protocol is described below.

The expression vector for ProUroguanylin was transformed into Arctic Express (DE3) (Agilent #230192) followed by selection on a 2xTYAG plate at 37˚C ON. A colony was used to inoculate a 5mL LB starter culture containing 200µg/mL ampicillin followed by ON incubation at 280rpm at 37˚C. The starter culture was subsequently used to inoculate a 400mL culture flask at an OD of 0.1. The culture was grown to an OD of 0.6, followed by addition of 0.5mM IPTG and incubation at 12˚C ON. Cells were harvested by centrifugation at 4000rpm at 4˚C for 15 minutes.

2.1.3 Purification of soluble ProGuanylin and ProUroguanylin

Cell pellets were resuspended in 25mL of 2xphospate buffered saline (PBS) (Gibco #70011044) per gram of weight of cells with 2xPBS buffer containing SigmaFast Protease inhibitor cocktail tablet EDTA free (1 tablet per 100mL), 0.2mg/mL of lysozyme (Merck Millipore #71412-3) and benzonase (Merck Millipore #01654, 50U/mL). Cells were lysed on ice by sonication in pulsed mode: six rounds of 30s bursts with a one-minute delay (intensity at 150W). The lysate was clarified by centrifugation in a 45ti rotor (Beckman) at 40,000rpm at 4˚C for 2hrs. The supernatant was filtered through a 0.22µm membrane.

The filtered supernatant was loaded on a HiTrap Chelating HP column (GE #17-0408-01) pre-immobilized with Cobalt solution and pre-equilibrated with 2xPBS. The column was washed with 2xPBS followed by a wash step with 50mM imidazole in 2xPBS. A gradient elution (50mM to 1M) was performed to elute the proteins. Eluate fractions containing the fusion protein were analysed by SDS PAGE. The desired fractions were pooled, and buffer exchanged in 1xPBS (Gibco #10010023) using PD10-columns (GE #17-0851-01). Protein concentrations were determined by spectrophotometry (Nanodrop1000 Thermo Scientific).

To remove the C-terminal His6-thioredoxin tag, fusion proteins were incubated with PreScission protease (GE # 27-0843-01) at room temperature (RT) for 3hrs. A subtractive purification using the Cobalt column pre-equilibrated in 2xPBS was performed. The flow-through containing the purified proforms was further purified by Superdex 75 2660 (GE) size exclusion chromatography on an Akta purifier (GE). Fractions containing monomeric proteins were pooled and concentrated using a centrifugal concentrator (Sartorius #VS2011) to a final concentration of 1mg/mL before being snap-frozen in liquid nitrogen.

2.1.4 Purification of ProUroguanylin from inclusion bodies

The pellet from the ultracentrifugation of the lysate above (refer to 2.1.3) was resuspended in 8M urea. The solution was clarified by centrifugation at 20,000rpm at RT for 10 minutes and filtering through a 0.22µm membrane (Stericup, Thermo Scientific #5670020). The supernatant was incubated with 5mL of Ni-Sepharose 6 Fast Flow medium (GE #17-5318-03) pre-equilibrated in 2xPBS. The solution was incubated for 1hr at RT with a magnetic stirrer. The nickel beads were washed with 20 volumes of 8M Urea in 2xPBS pH7.4, followed by 20 volumes of 2xPBS. Proteins were eluted with 1M imidazole in 2xPBS. The His6 thioredoxin tag removal was performed as described in 2.1.3.

2.1.5 Characterisation of ProUroguanylin and ProGuanylin

SDS-PAGE and mass spectrometry were used to determine the size and purity of proteins. 1µg and 5µg of proforms were analysed on a 12% SDS-PAGE gel, run at 200V for 40 minutes. The gel was stained with Instant Blue (Expedeon #ISB1L) for 1hr before destaining with deionized water for 30 minutes. MALDI-TOF mass spectrometry in the positive ion mode was performed on a Shimatzu Biotech AXIMA Assurance instrument using Shimadzu MALDI-MS software version 2.8.4, Shimadzu chips and EAM-1 matrices (Bio-Rad). Samples for MALDI-TOF MS analyses were prepared by diluting protein samples into a saturated EAM-1 matrix solution consisting of acetonitrile, water, trifluoroacetic acid (ratio 50:50:0.5). These samples were applied to the chip surface.

An ELISA was also performed to confirm the protein identities. 96-well microtiter plates (Nunc) were coated with 5µg/mL of the proforms and incubated ON at 4˚C. The plates were blocked using 3% Marvel/PBS for 1hr at RT. Polyclonal antibodies against the proforms were diluted at a starting concentration of 5µg/mL for ProUroguanylin (Ab171982) and 1 in 10 for ProGuanylin (Ab14427-50) (initial concentration unknown). Serial dilutions (1:4) was performed over 8 points on the assay plate followed by incubation at RT for 1hr. After washing 3 times with PBS-Tween (2%), 50µL of a 1:5000 dilution of horseradish peroxidase (HRP) conjugated goat anti-rabbit IgG (Sigma #A2074) was added for ProGuanylin, and goat anti-mouse IgG (Jackson Immuno Research #115-035-164) for ProUroguanylin. Following incubation at RT for 1hr, plates were washed 3 times with PBS-Tween (2%). 50µL of Tetramethylbenzidine (TMB) substrate (Sigma #T0440) was added to each well. The reaction was terminated after 10

minutes by adding 50µL of 0.5M sulphuric acid. Absorbance at 450nm was measured using an Envision plate reader (PerkinElmer).

2.1.6 Preparation of proforms for immunisation and antibody screening

The limit of endotoxin lipopolysaccharides (LPS) allowed in an immunising antigen is 80EU/mg. Above this limit, the purified protein was subjected to endotoxin removal using Polymyxin B resin. This resin has a specific interaction with endotoxin (Vesentini *et al.*, 2010). The resin was packed onto a column and pre-equilibrated with 30 column volumes of PBS before incubation with the purified ProGuanylin or ProUroguanylin. Subsequently the proteins were eluted with endotoxin-free 1xPBS by gravity flow.

To perform the primary screen of the hybridoma clones and IgG characterisation, biotinylated proforms were necessary. 2mg of each proform was enzymatically biotinylated using the BirA enzyme (Avidity LLC #BirA500) according to manufacturer's instructions. The efficiency of biotinylation was controlled by MALDI TOF mass spectrometry according to the protocol described 2.1.5.

2.2 Hybridoma campaign

2.2.1 Immunisation

Female CD1 mice aged 6-8 weeks were injected subcutaneously with 100µg of one of the following molecule: recombinant ProGuanylin, recombinant ProUroguanylin, Acetyl-Guanylin (human)-AEEAc-Lys(succinyl-KLH) amide (KLH-Guanylin) and Acetyl-Uroguanylin (human)-AEEAc-Lys(succinyl-KLH) amide (KLH-Uroguanylin) (Bachem #4092212 and #4092213, for KLH-Guanylin and KLH-Uroguanylin, respectively) in Freund's complete adjuvant (Sigma #F5881). Three subsequent boosts of 100µg each were administered through subcutaneous injection on day 7, 14 and 22 after the first immunisation in Freund's incomplete adjuvant (Sigma #F5506). Four days after the last injection, mice were sacrificed, and lymph nodes and spleen harvested. All animal research has been regulated under the Animals (Scientific Procedures) Act 1986 Amendment Regulations 2012, following ethical review by the Babraham Institute Animal Welfare and Ethical Review Body (AWERB) under the approved project license number 70/8084.

2.2.2 Serum titre determination

Peripheral blood was collected 6 days before immunisation, 14 and 21 days post-immunisation and serum recovered by centrifugation using serum separator tubes (Microvette #20.1280). ELISA was performed to assess the levels of immune response to the antigens. Antigens, either biotinylated-Guanylin (Bachem #4092214) or biotinylated-Uroguanylin (Bachem #4092215) were coated on plates at 1µg/mL at 4˚C ON. The plates were blocked using 3% Marvel/PBS at RT for 1hr. Serum samples were diluted in 3% Marvel/PBS and serial dilutions (1/200 over 5 points) applied onto assay plates in duplicate and incubated for 1hr at RT. After washing 3 times with PBS-Tween (2%), 50µL of a 1:5000 dilution of HRP conjugated goat anti-mouse IgG (Jackson Immuno Research #115-035-164) was added. Following incubation at RT for 1hr, plates were washed 3 times with PBS-Tween (2%). 50µL of TMB substrate (Sigma #T0440) was added to each well. The reaction was terminated after 10 minutes by adding 50µL of 0.5M sulphuric acid. Absorbance at 450nm was measured using an Envision plate reader (PerkinElmer).

2.2.3 Hybridoma generation

Cells were isolated from lymph nodes and/or spleens by mechanical disruption using the Gentle MACS dissociator (Miltenyi). Cells were fused with SP2/0 myeloma cells (ATCC) using a BTX electrofuser (ECM2001) before resuspending them in semi-solid media (CloneMatrix concentrate, Genetix), DMEM (Gibco), 20% FCS (SAFC), 2% GlutaMAX (Gibco), 1% sodium pyruvate (Sigma), 100U/mL penicillin, 100µg/mL streptomycin (Gibco), 10% hybridoma cloning factor (Roche), 2% oxaloacetate/pyruvate/insulin (Sigma), 2% hypoxanthine/azaserine (Sigma), containing FITC conjugated anti-mouse IgG monoclonal antibody (Jackson ImmunoResearch # 115-095-1649). Media and cells were plated into omni trays (Nunc) and cells were incubated at 37˚C, 7.5% CO_2-enriched atmosphere. After 16 days of incubation, secreting IgG colonies were picked by ClonePix robot (Molecular Devices) and inoculated onto 96 well plates (Costar) containing selection media (DMEM, 20% FCS, 2% glutaMAX, 100U/mL penicillin, 100µg/mL streptomycin, 10% hybridoma cloning factor, 2% oxaloacetate/pyruvate/insulin, 2% hypoxanthine and thymidine (Sigma)). After growing the hybridomas for a week, the supernatants were harvested using the MiniTrak robot (PerkinElmer).

2.2.4 Clones selection by HTRF assay

A Homogeneous Time Resolved Fluorescence (HTRF) biochemical assay was developed to measure the binding of IgGs (in hybridoma conditioned supernatants) to the four biotinylated targets using Europium cryptate conjugated streptavidin (Cisbio #610SAKLB) as the donor and AlexaFluor 647 conjugated goat anti-mouse Fc IgG (Jackson #115-605-164) as the acceptor. Test samples were incubated for 15hrs at RT with 2.5nM biotinylated-antigens premixed with 1nM Streptavidin-cryptate, and 7.5nM AlexaFluor 647 conjugated goat anti-mouse Fc IgG. The fluorescence was measured on an EnVision plate reader using a 320nm excitation filter and 665nm and 590nm emission filters. The raw data was initially analysed using the equation 665 nm / 590 nm x 10,000 and was then expressed as % ΔF using the equation (sample ratio - negative control ratio / negative control ratio x 100). Samples with a binding signal greater than 100% ΔF were taken forward for further analysis.

2.2.5 cDNA preparation and variable chain sequencing

The method used to sequence the hybridoma clones is described in Percival-Alwyn *et al.*, 2015. Briefly, heavy and light chain variable regions mRNA were isolated using Oligo $(dT)_{25}$ magnetic beads (Thermo Fisher Scientific #61002). SP2/0 MOPC abVκ mRNA was removed by targeted digestion with RNaseH (NEB # M0297L) at 37˚C for 1hr. Superscript III reverse transcriptase (Invitrogen SuperScript III kit #18080085) was used to transcribe the purified mRNA into cDNA at 44°C for 1hr. Poly(G) was added to the cDNA by incubation at 37°C for 1hr with dGTP (GE #28-4065-23) and terminal transferase (NEB #M0315L). Variable light and heavy chain DNA were amplified with oligo$(dC)_{25}$ and specific primers to the CH_1 or kappa constant domain (IgG77R and KconsR respectively) using Taq polymerase (Thermo #SP-0956/b) (details of the primers used in appendix 2). The chain termination method was used to sequence the PCR product.

2.2.6 IgG purification

From the primary screen results, hybridomas were selected and grown for 10 days at 37°C under a 7.5% CO_2-enriched atmosphere in HL-1 serum free media (Lonza #77201) supplemented with additives: 2% HybER™-Zero (Statens Serum Institute #71800) and 2% GlutaMAX (Gibco #35050-038). ProPlus resin bed Phytips (Phynexus #PTP-92-20-07) were used to purify the IgGs from the supernatants. Phytips were pre-equilibrated in PBS before capturing the IgG from the supernatant. The Phytips was washed 4 times after sample capture

with PBS before eluting the IgGs with an acidic elution buffer (100mM HEPES, 140mM NaCl, pH3). The eluate was neutralized by 200mM HEPES pH8. IgG concentrations were determined by measuring the OD280 using the EnVision plate reader.

2.3 Phage display selection

2.3.1 Soluble selections on naïve libraries

Phage libraries and magnetic streptavidin beads were blocked in 500µL 3% Marvel/PBS on a rotating disk at RT for 1hr, 20rpm. The phage libraries were subsequently deselected against the streptavidin beads on a rotary mixer at RT for 1hr, 20rpm. The phage libraries were captured with the relevant biotinylated antigen (biotinylated-Guanylin or biotinylated-Uroguanylin) in a 500µL final volume on a rotary mixer at RT for 1hr, 20rpm. A de-selection step was performed by adding 1µM free uroguanylin or guanylin to the relevant selection to prevent cross reactivity. Each selection was mixed with 50µL of blocked beads and equilibrated for 5 minutes before being transferred to a Kingfisher mL tube rack. Beads were washed 4 times from unbound phage in 0.1% PBS-Tween using the Kingfisher mL automated wash programme and released into 200µL of 10µg/mL trypsin in 0.1M sodium phosphate buffer. The bound phage was eluted by trypsin treatment on a rotary mixer at 37 °C for 30 minutes, 20rpm. Eluted phage was used to infect 1-5mL of TG1 cells, in the logarithmic phase of growth and incubated at 37°C for 1hr, 150rpm. Selection outputs were plated onto 2xTYAG bioassay plates and incubated overnight at 30°C. Single colonies representing each bacteriophage were picked into 96-well plates and incubated at 30°C ON, 25rpm. The rest of the cells were harvested in 2xTY with 17% glycerol, and stored at -80°C.

2.3.2 Selection rescue

For each selection, the bacterial scrape was used to inoculate 25mL of 2xTYAG in a 250mL flask to a starting OD600 of 0.1. Cells were grown to logarithmic phase at 280rpm at 37°C, before being infected with M13KO7trp helper phage at a multiplicity of infection (MOI) of 10. Cells were incubated at 37°C for 1hr, 150rpm. Cells were centrifuged at 3200rpm for 10 minutes and resuspended in 400mL of 2xTYAK media for growth at 25°C ON, 280rpm.

After overnight incubation, 1mL of culture was spun at 13000rpm for 5 minutes and put on ice until used for further selection. Input and output titres of phage were calculated for each

round of selection. To assess the stringency of the selections, a negative selection with no antigen was also performed at each round.

2.3.3 Phage ELISA

The single colonies picked in 96-well plates during the soluble selections were designated as "masterplates". They were duplicated using a sterilised 96-pronged replicator into deep 96-well daughter plates containing 500µL 2xTYAG. The colonies were grown at 37°C for 5hrs, 280rpm before being infected with K07 M13 helper phage to a MOI of 10. The plates were incubated at 37°C for 1hr, 150rpm. The media was changed to 2xTYAK and cells were grown at 25°C ON, 280rpm.

Nunc Maxisorp plates were coated with 50µL biotinylated-Guanylin or biotinylated-Uroguanylin at 2.5µg/mL overnight at 4°C. Plates were rinsed 3 x in PBS to remove unbound antigen, the plates and phage were then blocked in 3% Marvel-PBS at RT for 1hr. The plates were washed 3 times in PBS and 50µL of phage were added per well and incubated at RT for 1hr before being washed with 3x with PBS/0.1% Tween. 50µL of anti-M13-HRP (Amersham #27-9421-01) diluted 1/5000 in 3% Marvel-PBS at was added to each well and incubated at RT for 1hr. Plates were further washed 3x with PBS-Tween 0.1%. 50µL of TMB substrate (Sigma #T0440) was added to each well. The reaction was terminated after 10 minutes by adding 50µL of 0.5M sulphuric acid. Absorbance at 450nm was measured using an Envision plate reader (PerkinElmer).

2.3.4 Sequencing of clones and further selection process

88 positive clones of each selection that were not cross-reactive according to the Phage ELISA were sequenced and ranked. Clones were streaked out into single colonies on 2xTYAG plates and incubated at 30°C overnight. The scFv part of the DNA was amplified by PCR using specific primers pair (fdtetseq and pUC19reverse) before being sequenced using PCR L-link and mycseq10 primers (detailed in appendix 2).

Crude or purified monomeric preparations of scFvs were used in subsequent ELISA and competition ELISA to control the binding to the biotinylated and non-biotinylated version of the guanylin peptides. The scFv expression was induced by addition of 1mM IPTG to 2xTY medium at 30°C for 3hrs and the His-tagged scFv was purified from the extract using a nickel agarose column (Qiagen #30250). Monomeric scFv samples were purified using Superdex 75

10/300 GL (GE Healthcare #17517401) chromatography with an AKTA protein purifier and UNICORN software.

2.4 Phage display library generation

2.4.1 Preparation of a stop template DNA of the parents

Sequence diversification is introduced into the best antibodies by a targeted mutagenesis on the complementarity determining regions (CDR). As no mutagenesis reaction is 100% efficient, the sequence of the parent antibody will be expressed and displayed on phage alongside the mutant variants. Although their fraction in a mutant library might be as low as a few percent, parent clone molecules will easily outnumber any given variant. To overcome this problem for targeted libraries, stop codons are first introduced into the parent clone. The codons are placed in the area to be randomised, so that any mutated antibody variant will have replaced the stop codons by codons for amino acid residues and any non-mutated parent sequences will have retained the stop codons. When such a library is expressed the non-mutated parent sequences will be truncated and not be displayed and selected for.

Stop template primers were designed for the CDRs heavy chain CDR 3 (HCDR3) and light chain CDR 3 (LCDR3) of clones AB1000093 and AB1000107 (not displayed for MedImmune confidentiality). The stop template mutations were added to the sequence using the QuikChange Site-Directed Mutagenesis kit (Stratagene #200524) according to manufacturer's instructions. 10µL of the mutated and restricted DNA from the mutagenesis reaction was transformed into 100µL chemically competent CJ236 cells. After incubating DNA with cells for 5 minutes on ice, the mix was transformed on pre-warmed 2xTYAGC plates and incubated at 37°C ON. A single clone was restreaked on a plate and incubated at 37°C to ensure clonal purity. A new single colony was used to inoculate 3mL of 2xTYAGC media and the DNA was purified using a Miniprep kit (Qiagen #27104) according to manufacturer's instructions.

2.4.2 Production of uracil containing single stranded DNA (dU-ssDNA)

CJ236 colonies containing the stop template were grown in 5mL 2xTYAGC at 37°C to the logarithmic phase. Cells were infected with wild-type M13KO7 helper phage to a MOI of 10 and incubated at 37°C for 10 minutes. 1mL of media was used to inoculate 30mL of 2xTYAKU media (100 µg/mL ampicillin, 50µg/mL kanamycin, 0.25 µg/mL uridine) and cells were cultured at 37°C ON, 300rpm. Cells were centrifuged at 26,890g at 2°C for 10 minutes. 1/5 volume of

20% (v/v) PEG8000/2.5M NaCl were added to supernatants and incubated for 10 minutes at RT. Phage samples were pelleted at 11,950g at 2°C for 2 mins, and the phage pellet was resuspended in 0.5mL PBS. Debris were pelleted with a final centrifugation at 13,000rpm for 5 minutes. The dU-ssDNA template was purified using QIAprep Spin M13 kit (Qiagen # 27704) and eluted in 100µL. The DNA concentration was measured by absorbance at 260nm and the quality of the ssDNA was assessed on a 1% TAE agarose gel.

2.4.3 Kunkel mutagenesis

For each library a single mutagenic primer was designed to randomise blocks of up to 6 consecutive amino acids using NNS codons within degenerate oligonucleotides. Two libraries were designed for each CDR HCDR3 and LCDR3 of the clones AB1000093 and AB1000107. 0.7µg of each mutagenic oligonucleotide was phosphorylated at 37°C for 1hr using T4 polynucleotide kinase. Each reaction was performed in 1 x TM buffer, 1mM ATP, 5mM DTT, in a final volume of 20µL. The phosphorylated oligonucleotides were annealed to 20µg of dU-ssDNA, using 1 x TM buffer, in a 250µL final volume. The reaction was incubated at 90°C for 2 minutes, 50°C for 3 minutes followed by 20°C for 5 minutes. To the template mix, 21.5µL containing 30 units T4 DNA ligase, 30 units T4 DNA polymerase, 0.33mM ATP, 0.83mM dNTPs and 5mM DTT final concentration. The mix was incubated at 20°C for 3 hours. Each reaction was affinity-purified to 50µL water using the DNA High PCR product purification kit (Roche #1732676).

2.4.4 Preparation and electroporation of electrocompetent TG1 cells with libraries

A single TG1 colony was used to inoculate 60mL of 2xTY media at 30°C ON, 300rpm. 400mL of media was inoculated to an OD600 of 0.1 and grown to the logarithmic phase at 30°C, 300rpm. Cells were incubated on ice for 30 minutes before being centrifuged at 2700g at 2°C for 15 minutes. Cells were resuspended in 300mL ice-cold Milli-Q water. The centrifugation and wash steps were repeated before resuspending the cells in 50mL Milli-Q water, cells were centrifuged at 2210g at 4°C for 10 minutes. The centrifugation and wash steps were repeated once again before resuspending the cells in 5mL of Milli-Q water before being electroporated immediately.

35µL of mutagenesis reaction was mixed with 1.6 mL of electrocompetent TG1 cells. 4 x 400µL of cells were electroporated per library in a 0.2cm cuvette using the standard electroporation settings of 2.5kV field strength, 200Ω resistance, 25µF capacitance. Immediately after

electroporation, 1mL 2xTYG was added to each cuvette and cells were transferred to a 50mL Falcon tube and incubated at 37°C for 1hr, 150 rpm. Cells were plated on a 2xTYAG bioassay plate and incubated overnight at 30°C. A dilution series of each library were plated on 2xTYAG petri dishes to determine the number of transformants. Libraries were scraped into 10mL 2xTY with 17% glycerol and libraries were stored at -80°C.

2.5 Ribosome display lead optimisation

2.5.1 Building of a ribosome library

Preparation of the Parental scFv DNA Construct for Ribosome Display

The parent clone in pCANTAB6 was streaked onto a TYAG agar plate and grown at 37˚C overnight. A single colony was used to inoculate 15mL of 2xTYAG for overnight growth at 30˚C, 300rpm. The plasmid DNA was purified using the QIAamp Mini kit (Qiagen #51304) according to manufacturer's instructions. The above plasmid DNA and pUC-RD D3 vector were digested using the NEB enzymes NcoI and NotI at 37˚C for 90 minutes and the digestion product separated on a 1% agarose/TAE electrophoresis gel. Both vector and insert were purified using the Roche DNA purification kit (#1732676) according to manufacturer's instructions. The NotI-NcoI cut pUC-RD D3 vector and the NotI-NcoI cut parent scFv were ligated using a 1:5 ratio. The ligation was performed using the T4 ligation kit (NEB #M0202S) in a 30µL ligation reaction and the reaction was incubated 1hr at room temperature. 10µL of ligation product was transformed into 100µL chemically competent TG1 cells by heat-shock. The cells were incubated on ice for 30 minutes and heat-shocked at 42˚C for 45 seconds and placed back on ice for 2 minutes. 900µL 2xTYG was added to the reaction and shook at 37˚C for 1hr, 120rpm. The transformed cells were plated onto 2xTYAG agar plate.

Construction of Error–Prone Mutagenesis Libraries

The error-prone PCR is performed using the Diversify PCR Random Mutagenesis kit (Clontech #630703). The error rate can be adjusted by modifying manganese sulphate and dGTP concentrations. The conditions were chosen for the highest error rate (8.1 nucleotide changes per 1000bp) according to manufacturer's instructions (8mM $MnSO_4$, 2mM dGTP) with 10ng of scFv in pUC-RD D3 in a 50µL final volume. The scFv-coding region of antibodies AB1000107 and AB1000001 were amplified by PCR using primers MycRestore and germline VH gene specific primer SDCAT-CG (refer to appendix2). Two rounds of error-prone PCR using the following program: the thermal cycle was programmed for 3 minutes at 94°C as initial

denaturation, followed by 25 cycles of 30 seconds at 94°C for denaturation, 120 seconds at 68°C for annealing and extension. In between the two rounds of error-prone mutagenesis, the PCR products were separated on a 1% agarose/TAE gel and purified using the Roche DNA purification kit (#1732676) following the manufacturer's instructions.

A short non-structured region of the gene III sequence of filamentous phage was amplified by PCR for use as a 'tether' to allow protein display outside of the ribosomal tunnel. 10ng of pCANTAB6 was used as template to amplify the Gene III tether with the primers geneIIIfor2 and MycgeneIIIshortadapt using the PCR Master mix from Abgene (#SP-0488). The thermal cycle was programmed for 3 minutes at 94°C as initial denaturation, followed by 25 cycles of 30 seconds at 94°C for denaturation, 30 seconds at 55°C for annealing and 105 seconds at 72°C for extension and final extension at 72°C for 5 minutes. The PCR product was separated on 1.5% agarose/TAE gel and purified using the Roche DNA purification kit following the manufacturer's instructions.

A recombinatorial PCR to add gene III tether to the scFv coding sequence was performed using the PCR Master mix (Abgene #SP-0488) with 200ng of gel-purified SDCAT/mycrestore product and 200ng of gel-purified gene III tether. The first 5 cycles were performed without the use of primers and the thermal cycler was programmed for 3 minutes at 94°C as initial denaturation, followed by 5 cycles of 30 seconds at 94°C for denaturation, 30 seconds at 50°C for annealing and 105 seconds at 72°C for extension. At the beginning of the 5th annealing step, the PCR was paused and SDCAT family specific and T7te primers (see appendix 2) were added to the reaction mix and the programme resumed. The thermal cycler was programmed for 3 cycles of 30 seconds at 94°C, 30 seconds at 30°C and 105 seconds at 72°C followed by 15 cycles of 30 seconds at 94°C, 30 seconds at 50°C and 105 seconds at 72°C and a final extension at 72°C for 5 minutes. The PCR products were separated on a 1% agarose/TAE gel and the amplified fragment was gel purified using the Roche DNA purification kit following the manufacturer's instructions. The final ribosome display construct was reamplified to bulk up the converted scFv DNA using the PCR Master mix from Abgene (#SP-0488) with a new set of primers T7B and T6te (refer to appendix 2). The thermal cycle was programmed for 3 minutes at 94°C as initial denaturation, followed by 25 cycles of 30 seconds at 94°C for denaturation, 30 seconds at 55°C for annealing and 105 seconds at 72°C for extension and final extension at 72°C for 5 minutes. 5µL of PCR sample was checked on a 1% agarose/TAE gel for size and purity.

In vitro Transcription and mRNA Translation

The PCR sample was transcribed using the Ribomax Large Scale RNA production system (Promega #P1300) in a 50µL final volume. The transcription reaction was incubated at 37˚C for 2hrs. The DNA was removed using RNA qualified (RQ1) RNAse-free DNAse and the mRNA was purified using ProbeQuant G50 micro column (Amersham Biosciences #27-5335-01) according to manufacturer's instructions.

30µg of mRNA was cell-free translated using an in-house S30 *E. coli* extract. The translation mastermix was made of 38.5µL of 2M potassium glutamate, 26.6µL of 0.1mM magnesium acetate, 7µL of 5mg/mL Protein Disulphide Isomerase (PDI, Sigma #P3818), 77µL of Premix X (250mM Tris-acetate pH 7.5, 1.75mM of each amino acid, 10mM ATP, 2.5mM GTP, 5mM cAMP, 150mM acetylphosphate, 2.5mg/mL *E. coli* tRNA, 0.1mg/mL folinic acid, 7.5% PEG 8000) and 140µL of S30 *E.coli* extract. 300µL of the mastermix was added to 30µL mRNA on ice and mixed gently by pipetting up and down. The tube was transferred immediately to a 37˚C heat block for 9 minutes. The 330µL translation reaction was transferred into a pre-chilled microfuge tube containing 1250µL chilled heparin-block buffer (0.05M Tris-acetate pH 7.5, 0.15M NaCl, 0.05M magnesium acetate, 0.1% Tween-20, 2.5mg/mL heparin from Sigma #H9399) on ice to stabilise scFv-ribosome-mRNA complexes.

2.5.2 Selection and Capture of Specifically Bound scFv-Ribosome-mRNA Complexes

Ribosome display selections were performed as described in Groves and Nickson, 2012. Briefly, magnetic streptavidin beads were blocked in 1% de-biotinylated Marvel/PBS (final concentration) on a rotating disk at RT for 1hr, 20rpm before. 500µL of stabilised scFv-ribosome-mRNA complexes was mixed with 1% de-biotinylated Marvel/PBS and 50µL of the biotinylated antigen was added per library for overnight incubation at 4°C. Streptavidin magnetic beads were washed four times in HB buffer before capturing the antigen-bound complexes for 5 minutes at 4°C. Beads were washed 5 times with 800µL HB buffer to remove non-specifically bound complexes using the Kingfisher mL automated wash programme and released into 200µL water containing 10mg/mL *S. cerevisiae* RNA. Amplification of mRNA was performed by RT-PCR using Superscript II Reverse Transcriptase (Invitrogen, 18064-014) with T8te primer and a SDCAT VH family specific primer (SDCAT-CG for AB1000107 selections and SDCAT-CC for AB1000001 selections) (see appendix 2) in 20µL final volume with 12.25µL coming from the ribosome-bead-mRNA complexes. The mix was incubated at 42°C for 30

minutes before being amplified by PCR using 2x PCR master mix (Thermo CM-250 custom mix) with SDCAT-specific and T8te primers. The PCR was performed as follows: 94˚C for 3 minutes followed by 30 cycles at 94˚C for 30 seconds, 55˚C for 30 seconds and 72˚C for 105 seconds, and a last step at 72˚C for 5 minutes.

2.5.3 Further processing of the selection Output mRNA

To process outputs for a further round of selection, another round of PCR had to be performed on 50-200ng gel purified PCR using T7B and T6te primers. This PCR was performed using Vent DNA polymerase in a 50µL final volume with 25 cycles of 94˚C for 30 seconds, 62˚C for 30 seconds and 72˚C for 105 seconds. PCR was completed with a last step at 72˚C for 5 minutes.

To screen for the activity of the different PCR variants, 50ng of each PCR products were enzyme restricted with NcoI and NotI (NEB) and ligated into pCantab6 using T4 DNA ligase (Promega) according to manufacturer's instructions.

2.6 Characterisation of the antibodies

2.6.1 IgG conversion

Variable genes from antibodies of interest were amplified using PCR and cloned into pEU expression vectors. The heavy chain variable genes were digested with BssHII and BsmBI, then inserted into pEU23.4 mu IgG1. Light chain variable genes were digested with ApaLI and PacI, then inserted into pEU22.3 murine Kappa vector or pEU21.3 murine lambda vector. DNA quick ligase (NEB) was used for ligation reactions, and Z-competent DH5α cells were transformed. Successful cloning was confirmed using PCR with primers targeting the pEU backbone, products were loaded in a 1% agarose gel, which was ran at 130V for 20 minutes to check for the presence of an insert and confirmed using DNA sequencing. The DNA was later purified for positive clones using the QIAgen Midi Prep Plus Kit.

For antibody expression, DNA constructs of heavy and light chain variable genes were transfected into G22 cells using polyethylenimine (PEI) Max (Polysciences Inc). The transfected cells were incubated for 1 week at 34°C with shaking at 140rpm, 5% CO_2 and 70% humidity. Supernatant was harvested by centrifugation at 500g for 30 minutes at 4°C and filtered using a 0.22 µm membrane. MabSelect Sure resin (GE Healthcare Bio-sciences, Marlborough, USA) was used for purification, and antibody was eluted with 0.1M sodium citrate (pH3) in the high throughput method. Desalting was then performed using PD10 columns (GE Healthcare Bio-

sciences). A quality control check of the antibody was performed by SDS-PAGE. The gels were stained with Instant*Blue*™ to visualise the protein bands.

2.6.2 Specificity ELISA on the clones

96-well microtiter plates (Nunc) or streptavidin coated plates (Costar) were coated with 5µg/mL of proforms or biotinylated-Guanylin (Bachem #4092214) or biotinylated-Uroguanylin (Bachem #4092215) and incubated ON at 4˚C. The plates were blocked using 3% Marvel/PBS at RT for 1hr. scFvs or antibodies were tested as a single point or serially diluted into the assay plates in duplicate over 8 points and incubated for 1hr at RT. After washing 3 times with PBS-Tween (2%), 50µL of a 1:5000 dilution of HRP conjugated goat anti-mouse IgG (Jackson ImmunoResearch #115-035-164) was added. Following incubation at RT for 1hr, plates were washed 3 times with PBS-Tween (2%). 50µL of TMB substrate (Sigma #T0440) was added to each well. The reaction was terminated after 10 minutes by adding 50µL of 0.5M sulphuric acid. Absorbance at 450nm was measured using an Envision plate reader (PerkinElmer).

2.6.3 Competition ELISA

Competition ELISA was performed to confirm the specificity of scFv or IgG binding to the peptides as opposed to the tags (KLH and biotin). In other words, binding specificity was assessed based on the ability of free peptides in the solution to compete with immobilized tagged-peptides (which was used in the hybridoma screening). Plates were coated with biotinylated-peptides or biotinylated-proforms at 5µg/mL and incubated at 4˚C ON. Plates were blocked using 3% Marvel/PBS for 1hr at RT. The concentration of IgG or scFv that gave 80% of the maximum absorbance in a standard ELISA was incubated for 1hr at RT with a serial dilution of free guanylin (Bachem #H.2996.1000) or free uroguanylin (Bachem #H.2166.1000), from 0.21nM-3.3µM. After washing 3 times with PBS-Tween (2%), 50µL of a 1:5000 dilution of goat anti-mouse IgG (Sigma #Ab17198) was added. Following incubation at RT for 1hr, plates were washed 3 times with PBS-Tween (2%). 50µL of TMB substrate (Sigma #T0440) was added to each well. The reaction was terminated after 10 minutes by adding 50µL of 0.5M sulphuric acid. Absorbance at 450nm was measured using an Envision plate reader (PerkinElmer).

2.6.4 Epitope binning to identify antibody pairs

Antibodies were covalently bound to the surface of ester coupled pre-activated SensEye G Easy2Spot (SSens #1-09-04-006) using a Continuous Flow Microspotter (CFM) (Wasatch

Microfluidics). CFM uses a network of microchannels to cycle ligand solutions over a surface plasmon resonance (SPR) surface. A flow prints microarray spots by directing 70µL plugs of antibodies from a 96-well microplate into a fluidic manifold. The antibody solutions are arranged into a 4×12 array of 48 micro flow cells on the surface of the SPR substrate. The CFM cycles the solutions back and forth at 60µL/min.

The antibody plate contained the 90 IgGs prepared at 5µg/mL in 10mM NaOAc pH4.5 (GE Healthcare #BR-1003-50) and they were cycled for 15 minutes. Once the printing was done on the SensEye sensor, it was loaded into the SPRi reader (MX96, IBIS Technologies). 1M ethanolamine-HCl was injected across the SensEye sensor for 15 minutes to quench the excess reactive ester before washing it with system buffer. A sensor picture was used to define the reaction spots and the interstitial reference spots.

For the affinity measurement, a standard injection cycle of analyte (proforms or active peptides) followed by a regeneration was used. Antigens were injected at a concentration of 100nM and serially diluted 1 in 2 over 8 points for 3 minutes. Subsequently buffer was injected to define the dissociation rate. The sensor was regenerated using 10mM phosphoric acid pH2 for 1 minute. The data was analysed using Scrubber2 (BioLogic Software).

For epitope binning, both antigens and antibodies were flowed over the sensor, and injected immediately after one another before continuing with regeneration. Proforms were injected at 100nM for 3 minutes, followed by the antibodies at 7.5µg/mL for a further 5 minutes and then the sensor was regenerated using 10mM phosphoric acid pH2 for 1 minute. The data was analysed using SprintX (Ibis Technology).

2.6.5 Affinity measurement using Surface Plasmon Resonance (SPR)

Binding constants of the proforms, guanylin and uroguanylin were determined using a Biacore T100 instrument. Antibodies were immobilised at 10µg/mL on a CM3 chip by amine coupling to a density of 450RU. Serial dilutions of ProGuanylin, ProUroguanylin, guanylin and uroguanylin were prepared in the running buffer (PBS pH7.4, 0.05% Tween 20). The compound solutions were injected onto the surface of the chip at a flow rate of 50µL/min, contact time was 180 seconds and dissociation time 400 seconds. Sensorgrams were analysed using the Biacore T100 evaluation software and the binding constants determined using a 1:1 binding model.

2.7 Immunoassay to measure ProGuanylin and ProUroguanylin

2.7.1 Human samples

Studies on volunteers were performed by Dr. Claire Meek, Dr. Geoffrey Roberts, Dr. Benjamin Challis, and Pr Jørgen Jensen.

The study on healthy volunteers in the fasting and postprandial state was given ethical approval by the local research ethics committee (Reference 13/EE/0195).

The study on volunteers that undertook a gastrectomy and small bowel transplant was approved by the local National Health Service Research Ethics Committee and conducted in accordance with the ethical standards of the Helsinki Declaration of 1975 (Reference 16/EE/0338).

The study on volunteers that fasted over 7 days was approved by the Ethics committee at Norwegian School of Sport Sciences (Reference 15-220817).

The study on volunteers that presented a different range of osmolality was given ethical approval by the local research ethics committee (Reference 14/EE/1247).

The study on neuroendocrine tumour volunteers was approved by the local research ethics committee (Reference 14/EE/1059)

All human organoids studies were approved by local ethical review committee (Reference 09/H0308/24).

Glucose tolerance test or Liquid meal test

Following an overnight fast, participants were given a 50g, 75g or liquid standardised meal test (SMT). The SMT consisted of a 230mL bottle of Ensure plus, a balanced nutritional supplement containing 11g fat, 13g protein and 50g carbohydrate. Participants were also given 250ml of water after the meal was consumed. Blood samples were collected immediately prior to glucose/food ingestion, and at 15, 30, 45, 60, 90, 120 minutes post-ingestion.

Plasma samples

Blood was collected into EDTA and lithium heparin tubes and samples were immediately centrifuged for 10 minutes at 3500g at 4^{o}C. Plasma aliquots were snap frozen on dry ice and stored at -80^{o}C within 30 minutes.

Serum samples

Blood samples were taken and allowed to clot for 10 minutes after phlebotomy. Samples were then centrifuged for 10 minutes at 3500g at 4°C, separated and frozen on dry ice and stored at -80°C within 30 minutes.

2.7.2 In-house developed MSD assay

Antibodies AB1000011 and AB1000025 (anti-ProUroguanylin and -ProGuanylin respectively) were diluted to 50ng/µL and 5µL, respectively, coated on an assay plate (MSD #MA6000) and incubated at RT overnight. Plates were blocked using 1% PBS/BSA for 2hrs at RT. After washing 3 times with washing buffer of PBS-Tween (0.05%), 25µL of samples were added to each well and incubated for 2hrs at RT. Following incubation, plates were washed 3 times with washing buffer and 25µL of a second Sulfo-Tag labelled anti-proforms antibodies AB1000010 and AB1000028 prepared at 1µg/mL in Diluent 41 (MSD) was added per well for 1hr at RT. Once washed with washing buffer, 150µL of Read buffer 2X was added to each well before reading the plate immediately using a MSD Workbench. A standard curve was constructed by fitting a sigmoidal function to the absorbance obtained from the known proforms concentrations using MSD discovery software. The concentration of experimental samples was assessed by interpolating them to a standard curve using MSD discovery software as well.

2.7.3 Biovendor kit

ProGuanylin and ProUroguanylin were measured using the commercially available ELISA kits (Biovendor) following the manufacturer's instructions. Absorbance was measured at 450nm and 630nm using a Perkin Elmer 1420 multilabel counter (Perkin Elmer). Readings at 450nm were subtracted by the readings at 630nm. A standard curve was constructed by fitting a sigmoidal function to the absorbance obtained from the known proforms concentrations included in the kits. The concentration of experimental samples was measured by interpolation from the standard curve using GraphPad Prism software version 7.

2.8 Secretion assays

2.8.1 Solutions and chemicals

Standard saline solution contained 138mM NaCl, 4.5mM KCl, 4.2mM $NaHCO_3$, 1.2mM NaH_2PO_4, 2.6mM CaCl2, 1.2mM $MgCl_2$, 1mM D-glucose, 10mM HEPES, pH 7.4, osmolality ~300 mOsm/kg.

Modified saline solutions were used for some experiments. 'Buffer138 Na^+ free' solution contained 138mM N-Methyl-D-glucamine (NMDG), 4.5mM KCl, 1.2mM KH_2PO_4, 4.2mM $KHCO_3$, 2.6mM $CaCl_2$, 1.2mM $MgCl_2$, 10mM HEPES. 'Buffer138 Cl^- free' solution contained 138mM Sodium D-gluconate, 4.5mM Potassium D-gluconate, 4.2mM $NaHCO_3$, 1.2mM NaH_2PO_4, 5.2mM Calcium D-gluconate, 2.4mM Magnesium Gluconate, 10mM HEPES.

Lysis buffer contained 50mM Tris–HCl, 150mM NaCl, 1% IGEPAL-CA-630, 0.5% deoxycholic acid and supplemented with complete EDTA-free protease inhibitor cocktail (Roche).

Unless stated, all drugs and chemicals were obtained from Sigma (Poole, UK). Forskolin, isobutyl-1-methylxanthine (IBMX), phorbol 12-myristate 13-acetate (PMA), were dissolved in DMSO. Peptone, NaCl, mannitol, taurodeoxycholate (TDCA), bombesin acetate and carbachol were dissolved in water. Where DMSO is used as a solvent, the working concentration never exceeded 0.2 % (v/v).

2.8.2 Cell culture

Caco2-TC7 cell line

The Caco-2 cell line is a human intestinal cell line established from colonic adenocarcinoma and mature into enterocytes upon confluence. The TC7 cell line is a subclone of the Caco-2 cell line which was generated from Caco-2 at late passage (Caro *et al.*, 1995). TC7 cells were cultured in Dulbecco's modified Eagle's medium (DMEM, 4.5g/L glucose) supplemented with 10% Foetal Bovine Serum (FBS), 100units/mL penicillin, 100µg/mL streptomycin and 2mM L-glutamine. TC7 cells were incubated at 37°C, 5% CO_2 in 75 cm^2 flasks. The culture media was changed every 3 days. Every 5 days cells were trypsinised with 1X trypsin-EDTA, diluted and reseeded.

Organoids set up, maintenance and differentiation

Human tissues were obtained from the Human Research Tissue Bank at Addenbrooke's Hospital (Cambridge, UK) and processed within the same day.

Duodenal and colonic intestinal organoids were established from one human donor each by Dr Goldspink (Goldspink *et al.*, 2017) using a modified protocol from Sato *et al.*, 2009. Briefly, tissues were washed in ice cold PBS and chopped into 2-3mm pieces. Tissue pieces were incubated for 5 minutes in ice cold 30mM EDTA in PBS and transferred to cold PBS before shaking vigorously for 20s. The incubation in EDTA and shaking steps (in new cold PBS

fractions) were repeated 4 times. Fractions presenting crypts were filtered through a 70µm cell strainer (Thermo Fisher) to remove villi. The crypts were centrifuged at 200g for 3 minutes, resuspended in Cultrex PathClear Reduced Growth Factor BME (Bio-Techne) and 20µL drops were polymerised at 37°C for 30 minutes in 48-well plates (Nunc). 250µL organoid medium (100µg/mL mouse Noggin (R&D), 50µg/mL human EGF (Invitrogen), 2mM L-Glutamine (Invitrogen), 100units/mL Pen/100µg/mL Strep (Invitrogen), 1x B27 (Invitrogen), 1x N2 (invitrogen), 1mM NAC (Sigma), 10nM Gastrin (Sigma), 10mM nicotinamide, 500nM A83-01 (Tocris), 10nM SB202190 (Sigma), 10µM ROCK inhibitor y27632 (Tocris), Wnt-3a and R-Spondin-1 (RSPO1) conditioned medium were used and generated following the manufacturer's instructions (ATCC and Trevigen, respectively) and adapted according to Fujii *et al.*, 2015.

To maintain the organoid cell line, medium was changed every 3 days, with organoids passaged every 10 days. For the passage of the organoids cell lines, domes were harvested in 1X TrypLE (Life technologies) and trypsinised at 37°C for 10-15 minutes, cells were centrifuged at 300g for 3min, resuspended in BME and 20µl drops were polymerised at 37°C for 30min. 250µL organoid medium was added per well.

Organoids were maintained in an undifferentiated state by the high concentration of Wnt-3a conditioned medium. To differentiate the organoids, wells were rinsed 3 times with Advanced DMEM/F12 medium over the course of an hour and 250µL of differentiation medium was added (15% RSPO1 conditioned medium, 100µg/mL human Noggin (R&D), 50µg/mL human EGF (Invitrogen), 2mM L-Glutamine (Invitrogen), 100units/mL Pen, 100µg/mL Strep (Invitrogen), 1x B27 (Invitrogen), 1x N2 (invitrogen), 1mM NAC (Sigma), 10nM Gastrin (Sigma) in Advanced DMEM/F12 medium) per well. Medium was changed every day for 7-10 days before experiments.

Air Liquid interface (ALI) monolayer cultures

ALI cultures were set up in 24 well plates (Costar) with 0.4µm pore cell inserts (BD Falcon) with a transparent PET membrane ideal for observing cell cultures as adapted from Wang *et al.*, 2015. TrypLE dissociated organoids (Cf. section on organoids maintenance) were seeded onto BME-coated transwells on the apical surface at 2 x 10^4 cells in WENR media (media on both apical and basolateral side). This media was replaced after 24hrs. Differentiation was induced at day 3 with differentiation media (See above Organoids differentiation) changed every other

day. Once cells had formed a confluent monolayer, air liquid interface was initiated with the removal of the media from the apical side. The cultures were grown for 2 weeks with periodical removal of mucus produced on the apical side and media on the basolateral side was changed every other day.

2.8.3 ProGuanylin and ProUroguanylin secretions

For ProGuanylin and ProUroguanylin secretion experiments, TC7 were seeded for 9 days on a 24-well plate or human organoids were seeded into BME domes in 48-well plates and differentiated for 8-9 days as previously described. The wells were washed 3 times in warm basal medium containing 1mM glucose and 0.1% BSA. Test agents were dissolved in the same basal medium and 250µL applied for TC7 secretions, or 150µL applied for organoid secretions. For organoid secretions, treatments were added to the organoids domes and incubated at 37°C for 4hrs, 8hrs, or 24hrs. Supernatants were removed from the organoids and spun at 350g at 4°C for 10 minutes, transferred to a fresh Lo-bind tube (Eppendorf) and snap frozen on dry ice.

For experiments that required cell lysates to measure total proforms or total protein levels, the cells were lysed in 150µL of lysis buffer on ice for 30 minutes. Lysates were collected and centrifuged at 10,000g at 4°C for 10 minutes and the supernatants was snap frozen until measurement.

To isolate RNA, the cells were lysed with TRI-Reagent (Sigma), collected and snap frozen until RNA extraction (see section 2.10.1).

Proforms were measured using the MSD assay (see section 2.7.2). Proforms secretions were calculated first as the amount produced in pg/mL and secondly as fold change produced in comparison to wells treated with the basal condition.

2.8.4 BCA assay to measure total protein levels

BCA assay were performed on cell lysis (Thermo Fisher) according to manufacturer's instructions. Briefly, 25µL of each standard or unknown sample were pipetted into a 96 microplate (Costar). 200µL of the WR mix (WR ratio = 1:8) was added to each well and mixed thoroughly. The plate was incubated at 37°C for 30 minutes. The absorbance was measured at 562nm on a plate reader (Tecan M1000).

2.9 Ussing Chamber

Human tissue (ascending colon) was obtained through Addenbrooke's Hospital Tissue Bank from patients undergoing partial colectomy. After histological verification, the piece of intestine was transported in ice-cold L-15 medium to level 2 biosafety cabinet. It was washed with Ringer solution containing 120mM NaCl, 3mM KCl, 0.5mM $MgCl_2$, 1.2mM $CaCl_2$, and 23mM $NaHCO_3$, with 10mM glucose. Serosa and most of the muscular layer were stripped away with fine forceps. The segment was mounted in an Ussing chamber (EM-LVSYS-4 system with P2400 chambers and P2405 slider; Physiologic Instruments). The active epithelial surface area of each segment was 0.25cm^2. Both parts of the Ussing chambers were filled with Ringer solution, maintained at 37°C, and continuously bubbled with 5% CO_2/95% O_2 (vol/vol). The transepithelial potential difference was continuously monitored under open circuit conditions, using a DVC 1000 amplifier (WPI) and recorded through Ag-AgCl electrodes and 150mM NaCl agarose bridges. Recordings were collected and stored using a DVC 100 amplifier (WPI) connected to a Digidata 1440A A/D converter and AxoScope 10.4 acquisition software (Molecular Devices). First, transepithelial resistance and potential difference were allowed to stabilise for 20 to 30 minutes. During this period, transepithelial resistance was assessed by measuring voltage changes in response to 45µA pulses lasting 2.5 seconds, applied every 100 seconds. After stabilization of the electrical parameters, solutions from both sides were removed. Both sides of the chamber were refilled with 1.2mL of fresh Ringer solution containing 10mM glucose, 0.1% fatty acid–free BSA, 10µM amastatin and 500 kIU/mL aprotinin. To prevent extensive foam formation, Infacol (Forest Laboratories) was added to the both compartments (1:100000 dilution). At 15, 45 and 90 minutes after the solution exchange, samples (120µL) were taken from both compartments and assayed for ProGuanylin/ProUroguanylin content. Fresh solution was added to replenish volumes lost by sampling. At 45 minutes after the second pair of samples was taken, forskolin (10µM) and IBMX (100µM) were added bilaterally. Reported secretion values were normalised for 1cm^2 of the tissue and a 60-minute secretion period.

2.10 Measurement of transcript levels

2.10.1 mRNA extraction

Tissue or cells were homogenised in TRI-Reagent, and RNA was extracted using an adjusted manufacturer's (Sigma) protocol. Homogenised tissues/cells were transferred to new

microcentrifuge tubes and incubated at RT for 5 minutes. 50µL of chloroform was added, the mix was shaken vigorously before incubating it at RT for 15 minutes. Tubes were centrifuged at 12,000g at 4˚C for 15 minutes and the aqueous layer was carefully transferred into a clean microcentrifuge tube. 500µL of isopropanol was added to each tube; they were mixed thoroughly and incubated at RT for 10 minutes. To pellet the RNA, tubes were centrifuged at 12,000g at 4˚C for 10 minutes the supernatant removed. 1mL of 70% ethanol was used to wash the pellet and the tubes were centrifuged at 12000g at 4˚C for 15 minutes. The pellets were air-dried at RT and RNA was dissolved into 20µl of RNAse free water. The RNA was treated with DNAseI (Ambion) according to manufacturer's instructions. Following a 20 minutes incubation at 37˚C, DNAse inactivation reagent was added to each tube. After 2 minutes incubation, the samples were centrifuged at 12,000g for 2 minutes. RNA samples were transferred to new tubes and snap frozen on dry iced before being stored at -80˚C.

2.10.2 Reverse Transcription

2µg of RNA was reverse transcribed with random primers via High-Capacity cDNA Reverse Transcription Kit (Thermo Fisher) according to manufacturer's protocol. Reverse transcription was performed in a 20µL final volume with a first step at 25°C for 10 minutes, followed by 37°C for 2hrs and a final step of 85°C for 5 minutes. cDNA was stored at -80°C and used neat in subsequent PCR reactions.

2.10.3 Quantitative RT-PCR

Quantitative PCR were performed using 1µL of cDNA template, 5µL of TaqMan Fast Universal PCR Mastermix (AppliedBiosystems), 3µL of RNase-free water and 1µL of FAM-dye labelled TaqMan Gene expression assay probe (Applied Biosystems) (see appendix 3 for probes). Each reaction was incubated at 90˚C for 2 seconds followed by 40 cycles of 90˚C for 1 second followed by 60˚C for 20 seconds using ABI QuantStudio 7 qRT-PCR machine. Available sequences for the TaqMan probes are shown in appendix 3.

2.11 LDH assay

Cell culture supernatant and lysate samples were assessed using a Lactate Dehydrogenase Activity Assay Kit (Sigma–Aldrich) adapted from manufacturer's instructions. Briefly, supernatants were diluted 1 in 5 and cell lysis samples were diluted 1:11 in cold LDH assay buffer. Samples were centrifuged at 10,000g at 4˚C for 15 minutes to remove insoluble

materials. 50µL of each sample was pipetted into a 96-well flat bottom plate (Costar) as well as the NADH standards. 50µL of master reaction mix was added to each well and the plate was incubated at 37 ˚C for 30 minutes before OD was measured at 450nm and 690nm. OD690 was subtracted to OD450 as well as the background. Data was plotted as a percentage of LDH activity in the supernatant over the total LDH activity in cell lysate and supernatant.

2.12 Mass Spectrometry to analyse peptides levels

2.12.1 Preparation of samples for Mass Spectrometry

Peptides from tissue homogenates, plasma, organoid secretion, and intestinal content samples were extracted in 80% acetonitrile (ACN) in water. Samples were spun at 12,000g for 10 minutes and the supernatants were transferred to new Lo-bind tubes (Eppendorf). Samples were dried using a SPE Dry evaporator system (Biotage) and resuspended in 200µL 0.1% formic acid (FA) in water. The samples followed a solid phase extraction (SPE) step to purify the peptides. Samples were loaded on a HLB PRIME µElution plate (Waters) and washed first with 0.1% FA in water. Samples were washed by addition of 200µL of 5% methanol and 1% acetic acid in water. The samples were eluted by addition of 2 x 25µL of 60% methanol 10% acetic acid in water.

To remove disulphide bonds and obtain linear peptides, samples were reduced and alkylated. Eluted samples were dried using SPE Dry evaporator system. Peptides were reconstituted in 200µL of 10mM DTT in 50mM ammonium bicarbonate solution and incubated at 60˚C for 1hr. 40µL of 100mM iodoacetamide (Sigma) in 50mM ammonium bicarbonate solution was added to the samples and incubated in the dark at RT for 30 minutes. 25µL of 1% FA in water was added to the samples to acidify the samples.

For samples that were trypsinised, the enzyme digest was performed before the addition of 1% FA in water. This step was done by addition of 10µL of trypsin (Promega #V511C 20µg in 40µL) at 100µg/mL.

2.12.2 Nano-LC-MS

Method as described in Kay *et al.*, 2017: “Peptide extracts were analysed using a Thermo Fisher Ultimate 3000 nano-LC system coupled to a Q Exactive Plus Orbitrap mass spectrometer (ThermoScientific, San Jose, USA). The analysis was performed using nano-flow-based separation and electrospray approaches due to the low amount of material present in the

samples. The extracts were injected onto a peptide trap column (0.3 × 5mm; ThermoFisher Scientific) at a flow rate of 20µL/min and washed for 10 minutes before switching in line with a nano easy column (0.075 × 250mm; ThermoFisher Scientific) flowing at 300nL/min. Both nano and trap column temperatures were set at 45°C during the analysis. The buffers used for nano-LC separations were A: 0.1% formic acid in water (v/v) and B: 0.1% formic acid (v/v) in 80:20 ACN/water. Initial starting conditions were 2.5% B (equating to 2% ACN), and held for 5 minutes. A ramp to 50% B was performed over 145 minutes, and the column then washed with 90% B for 20 min before returning to starting conditions for 20 minutes, totalling an entire run time of 190 min. Electrospray analysis was performed using a spray voltage of 1.8 kV, the tune settings for the MS used an S-lens setting of 70 v to target peptides of higher *m/z* values. A full scan range of 400–1600 *m/z* was used at a resolution of 75,000 before the top 10 ions of each spectrum were selected for MS/MS analysis. Existing ions selected for fragmentation were added to an exclusion list for 30 s.

The acquired LC/MS files were searched using Peaks 8.0 software (Waterloo, ON, Canada) against the mouse and human Swissprot databases (downloaded on 06/May/2016). A no-digest setting was used, which enabled peptides of up to 65 amino acids in length to be matched, and precursor and product ion tolerances were set at 10 ppm and 0.05 Da, respectively. A fixed post-translational modification of carbamidomethylation was applied to cysteine residues, whilst variable modifications included methionine oxidation, N-terminal pyro-glutamate, N-terminal acetylation and C-terminal amidation. A false discovery rate value of 1% was used to filter the results, with a minimum of 1 unique peptide also required."

Raw data files were analysed using Xcalibur (v4.0) (Thermo Fisher Scientific). Peptide peak areas were obtained by integrating the area under the peak of an extracted ion chromatogram.

2.13 Transgenic mice generation

All experimental procedures were approved by local ethical review bodies and were performed in accordance with the Animal (Scientific Procedures) Act 1986, Home Office guidelines, local establishment guidelines. Experiments were performed under Fiona Gribble's project licence (70/7824). C57BL/6 mice were purchased from Charles River UK.

The 3 exons coding for *Guca2a* (Guanylin) from the start codon to the stop codon in the murine-based BAC RP23-104G3 (Source Bioscience) was initially replaced by a counter-selection cassette RpsL-neo (GeneBridges) and subsequently by the Venus (EYFP) sequence (Rekas *et al.*, 2002) using Red/ET recombination technology (Genebridges). The RpsL/Neo (FSD001/FSD002) or Venus (FSD003/FSD004) sequences were amplified by PCR with Phusion-polymerase adding *Guca2a*-gene specific 3' and 5' sequences (see appendix 2 for primers). Homologous recombination was performed by co-transformation of the PCR product and the plasmid pRedET (which provides the recombination enzymes) into DH10B *E. coli* strain containing the BAC vector. Positive recombinants were isolated using appropriate antibiotic selection and characterised by PCR. The identity and correct positioning of the introduced Venus sequence was confirmed by direct sequencing using oligonucleotides FSD045-FSD076 in appendix 2 and restriction analysis using the ZraI enzyme (NEB) for DNA fingerprinting.

The 3 exons coding for *Guca2b* (Uroguanylin) in the murine-based BAC RP23-440N21 (Source Bioscience) was replaced by the counter-selection cassette RspL/Tet fused to the Venus sequence. The Venus (FSD033/FSD034) and RpsL/Tet (FSD035/FSD036) sequences were amplified by PCR to add the homology arms to RpsL/Tet and Venus respectively. The final RpsL/Tet-Venus product was amplified by PCR using the FSD037 and FSD038 primers combination. The RpsL/Tet counter-selection cassette was later removed using an oligonucleotide (FSD039) covering the 3' promoter sequence and the 5' Venus sequence. Similarly, homologous recombination was performed by co-transformation of the PCR product and the plasmid pRedET into DH10B *E. coli* strain containing the BAC vector. The identity and correct positioning of the introduced Venus sequence was confirmed by direct sequencing using oligonucleotides FSD110-FSD127 and restriction analysis using the XhoI enzyme (NEB) for DNA fingerprinting.

The large construct Maxi-Prep (Qiagen) was used to purify the BAC DNAs for microinjection. It was diluted to 1ng/µL into the injection buffer (10mM Tris-HCl (pH 7.5), 0.1mM EDTA, 100mM NaCl, 0.03 mM spermine, and 0.07mM spermidine). The Central Biomedical Services (Cambridge University) performed the pronuclear injection of C57BL/6 mice ova which were implanted into pseudopregnant females. Integration of the transgene was screened by PCR on the pups' ear clips after extracting the DNA by proteinase K digestion using the primers GFPF1 and GFPR1. Out of two Guanylin-Venus founders, only one passed the transgene to

their offspring (mouse 26) and presented detectable fluorescence. It was backcrossed to a C57BL/6 background up to 5 generations.

2.14 Immunohistochemistry

Tissues were fixed in 4% paraformaldehyde (PFA) (Alfa Aesar) ON at RT, dehydrated in 15% for 6hrs and finishing with 30% sucrose ON at 4˚C. Tissues were embedded in OCT (VWR) prior to slicing. Tissues sections were blocked in 10% donkey serum, 0.05% Tween-20 and 1% BSA. Slides were stained with primary antisera of interest in the same blocking solution ON at RT (Appendix 4). Slides were washed in blocking solution and incubated with appropriate secondary antisera diluted 1:300 and Hoescht diluted 1:1300 for 1hr. Tissue stained with secondary antisera only served as controls. Coverslips were mounted with hydromount (Fisher Scientific). Images were taken using a Leica TCS SP8 X confocal microscope with Leica Application Suite X software.

2.15 Whole mounted tissue immunostaining

The following method was adapted from that developed by Winton and Ponder, 1990. Excised tissues were stripped of adipose tissue and muscle layers (removal of the muscle layer greatly reduces immunofluorescent background). tissues were pinned onto 3% agar filled petri dishes, cut open and washed with PBS using a plastic pipette. The colons were then fixed for 3hrs at room temperature using 4% PFA (Alfa Aesar) and subsequently washed with PBS. Residual mucus was removed from the fixed tissue by incubation with 50mL of demucifying solution for 20 minutes at RT followed by 4x PBS washes. The fixed colons were transferred to 50mL Falcon tubes containing blocking solution (PBS with 0.1% Triton-X 100 and 10% goat serum) and left ON at 4°C. The following morning tissues were incubated for 4hrs at room temperature with primary antibodies to GFP diluted in wash solution containing 1% goat serum and 0.1% Triton-X 100 in PBS. Tissues were placed in wash solution ON. Tissues were incubated with goat secondary antibody (1:300) for 3 hours at room temperature. Following further washing ON at 4°C, tissues were incubated with 1:2000 Hoescht nuclear stain (in PBS) for 30 minutes at RT followed by 1hr period of PBS washes. Finally, tissues were divided in half and mounted onto microscope slides using Hydromount (National Diagonistics). Wholemounts were imaged using the Axio Scan.Z1 system (Zeiss). Tiles of extended depth of focus (EDF) images were taken for the labelled channel using a PlanApoChromat 20x/0.8 M27 objective, a Hamamatsu Orca Flash camera and an inbuilt autofocus function. The depths used

for the EDF images were customised for the wholemount and depended on tissue thickness. Following acquisition, the tiled images were stitched together with shading correction.

2.16 Primary murine intestinal single-cell suspension for fluorescence-activated cell sorting

Guanylin-Venus mice were killed by cervical dislocation and the gut collected into ice-cold Leibovitz-15 (L-15) medium. 4 distinct parts of 3 cm corresponding to the duodenum, jejunum and ileum as well as the colon were treated separately. Each intestine part was opened longitudinally, rinsed in phosphate buffered saline. The outer muscle layer was removed. Each epithelium was digested in 10mL with 15mM EDTA (or 30mM for colon) and 1 mM DTT in Ca^{2+}-free PBS for 7 minutes at RT. Tissue pieces were transferred in 15mL Ca^{2+}-free PBS with 10µM ROCK inhibitor y27632 (Tocris) and shaken for 30 seconds. The incubation steps in EDTA solution followed by the shaking steps were repeated 5 times. The tissue pieces were transferred into a 10mL Trypsin 0.25% EDTA, 100mg/mL DNAseI and incubated at 37°C for 5 minutes. Cells were spun at 500g at 4°C for 5 minutes and resuspended into 10mL of washing solution (of Hanks' buffered salt solution (HBSS) supplemented with 10% FBS and 5µM ROCK inhibitor y27632) and filtered using both 100µm and 50µm cell filters. 150µL of the washing solution containing an anti-CD45-PE antibody (1/500) (Thermo Fisher #MA110233) and incubated on ice for 1hr. Cells were spun at 500g at 4°C for 5 minutes, resuspended in 200µL of the washing solution containing DAPI and incubate for 5 minutes. A final centrifugation was performed, and cells were resuspended in 500µL of the washing solution containing 5µM DRAQ5 (Fisher Scientific #15530617). Cells were transferred to a 5mL polypropylene 12*75mm FACs tube (Falcon #352063). Single cell suspensions were separated immediately by flow cytometry using a MoFlo Beckman Coulter Cytomation sorter (Coulter Corp., Hialeah, FL) by the Flow Cytometry Core Facility at the Cambridge Institute for Medical Research. Side scatter, forward scatter, and pulse-width gates were used to exclude debris aggregates and doublets. Dead cells were excluded using DAPI staining and live cell-shape remains were removed by DRAQ5 staining. Cells were sorted and collected into a positive (YFP+) population with high green fluorescence and non-fluorescent negative cells population for each tissue. Cells were sorted into lysis buffer for mRNA extraction

2.17 RNA sequencing

Total RNA from FACS-isolated cells was extracted using RNAeasy Micro Plus kit (Qiagen) according to the manufacturer's instructions. The Bioanalyser RNA Pico kit (Agilent) was used to assess the quality and quantity of the RNA extracted. RNA samples with RNA integrity number values between 8.6 and 10 were used. Libraries were prepared and amplified using SMARTer Pico V2 Mammalian prep kit (Takara) from 10ng of RNA. Libraries were single-end 50 base pair sequenced at CRUK Cambridge on the Illumina HiSeq 4000 platform. The average total number of reads in each sample was 32.3 million with an average of 21.4 million mapping once to the mouse genome GRCm38 using STAR (Dobin *et al.*, 2013). Read counts per gene was determined using STAR and differential gene expression was determined using DESeq2.

2.18 Statistical analysis

Statistics on samples was performed using GraphPad Prism 7.04 (GraphPad Software, La Jolla, CA, USA), with a threshold for significance of $p = 0.05$. Specific details for the statistical analysis of each experiment are described in the corresponding figure legends.

Chapter 3: Generation of monoclonal antibodies against ProGuanylin and ProUroguanylin and development of an immunoassay

3.1 Introduction

3.1.1 Lack of tools to study ProGuanylin and ProUroguanylin

Understanding the physiology and pathophysiology of the guanylin peptides in health and disease states has been limited by the lack of specific monoclonal antibodies against the active peptides and their prohormone precursors.

Commercially available antibodies from the main commercial distributors (Abcam, Santa Cruz antibodies) are polyclonal and do not distinguish between the proforms and the bioactive versions of the guanylin-related peptides. The only available kit used routinely referred to in the published literature was developed by Biovendor which cost £683 per kit.

Not only are reliable antibodies difficult to find but recombinant versions of prohormone precursors ProGuanylin and ProUroguanylin are not commercially available. The production of ProGuanylin solubly-expressed in *E. coli* was described in Lauber *et al*. This method was optimised to produce ProUroguanylin (Lauber *et al.*, 2002).

3.1.2 Generation of antibodies by hybridoma campaign

Since 1975 hybridoma campaigns have been widely used to create monoclonal antibodies based on the techniques originally described by Köhler and Milstein (Köhler and Milstein, 1975). A campaign is initiated by repeatedly immunising a mouse with a target antigen which will trigger an immune response. B cells from the spleen (or lymph nodes in our case) are then isolated and fused with an immortal myeloma cell line. The fused cells have the capacity of dividing perpetually and the ability to produce antibodies. The hybridoma cells secrete antibodies in the media that can subsequently be assayed in ELISA or other immunoassays to determine the antibody specificity (figure 3.1).

Other approaches are available to produce antibodies against a specific target and these include phage display, ribosome display, yeast display and computational methods. However, a hybridoma campaign is considered a fast and efficient method to produce and identify large numbers of IgG antibodies usually with nanomolar (nM) or subnanomolar affinity to their targets due to the *in vivo* round of selection and affinity maturation.

MedImmune has a state-of-the-art technology platform to produce and characterise monoclonal antibodies in a short and efficient way. The Clonepix FL machine for instance is able to pick hybridoma colonies growing in semi-solid media and check for monoclonality.

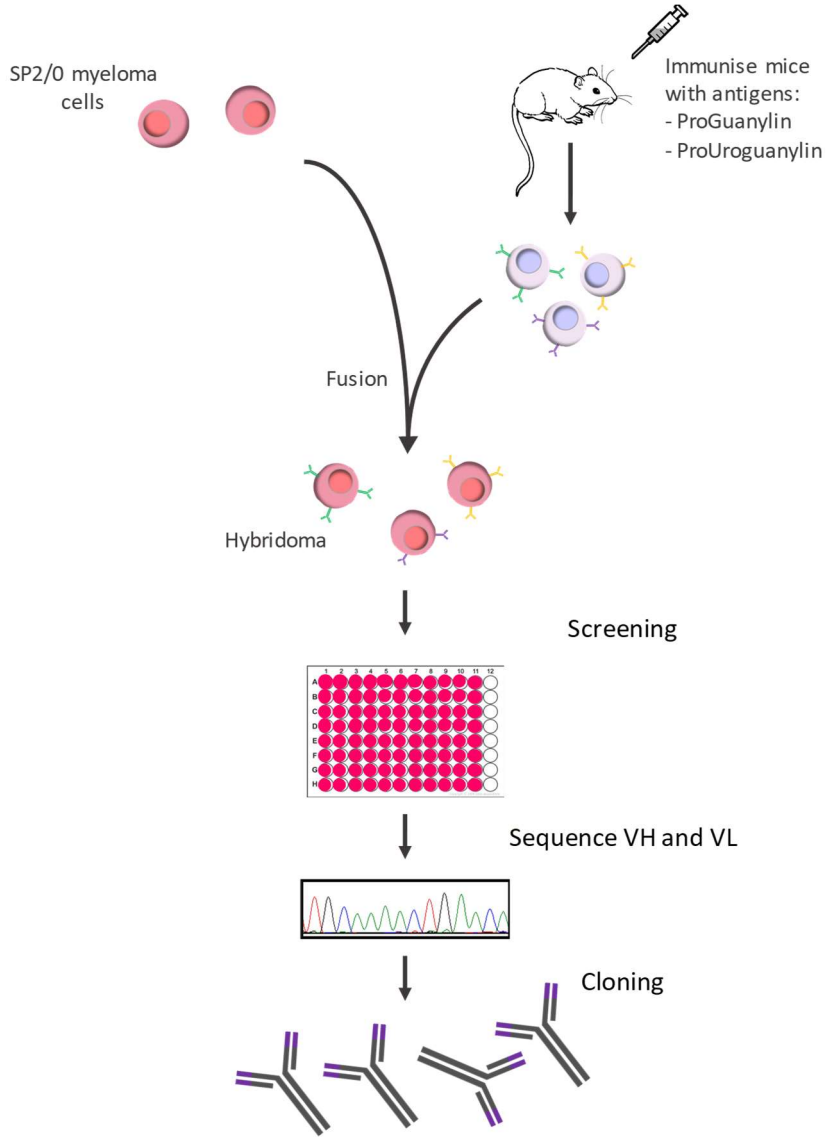

Figure 3.1: Hybridoma process for the generation of antibodies against Guanylin or Uroguanylin. Female CD1 mice were immunised with a series of antigen injections over 28 days. Antibody-producing B cells from lymph nodes or spleen were fused with a myeloma (B cell cancer) by electrofusion. IgG-secreting hybridomas were selected and incubated for 15 days in semi-solid media containing an anti-IgG-FITC antibody, and subsequently picked by Clonepix FL. Colonies were grown for a further 3-5 days before being screened for activity. The positive clones were cherry-picked, sequenced, and then small-scale IgGs were expressed, and purified. IgGs were further characterised.

3.1.3 Aim

To generate novel monoclonal antibodies against ProGuanylin and ProUroguanylin by:

a) Designing and producing ProGuanylin and ProUroguanylin in *E. coli*.
b) Generating hybridoma antibodies by mice immunisation.
c) Screening the clones of interest in ELISA assays and epitope binning to find pairs of compatible antibodies to detect ProGuanylin or ProUroguanylin.
d) Developing an immunoassay as sensitive as the commercially available ELISA.

3.2 Results

3.2.1 Production of the ProGuanylin and ProUroguanylin

3.2.1.1 Generation of ProGuanylin and ProUroguanylin fusion proteins

C-terminally His6 –tagged ProGuanylin was expressed in Origami 2 (DE3) and affinity purified following the protocol of Thomas Lauber *et al*. 25mg of ProGuanylin was obtained at a yield of 5.6mg/L. The same protocol was used to overexpress and purify ProUroguanylin with limited success due to poor solubility when expressed in *E. coli*. Therefore, the expression and purification protocol for ProGuanylin was adapted and optimised. Sixty-eight expression conditions were tested in attempt to generate sufficient quantity of protein for subsequent experiments. Expression in Arctic Express (DE3) at 12˚C overnight with 0.5mM IPTG was found to yield the highest quantities of ProUroguanylin as determined by SDS-PAGE (figure 3.2). On review of the literature, this adapted method is the first to describe production of soluble ProUroguanylin. However, the protein yield was poor (30.5µg/L). Therefore, to achieve the quantities required for immunisation and screening the production was scaled up. In all, a total of 62 litres of cultures were generated to produce 2mg of purified ProUroguanylin.

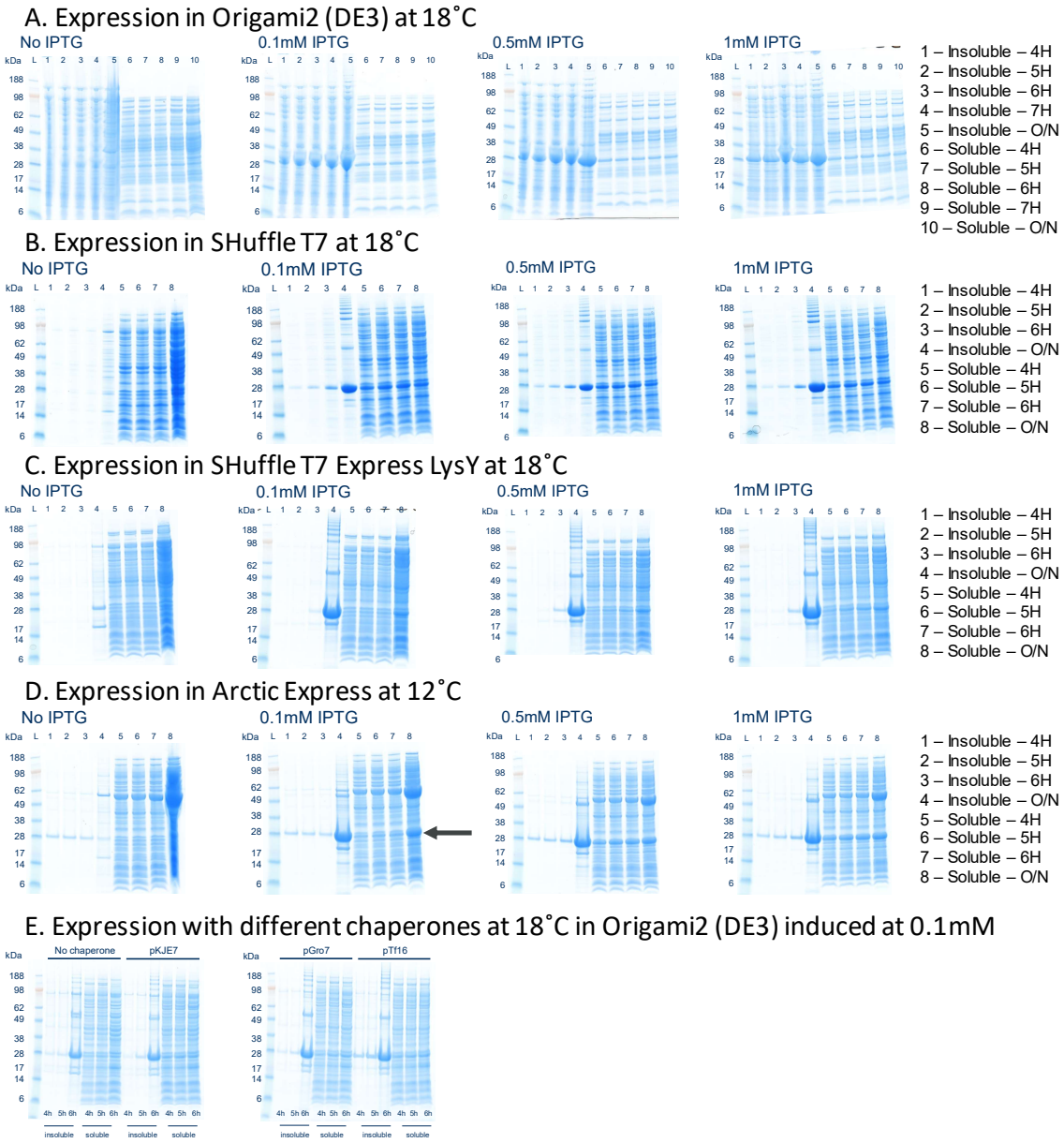

Figure 3.2: Assessment of the optimal condition for ProUroguanylin expression by SDS-PAGE. Expression assessed in (**A.**) Origami 2 (DE3) at 18˚C, (**B.**) Shuffle T7 at 18˚C, (**C.**) SHuffle T7 Express LysY at 18˚C, (**D.**) Arctic Express at 12˚C and (**E.**) in Origami 2 (DE3)0.1mM IPTG at 18˚C in presence of chaperones (pKJE7, pGro7 or pTf16) . For (**E.**) only soluble fractions were analysed by SDS-PAGE. Protein expression was examined at 4hrs, 5hrs, 6hrs, 7hrs and overnight following induction with varying concentrations of IPTG (0.1mM, 0.5mM, and 1mM). The expected value for the protein of interest (ProUroguanylin - Avi Tag - Prescission protease cleavage site – linker - His6 Tag – Thioredoxin) is 29.4kDA. The arrow represents the condition that was chosen to produce the soluble version of ProUroguanylin: expression in Arctic Express (DE3) at 12˚C overnight with 0.5mM IPTG.

It was apparent that adopting this soluble protocol would not yield enough ProUroguanylin therefore, in order to generate the required 5mg of protein for immunisation, an alternative protocol was developed. Since the correct conformation of the protein was not essential for immunisations in mice, a significant larger quantity of the protein was isolated and purified

from inclusion bodies. Using this approach, 9.3mg of ProUroguanylin was purified from the inclusion bodies with an average yield of 520µg/L. This was a sufficient quantity to pursue immunisations and screening for the ProUroguanylin protein.

Endotoxins or lipopolysaccharide (LPS) are the membrane components of Gram-negative bacteria and are immunogenic. The purified proforms -soluble ProGuanylin and ProUroguanylin from inclusions bodies were found to contain high levels of endotoxins (>200EU/mg) and not suitable for immunisation (80EU/mg allowed for immunisation). Endotoxin levels were reduced by using polymyxin B agarose (Sigma P1411). The interaction between polymyxin B and endotoxin (LPS) is specific (Vesentini *et al.*, 2010). After incubation with the resin, the endotoxin levels were reduced to 8.96EU/mg and 75.8 EU/mg for ProGuanylin and ProUroguanylin, respectively.

3.2.1.2 Characterisation of the ProGuanylin and ProUroguanylin

The proforms were characterised using SDS-PAGE and MALDI-TOF mass spectrometry to determine size and purity. Observed masses on mass spectrometry were consistent with the presence of AviTag on ProGuanylin and ProUroguanylin (12307.9Da and 11454.0Da, respectively) (figure 3.3). The proteins were both >95% pure, appeared monomeric by SDS-PAGE and single species by mass spectrometry. The ELISA using commercially available antibodies (Abcam #Ab14427-50 for ProGuanylin and #Ab171982 for ProUroguanylin) further confirmed their identities (Figure 3.4).

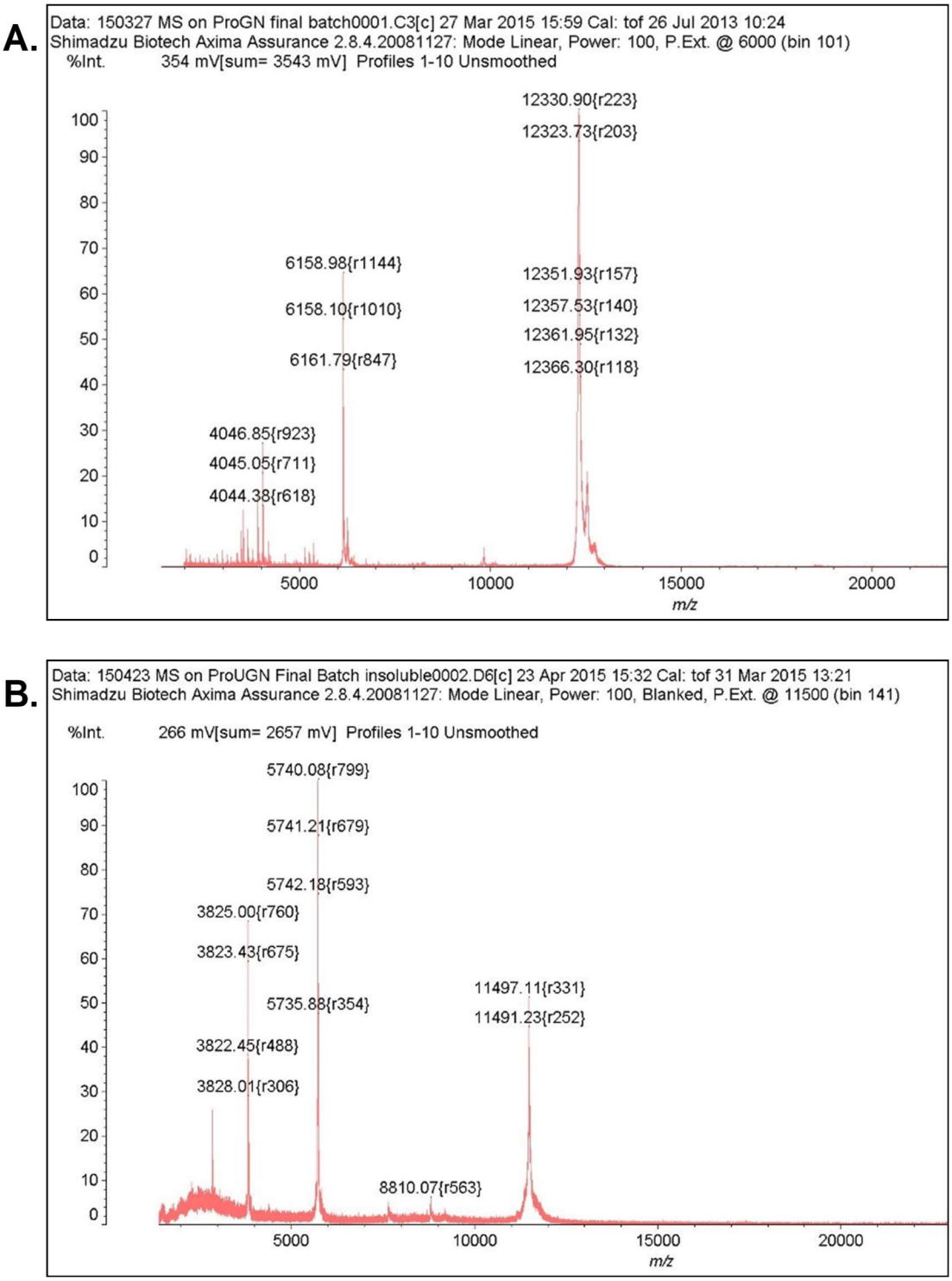

Figure 3.3: Characterisation of the proforms of ProGuanylin and ProUroguanylin by Mass Spectrometry. MALDI-TOF mass spectrometry of (**A.**) ProGuanylin and (**B.**) ProUroguanylin in the positive ion mode was performed on a Shimatzu Biotech AXIMA Assurance instrument using Shimadzu MALDI-MS software version 2.8.4 using. The expected molecular weights for ProGuanylin and ProUroguanylin are 12.3kDa and 11.5kDa, respectively.

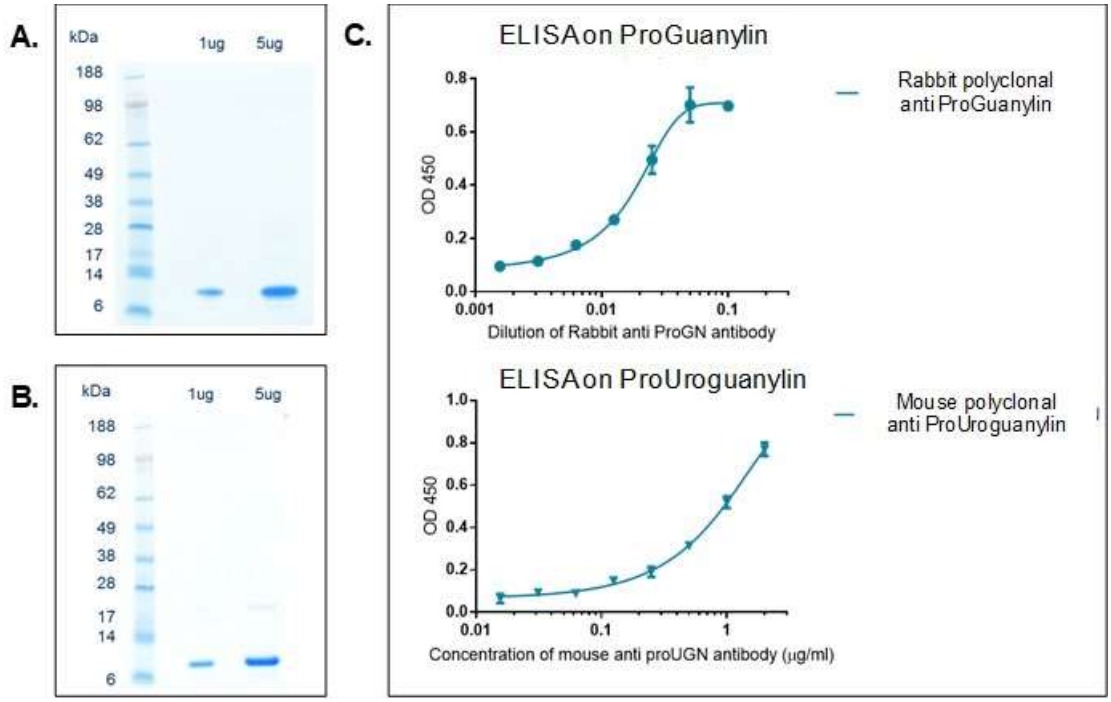

Figure 3.4: Characterisation of the proforms of ProGuanylin and ProUroguanylin by SDS PAGE and ELISA. SDS PAGE was performed on 1µg and 5 µg of (**A.**) ProGuanylin and (**B.**) ProUroguanylin to control their quality. The expected molecular weights for ProGuanylin and ProUroguanylin are 12.3kDa and 11.5kDa, respectively. Both proforms are recognised by commercially available polyclonal antibodies in (**C.**).

To enable screening, proforms purified from the soluble fractions were specifically biotinylated on the AviTag by BirA enzymatic reaction (Cull and Schatz, 2000) (Avidity #BirA500). The biotinylation was confirmed by MALDI TOFF mass spectrometry (figure 3.5).

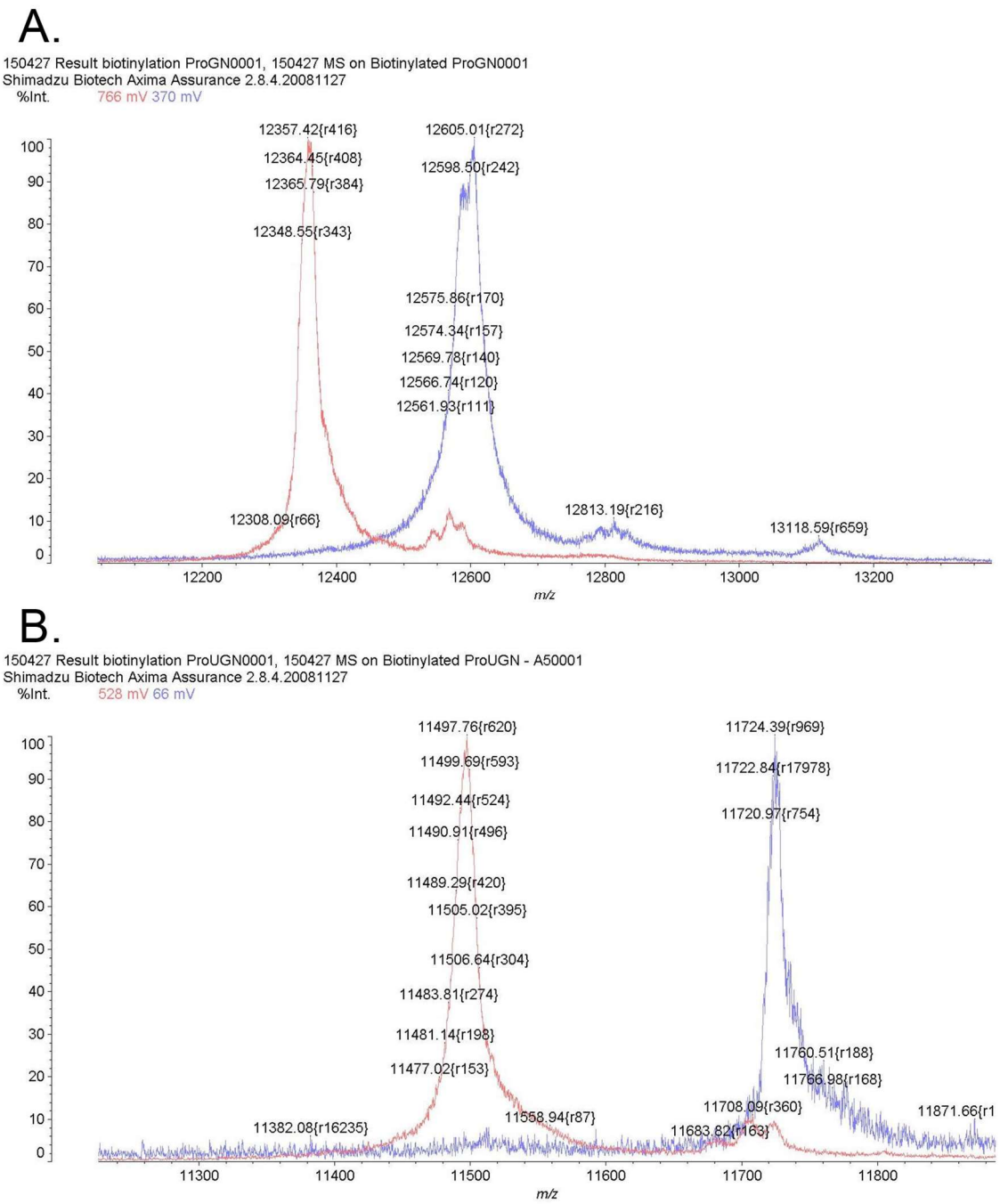

Figure 3.5: Assessment of biotinylation efficiency by Mass spectroscopy. ProGuanylin and ProUroguanylin were enzymatically biotinylated using BirA enzyme. (**A.**) shows the mass spectra for ProGuanylin before (red) and after (blue) biotinylation. (**B.**) shows the mass spectra for ProUroguanylin before (red) and after (blue) biotinylation.

3.2.2 Generation of monoclonal antibodies

3.2.2.1 Mouse immunisation and hybridoma generation

Mice were immunised with 100µg of ProGuanylin or ProUroguanylin following a 28-day immunisation schedule. Serum titres (prebleed, day 13 and day 20) were measured using an

ELISA that detected binding to biotinylated-proforms. Strong serum titres were obtained for the mice immunised with ProGuanylin and ProUroguanylin (data not shown).

For antibody production, hybridomas were generated from lymphocytes extracted from immunised mice that presented the highest serum titres among each group. To identify IgG-secreting colonies, fusions were plated into a semi-solid media containing a FITC-labelled antibody against IgG. ClonePix FL was used to identify IgG-secreting colonies. Percentages of IgG secreting for the two immunising antigen groups are shown on table 3.1.

	ProGuanylin	ProUroguanylin
Hybridoma colonies	5691	4077
IgG secreting colonies	754	60
% of IgG secreting colonies	13.2%	1.4%
HTRF binders to biotinylated antigens	35	10
% of binders/IgG secreting colonies	4.6%	16.7%
Binders after further characterisation	11	4

Table 3.1: Summary of the hybridoma campaign to ProGuanylin and ProUroguanylin targets. All IgG-secreting hybridomas were picked and IGs screened in the primary screens. The table contains the final results of binders after characterisation.

3.2.2.2 Screening of hybridoma clones

All of the IgG-secreting hybridoma colonies were tested for binding to the four biotinylated targets in a HTRF direct binding assay. Among the 814 IgG supernatants tested, 35 clones were found to bind to biotinylated-ProGuanylin and 10 clones bound to biotinylated-ProUroguanylin (table 3.1). The 45 hybridoma supernatants that were positive in the HTRF assay were sequenced and IgG-purified using a small-scale automated plate-based method. To assess the sequence diversity of the panel of antibodies, the variable region CDR3 was sequenced. 42 out of 45 clones presented a unique sequence, equivalent to 93.3% diversity.

The specificity of the 45 antibodies was confirmed using an ELISA assay against each potential target: biotinylated-ProGuanylin, biotinylated-ProUroguanylin, biotinylated-Guanylin, biotinylated-Uroguanylin, Guanylin-KLH, Uroguanylin-KLH and KLH only (those last targets are developed more in Chapter 4). The ELISA was performed at a single sample dilution. From the 35 antibodies directed against ProGuanylin, 26 showed exclusive binding to ProGuanylin. Five out of 10 antibodies directed against ProUroguanylin showed exclusive binding to ProUroguanylin (figure 3.6).

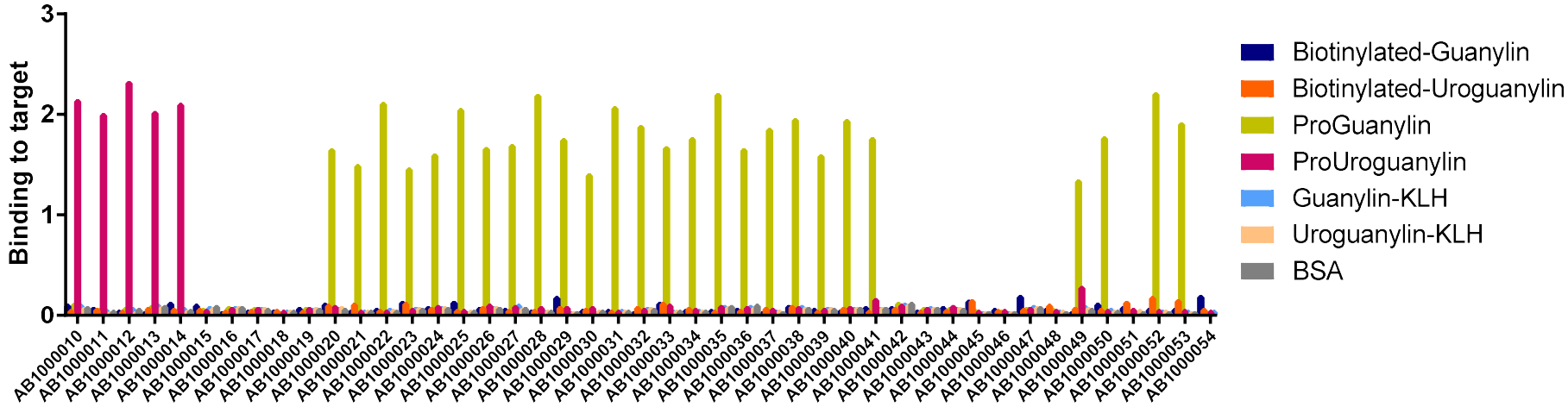

Figure 3.6: Screening for ProGuanylin and ProUroGuanylin specific clones by direct binding ELISA on the antibodies produced from the hybridoma campaign. A direct binding ELISA was performed on the positive IgG-secreting hybridoma colonies clones selected by the HTRF assay where 35 clones were found to bind ProGuanylin and 10 clones were found to bind ProUroguanylin.

3.2.3 Determination of the specificity and binding of the panel of antibodies

3.2.3.1 Affinity measurement and identification of antibody pairs by Epitope binning

All 45 antibodies identified by primary screens were covalently conjugated to a SensEye for affinity measurements and epitope binning assay using IBIS-MX96, which is based on surface plasmon resonance. From the panel of 45 antibodies, 25 clones did not bind the SensEye and were subsequently excluded from further analysis. It was likely that these antibodies were not compatible with the surface chemistry of SensEye. The binding of each antibody to its target (either ProGuanylin or ProUroguanylin) was analysed. The KD was measured for 11 of the 16 antibodies and demonstrated binding to ProGuanylin and binding to ProUroguanylin for 3 out of the 4 antibodies (table 3.2). Some antibodies presented a high affinity to their targets such as AB100030 (KD=597pM) and AB100033 (644pM) due to low off-rates. The KD of AB100011 was impossible to determine as the binding was biphasic with an initial fast off-rate followed by a second slower off-rate phase. However, the kd was measured on the slower off-rate phase and was the lowest among the panel of antibodies.

	AB100010	AB100011	AB100012	AB100013	AB100020	AB100021	AB100023	AB100024	AB100025	AB100027	AB100028	AB100030	AB100032	AB100033	AB100034
Target	ProUGN	ProUGN	ProUGN	ProUGN	ProGN	ProGN	ProGN	ProGN	ProGN	ProGN	ProGN	ProGN	ProGN	ProGN	ProGN
ka	2.46E+05		9.45E+04	1.08E+05	9.75E+05	1.70E+05	1.36E+06	1.56E+05	1.03E+06	3.42E+05	1.55E+05	1.74E+06	7.40E+05	1.94E+06	4.73E+05
kd	1.74E-03	5.40E-04	1.99E-03	2.03E-03	1.84E-02	1.24E-02	5.41E-02	3.19E-03	4.66E-03	1.10E-02	9.89E-03	1.04E-03	2.35E-02	1.25E-03	7.72E-03
Rmax	96.34		36.08	34.9	149.9	33	57.96	66.37	85.91	63.8	58.83	49.66	76.58	37.63	82.86
KD	7.09nM		21.03nM	18.8nM	18.9nM	75nM	39.81nM	20.50nM	4.521nM	32.11nM	63.84nM	597.21pM	31.76nM	644.55pM	16.34nM
Res sd	2.86	1.55	1.32	2.44	2.10	1.37	2.72	2.05	1.36	1.87	1.86	1.73	1.68	1.52	1.13

Table 3.2: Affinity results of the panel of antibodies to their targets measure using the IBIS-MX96. ProGN means ProGuanylin and ProUGN means ProUroguanylin.

The IBIS technology was also used to perform epitope binding to identify antibody pairs that bind different epitopes on the same antigens. Having antibody pairs will enable the development of assays to detect proform and active peptides of guanylin and uroguanylin. A signal will be detected only when two antibodies bind to non-overlapping epitopes. The epitope binding results are presented in figure 3.7 and demonstrate identification of several antibody pairs capable of detecting ProGuanylin. The coated antibodies AB100030 and AB100025 appeared most promising with a diversity of potential secondary antibody: AB100037, AB100038, AB100028, AB100031 and AB100041. Out of the 4 antibodies that showed binding to ProUroguanylin, only one pair of antibodies was able to detect ProUroguanylin: AB100010 and AB100011. The signal was stronger when AB100010 was covalently bound to SensEye compared to AB100011 but that could be due to a difference in conjugation efficiencies to SensEye.

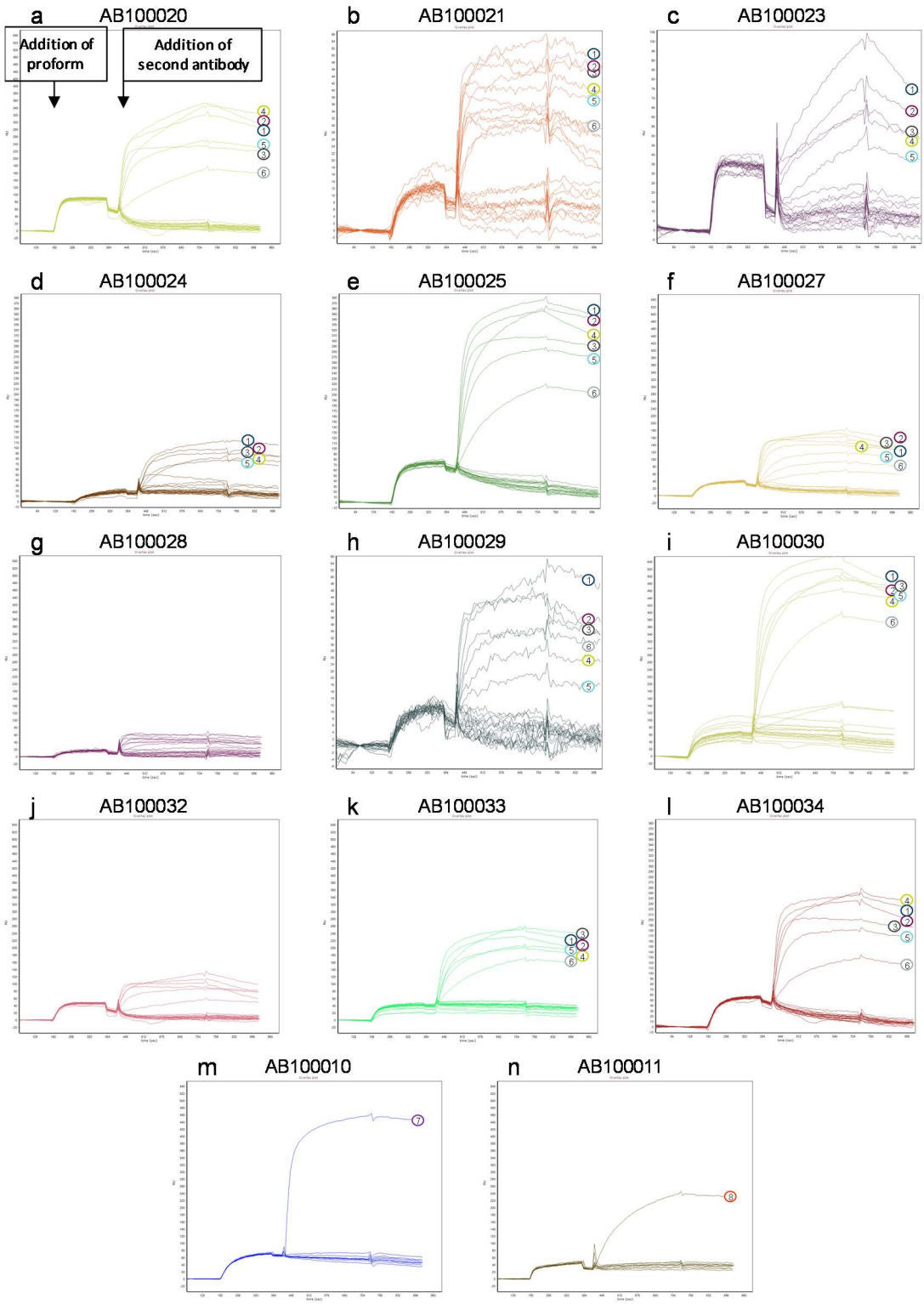

Figure 3.7: Epitope binding of antibodies to propeptides using SPR technology IBIS MX96 to identify antibody pairs. Each of the composite sensorgrams A-L represents the binding of free ProGuanylin in the flow cell to the covalently immobilised antibody (labelled on the top of each composite sensorgram), followed by individual binding events of secondary antibodies 1-6 to ProGuanylin. Similarly, M-N represent the binding of free ProUroguanylin in the flow cell to the covalently immobilised antibody, followed by individual binding events of secondary antibodies 7-8 to ProUroguanylin. The identities of the secondary antibodies are: 1/ AB1000037 2/ AB1000038 3/ AB1000028 4/ AB1000031 5/ AB1000041 6/AB1000021 7/ AB1000011 8/ AB1000010

Four of the antibodies implicated in a potential pair to detect ProUroguanylin and ProGuanylin did not bind to the SensEye and therefore the affinity to the proforms was not measured. It was decided to perform another experiment using a Biacore instrument - based on surface plasmon resonance as well. Eight of the antibodies involved in pairs detecting the ProGuanylin or Proguanylin were covalently bound to a CM3 chip by amine coupling. Different concentrations of the ProGuanylin and ProUroguanylin allowed the measurement of the binding constants using a 1:1 binding model. The sensorgram presenting the binding of AB1000010 and AB1000011 to ProUroguanylin and AB1000025, AB1000028, AB1000030, AB1000031, AB1000037 and AB1000041 to ProGuanylin are presented in figure 3.8 and the binding constants are summarised in table 3.3.

Antibody name	Target	Origin	KD measured by IBIS	KD measured by Bioacore
AB1000010	ProUroguanylin	Hybridoma selection	7.09E-09	6.17E-09
AB1000011	ProUroguanylin	Hybridoma selection	N/D	2.94E-09
AB1000025	ProGuanylin	Hybridoma selection	4.52E-09	3.64E-09
AB1000028	ProGuanylin	Hybridoma selection	6.38E-08	2.89E-09
AB1000030	ProGuanylin	Hybridoma selection	5.97E-10	1.12E-09
AB1000031	ProGuanylin	Hybridoma selection	N/D	6.99E-10
AB1000037	ProGuanylin	Hybridoma selection	N/D	8.04E-10
AB1000041	ProGuanylin	Hybridoma selection	N/D	1.06E-09

Table 3.3: Affinity results of the panel of antibodies to ProGuanylin or ProUroguanylin. Affinity measurement was performed using the IBIS and Biacore T100 instrument. The data was analysed using Scrubber2 (BioLogic Software) and the Biacore T100 evaluation software respectively using a 1:1 binding model.

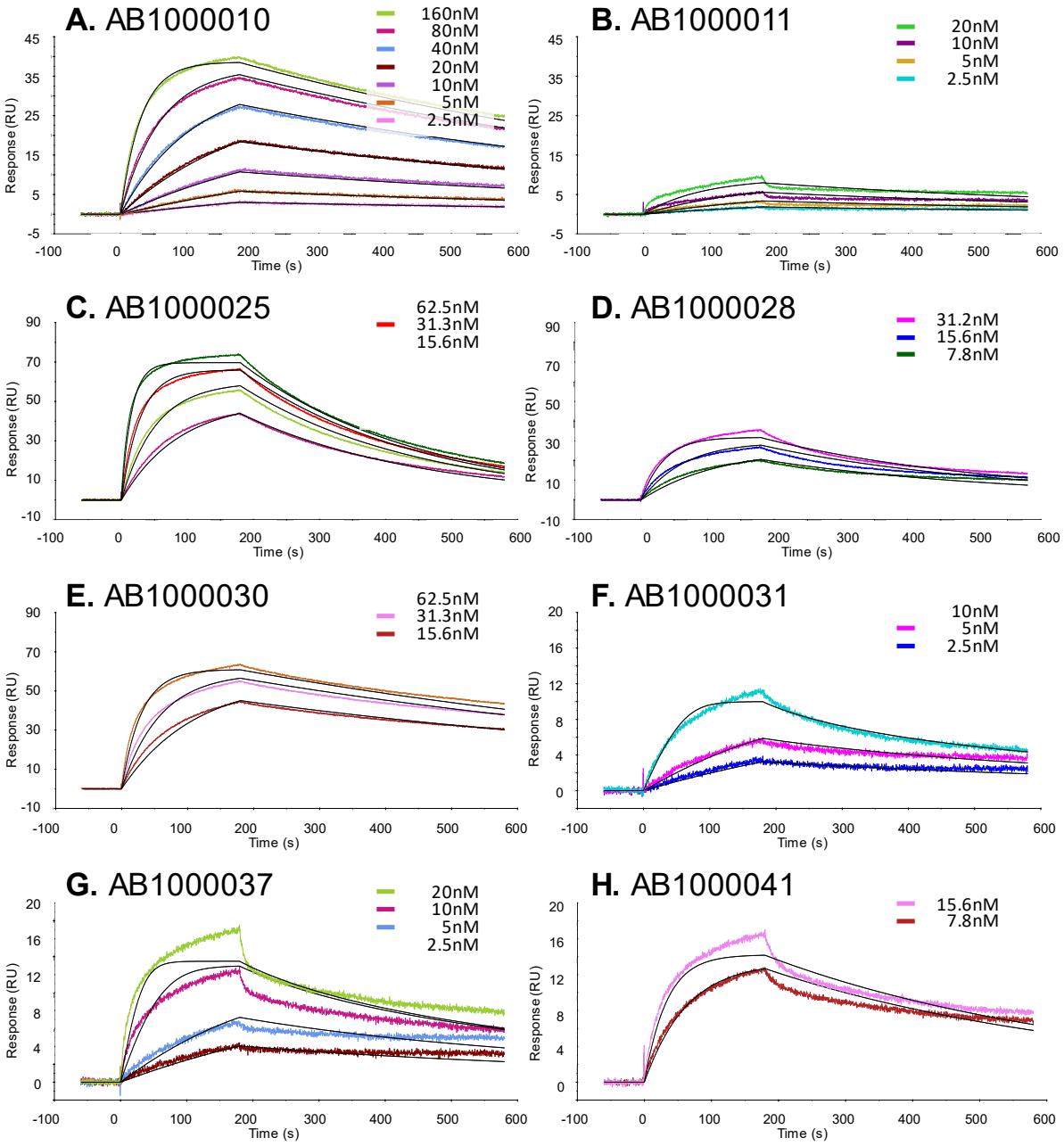

Figure 3.8: Determination of the antibodies' affinity to ProGuanylin of ProUroguanylin using Biacore.
Kinetic binding experiment with antibodies A. AB1000010 B. AB1000011 C. AB1000025 D. AB1000028 E. AB1000030 F. AB1000031 G. AB1000037 H. AB1000038 on the Biacore T100 instrument (Response Units (RU) as function of time). The antibodies were immobilised at 10µg/ml on the CM3 chip. The flow rate was 50µl/min, the contact time was 180 seconds while the dissociation time was 400 seconds. The data was analysed using the Biacore T100 evaluation software using a 1:1 binding model and the fit is represented by the black line.
In (**A.**) ProUroguanylin was used at a concentration ranging between 2.5nM and 160nM. In (**B.**) ProUroguanylin was used at a concentration ranging between 2.5nM and 20nM. In (**C.**) and (**E.**) ProGuanylin was used at a concentration ranging between 7.81nM and 62.5nM. In (**D.**) ProGuanylin was used at a concentration ranging between 7.81nM and 31.25nM. In (**F.**) ProGuanylin was used at a concentration ranging between 1.25nM and 10nM. In (**G.**) ProGuanylin was used at a concentration ranging between 1.25nM and 20nM. In (**H.**) ProGuanylin was used at a concentration ranging between 7.81nM and 15.63nM.

All tested antibodies presented a high affinity (nanomolar affinity) for either ProGuanylin or ProUroguanylin. The antibodies AB1000031 and AB1000037 showed picomolar affinity.

However, the Biacore T100 evaluation software was unable to fit the curves properly using a 1:1 binding model. This is probably due to bivalent binding and, therefore, the KD needs to be interpreted with some reservation, although it does provide an estimation of the affinity.

Biacore sensorgrams frequently exhibit deviation of the first-order kinetics and different causes can explain such a result (Kalinin, Ward and Winzor, 1995; Morton, Myszka and Chaiken, 1995; O'Shannessy and Winzor, 1996). The antibody could have a multivalent property and recognize two or more parts of the target (ProGuanylin or ProUroguanylin) invalidating the first-order binding model. Another potential cause would be the heterogeneity of the antibody or the target. It can be assumed that the proforms exist as a homogeneous solution as it presented a 1:1 binding model fit with some of the antibodies. Even though the antibodies were purified by affinity followed by size exclusion chromatography, potential degradation of the antibodies with time would modify the homogeneity of the solutions. Finally, a potential explanation of the bivalent binding would be the masking of potential sites by the proform.

A common approach to overcome bivalent binding to measure the affinity of antibodies to their targets is to perform the experiment using the Fab or the scFv part of the antibody (Muller-Loennies *et al.*, 2000). This methodology was however not pursued as it would have been time consuming and the affinity measurement was not essential for the completion of the project.

3.2.3.2 Development of an immunoassay for the measurement of the proforms

To compare the different possible pairs of antibodies that were identified by epitope binning for ProGuanylin, each potential pair of antibodies were tested in the Meso Scale Discovery (MSD) electrochemiluminescence assay which measures the light emitted when a voltage is applied. The MSD immunoassay has been regularly evaluated against competitor immunoassays (Becton Dickinson Cytometric Bead Array, ELISA) and has proven a more reliable, accurate and with a broader dynamic range assay to measure cytotoxins (Chowdhury, Williams and Johnson, 2008; Dabitao *et al.*, 2011), pharmacodynamic responses in tumours (Gowan *et al.*, 2007) or incretin hormones (Bak *et al.*, 2014; Meek *et al.*, 2016).

In order to perform a MSD assay, one of the 2 antibodies involved in a pair is used to coat the MSD plate while the second antibody is labelled with a Sulfo-tag. Antibodies AB1000025 and

AB1000030 were both used as capture antibodies and were coated on a plate. Antibodies AB1000028, AB1000031, AB1000037 and AB1000041 were labelled with a Sulfo-Tag and used as detection antibodies. Three concentrations of ProGuanylin were used with each antibody configuration and the pair that gave the highest MSD response was the pair formed by AB1000025 and AB1000028-Sulfo-Tag (figure 3.9 A). The antibody pairs were also tested in the reverse configuration where AB1000028 was used as the capture antibody and Sulfo-Tag labelled AB1000025 used as the detection antibody. This new configuration was not as effective as the pair with AB1000025 as the capture antibody (figure 3.9 B).

The best combination of antibodies to detect ProUroguanylin was easier to find as only two antibodies worked as a pair (AB1000010 and AB1000011). Both were labelled with the Sulfo-tag and used as capture antibody. Three concentrations of ProUroguanylin were used with each antibody configuration and both antibody configurations gave similar MSD response (figure 3.9 C).

The final assay to detect ProGuanylin gave a range of detection from 200-200,000pg/ml and intra-assay CVs of <5%. The final assay to detect ProUroguanylin gave a range of detection from 300-200,000pg/ml and intra-assay CVs of <5%.

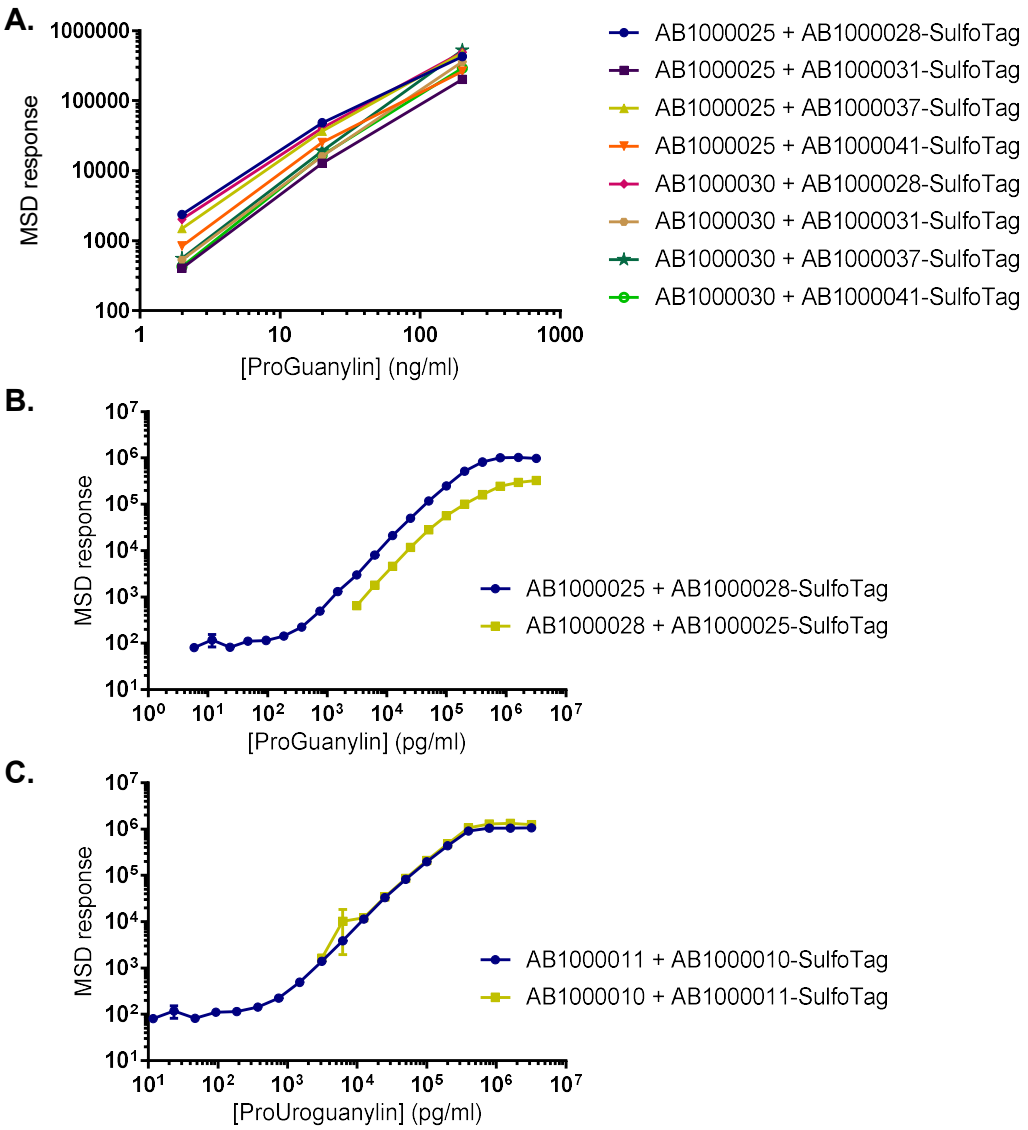

Figure 3.9: Assessing the best pair of antibodies to capture and detect ProGuanylin or ProUroguanylin in the Meso Scale Discovery assay. (A). MSD response to set concentration of ProGuanylin with all potential antibody combinations. (**B.**) Assessment of the limit of detection of ProGuanylin by the AB1000025 and AB1000028 antibody pair with either the AB1000025 coated to the plate and AB1000028 tagged or vice versa. (**C.**) Assessment of the limit of detection of ProUroguanylin by the AB1000010 and AB1000011 antibody pair with either the AB1000025 coated to the plate and AB1000028 tagged or vice versa.

3.3 Discussion

3.3.1 Expression of the ProGuanylin and ProUroguanylin

A method to produce ProGuanylin in solution was previously been described by Lauber *et al*. This method was used to express soluble ProGuanylin in bacteria and purify it from the cytoplasm by affinity purification. However, when using the same protocol for ProUroguanylin, the protein was mainly expressed in inclusion bodies. This was not an unexpected result as the two prohormones only share 28.9% of their identity and might have

different physical and chemical properties which could lead to a different expression behaviour.

In order to obtain soluble ProUroguanylin from *E. coli* expression, a diverse range of expression conditions were thoroughly analysed: different bacteria strains engineered to help the expression of proteins in solution, temperature, expression time, and IPTG concentration for induction of the protein expression were tested. After optimisation of soluble expression, the protein yield was very low. Moreover, the purification was done in 3 steps: ProUroguanylin-$(His)_6$Tag-TRX was affinity purified followed by the cleavage of $(His)_6$Tag-TRX from the proform and purified again to remove $(His)_6$-thioredoxin tag. Each purification step generated protein loss leading to a total loss of 60% at the end of the process. Hence, in total only 40% of the material required for the immunisations could be produced as soluble and so other approaches needed to be investigated.

To immunise mice, recombinant proteins are vortexed in Freund's Complete Adjuvant or Incomplete Freund's Adjuvant which is a denaturant. This step will unfold the proteins. As maintaining protein conformation is not a prerequisite for immunisations, it was decided to produce the protein from the inclusion bodies, in an aggregated state. For the isolation of specific antibodies against ProUroguanylin, ProUroguanylin aggregates were used for immunisation and soluble ProUroguanylin was only used for the screening and characterisation in order to isolate binders recognising the native ProUroguanylin.

If time was not a limiting factor, different strategies could have been developed in attempt to express higher levels of ProUroguanylin in the soluble fraction. First, redesigning the DNA vector to increase the size of the His_6-tag to a His_{10}-tag would have helped protein binding to the purification column during the affinity purification. Another strategy to achieve such a result would have been to place the His-tag at the C- or N-terminus of the protein. The poor binding of the protein to the affinity column could also be explained if the protein was produced as soluble aggregates (Dümmler, Lawrence and de Marco, 2005). Soluble aggregates do not bind properly to an IMAC column, but addition of mild detergents may help to dissociate the soluble aggregates and increase the efficiency of the protein binding to the column. Finally, the use of different expression hosts might have achieved an improved soluble expression profile.

In addition, other solubilisation tags could have been used to assist in the proper folding of the protein instead of the thioredoxin-tag such as a poly(NANP) tag. Other solubilisation tags have a dual role as affinity tags and could have replaced both His-tag and thioredoxin-tag such as MBP and GST. To improve the purification step removing the solubilisation and purification tags, different cleavage sites could have replaced the PreScission protease cleavage site to use different enzyme with higher yield such as enterokinase, Factor Xa, or Thrombin. A final strategy would have been to develop a purification method from the inclusion bodies. However, for this strategy it would have been necessary to develop assays to control the conformation of the protein.

3.3.2 Results of the hybridoma campaign

A hybridoma campaign is considered a fast and efficient method to find large numbers of antibodies in IgG format usually with nanomolar or subnanomolar affinity to their targets. The goal of this work was to find pairs of antibodies directed specifically to the proforms in order to perform assays to detect them in human samples. The hybridoma campaign was successful in finding pairs of antibodies against ProGuanylin and ProUroguanylin. Several options can be used to quantify ProGuanylin as AB1000030 and AB1000025 managed to bind the target which was consecutively recognised by AB1000037, AB1000038, AB1000028 or AB1000031. To quantify ProUroguanylin, one pair of antibodies was found to bind in a sandwich format: AB1000010 and AB1000011.

Both assays have a broad range of detection. When comparing the MSD assay to the commercially available kit, Biovendor states that their ProGuanylin ELISA to be able to detect between 0.31-10ng/ml of protein, whereas this newly-developed MSD assay is able to measure levels of ProGuanylin ranging from 0.2-200ng/ml. Biovendor states that their ProUroguanylin ELISA kit is able to detect between 0.8-40ng/ml, but the newly developed MSD assay is able to measure levels of ProUroguanylin ranging from 0.3-200ng/ml.

In conclusion, the hybridoma campaign was successful in producing monoclonal antibodies against ProUroguanylin and ProGuanylin. Both proforms have now at least one pair of antibodies that can be used to measure quantitatively their concentrations in human biospecimens. The Biovendor protocol supplied for both assays also recommends diluting the plasma or serum samples to be in the calibration range. An advantage of the broad dynamic

range of the MSD assay is that no further dilution of serum or plasma samples is required, thereby minimising introduction of potential error through, for example, pipetting.

Chapter 4: Generation of monoclonal antibodies against the bioactive peptides guanylin and uroguanylin

4.1 Introduction

4.1.1 Historically known active peptides and antibodies availability

Human guanylin and uroguanylin are both expressed on chromosome 1 and translated as pre-prohormones consisting of 115 and 112 amino acids, respectively (Hill *et al.*, 1995; Magert *et al.*, 1998). The 21 amino acid signal peptide is cleaved leading to the formation of ProGuanylin, a 94 amino acid peptide (Kuhn *et al.*, 1995). Following secretion from the cell, ProGuanylin is cleaved further by an unknown proteolytic process resulting in guanylin, a 15-amino acid biologically active peptide (de Sauvage *et al.*, 1992; Mark G Currie *et al.*, 1992). Similarly, following cleavage of the signal peptide, the uroguanylin pre-proform, is processed to yield an 86 amino acid peptide, ProUroguanylin (Hamra *et al.*, 1996), which is released from the cell and processed further into a 16-amino acid peptide called uroguanylin (Kita *et al.*, 1994; Miyazato *et al.*, 1996). A second 24-amino acid peptide version was isolated and characterised as another potential peptide derived from the ProUroguanylin sequence; and called GCAP-II (Hess *et al.*, 1995).

Whilst the biological activity of the proforms is debated (Kuhn *et al.*, 1993; Schulz *et al.*, 1999), the bioactive guanylin and uroguanylin peptides potently activate the GC-C receptor.

To date, the most commonly employed methods for measuring and studying these peptides include radioimmunoassay (RIA), electrospray mass spectrometry and cGMP assays. No monoclonal antibodies are commercially available that bind specifically to the guanylin and uroguanylin peptides.

4.1.2 Generation of antibodies by phage display

Phage display is a commonly used technique for the isolation and maturation of antibodies to a target using M13 bacteriophage. The M13 bacteriophage displays on its surface 5 coat proteins that are directly encoded by genes packaged within the bacteriophage. Genes can be cloned and enclosed in the bacteriophage resulting in expressed proteins that are displayed on the bacteriophage surface (Smith, 1985). In the case of antibody phage display, phage libraries were generated in which genes encoding for single chain variable fragment (scFv)

were cloned in a phage display vector. ScFvs are fusion proteins encoding the variable regions of the heavy (V_H) and light (V_L) chains of the antibody. Both chains are connected by a flexible linker to form the scFv and the structure can be used for antibody phage display. Consequently, scFvs fused to the pIII coat protein are expressed on the M13 bacteriophages (McCafferty *et al.*, 1990).

MedImmune has produced libraries containing between 10^{10}-10^{11} different phages, that were engineered to isolate clones against all targets which can be a protein, a peptide or DNA (Tristan J. Vaughan *et al.*, 1996; Lloyd *et al.*, 2008). The most common way to select for clones of interest is through an *in vitro* binding incubation in which the phage library binds to a target of interest. Unattached phages are washed off before elution of the phage of interest and propagating them for further rounds of selection (figure 4.1). After several rounds of selection, clones can be screened, and their identity determined by sequencing. Initial characterisation of the panel of clones is done by phage ELISA in which phages bind to a target coated on a plate. The specific binding is detected by an anti-phage antibody which will give a "yes-no" answer. Characterisation of the binding is studied by the production of a soluble scFv, which can be used in competition assays. The resulting V_H and V_L sequences of interest are reformatted into mammalian expression vectors containing the light or heavy chain constant domains.

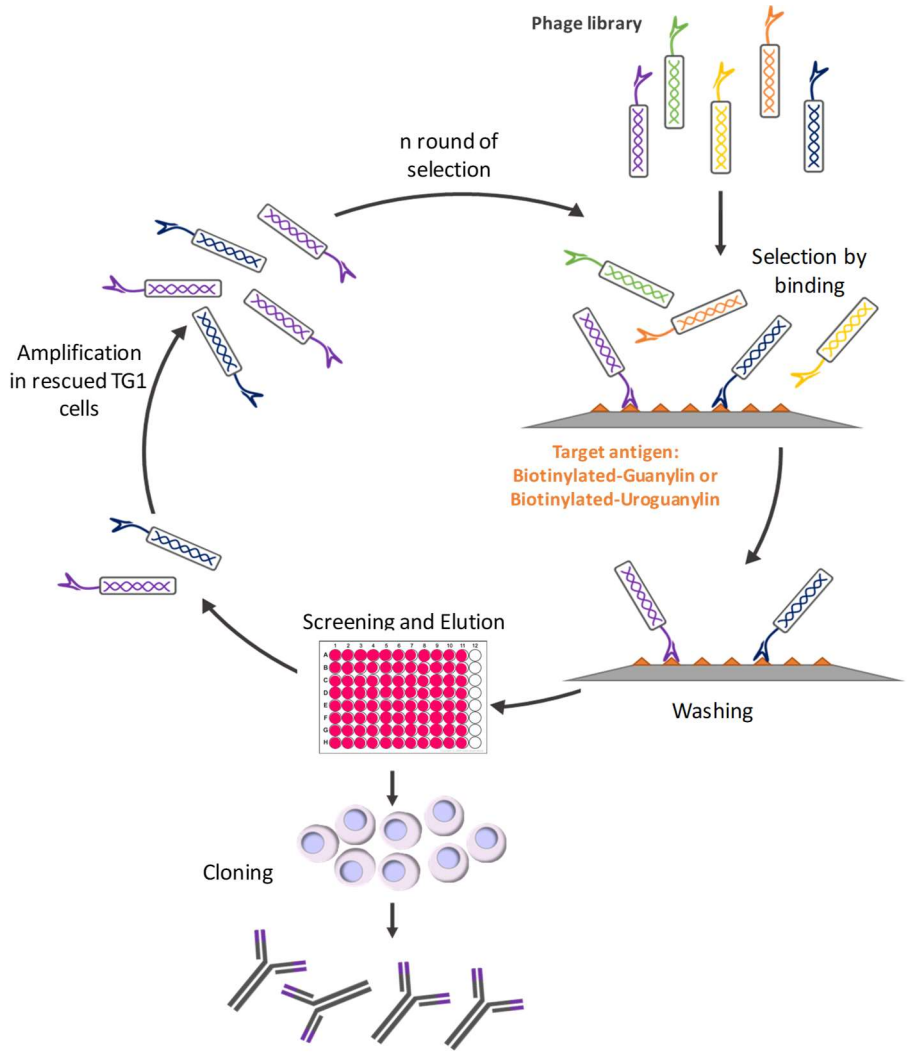

Figure 4.1: Phage Display selection process for the selection of clones against Guanylin or Uroguanylin. M13 bacteriophage expresses a single scFv fused to the pIII protein -determined by the sequence of the phagemid. The phage libraries are selected by binding to the biotinylated targets which are separated using magnetic streptavidin beads. Following their elution from the beads, bacteriophage infect TG1 bacterial cells. The bacteriophage infected cells are rescued allowing the cells to produce a new pool of phagemids of interest that can be used subsequently in further rounds of selections. The positive clones from the screening were cherry-picked, characterised in ELISA and competition ELISA, sequenced, and then small-scale IgGs were expressed and purified. IgGs were further characterised. Figure adapted from Clackson and Lowman, 2004.

4.1.3 Options to optimise epitope binding

Several options are available to optimise the affinity of an antibody to its target. Phage display is, again, a common tool to improve the affinity of an antibody to its target and can typically be increased by up to 1000-fold (Schier, McCall, *et al.*, 1996). Targeting mutations to the complementary determining regions (CDRs) is a preferential way to increase the affinity as they are responsible for antigen binding. The CDR3 is usually the major determinant of antibody-binding specificity, and the varied length and biochemical properties of V_H CDR3 is the main contributor to the sequence diversity (Zemlin *et al.*, 2003; Barderas *et al.*, 2008).

Affinity maturation by targeted mutagenesis on the V_H CDR3 and V_L CDR3 is a common method to mature the affinity of an antibody to its target (Yang *et al.*, 1995).

Another common method to optimise the binding of an antibody to its target is ribosome display. This technique is based on *in vitro* translation that prevents the newly synthesised protein (scFv) from leaving the ribosome by removal of the stop codon that causes stalling. Therefore, the encoding gene sequence (mRNA) and scFv peptide are linked together in a ribosomal complex, coupling phenotype and genotype. Those complexes are used in selection against an immobilised target and similarly to phage display the unbound scFv-mRNA-ribosomes complexes are washed off. The mRNA isolated and purified can be used in subsequent rounds of selection (figure 4.2) As well as performing rounds of selection, mutations can be introduced into the mRNA sequences using low-fidelity DNA polymerase and can be performed between rounds of selection, conferring a directed evolution of proteins for higher binding affinity. For example, antibodies optimised against insulin showed a 40-fold improvement compared to its progenitor by accumulating point mutations during ribosome display cycles (Hanes *et al.*, 2000).

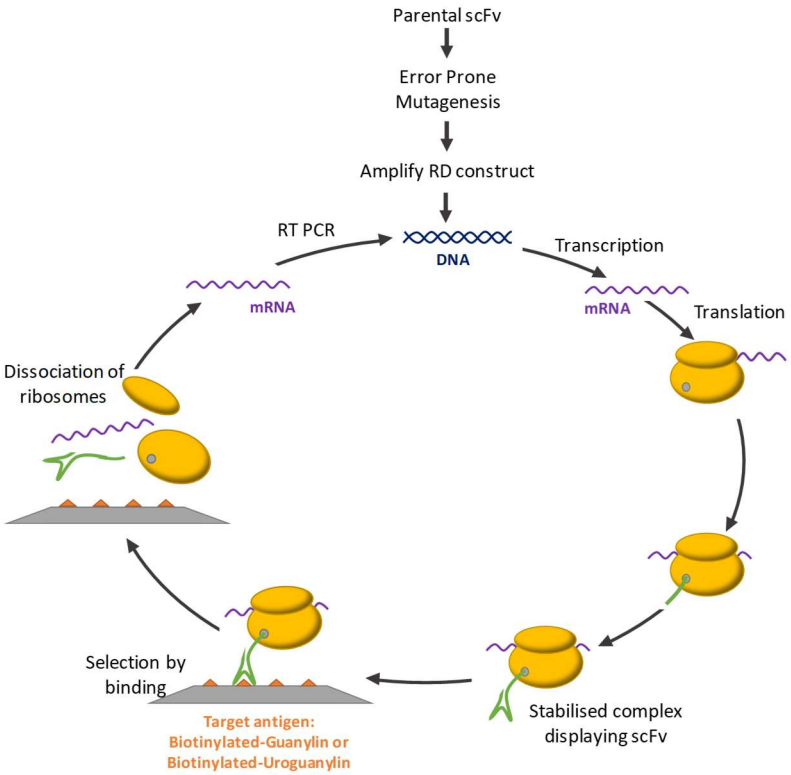

Figure 4.2: Ribosome display process for the selection of clones against guanylin or uroguanylin. After performing Error Prone mutagenesis on the parental scFv, the mutated DNA was transcribed *in vitro*. The mRNA was translated using a cell-free system allowing the generation of a stabilised mRNA-ribosome displaying a scFv by removal of the stop codon causing stalling. Selections were performed on the complex by binding to the immobilised target biotinylated-Guanylin or biotinylated-Uroguanylin. After washing away the non-binding complexes and disrupting the ribosome complex, the mRNA was reverse transcribed, and the signal amplified by PCR. Several rounds of selection were performed with decreasing levels of target antigens. Once the round of selections performed, the DNA was cloned back into phage libraries to perform some screening. Diagram adapted from Groves and Osbourn, 2005.

4.1.5 Liquid chromatography and mass spectrometry as a new powerful tool in peptidomics

Liquid chromatography coupled to mass spectrometry (LC-MS) is used in the detection and quantification of peptides. It is an analytical technique that uses the physical separation capabilities of liquid chromatography (LC) with the mass analysis capabilities of mass spectrometry (MS), and can detect the mass-to-charge ratio (m/z) of charged particles or ions within a sample.

Samples are injected into a chromatography column that will separate according to physico-chemical properties (for example, size, charge, hydrophobicity). The most widely used variant is the reverse-phase (RP) mode of the partition chromatography technique, which separates analytes according to their hydrophobicity. The more hydrophobic an analyte, the longer it will take to elute. Once eluted, the analytes introduced into a MS system are ionized by application of high temperature in combination with a voltage resulting in the ions moving

from the liquid to gas phase. The gaseous analytes are then applied to an analyser that will determine the mass-to-charge value of the analyte (Kebarle, 2000). The mass-to-charge value is a unique signature of a peptide/analyte.

An analyte can be analysed further by Tandem-MS/MS. In this method, the gaseous analyte is fragmented by collision with atoms of an inert gas (helium or nitrogen). Fragmented analytes will re-enter the MS analyser and the new mass-to-charge ratio re-evaluated. The fragmentation occurs in between amino acid residues and the sequence of the peptide can be assessed using analysis software (PEAKS).

In conclusion, mass spectrometry is a powerful tool to assess which peptides are present in a sample and can analyse all peptides in the same sample. Recently, LC-MS/MS is becoming a prominent method to assess the peptides in a sample as well as to quantify them (Chambers *et al.*, 2014; Cox *et al.*, 2016; Kay *et al.*, 2017).

4.1.4 Aims

To generate novel monoclonal antibodies for the bioactive versions of the human guanylin and uroguanylin peptides by:

e) Generating hybridoma antibodies by immunisation of mice.
f) Naïve phage display using biotinylated-Guanylin or biotinylated-Uroguanylin.
g) Screening the clones of interest in ELISA assays and competition ELISA.
h) Affinity maturation of the lead clones to improve affinity to their targets by phage or ribosome display.
i) Developing an IP method to pull out the peptides from human samples and measure them by mass spectrometry.

4.2 Results

4.2.1 Generation of a monoclonal antibody against guanylin by a hybridoma campaign

As described in Chapter 3, a hybridoma campaign was performed to generate specific antibodies to the historically known active peptides. Mice were immunised with 100µg of KLH-Guanylin and KLH-Uroguanylin over a 28-day immunisation programme. Serum titres (prebleed, day 13 and day 20) were measured by ELISA for binding to biotinylated peptides. Low serum titres were obtained for the mice immunised with KLH-Guanylin or KLH-Uroguanylin (data not shown). This result was not unexpected since KLH is a high molecular weight (MW) and immunogenic protein, most of the immune response would be targeted against it. Conversely only a small fraction of the immune response would be directed against the peptides linked to it because they are composed of very small numbers of amino acids (guanylin: 15 amino acids; uroguanylin: 16 amino acids).

Hybridomas were generated from lymphocytes extracted from all immunised mice as no difference could be made between serum titres among each group. IgG-secreting colonies were then picked and screened for their specificity to guanylin and uroguanylin. The percentages of IgG secreting for the two immunising antigen groups are shown in table 4.1.

	KLH-Guanylin	KLH-Uroguanylin
Hybridoma colonies	2598	3358
IgG secreting colonies	376	961
% of IgG secreting colonies	14.4%	28.6%
HTRF binders to biotinylated antigens	9	0
ELISA binders to KLH peptides	10	26
Binder after primary screen	19	26
% of binders/IgG secreting colonies	2.7%	2.7%
Binders after further characterisation	1	0

Table 4.1: Summary of the hybridoma campaign to guanylin and uroguanylin targets. All IgG-secreting hybridomas were picked and IgGs screened in the primary screens. The table contains the final results of binders after characterisation.

4.2.2 Screening of hybridoma clones and specificity

All IgG-secreting hybridoma colonies were tested for binding to the biotinylated targets in a HTRF direct binding assay. Among the 1337 IgG supernatants tested, 9 clones bound biotinylated-Guanylin, whereas no clones bound biotinylated-Uroguanylin (table 4.1). It was possible that due to the small size of guanylin and uroguanylin, biotinylation of the peptides may have affected their conformation or sterically hindered binding of antibodies to the

peptides, leading to the low or null number of binders observed. An ELISA using the KLH conjugated peptides was used as an alternative assay to screen for potential binders. The ELISA identified 26 binders to KLH-Uroguanylin and 10 additional binders to KLH-Guanylin.

The specificity of the 45 antibodies was confirmed using an ELISA assay against each potential target and negative controls: biotinylated-Guanylin, biotinylated-ProGuanylin, biotinylated-ProUroguanylin, biotinylated-Uroguanylin, Guanylin-KLH, Uroguanylin-KLH and KLH only. The ELISA was performed at a single sample dilution (figure 4.3). Four out of 9 antibodies for the biotinylated-Guanylin showed specificity against its antigens. All binders to KLH peptides were cross-reactive to KLH-Guanylin and KLH-Uroguanylin. The antibody AB1000001 (raised against KLH-Guanylin) was able to bind the biotinylated-Guanylin, but also able to bind the coated biotinylated-ProGuanylin.

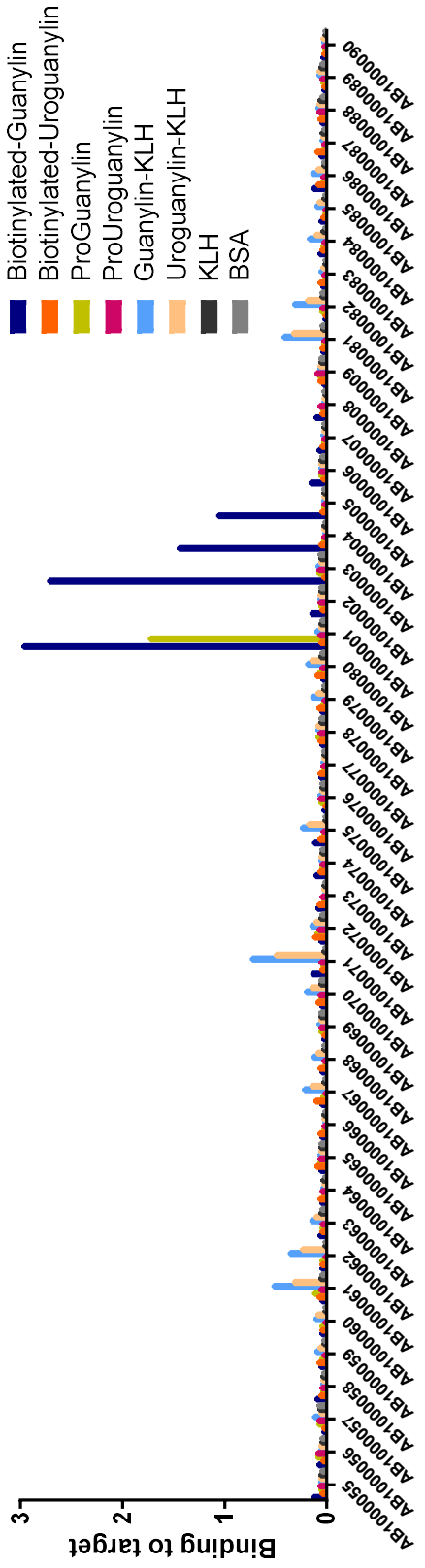

Figure 4.3: Screening for guanylin and uroguanylin specific clones by direct binding ELISA on the antibodies produced from the hybridoma campaign. A direct binding ELISA was performed on the positive IgG-secreting hybridoma colonies clones selected by the HTRF assay where 9 clones were found to bind to biotinylated-Guanylin and none were found to bind to biotinylated-Uroguanylin. 19 and 26 more clones were found binding to Guanylin-KLH and Uroguanylin-KLH respectively and were characterised further.

To identify antibodies directed against guanylin and uroguanylin, the ten strongest cross-reactive binders to KLH-Guanylin and KLH-Uroguanylin were analysed in a competition ELISA. An increasing concentration of free guanylin or uroguanylin was used to compete against a constant concentration

of coated KLH-Guanylin or KLH-Uroguanylin. None of the antibodies that were isolated from the KLH-peptide screening bound the free peptides (figure 4.4 B and C). This finding may be explained if these clones recognise epitope(s) at the C-termini of the peptides where they bind KLH. This is further supported by the observation that the C-termini of the two peptides are almost identical.

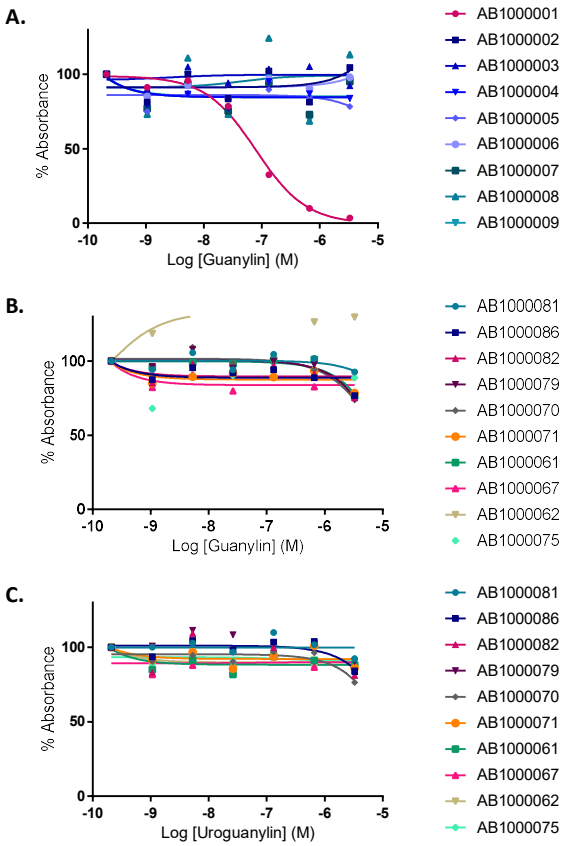

Figure 4.4: Characterisation of guanylin peptides antibodies isolated from the hybridoma campaign. A. Competition ELISA performed on the strongest binders to biotinylated-Guanylin. Serially diluted concentrations of free guanylin were used to compete against a constant concentration of coated biotinylated-Guanylin. AB100001 in pink binds Free guanylin. **B** and **C.** Competition ELISA performed on the strongest binders to peptide-KLH. Serially diluted concentrations of free peptide were used to compete against a constant concentration of coated peptide-KLH. None of the antibodies bind free guanylin or free uroguanylin.

A similar competition ELISA was performed on the clones binding to biotinylated-Guanylin (selected from the HTRF assay). An increasing concentration of free guanylin was used to compete against a constant concentration of coated biotinylated-Guanylin. The titratable effect of free guanylin was only observed in AB1000001, indicating specific binding. No titratable effect was observed for the eight other antibodies. This suggests that biotinylation was a critical structural determinant of the epitope recognised by these antibodies (figure 4.4C).

The cross-reactivity of AB1000001 to guanylin and ProGuanylin in the single-point specificity was further investigated. An ELISA was performed with fixed amount of biotinylated-ProGuanylin or biotinylated-Guanylin captured on the plate against a titration of AB1000001 (figure 4.5A and B). The dose-dependent signals observed for both ProGuanylin and guanylin indicated that AB1000001 recognises both antigens. However, when AB1000001 was coated to the plate followed by incubation with dilution series of biotinylated-ProGuanylin or biotinylated-Guanylin, in solution dose dependent binding was detected only for biotinylated-Guanylin (figure 4.5C and D). In conclusion, AB1000001 is specific for guanylin when it is in solution and not bound to an assay plate. The binding to ProGuanylin when immobilised was most likely an *in vitro* artefact as a result of biotinylated-ProGuanylin presenting non-conformational epitopes.

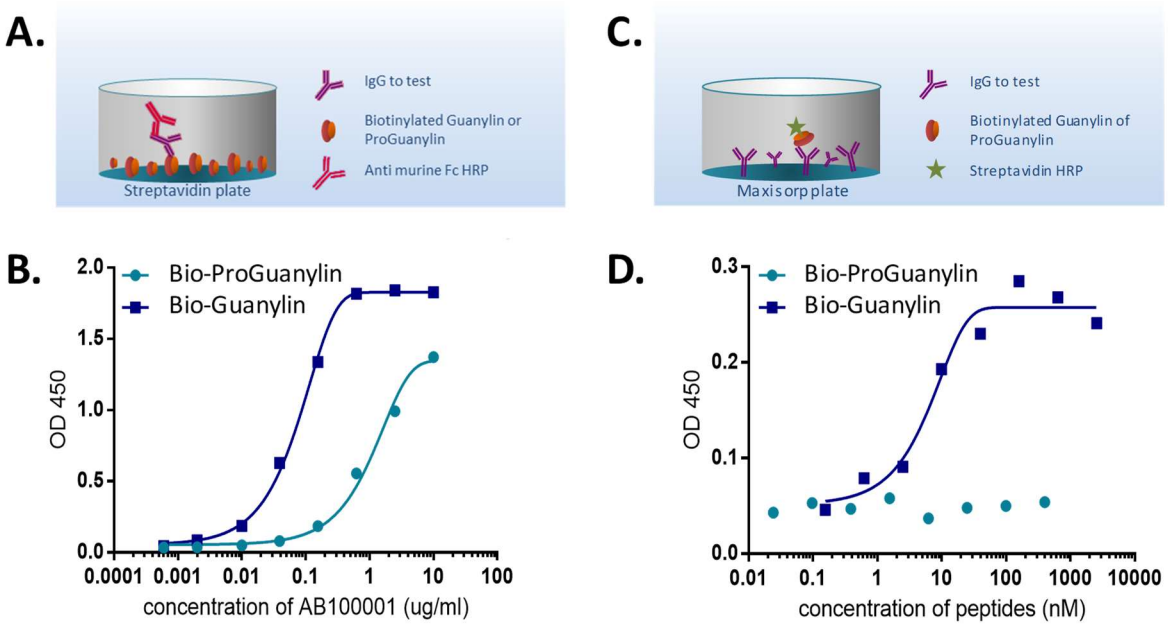

Figure 4.5: Specificity characterisation of AB1000001 for guanylin and ProGuanylin. In **A.** and **B.**, biotinylated-Guanylin or biotinylated-ProGuanylin was immobilised to a streptavidin plate and incubated with a dilution series of AB1000001, followed by antimouse IgG HRP detection. In **C.** and **D.**, AB1000001 was immobilised to a Maxisorp plate and incubated with a dilution series of biotinylated-Guanylin or biotinylated-ProGuanylin, followed by streptavidin-HRP detection.

Despite the high number of clones screened, no specific antibodies against uroguanylin were found using the hybridoma technique, and only one antibody AB1000001 was specific to guanylin.

Clones that bound to biotinylated-Guanylin, Guanylin-KLH or Uroguanylin-KLH were identified in the primary screen. After further detailed characterisation, the binders to Guanylin-KLH and

Uroguanylin-KLH were found to be cross-reactive and did not bind the free peptide. It is highly possible that the clones that bound Guanylin-KLH and Uroguanylin-KLH were binding the link between the KLH and the peptide. Identity between human peptides and mouse endogenous peptides is high: 93% and 81% for guanylin and uroguanylin, respectively. Therefore, the mice immune response during the hybridoma campaign would generate antibodies against non-identical parts of the peptides. The main immune response was directed against the KLH or the peptides' C-terminal epitope linked to KLH. Also, the C-termini of the peptides have a strong identity between guanylin and uroguanylin which may account for the cross-reactivity.

4.2.3 Lead isolation of guanylin and uroguanylin binders by Naïve Phage Display Selection

Antibodies targeting guanylin or uroguanylin were generated using a naïve phage display selection approach. Three naïve bacteriophage libraries were used: Bone Marrow Vault$_{trp}$ (BMV$_{trp}$) library which was isolated from bone marrow, Combined Spleen$_{trp}$ (CS$_{trp}$) isolated from spleen and DP47$_{trp}$ a library based on the V_H CDR3 framework of the DP-47 gene segment, the most frequently used V_H gene segment in the V_H gene rearrangements (Brezinschek *et al.*, 1997).

Libraries were selected for 2 rounds, with the first round of selection performed using 100nM of biotinylated human guanylin (or uroguanylin) followed by a second round of selection using 50nM biotinylated human guanylin (or uroguanylin). To remove guanylin/uroguanylin cross-reactive clones, de-selections were performed using 1µM of the opposite free peptide. Output titres were measured at each round of selection and reported in tables 4.2 and 4.3.

	Selection performed for Lead Isolation of clones to guanylin					
Round of selection	BMVtrp	CStrp	DP47	BMVtrp	CStrp	DP47
Round 1: 100nM biotinylated-Guanylin	Deselected with free uroguanylin			No deselection		
Output titre CFU/ml	3700	1900	7600	3500	4000	1500
Round 2: 100nM biotinylated-Guanylin	Deselected with free uroguanylin			Deselected with free uroguanylin		
Output titre CFU/ml	5.50E+05	2.13E+06	2.08E+03	1.88E+05	8.40E+06	7.80E+04

Table 4.2: Round of selection and output of initial lead Isolation of clones against human guanylin by phage display selection. Round 1 of selection used 100nM biotinylated human guanylin and half of the libraries were de-selected against 1µM free human uroguanylin. Round 2 used 50nM biotinylated human guanylin and all libraries were subjected to a de-selection against 1µM free human uroguanylin.

	Selection performed for Lead Isolation of clones to uroguanylin					
Round of selection	BMVtrp	CStrp	DP47	BMVtrp	CStrp	DP47
Round 1: 100nM biotinylated-Uroguanylin	Deselected with free guanylin			No deselection		
Output titre CFU/ml	3100	1100	1500	3100	1100	1500
Round 2: 100nM biotinylated-Uroguanylin	Deselected with free guanylin			Deselected with free guanylin		
Output titre CFU/ml	6.75E+05	4.74E+06	1.84E+05	1.34E+06	1.59E+06	1.82E+05

Table 4.3: Round of selection and output of initial lead Isolation of clones against human uroguanylin by Phage Display selection. Round 1 of selection used 100nM biotinylated human uroguanylin and half of the libraries were de-selected against 1µM free human guanylin. Round 2 used 50nM biotinylated human uroguanylin and all libraries were subjected to a de-selection against 1µM free human guanylin.

The output titre is a quality control measurement of the selection method and an expected output titre would be 10^3-10^6 colony forming units (cfu) per ml. Selections were performed at a high concentration of biotinylated target, however the first round of selection gave low output titres. The similar step without deselection did not particularly increase the output titres. The second round of selection was performed with a de-selection step giving expected titres but most probably with a low sequence diversity. The diversity per library selection was not calculated due to costs.

4.2.4 Screening of clones from the Lead isolation by phage display

Eighty-eight scFv binders to guanylin and 176 scFv binders to uroguanylin were isolated and crude fractions of scFvs were prepared and analysed in a single-point binding ELISA. Positive clones were sequenced and ten unique binders to each target with high sequence diversity were expressed as scFvs by the Biologics Expression team at MedImmune. The 10 purified scFvs were characterised by ELISA and the scFv concentration giving 80% of the maximal absorbance was used to perform a competition ELISA. This assay was performed to assess scFvs' ability to bind the free peptide version (figure 4.4A and 4.5A). A smaller panel of 5 clones were consequently selected for IgG conversion and the V_H and V_L sequence were cloned into murine pEU vectors (IgG1 format). Similar binding assays were performed on the panel of antibodies (figure 4.4B and 4.5B) and IC_{50} were calculated for the 5 IgGs. IC_{50} measurements are summarised in table 4.5.

For the uroguanylin binders, AB1000107 antibody was the strongest uroguanylin binder with an IC_{50} of 850nM. A second antibody AB1000110 displayed a similar affinity but was cross-reactive to guanylin (data not shown). AB1000107's affinity to uroguanylin was low and required optimisation.

For the guanylin binders, antibodies from the phage display's isolation did not present a lower IC_{50} when compared to the hybridoma antibody AB1000001. The strongest guanylin binders from the lead isolation were AB1000092 and AB1000093 with a measured IC_{50} of 519nM and 692nM, respectively. AB1000001, AB1000092 and AB1000093 antibodies did not display a sufficient affinity for guanylin therefore affinity maturation was required.

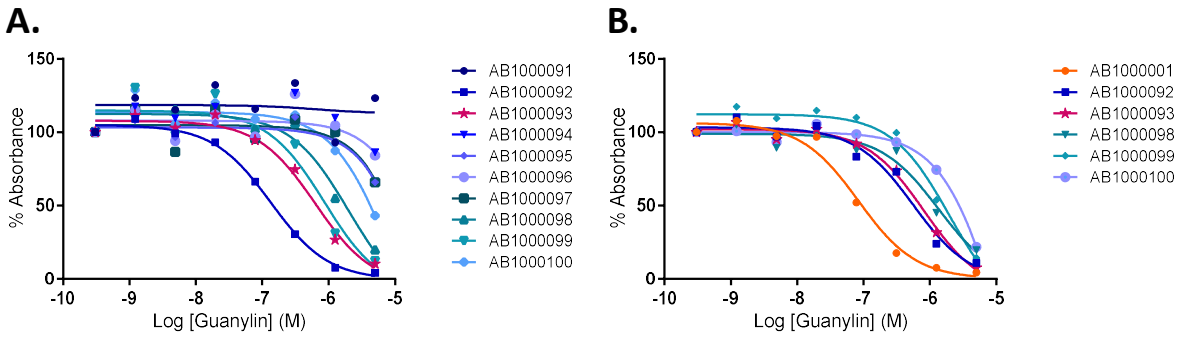

Figure 4.4: Characterisation of the guanylin binders' scFv and IgGs from the lead isolation by phage display. A competition ELISA was performed on the 10 leads expressed as scFv in (**A.**) and on the 6 leads expressed as IgGs in (**B.**) The clone represented in orange is the IgG obtained from the hybridoma campaign and used subsequently for lead optimisation by error-prone mutagenesis. The clone represented in pink was used subsequently for lead optimisation by site-directed mutagenesis.

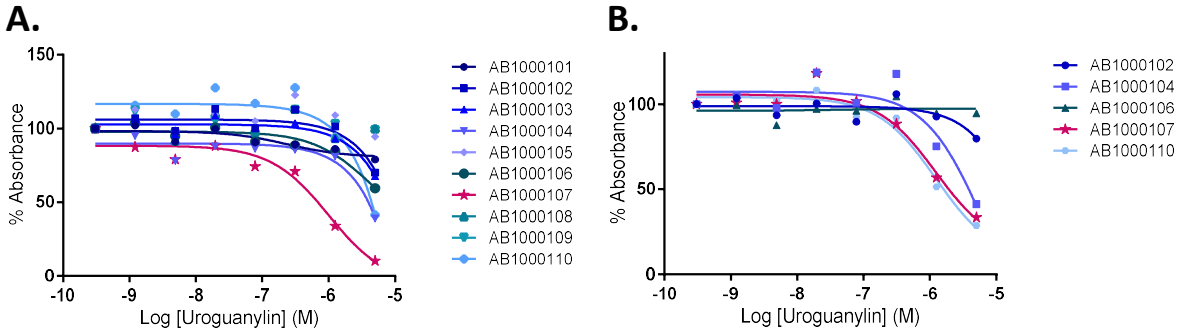

Figure 4.5: Characterisation of the uroguanylin binders' scFv and IgGs from the lead isolation by phage display. A competition ELISA was performed on the 10 leads expressed as scFv in (**A.**) and on the 6 leads expressed as IgGs in (**B.**) The clone represented in pink was used subsequently for lead optimisation by site-directed mutagenesis

4.2.5 Affinity maturation by targeted mutation on V_H and V_L CDR3

A summary of the lead optimisation of the antibodies against guanylin or uroguanylin was performed using different methods which are summarised in two flow charts: figures 4.7 and 4.9.

While AB1000001 has a stronger IC_{50} to guanylin compared to AB1000092 and AB1000093, experience at MedImmune showed that antibodies originating from a hybridoma campaign, would have already matured their CDR3 through rounds of *in vivo* selection. The V_H CDR3 of

AB1000092 was shorter than the V_H CDR3 of AB1000093 which reduced the possibility for mutations. AB1000092 was subsequently discarded and affinity maturation by targeted mutation on the V_H and V_L CDR3 was performed on AB1000093 for guanylin and AB1000107 for uroguanylin.

For maturation, two overlapping libraries targeting the V_H CDR3, and two overlapping libraries targeting the V_L CDR3 were generated for each antibody, culminating in a total of 8 scFv phage libraries. Libraries were produced by Kunkel reaction, replacing 6 consecutive codons with NNS codons (where N=A/C/G/T and S=C/G) in the CDRs. Four rounds of selection were proceeded on all libraries using more stringent conditions than during the lead isolation. While the first round of selection was performed using a concentration of 100nM of biotinylated-peptide, the last round of selection used a concentration of 400pM of biotinylated-peptide (figure 4.6).

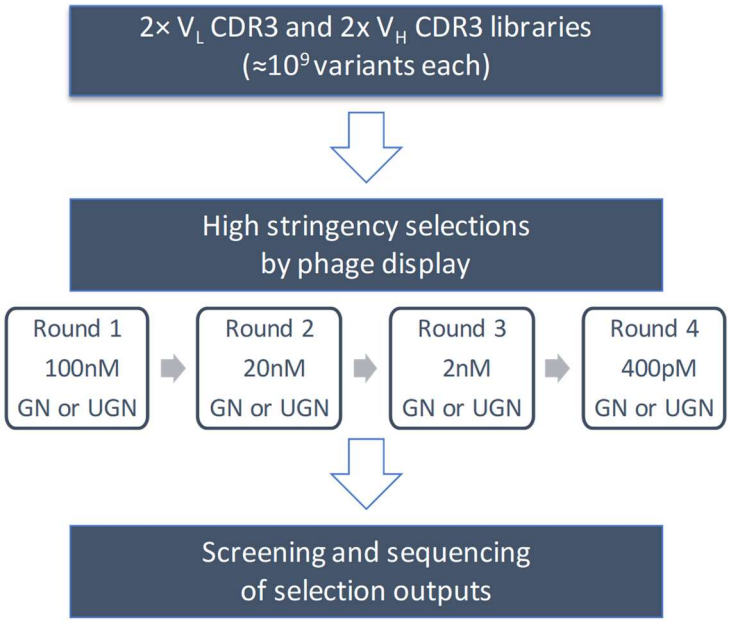

Figure 4.6: Flow chart summarising the lead optimisation by phage display selection after site-directed mutagenesis. Two site-directed mutagenesis were performed on each V_H and V_L to cover the CDR3 sequence. The 8 libraries were selected by phage display over 4 rounds of selection using 100nM, 20nM, 2nM and 400pM of biotinylated-target antigen and de-selected against 1µM free human guanylin or uroguanylin. The round 4 was screened in Phage ELISA and positive clones were sequenced and further characterised.

Output titres for the maturation selection ranged from 2.2 x10^5 to 8.7 x 10^7 and sequencing diversity was assessed (table 4.4). Amino acid sequences are not shown due to MedImmune confidentiality.

Library	Antigen	Output titres (cfu/ml)				Sequence diversity	
		R1	R2	R3	R4	R2	R4
93H3.1	Guanylin	2.6E+07	4.4E+07	3.4E+07	3.2E+07	100%	100%
93H3.2	Guanylin	1.4E+06	2.7E+06	1.5E+06	4.8E+05	100%	68%
93L3.1	Guanylin	2.6E+05	1.2E+07	1.0E+07	4.7E+06	100%	64%
93L3.2	Guanylin	3.3E+05	1.1E+07	6.4E+06	3.3E+06	93%	78%
107H3.1	Uroguanylin	1.3E+07	5.7E+07	4.0E+07	1.8E+07	93%	84%
107H3.2	Uroguanylin	2.2E+05	6.7E+07	4.4E+07	4.0E+06	93%	41%
107L3.1	Uroguanylin	2.2E+07	5.7E+07	4.7E+07	1.2E+07	93%	63%
107L3.2	Uroguanylin	8.7E+07	6.4E+07	3.6E+07	5.6E+06	98%	34%

Table 4.4: Output titres and sequence diversity of selections from affinity maturation of AB1000093 and AB1000107. Rounds 1, 2, 3 and 4 of selection used 100nM, 20nM, 2nM and 400pM of biotinylated human guanylin or uroguanylin respectively. The % sequence diversity across each library was calculated from the number of unique sequences within 44 clones.

All single picked clones were prepared as crude fractions of scFvs and analysed in a single-point binding ELISA. The strongest binders were expressed as scFvs by the biologics expression team at MedImmune and those 11 purified scFvs were characterised by competition ELISA to assess their ability to bind the free peptide version (figure 4.8A and 4.10A).

For the uroguanylin binders (figure 4.8A), the clones did not show a major improvement with only a two-fold improvement in IC_{50} compared to the parent clones AB1000107. It was decided to perform a maturation of the antibodies differently using an error prone mutagenesis on the 5 clones which presented a slight improvement in IC_{50}. AB1000126, AB1000127, AB1000128, AB1000131 and AB1000133) scFvs were pooled for a next step of optimisation.

For the guanylin binders (figure 4.10A), all the clones presented an improvement compared to the parent clone AB1000093. While the clones coming from the V_H CDR3 site-directed mutagenesis (AB1000136-AB1000145) had a similar improvement in affinity, the clone coming from the V_L CDR3 site-directed mutagenesis AB1000146 had the strongest affinity improvement with an IC_{50} of 2.1nM (300-fold improvement). Five of the 10 clones that showed an improvement from the V_H CDR3 site-directed mutagenesis (AB1000137, AB1000139, AB1000142, AB1000144 and AB1000145) were selected to be expressed as IgG with either the light chain from the progenitor clone (AB1000093) or the light chain from the clone AB1000146. AB1000146 light chain was also co-expressed with the parental heavy chain AB1000093. Due to rearranging heavy and light chains, the IgGs had to be nicknamed differently: Flo08-Flo18. A summary of the antibody panel is shown in table 4.5. Antibodies were compared in a final competition assay to assess their ability to bind the free peptide and

compare their IC_{50} (figure 4.10B). The antibody with the largest improvement was Flo13 (IC_{50} = 3.2nM).

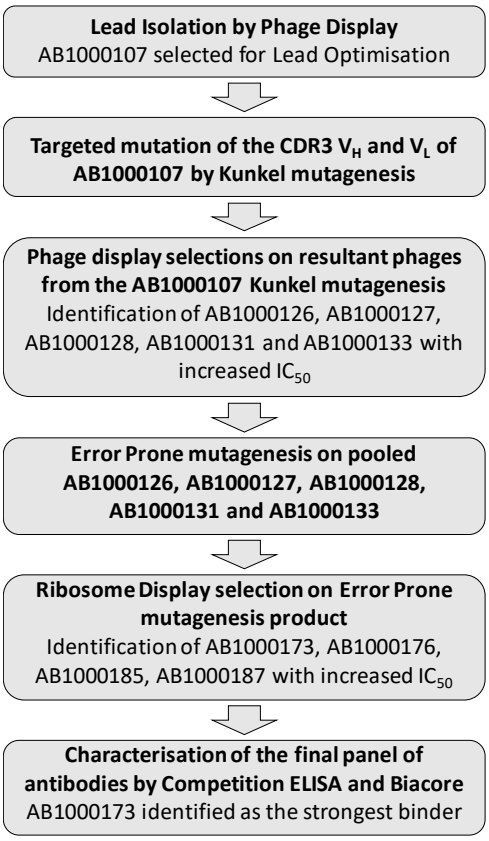

Figure 4.7: Flow chart summarising the generation of antibodies against uroguanylin.
Lead isolation was performed by phage display. Site-directed mutagenesis of the V_H and V_L CDR3 were performed on one variant followed by further rounds of phage display selection. The resultant phages with increased IC_{50} were pooled and error prone mutagenesis was performed on them. Ribosome display selection were performed, and the final characterisation identified AB1000173 as the lead antibody to detect uroguanylin.

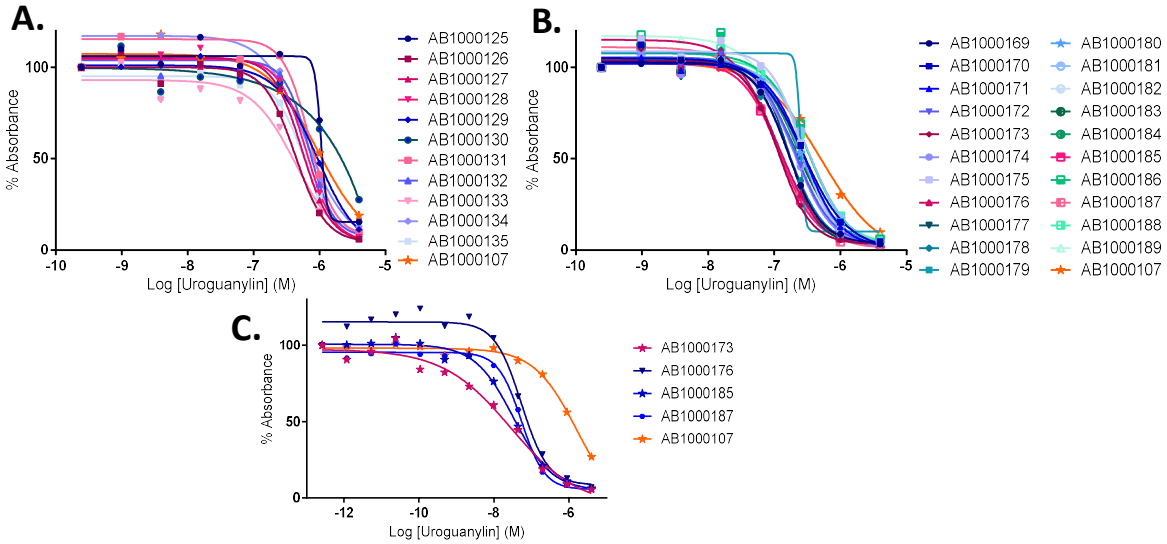

Figure 4.8: Characterisation of the uroguanylin scFv and IgG binders from the lead optimisation. In (**A.**) a competition ELISA was performed on the 11 scFv leads from the site-directed mutagenesis. (**B.**) presents the panel of scFvs generated by error prone mutagenesis on the pool of scFvs with higher IC_{50} compared to the parent AB1000107 (AB1000126, AB1000127, AB1000128, AB1000131 and AB1000133) in a competition ELISA. In (**C.**) the 4 leads expressed as IgGs were compared in a final competition ELISA including the parent antibody AB1000107. The clone represented in orange is the parental clone used for lead optimisation. The clones represented in pink are the leads from each step of the optimisation.

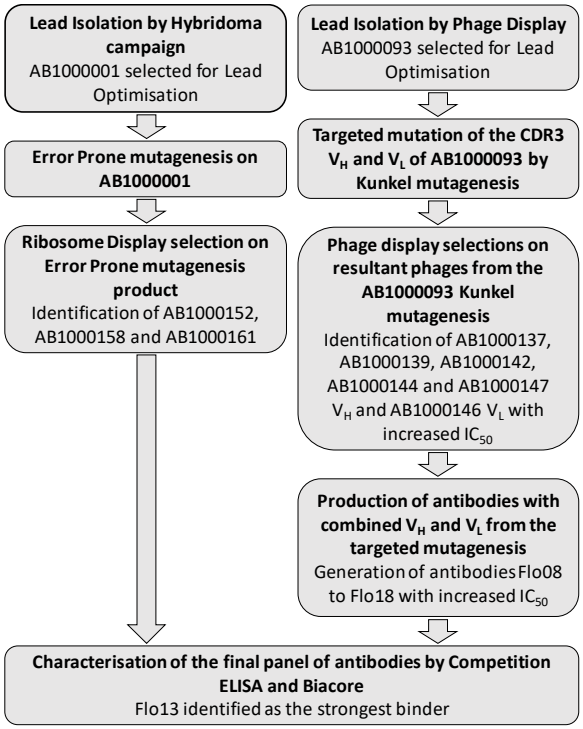

Figure 4.9: Flow chart summarising the generation of antibodies against guanylin. Lead Isolation was performed both by hybridoma and a phage display campaign. Error prone mutagenesis was performed on AB1000001 identified from the hybridoma campaign followed by ribosome display selection. Site-directed mutagenesis of the V_H and V_L CDR3 was performed on the variant identified by phage display. V_H and V_L with higher IC_{50} were recombined to generate a new panel of antibodies. Final characterisation of the panel of antibodies identified Flo13 as the lead antibody to detect guanylin.

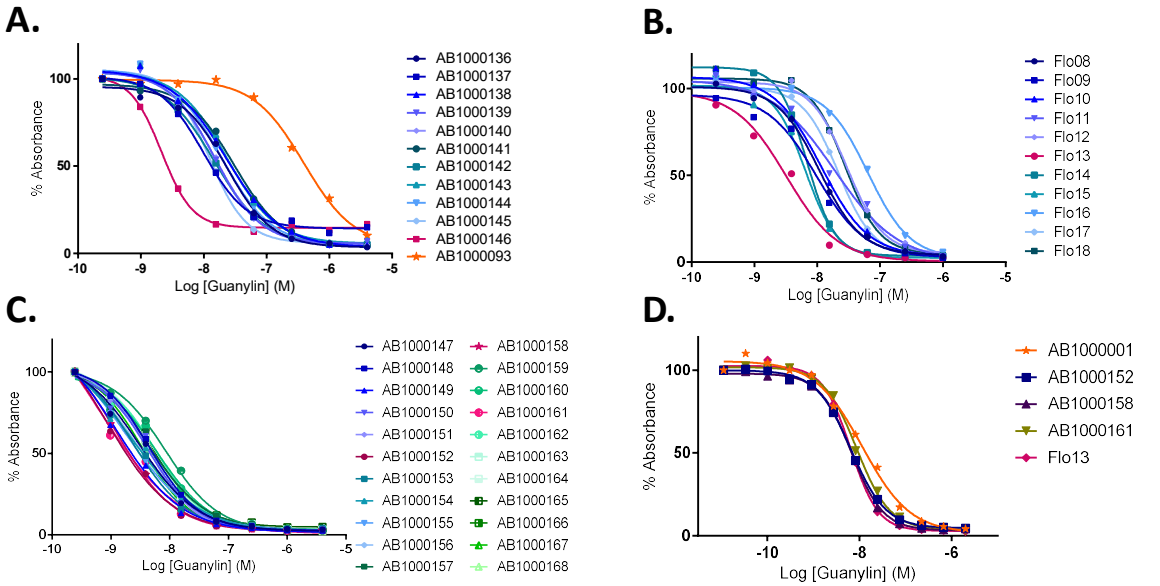

Figure 4.10: Characterisation of the guanylin scFv and IgG binders from the lead optimisation. In (**A.**) a competition ELISA was performed on the 11 scFv leads from the site-directed mutagenesis. In (**B.**) the antibodies generated from the V_H and V_L recombination from these scFvs where tested in a competition ELISA. In (**C.**) a competition ELISA was performed on 22 scFvs from the lead optimisation by error-prone mutagenesis. In (**D.**) the 3 leads expressed as IgGs were compared in a final competition ELISA including the parent antibody AB1000001 and the best antibodies from the lead optimisation by site directed mutagenesis Flo13.
The clones represented in orange are the parental clones used for lead optimisation. The clones represented in pink are the leads from the optimisation and were used for further characterisation.

4.2.6 Affinity maturation by error prone mutagenesis on AB1000001 and affinity matured products of AB1000107

The aim of the lead optimisation steps was to obtain antibodies with low nanomolar to subnanomolar affinity for guanylin or uroguanylin. The antibodies isolated did not present a high enough affinity, especially for the uroguanylin binders.

An alternative approach had to be considered to improve the binding to the targets. When the site directed mutagenesis of the V_L and V_H CDR_3 is unsuccessful to reach an affinity target, another commonly used method is error prone mutagenesis on the scFv sequence. In error prone ribosome display libraries, prior to subsequent rounds of selection, mutations are introduced into the mRNA using low-fidelity DNA polymerase for amplification, resulting in error-prone PCR. An advantage of ribosome display compared to other selections method is that more mutations can be introduced after each round of selection allowing directed evolution.

Uroguanylin AB1000126, AB1000127, AB1000128, AB1000131 and AB1000133 scFvs sequences were pooled together. Those scFvs originated from the lead optimisation by phage display of the parent clone AB1000107 and were identified as 107pool. Three rounds of error prone mutagenesis were performed on the 107pool as well as the AB1000001 sequence (Cf. 4.2.1 and 4.2.2). The mutated DNA was transcribed in vitro, and the mRNA was translated using a cell-free system allowing the generation of a stabilised mRNA-ribosome complex displaying a scFv. Three rounds of selections on the mutated 107pool or mutated AB1000001 were performed on the complex by binding to the immobilised target biotinylated-Uroguanylin or biotinylated-Guanylin respectively at 10nM, 2nM and 400pM. The mRNA was reverse transcribed, and the signal was amplified by PCR. The final amplification was enzyme-restricted and ligated into pCantab6 vectors.

Once transformed into *E. coli*, 176 clones were picked after the third round of selection and crude fractions of scFvs were prepared and analysed in a single-point binding ELISA. The 24 strongest binders with specific sequences that produced a signal in the ELISA were selected and expressed as scFvs by the biologics expression team at MedImmune. Purified scFvs were characterised by competition ELISA to assess their ability to bind the free peptide version and measure their IC_{50}.

For the uroguanylin binders, all clones showed an improvement in IC_{50} compared to the progenitor AB1000107 in the scFv competition ELISA (figures 4.8B). Four binders (AB1000173, AB1000176, AB1000185 and AB1000187) presenting the strongest affinity were reformatted into IgG and tested once again in a competition ELISA (figure 4.8C). A clone presenting 2 changes in its V_H CDR2, AB1000173, displayed the best improvement with an IC_{50} of 28nM.

For the guanylin binders, three clones AB1000152, AB1000158 and AB1000161 were reformatted into IgG and tested in a competition ELISA (figures 4.10C and 4.10D). They showed a 10-fold improvement in IC_{50} than its progenitor AB1000001 (6.5nM, 6.6nM and 8.7nM). However, those clones did not show a stronger affinity than the IgG Flo13, which came from the lead isolation/optimisation by phage display and presented an IC_{50} of 3.2nM. (Cf. table 4.5)

4.2.7 Determination of the binding specificity of the panel of antibodies

A panel of 4 antibodies were selected for a final affinity measurement using the Biacore T100 instrument. Two of the antibodies binding guanylin (Flo13 and AB1000152) and two of the antibodies binding uroguanylin (AB1000173 and AB1000185) were covalently bound to a CM3 chip by amine coupling. Different concentrations of the guanylin and uroguanylin allowed the measurement of the binding constants using a 1:1 binding model. The sensorgrams presenting the binding of Flo13 and AB1000152 to guanylin and AB1000173 and AB1000185 to uroguanylin are presented in figure 4.11 and the binding constants are summarised in table 4.5.

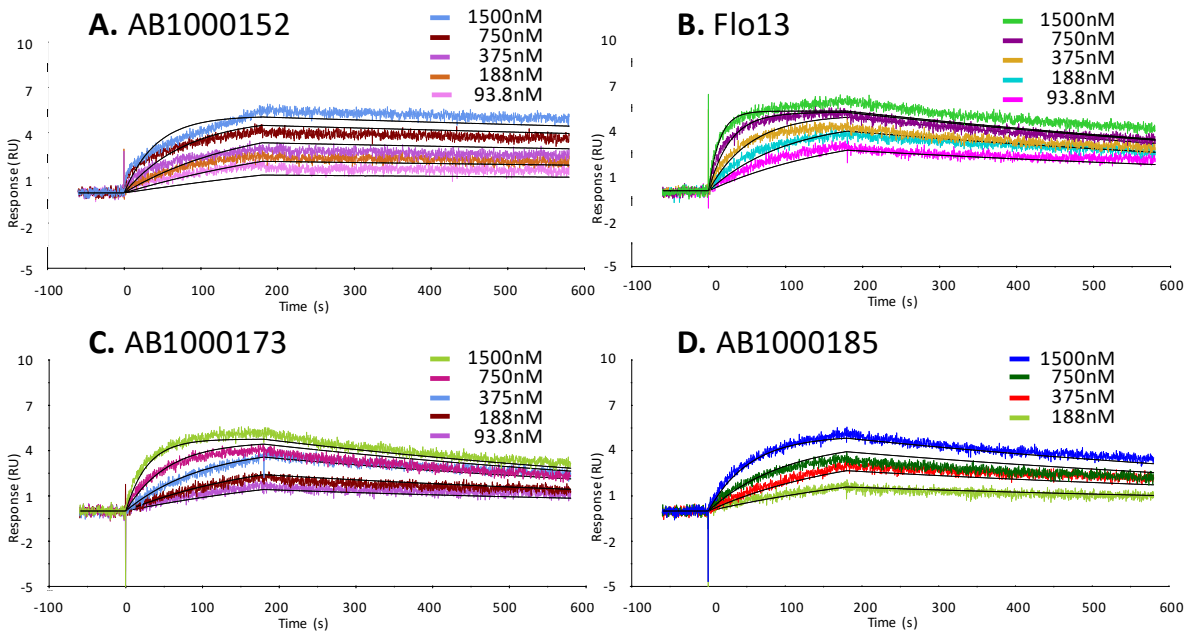

Figure 4.11: Determination of the antibodies' affinity to their targets using Biacore.
Kinetic binding experiment with antibodies (**A.**) AB1000152 (**B.**) Flo13 (**C.**) AB1000173 (**D.**) AB1000185 on the Biacore T100 instrument (Response Units (RU) as function of time). The antibodies were immobilised at 10µg/mL on the CM3 chip. The flow rate was 50µL/min, the contact time was 180 seconds while the dissociation time was 400 seconds. The data was analysed using the Biacore T100 evaluation software using a 1:1 binding model and the fit is represented by the black lines.
In (**A.**) and (**B.**) guanylin was used at a concentration ranging between 93.8nM and 1500nM. In (**C.**) uroguanylin was used at a concentration ranging between 93.8nM and 1500nM. In (**D.**) uroguanylin was used at a concentration ranging between 187.5nM and 1500nM.

All tested antibodies presented a nanomolar affinity for either guanylin or uroguanylin. The Biacore T100 evaluation software managed to fit the curves properly using a 1:1 binding model for all antibodies to their target; but, the response unit was low and the signal noisy. The small size of guanylin and uroguanylin, 15 and 16 amino acids respectively, are responsible for the sensorgrams' quality and are not uncommon in the literature for such small peptides (Zhang and Oglesbee, 2003).

The first aim of this chapter was to find pairs of antibodies that would bind guanylin or uroguanylin in an immunoassay. Concerned by the size of the peptides and potential steric hindrance from each of the antibody, the plan was to use the antibodies for either immunoprecipitation or use of magnetic beads coated with the antibodies to isolate the peptides. Once isolated from serum, plasma or supernatants, levels of guanylin peptides could be measured by mass spectrometry. Commercially available guanylin or uroguanylin could be used as standards to develop a quantitative method.

Antibody name	Target	Origin	Heavy chain name	Light chain name	scFv IC_{50} measured by Competition ELISA	IgG IC_{50} measured by Competition ELISA	KD measured by Bioacore
AB1000001	Guanylin	Hybridoma selection	AB1000001 VH	AB1000001 VL	Not Applicable	7.66E-08	
AB1000092	Guanylin	Lead Isolation by Phage Display	AB1000092 VH	AB1000092 VL	1.34E-07	5.19E-07	
AB1000093	Guanylin	Lead Isolation by Phage Display	AB1000093 VH	AB1000093 VL	6.31E-07	6.92E-07	
AB1000098	Guanylin	Lead Isolation by Phage Display	AB1000098 VH	AB1000098 VL	1.97E-06	9.21E-07	
AB1000099	Guanylin	Lead Isolation by Phage Display	AB1000099 VH	AB1000099 VL	8.63E-07	1.12E-06	
AB1000100	Guanylin	Lead Isolation by Phage Display	AB1000100 VH	AB1000100 VL	8.23E-06	5.72E-06	
AB1000102	Uroguanylin	Lead Isolation by Phage Display	AB1000102 VH	AB1000102 VL	1.11E+00	1.33E-06	
AB1000104	Uroguanylin	Lead Isolation by Phage Display	AB1000104 VH	AB1000104 VL	5.03E-03	1.26E-06	
AB1000106	Uroguanylin	Lead Isolation by Phage Display	AB1000106 VH	AB1000106 VL	4.37E-06	N/D	
AB1000107	Uroguanylin	Lead Isolation by Phage Display	AB1000107 VH	AB1000107 VL	1.00E-06	8.59E-07	
AB1000110	Uroguanylin	Lead Isolation by Phage Display	AB1000110 VH	AB1000110 VL	1.75E-03	8.70E-07	
AB1000126	Uroguanylin	Lead Optimisation of AB100107 by targeted CDR modification	AB1000126 VH	AB1000107 VL	2.59E-07	1.056E-07	
AB1000127	Uroguanylin	Lead Optimisation of AB100107 by targeted CDR modification	AB1000127 VH	AB1000107 VL	1.84E-07	1.476E-07	
AB1000128	Uroguanylin	Lead Optimisation of AB100107 by targeted CDR modification	AB1000128 VH	AB1000107 VL	2.07E-07	3.192E-07	
AB1000131	Uroguanylin	Lead Optimisation of AB100107 by targeted CDR modification	AB1000131 VH	AB1000107 VL	3.35E-07	5.737E-07	
AB1000132	Uroguanylin	Lead Optimisation of AB100107 by targeted CDR modification	AB1000132 VH	AB1000107 VL	1.25E-07	1.136E-07	
AB1000133	Uroguanylin	Lead Optimisation of AB100107 by targeted CDR modification	AB1000133 VH	AB1000107 VL	2.82E-07	1.886E-07	
AB1000135	Uroguanylin	Lead Optimisation of AB100107 by targeted CDR modification	AB1000135 VH	AB1000107 VL	3.68E-07	2.072E-07	
Flo08	Guanylin	Lead Optimisation of AB1000093 by targeted CDR modification	AB1000137 VH	AB1000093 VL	9.896E-09	1.094E-08	
Flo09	Guanylin	Lead Optimisation of AB1000093 by targeted CDR modification	AB1000139 VH	AB1000093 VL	1.493E-08	9.733E-09	
Flo10	Guanylin	Lead Optimisation of AB1000093 by targeted CDR modification	AB1000142 VH	AB1000093 VL	1.476E-08	1.156E-08	
Flo11	Guanylin	Lead Optimisation of AB1000093 by targeted CDR modification	AB1000144 VH	AB1000093 VL	1.912E-08	1.91E-08	
Flo12	Guanylin	Lead Optimisation of AB1000093 by targeted CDR modification	AB1000145 VH	AB1000093 VL	1.21E-08	2.991E-08	
Flo13	Guanylin	Lead Optimisation of AB1000093 by targeted CDR modification	AB1000137 VH	AB1000146 VL	9.896E-09	3.232E-09	2.34E-08
Flo14	Guanylin	Lead Optimisation of AB1000093 by targeted CDR modification	AB1000139 VH	AB1000146 VL	1.493E-08	6.858E-09	
Flo15	Guanylin	Lead Optimisation of AB1000093 by targeted CDR modification	AB1000142 VH	AB1000146 VL	1.476E-08	6.592E-09	
Flo16	Guanylin	Lead Optimisation of AB1000093 by targeted CDR modification	AB1000144 VH	AB1000146 VL	1.912E-08	6.432E-08	
Flo17	Guanylin	Lead Optimisation of AB1000093 by targeted CDR modification	AB1000145 VH	AB1000146 VL	1.21E-08	2.147E-08	
Flo18	Guanylin	Lead Optimisation of AB1000093 by targeted CDR modification	AB1000093 VH	AB1000146 VL	2.123E-09	2.781E-08	
AB1000152	Guanylin	Lead Optimisation by Error Prone mutagenesis on AB1000001	AB1000152 VH	AB1000152 VL	8.523E-10	6.509E-09	2.00E-08
AB1000158	Guanylin	Lead Optimisation by Error Prone mutagenesis on AB1000001	AB1000158 VH	AB1000158 VL	1.247E-09	6.639E-09	
AB1000161	Guanylin	Lead Optimisation by Error Prone mutagenesis on AB1000001	AB1000161 VH	AB1000161 VL	6.327E-10	8.657E-09	
AB1000173	Uroguanylin	Lead Optimisation by Error Prone mutagenesis on Flo01-Flo05	AB1000173 VH	AB1000173 VL	1.155E-07	2.845E-08	5.63E-08
AB1000176	Uroguanylin	Lead Optimisation by Error Prone mutagenesis on Flo01-Flo05	AB1000176 VH	AB1000176 VL	1.113E-07	5.404E-08	
AB1000185	Uroguanylin	Lead Optimisation by Error Prone mutagenesis on Flo01-Flo05	AB1000185 VH	AB1000185 VL	1.192E-07	3.31E-08	9.19E-08
AB1000187	Uroguanylin	Lead Optimisation by Error Prone mutagenesis on Flo01-Flo05	AB1000187 VH	AB1000187 VL	1.147E-07	5.403E-08	

Table 4.5: Affinity results of the panel of scFv and antibodies to their targets. IC_{50} were measured for both the scFv and the IgGs by competition ELISA. The KD was measured for the best binders to guanylin and uroguanylin using the Biacore T100 instrument with a 1:1 binding model.

4.2.7 New knowledge about the sequence of the murine active Guanylin peptide by mass spectrometry

Concomitantly towards the end of the antibodies' lead optimisation, the Gribble/Reimann group developed new protocols and techniques to study peptide levels and secretions from different biological sources. Kay *et al.* looked at peptides from human and mouse colonic tissues' homogenates as well as colonic primary intestinal culture supernatants to detect insulin-like peptide 5 peptides and measured an increase in secretion in response to L-cell stimuli (Kay *et al.*, 2017). A similar method and analysis was applied on mouse and human homogenates in the first instance.

Initial analysis was performed on homogenates from mouse tissues (duodenum, jejunum, ileum, colon and rectum). GUC2A (guanylin) peptides were successfully detected after reduction/alkylation and Nanoflow-LC-MS analysis (figure 4.12). However, the method was not sensitive enough to detect GUC2A peptides in human homogenates. GUC2B (uroguanylin) peptides were not detected in either murine or human tissue homogenates.

The database search matched peptides throughout the entire GUC2A prohormone sequence except for the signal peptide (amino acid residues 1-21). In figure 4.12, blue box represents a sequence identified by LC-MS/MS that matches the murine GUC2A sequence. The peptides peak area (and therefore the concentration of peptide) is represented by the blue gradient. The historically known sequence from Swissprot database is highlighted by the black box below the protein sequence. An interesting observation originating from this peptide search was that the Swissprot entry for the historically known activating guanylin peptide 102-116 was present at extremely low levels in homogenates from jejunum and colon only.

This experiment also highlighted the presence of other GUC2A peptides at higher levels compared to the historically known guanylin peptide 102-116. A version of the known guanylin peptide supplemented by a glutamic acid (D) on the N-terminal (figure 4.13A) was found in murine homogenates from duodenum, jejunum, ileum and colon tissues in detectable levels (figure 4.12). Two other peptides distinguished themselves by the levels found across the tissues (based on peptide peak area): the peptide 22-49 and the peptide 60-116 (figure 4.13B and C). While the peptide 22-49 does not present the C-terminal sequence proposed to activate the GC-C receptor, the peptide 60-116 does.

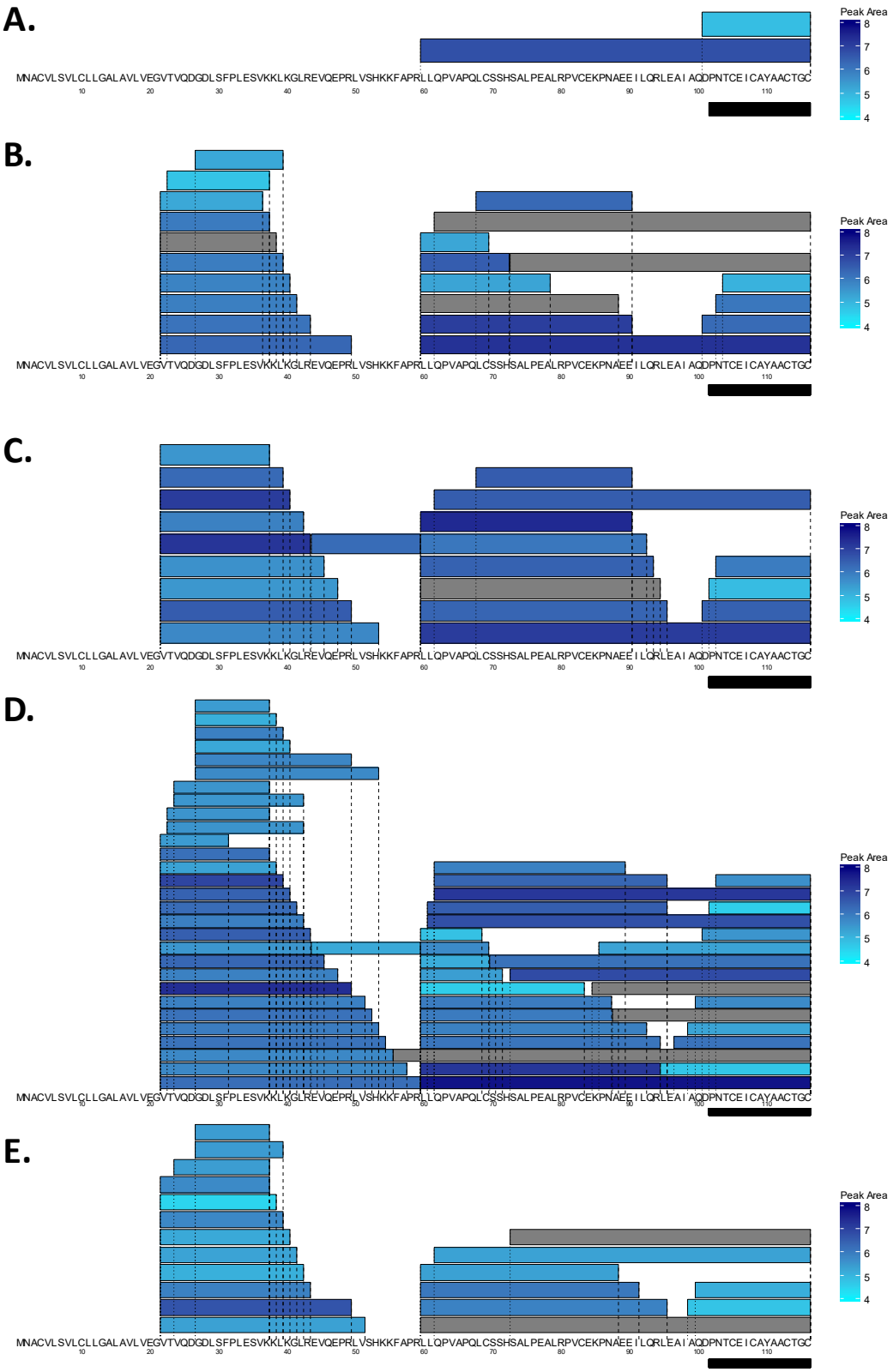

Figure 4.12: GUC2A (guanylin) peptides detected in murine homogenates. Murine homogenates of duodenum (**A.**), jejunum (**B.**), ileum (**C.**), colon (**D.**) and rectum (**E.**) were analysed by LC-MS/MS. Each blue box represents a sequence identified by LC-MS/MS that matches the murine GUC2A sequence. The peptide peak area (log10 scale) is represented by the blue gradient. The historically known sequence from Swissprot database is highlighted by the black box below the protein sequence.

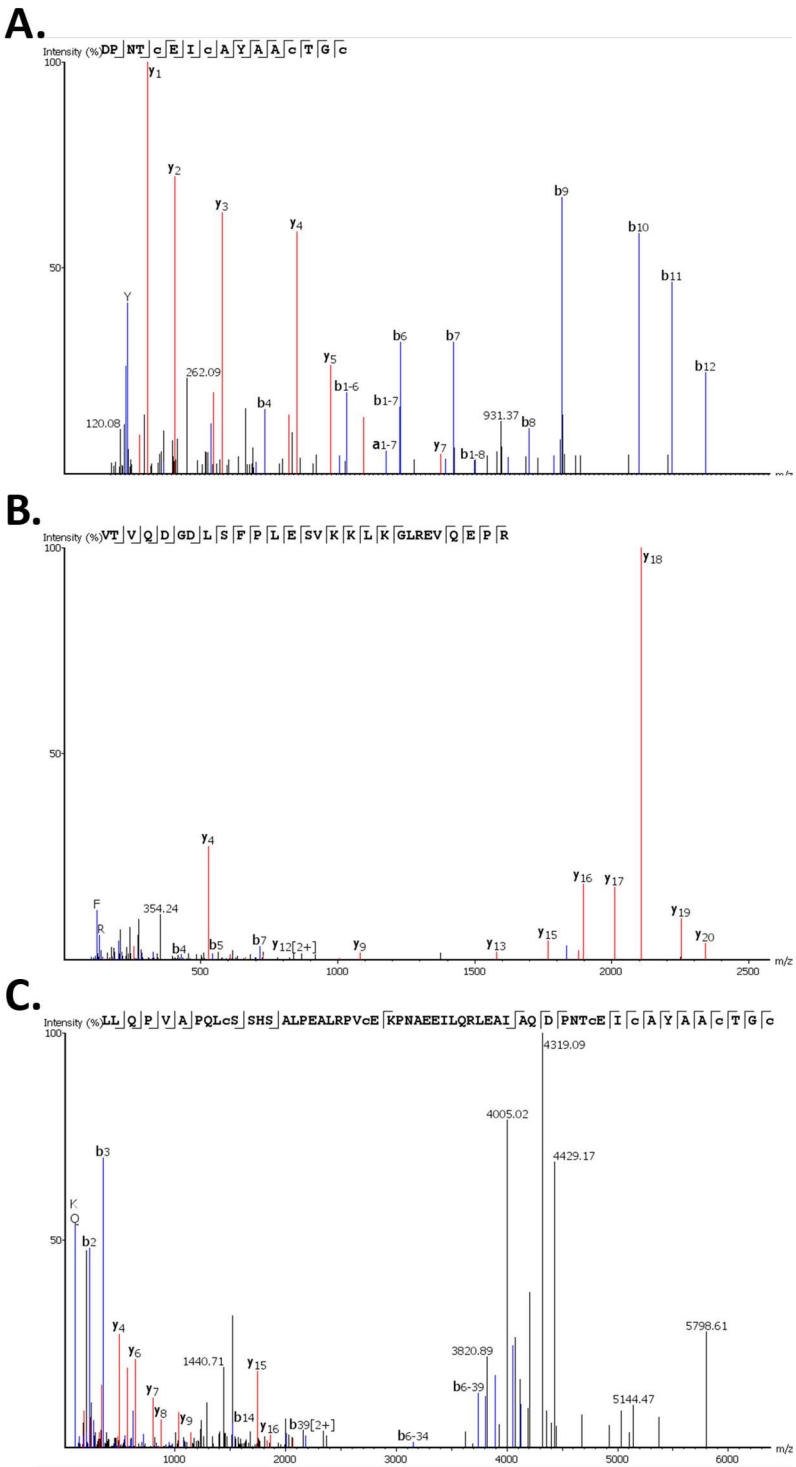

Figure 4.13: Product ion spectrum of detected peptides of GUC2A from murine ileal secretion. (**A.**) Product ion spectrum of the $[M+2H]^{2+}$ ion of the GUC2A peptide 101-116 (m/z=931.845) found in culture media of murine ileal organoids. (**B.**) Product ion spectrum of the $[M+6H]^{6+}$ ion of the peptide 22-49 (m/z=528.297) found in secretion of murine ileal organoids. (**C.**) Product ion spectrum of the $[M+5H]^{5+}$ ion of the peptide 60-116 (m/z=1284.821) found in lysis of murine ileal organoids.

To confirm the existence of different GUC2A peptides in mouse, investigations using the LC-MS/MS were done on different sample types: organoid secretion (culture supernatants),

intestinal content and plasma. Consistent with what was previously observed in tissue homogenates, the peptides 22-49 and 60-116 were highly represented (based on peptide peak area) in the supernatants and lysates of the ileal organoid' secretion assay, as well as in the luminal content (figure 4.14). Another interesting highly expressed peptide was the peptide 60-90. In mouse plasma, only 3 peptides from GUC2A were identified: 22-39, 22-49 and 60-116. The historically known peptide 102-116 was not detected.

The combination of multiple sources of tissues and fluids, studied here by LC-MS/MS differed from those in the literature (Currie *et al.*, 1992) and the Swissprot database. Previously proline as the first amino acid was assessed by automated Edman degradation sequence analysis and electrospray mass spectrometry from rat jejunum. The peptides were purified by a 10 minutes boiling step in 1M acetic acid. Such step could have degraded the natural hormone and would not reflect its true sequence. The peptide extraction method used in this chapter was based on 80% ACN in water (v/v) which denatures the protein instead of degrading them. The mass spectrometry data in conjunction with the peptide extraction method argues against the established guanylin sequence. A strong candidate for a potential active peptide would be the peptide 60-116. This peptide has been the most abundant and presenting the amino acid sequence 112-116 proposed to activate the GC-C receptor: ACTGC.

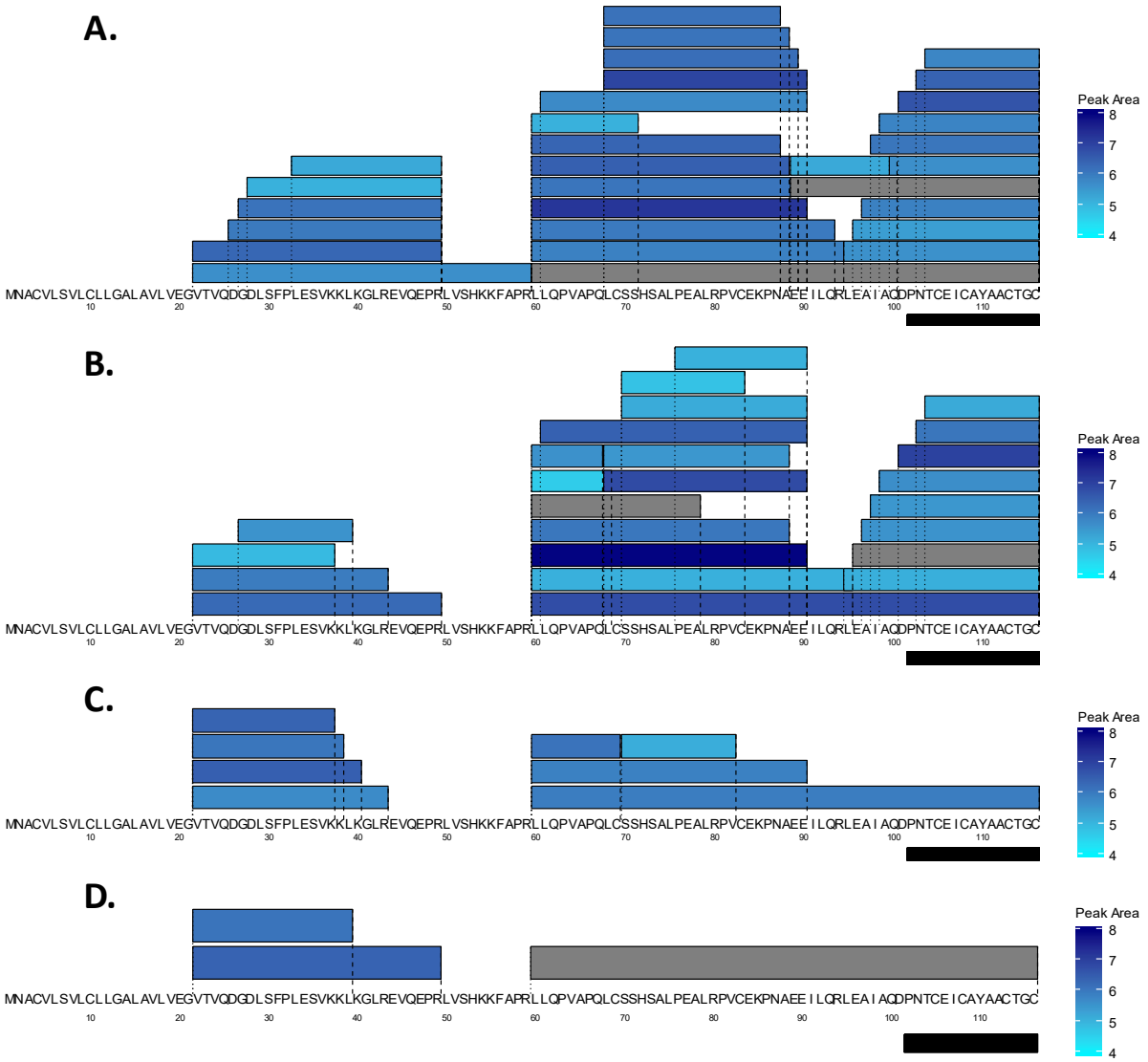

Figure 4.14: GUC2A (guanylin) peptides detected in murine ileal organoid secretion intestinal content and serum. Secretion of murine ileal organoids and peptides were analysed in supernatant (**A.**) and cell lysis (**B.**). Murine luminal content for the different part of the gut was analysed in (**C.**) as well as murine plasma samples in (**D.**) Each blue box represents a sequence identified by LC-MS/MS that matches the murine GUC2A sequence. The peptide peak area (log10 scale) is represented by the blue gradient. The historically known sequence from Swissprot database is highlighted by the black box below the protein sequence.

4.2.8 Mass spectrometry analysis on human samples to uncover the active guanylin sequence

Due to doubts regarding the existence of the previously described murine guanylin active peptide sequence and establishing the true sequence of the bioactive human guanylin peptide similar studies were undertaken on human samples. Human colonic secretion performed in Ussing chambers as well as human plasma were looked at in a similar method as in 4.2.7.

The historically known peptide described in the literature was not found in any human samples analysed. The longer peptide 100-115 containing an additional Aspartic acid on the N-terminal sequence was found in the secretion of human colonic tissue using the Ussing

chamber (assay performed by Juraj Rievaj, University of Cambridge) (figures 4.15A and B). Peptide 22-49 was the second and only peptide which was detected in the secretion samples (figures 4.15C and D). Those 2 peptides were also detected in human intestinal homogenates. These findings are summarised graphically as the levels found per tissue (based on peptide peak area) in chapter 7 (Cf. figure 7.10).

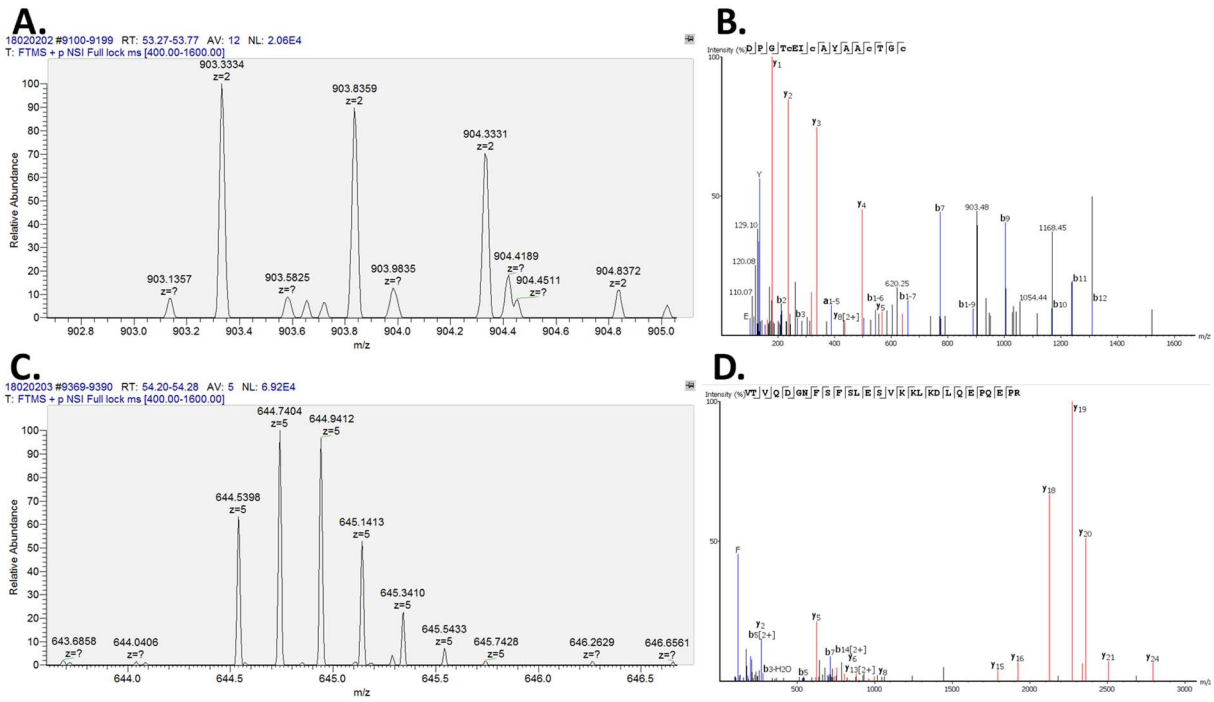

Figure 4.15: GUC2A (guanylin) peptides detected in secretion of human colonic tissue in Ussing chamber. (**A.**) Mass spectrum displaying the ^{13}C isotope pattern of the GUC2A peptide 101-116 from the peak at 53.4 minutes and its product ion spectrum of the $[M+2H]^{2+}$ ion (m/z=903.333) in (**B.**) found in secretion of human colonic tissue in Ussing chamber in the apical compartment. (**C.**) is the Mass spectrum displaying the ^{13}C isotope pattern of the GUC2A peptide 22-49 from the peak at 54.04 minutes and its product ion spectrum of the $[M+5H]^{5+}$ ion (m/z=644.541) in (**D.**) found in secretion of human colonic tissue in Ussing chamber in the apical compartment.

While one of the most common forms of the peptides detected in mouse was longer (amino acid residues 60 to 116), a similar peptide was not detected in human samples. The presence of the peptide 22-49 in human samples was the starting point of a hypothesis assigning a potential cleavage site after the arginine residue on position 49. The theorised peptide -once cleaved- would result in a 66 amino acid residues peptide 50-115; peptide which would be too long to be detected using the mass spectrometry method.

When all previous mass spectrometry experiments performed on human serum or plasma from healthy volunteers failed to detect the guanylin peptides, an experiment performed by Dr Richard Kay (University of Cambridge) managed to detect GUC2A peptides in plasma

samples from healthy volunteers undergoing a long fasting (Cf. chapter 5). A proteomic approach was used to analyse the samples instead of a peptidomic approach -as previously used. In a proteomic approach, samples are cleaved with an enzyme treatment after the reduction-alkylation treatment. In the case of this study trypsin was used, which cuts after the arginine and lysine residues. An interesting outcome was the presence of 2 new peptides that were not previously detected: peptides 55-83, 84-93 (figure 4.16). This result was consistent with the previously described hypothesis, a longer hidden version of the peptide which was not detectable with a peptidomic approach was unveiled by proteomics. The N-terminal part of the hypothesised longer peptide that was not detected in this experiment was from the residues 50-55 which would have cleaved at the lysine residue 52, making it too small to be detected.

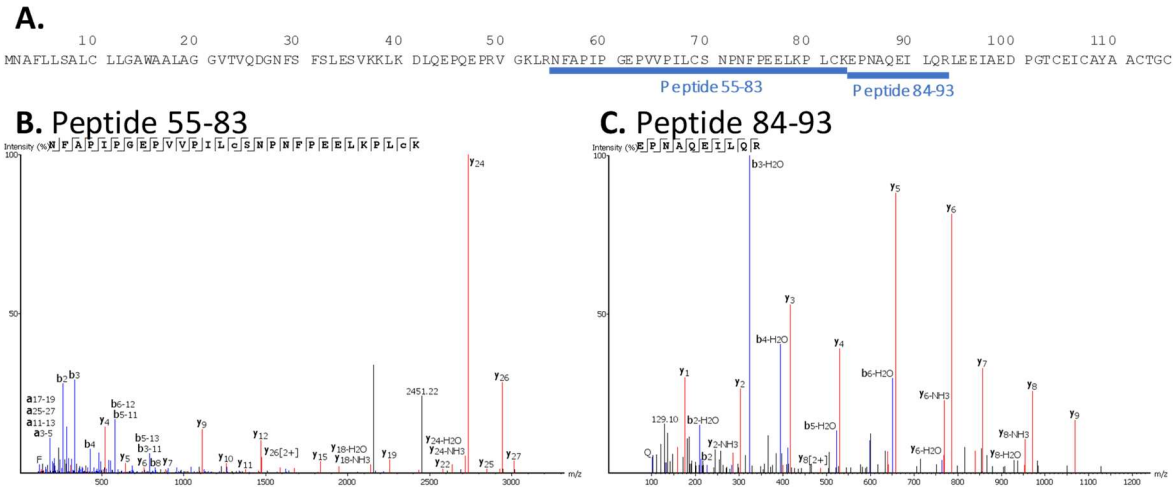

Figure 4.16: Proteomic analysis of human plasma where GUC2A (Guanylin) peptides were analysed after reduction and alkylation followed by trypsin treatment. (**A.**) Localisation of the peptides 55-83 and 84-93 on GUC2A's human amino acid sequence, identified by LC-MS/MS after trypsin treatment (**B.**) Product ion spectrum of the $[M+3H]^{3+}$ ion of the GUC2A peptide 55-83 (m/z=1092.903) found in human serum. (**C.**) Product ion spectrum of the $[M+2H]^{2+}$ ion of the peptide 84-93 (m/z=599.316) found in human serum.

This result supported previous suspicions regarding the existence of a potential longer version peptide 50-115 in human plasma. If a proteomic approach allows to form a hypothesis about a longer form present in the plasma, a caveat of this experiment is that the use of trypsin could cleave the ProGuanylin form and provide an identical result. Therefore, the use of trypsin cleavage does not corroborate completely the theory of a longer peptide. In other words, a potential other explanation of the presence of peptides 55-83 and 84-93 in the proteomic approach would be that ProGuanylin (amino acid residues 22 to 115) could produce identical peptides by trypsin treatment.

To corroborate the theory, a strategy was employed to uncover the potential longer peptide by using another cleavage enzyme, cutting at different sites. Chymotrypsin, an enzyme cutting on the C-terminal of phenylalanine, tyrosine and tryptophan in position P1, was employed on the same plasma sample. Positions of cleavage sites were after residues 29, 31, 56 and 109 in the GUC2A sequence (without considering the signal peptide). This approach was unsuccessful as no GUC2A peptides were detected by mass spectrometry on the chymotrypsin-cleaved plasma sample. Using an enzyme to cleave peptides for a proteomic approach can make analysis complicated as it significantly increases the number of peptides to read by the mass spectrometry. The absence of peptides in the mass spectrometry read out, does not mean they are not present in the sample but only that they have not been detected.

In conclusion, the historically known peptides were not present in sufficient quantities to attest of their endogenous presence in mouse and human. A 57 amino acid long peptide was identified in mouse. This peptide is the most represented peptide in homogenates, intestinal content, secretion and serum samples. It encompasses the conserved C-terminal motif which is required for GC-C receptor activation (Schulz *et al.*, 1999). Other smaller peptides were present and could be the result of further processing of this 57-amino acid peptide.

Human levels of GUC2A and GUC2B peptides were constantly lower compared to mouse. So far, the longer peptide was not detected in human samples, even though some preliminary proteomics data were encouraging.

4.3 Discussion

4.3.1 Antibody isolation by hybridoma campaign against small peptides

A hybridoma campaign is a fast and efficient method to find large numbers of antibodies in IgG format with nanomolar or subnanomolar affinity to their targets. MedImmune has successfully produced antibodies specifically directed against peptides of 30 amino acids using the hybridoma platform, so it was with confidence that a hybridoma campaign was performed to generate antibodies against historically known guanylin and uroguanylin which are 15 and 16 amino acids long, respectively. Despite the high number of clones screened, no specific antibodies against uroguanylin were found using the hybridoma technique, and only one antibody AB100001 was specific to guanylin.

Clones that bound to biotinylated-Guanylin, Guanylin-KLH or Uroguanylin-KLH were identified in the primary screen. After more characterisation, the binders to Guanylin-KLH and Uroguanylin-KLH were found to be cross-reactive and did not bind the free peptide. It is highly possible that the clones that bound KLH-Guanylin and KLH-Uroguanylin were binding the link between the KLH and the peptide. Identity between human peptides and mouse historically known peptides is significant: 93% and 81% for guanylin and uroguanylin, respectively. Therefore, the murine immune response during the hybridoma campaign would generate antibodies against non-identical parts of the peptide and the main immune response was directed against the KLH.

4.3.2 Lead isolation using display methods compared to a hybridoma approach

Currently, antibody phage display is widely used for generation of therapeutic biologicals. For example, in 2002, adalimumab (Humira) was the first phage display derived antibody to be granted a FDA approval and was produced by CAT/Abbott laboratories (Frenzel, Schirrmann and Hust, 2016). Using a phage display platform has various advantages compared to a hybridoma platform when developing therapeutic antibodies. A first benefit compared to the hybridoma is the *in vitro* approach that can by-pass the use of animals and allow the development of antibodies on more complicated targets such as toxin (Garet *et al.*, 2010). Another advantage of working with such a platform is the valuable selection strategies that can be employed on the rounds of selections. Rounds of selection can be performed using ortholog targets allowing scientists to look for cross reactive antibodies between species, a strategy which is unachievable with a hybridoma approach. For instance, a cross reactive

antibody was developed against a GLP1-receptor by a member of the Gribble/Reimann lab (Biggs *et al.*, 2018).

In this work, monoclonal antibodies were generated against the historically known active peptide guanylin and uroguanylin using naïve phage libraries. The selection process led to the production of large panels of potential clones, and high throughput screening techniques were used to screen them. Phage ELISA and sequence assessment were used for screening the clones. Although the time-frame to isolate guanylin and uroguanylin binders by phage display was much shorter than the isolation of antibodies by a hybridoma approach, the clones proved to have low affinity to their targets (690nM and 860nM for guanylin and uroguanylin respectively). Albeit low affinity to their targets, competitive ELISA demonstrated specificity of the antibodies to biotinylated peptides as well as the free active peptides.

4.3.3 Affinity maturation approaches using display methods

The low affinity of the generated antibodies to their targets were not unexpected and maturation was necessary to obtain the desired efficiency. Affinity maturation by display methods can prove to be efficient with improvement to femtomolar antigen-binding affinity (Boder, Midelfort and Wittrup, 2000).

To achieve a sufficient affinity improvement, AB1000093 and AB1000107 mutant libraries were generated by targeting the V_H and V_L CDR3 by Kunkel mutagenesis. AB1000001 isolated from the hybridoma approach had a stronger affinity to guanylin compared to the phage display isolated AB1000093 but rounds of *in vivo* selection on the CDR3 do allow a small window of improvement. The new mutated libraries were processed in more stringent rounds of selection by decreasing the concentration of antigen: up to 400pM of antigen. A 200-fold improvement was reached for the guanylin antibody Flo13 when compared to the progenitor antibody AB1000093 and the affinity reached an IC_{50} value of 3.2nM. The maturation of the AB1000107 antibody was not as effective with only an 8-fold improvement, reaching an IC_{50} of 105nM.

Concomitantly to the affinity maturation by phage display, the antibody AB1000001 (and later the affinity matured AB1000107 clone) was matured by error prone mutagenesis and ribosome display selections. Ribosome display is used on a regular basis to mature lead antibodies derived from phage display or from immunised animals. This technology can evolve

the antibody libraries by introducing random mutations in between the selection cycles and therefore perform directed evolution (Groves and Osbourn, 2005). After 3 rounds of stringent selection on the mutated AB1000001 library, a new lead antibody was found for guanylin with a 12-fold improvement in IC_{50}.

When error prone mutagenesis and ribosome display selection were performed on the pool of matured clones from the phage display maturation of AB1000107, a new antibody with V_H CDR2 modifications was found for uroguanylin with a 4-fold improvement succeeding in an IC_{50} of 28.4nM (30-fold improvement from progenitor AB1000107's IC_{50}).

Plenty of different approaches using both phage display and ribosome display techniques could be used to improve further the affinity of the antibodies to the historically known active peptides. A systematic but laborious approach, sometimes employed in industry, would be to perform targeted mutagenesis on all CDRs and look at combination of V_H and V_L CDRs. Combinations of the highest affinity mutant heavy chains with the highest affinity mutant light chains provide the potential to generate new antibodies with additive affinities. A similar approach called CDR walking mutagenesis was proven successful and is done by maturating the antibody's CDR consecutively (Yang *et al.*, 1995).

A relatively quicker method would be to perform more rounds of error prone mutagenesis followed by stringent ribosome display selection. The sequencing of those clones could show patterns of mutations in specific CDRs suggesting where to perform targeted CDR mutagenesis. It is for instance a method that could have been employed on the uroguanylin antibody: a 4-fold improvement obtained by 2 modifications in the V_H CDR2 is a strong incentive suggesting that the CDR2 might be strongly implicated in the binding to Uroguanylin.

Another approach to perform affinity maturation is chain shuffling when either the V_H or the V_L gene is replaced by random combinatorial immunoglobulin libraries (Kang, Jones and Burton, 1991).

4.3.4 Conclusion on the generation of antibodies against guanylin peptides

In this chapter, monoclonal antibodies were generated against the peptides described in the literature as the bioactive forms. Several techniques were used to isolate antibodies including a hybridoma campaign and phage display selection on naïve libraries and antibody affinities were improved through several rounds of maturation, using display methods such as targeted

mutation on V_H and V_L followed by phage display and error prone mutagenesis followed by ribosome display. Affinities were improved to reach a KD of 3.2nM and 28.4nM for antibodies against guanylin and uroguanylin. The affinity of the antibodies against uroguanylin is not considered as high enough and further maturation would need to be performed on this antibody to increase it. Other methods are available to perform affinity maturation of an antibody to its target. Yeast display is commonly used for affinity maturation which has generated antibodies with femtomolar affinity (Boder, Midelfort and Wittrup, 2000). This method can overcome some difficulties that are encountered when using the phage display approach. One of the limitations of the phage display method is its potential bias due to host infectivity by the phage as well as its toxicity on the host (Riechmann and Weill, 1993; Schier, Bye, *et al.*, 1996) and its potential library bias due to expression of the library in a prokaryotic host. *E. coli* that can present difficulties to express several disulphide-bonded eukaryotic proteins by lack of chaperones (Boder and Wittrup, 1997; T J Vaughan *et al.*, 1996). An alternative approach to the maturation of protein is the use of computational *in silico* modelling to support the affinity maturation process (Jorgensen, 2004; Clark *et al.*, 2006; Thakkar *et al.*, 2014). The maturation of an antibody is a time-consuming task and countless techniques have been developed to optimise the affinity to a target, however one of the main constraints in industry and academia is time.

Furthermore, the goal behind this work was to establish an immunoassay involving 2 antibodies able to bind guanylin or uroguanylin in a sandwich type of assay. So far, I managed to only produce a range of antibodies that were not able to bind different epitope of the peptides. This is probably due to the small size of the peptides (15 and 16 amino acids respectively), preventing the development of an immunoassay with 2 antibodies. A potential assay that could measure the levels of guanylin and uroguanylin would be a competitive ELISA. Biotinylated targets could be coated on a streptavidin plate and would compete for the antibody against guanylin peptides present in unknown or standard samples. A limitation of this type of competitive assay is supposed to be 4/5 times less sensitive.

Concomitantly to the affinity maturation, the Gribble/Reimann lab developed a new peptidomic approach to look at a variety of samples allowing to describe exactly the different guanylin peptides present in each sample. The historically described guanylin active peptide was not found in several mouse and human samples (such as tissue homogenates, plasma,

intestinal content, and organoids secretion and cell lysate), but longer version were detected. The antibodies being able to target the C-terminus part of the guanylin amino acid sequence would potentially bind the endogenous forms. An experiment involving both an immunoprecipitation with the antibodies followed by LC-MS/MS would be a perfect way to investigate the prevalent form of peptides that bind to the antibodies and also the sequence of the endogenous peptides. Unfortunately, this was not pursued further. This method could be used as an assay to measure the different forms of guanylin peptides binding to the antibody.

4.3.5 Redefining the guanylin active peptides

This chapter has mainly focused on designing antibodies on what was thought to be the active guanylin peptides: guanylin (101-115) and uroguanylin (103-111). Since the discovery of guanylin in 1992 in rat and human by Currie and de Sauvage respectively, techniques used to assess the amino acid sequence have improved tremendously. One of them is LC-MS/MS mass spectrometry. New data using this highly sensitive method brought light to a different processing of the guanylin active peptide described in the literature with a different cleavage site on the N-terminal side of it.

Currie was the first to describe the purification and characterisation of a 15 amino acids guanylin from rat jejunum (M G Currie *et al.*, 1992). The purification was achieved on frozen jejunum tissue, and were thawed, minced and boiled for 10 minutes in 1M acetic acid solution. The peptide sequence was assessed by automated Edman degradation sequence analysis and electrospray mass spectrometry. The resulting sequence was a 15-amino acid peptide characterised by an N-terminal proline. While this sequence was rarely questioned, the authors acknowledged that the guanylin peptide could be the result of a truncated form that had bioactivity but could be derived from a larger precursor. A hypothesis on the purification of a 15-amino acid peptide would be that the harsh acetic acid boiling step cleaved the aspartic acid and proline bond.

Once identified in rat, multiple groups tried to identify the guanylin in different species and de Sauvage was first to describe it in human (de Sauvage *et al.*, 1992). After identifying the full-length human guanylin cDNA, it was transfected into a human embryonic kidney cell line which expressed the proform. Peptides were generated by trypsin or acid treatment on the purified ProGuanylin and the C-terminal sequence of ProGuanylin was found to activate the

GC-C. de Sauvage *et al.* highlighted that a more physiologic processing site would be after the basic 93rd arginine residue and emitted the hypothesis that the previously described rat peptide was probably not the correct N-terminal sequence.

However, Currie's and de Sauvage's observations about the N-terminal sequence of the guanylin peptides were disregarded or unnoticed by the scientific community. Discrepancies on the rare reviews on guanylin quoted those papers but never mentioned a potential longer form of the active peptide. One paper found a 16-amino acid version of guanylin starting with an aspartic acid. However, they concluded that this version was not biologically active (Yamaguchi *et al.*, 1995). Later, research was completed by accepting the 15-amino acid peptide as being the endogenous active version. No questioning on the difficulty to cleave between an aspartic acid and proline residue *in vivo* was mentioned in the literature again.

While the mass spectrometry data produced in this chapter highlighted evidence of a different endogenous guanylin in mouse, no conclusions can be drawn on the longer versions yet. The biological activity of the longer versions (peptides 60-116 or 101-116) found in the different array of mouse samples need to be confirmed.

In humans, the guanylin peptide's current version not being found in any samples, and the detection of a peptide with an additional aspartic acid on the N-terminal (101-116) tends to refute the current understanding of the human guanylin peptide. A hypothesis emitted in this chapter was the presence of an even longer peptide which could not be detected by mass spectrometry as too long. However, more experiments need to be performed on human samples to confirm the presence of this longer peptide and its activity.

When studied by mass spectrometry, human and mouse samples rarely exhibited uroguanylin peptides that presented the C-terminal active part and therefore the literature cannot be confirmed or opposed.

Chapter 5: Quantification of guanylin-related peptides in humans.

5.1 Introduction

In humans, guanylin-related peptides have not been extensively characterised due to a lack of validated reagents and assays required for their quantification. Only a few reports have described their attempt to measure circulating levels of active guanylin and uroguanylin, with initial attempts done with an early developed radioimmunoassay (RIA) (Kuhn *et al.*, 1994). In healthy volunteers the authors reported a measured guanylin concentration of 40fmol/ml of in EDTA plasma samples (fasting status was not reported) (Kuhn *et al.*, 1995) and 5fmol/ml for uroguanylin in EDTA plasma samples from fasted healthy volunteers (Kinoshita, Fujimoto, *et al.*, 1997). Despite the interest in these hormones due to their potential roles in energy homeostasis and carcinogenesis (Valentino *et al.*, 2011; Begg *et al.*, 2014; C. Folgueira *et al.*, 2016), the lack of a reliable and user-friendly method to analyse all the guanylin-related peptides has prevented advancements in our understanding of their physiological and pathophysiological roles.

Chapter 3 described the development of two assays that are capable of measuring both ProGuanylin and ProUroguanylin. In this chapter, I describe the utility of these assays in the measurement of ProGuanylin and ProUroguanylin in human biosamples, including serum and plasma. Antibodies and MSD assays were developed using ProGuanylin and ProUroguanylin that were produced *in vitro* in *E. coli*. Of potential concern was the potential lack of specificity of the antibody pairs to the endogenous proforms because the antibodies were raised against peptides produced in *E. coli* and the presence of the AVI-tag could be essential in the binding of the antibody pairs to the recombinant proforms (Cf. to chapter 3). It was also uncertain whether the binding of antibody pairs to non-specific molecules present in biological samples would occur.

Another aim of this study was to compare the MSD assays I developed with the commercially available ELISAs that are marketed for the quantification of guanylin-related peptides in human samples. I also sought to compare their respective calibration ranges and, limits of detection. Online protocols obtained for the Biovendor kit (www.biovendor.com) displayed different incubation steps and sample handling requirements for ProGuanylin and ProUroguanylin. In light of this, one advantage of the assays I developed is the similar protocol

used for each prohormone which promotes user-friendliness and the ability to perform the assays in parallel.

It was anticipated that the developed assays would be capable of measuring ProGuanylin and ProUroguanylin in human plasma and serum samples and provide approximate reference ranges for healthy volunteers in fasting and post-prandial states, as well as in other physiological and pathological situations. Earlier studies examined a potential role for guanylin peptides as biomarkers in patients with neuroendocrine tumours (Kuhn *et al.*, 1995) or kidney disease (Kinoshita, Fujimoto, *et al.*, 1997; Kinoshita, Nakazato, *et al.*, 1997; Kinoshita *et al.*, 1999), which was also attempted as part of this study to help establish reference ranges that may aid disease diagnosis, response to treatment and surveillance. For example, establishment of reference ranges have been of value in our understanding of human gut peptide secretion in response to a variety of stimuli (Meek *et al.*, 2016).

The aims of this chapter were firstly, to test the developed MSD assays on human samples and compare them with the commercially available ELISA kits, specifically in terms of their calibration range, as well as limits of detection. Secondly, to provide reliable reference ranges for both ProGuanylin and ProUroguanylin in healthy, fasted human volunteers, and investigate effects of standardised liquid meal test or an oral glucose challenge (OGTT) on the circulating levels of the proforms. Finally, ProGuanylin and ProUroguanylin levels were also determined in subjects with midgut metastatic neuroendocrine tumours with carcinoid syndrome and other conditions characterised by impaired gastrointestinal function including following prophylactic total gastrectomy and small intestine transplant.

To do so, studies on volunteers were performed by several clinicians (Dr Meek, Dr Roberts, Ft Challis and Pr Jensen) and glucose tolerance and liquid meal tests were achieved according to methods detailed in section 2.7.1. ProGuanylin and ProUroguanylin were measured in Serum, Lith Hep plasma or serum samples using both the commercially available ELISA kit and the newly developed MSD assay with methods described in sections 2.7.2 and 2.7.3.

5.2 Results

5.2.1 Evaluation of the MSD assay on human plasma samples and comparison with the commercially available Biovendor kit

Antibody pairs capable of detecting either ProGuanylin or ProUroguanylin and the newly developed MSD assays were compared to the commercially available kit from Biovendor. ProGuanylin levels were measured in 80 lithium heparin (Lith Hep) plasma samples (from 40 different participants) using both the ProGuanylin ELISA kit from Biovendor and the ProGuanylin MSD assay. Similarly, the ProUroguanylin ELISA kit from Biovendor and the ProUroguanylin MSD assay were used to determine the levels of ProUroguanylin. Biovendor standards were tested in the MSD assays and standards from the MSD assays were tested in the Biovendor ELISA kits at the concentration that was used in each respective experiment. Measurements from all assays were done in parallel and at the same time in order to mitigate the effects of possible freeze/thaw degradation. The results are presented in figure 5.1.

Interestingly, both assays were able to detect the standards from the other kit (figures 5.1 A and B). While MSD assays managed to read all 8 standard points from the Biovendor kits, the Biovendor kit was not able to detect the 3 highest MSD standard concentrations because these were too high and therefore above the range of detection (data not shown). The ProUroguanylin MSD assay was able to detect the expected standard concentrations of the Biovendor kit with a slope of 1.13. The Biovendor kit was not able to correctly detect the ProUroguanylin standard concentrations which were underestimated (slope of 0.73). Regarding the ProGuanylin standard concentrations, the Biovendor kit also underestimated the expected values of the standard concentrations with a slope of 0.39. However, the MSD assay measured Biovendor concentrations that were higher than expected (slope was 1.75). The discrepancy between measured and expected concentrations are unclear. Factor differences between expected and measured values were 1.75 and 0.39 for the MSD assay and the Biovendor assay, respectively. One potential explanation may be human error when reconstituting the ProGuanylin powder provided by the Biovendor kit. Another explanation is the different buffers used for diluting the standards. For example, MSD standards were diluted in PBS with BSA whereas the Biovendor standards were diluted in a proprietary diluent.

In conclusion both assays could detect the standards from the other kit, but the MSD assays were able to detect the standard concentrations more accurately than the Biovendor kits could detect the MSD standards.

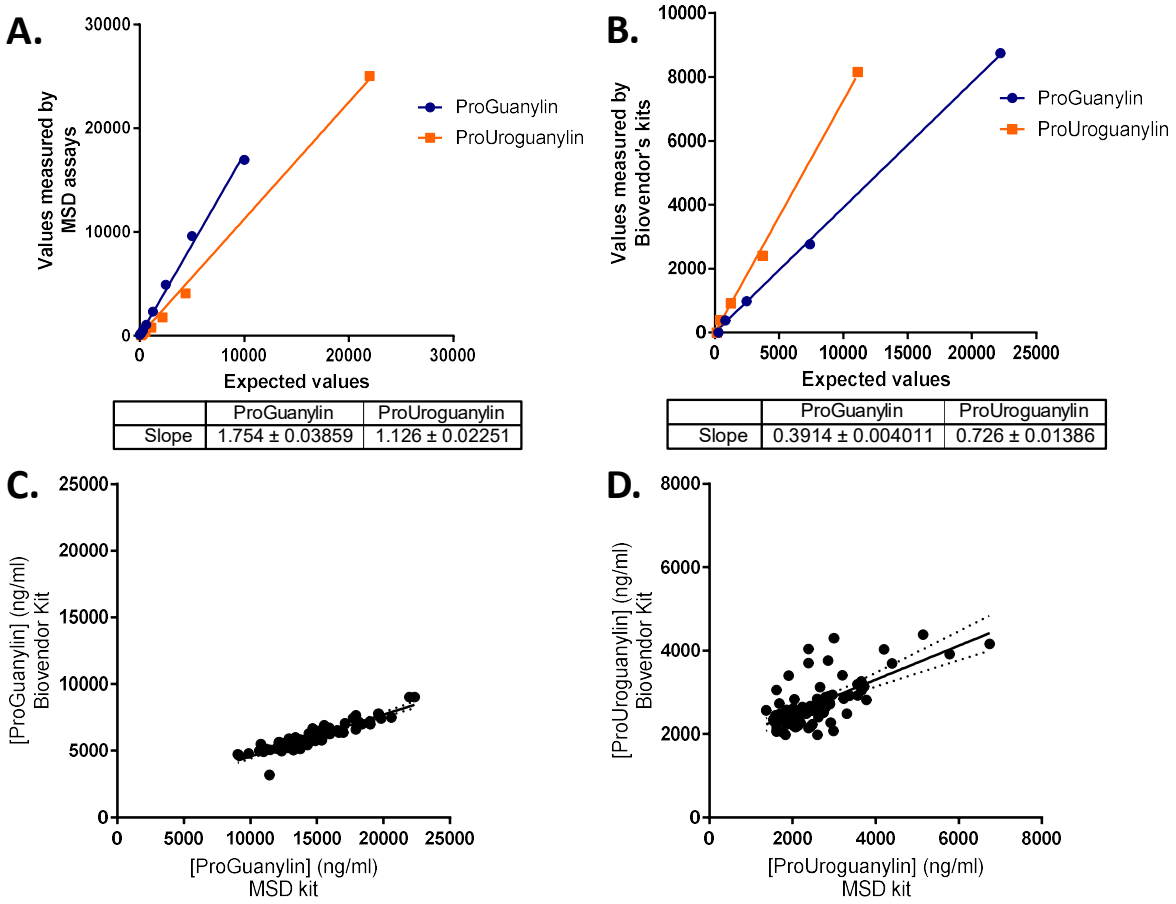

	ProGuanylin	ProUroguanylin
Slope	1.754 ± 0.03859	1.126 ± 0.02251

	ProGuanylin	ProUroguanylin
Slope	0.3914 ± 0.004011	0.726 ± 0.01386

E.

	ProGuanylin Biovendor Vs MSD kit	ProUroguanylin Biovendor Vs MSD kit
Slope	0.3141 ± 0.01559	0.4073 ± 0.04944
Y-intercept	1428 ± 232	1674 ± 135.7
R^2	0.8389	0.4652

Figure 5.1: Comparison of the Biovendor kit with the newly developed MSD kit on human Lith Hep plasma samples. In (**A.**) and (**B.**), standards from each kit were tested in each other's assay. In the Biovendor ELISA kits, MSD standards concentrations were higher than the detection limit of the ELISA kits assay. Slopes values were reported in the table underneath the plots. N = 80 Lith hep plasma samples were measured for ProGuanylin (**C.**) and ProUroguanylin (**D.**) using the commercially available Biovendor ELISA kit and the MSD assay. Obtained values and linear regression were plotted. The linear regression results are summarised in the table (**E.**) including the slope, the Y-intercept and the R^2.

Human plasma samples were measured using both the MSD assay and Biovendor kit (figure 5.1 C, D and E). The measured ProGuanylin levels correlated well between both assays with a coefficient of determination (R^2) of 0.84. An intriguing result was the difference in concentration measured by both assays: identical plasma samples presented a 2-fold

difference depending on which assay was used. This result was expected as the standard concentrations presented a discrepancy between both assays.

ProUroguanylin levels did not correlate as well between the 2 assays, when compared with the ProGuanylin assay (coefficient of determination (R^2) of 0.47). Similarly, ProUroguanylin concentrations measured with the Biovendor kit were lower than proforms concentrations measured with the MSD assay. Again, this was expected based on differences found with the respective standard concentrations detected by the assays.

In conclusion, the MSD assays appeared more sensitive and had a broader dynamic range than the commercially available Biovendor ELISA kits. Correlations between both assays were relatively good suggesting that experiments requiring relative values could be performed with the Biovendor kit. However, the MSD assay is capable of more accurately measuring absolute peptide values. As alluded to above, another advantage of the MSD assay is that proform assays use the same protocol, whereas the protocols of the two ELISA kits differ in terms of dilution and incubations time and is less user friendly.

5.2.2 ProGuanylin and ProUroguanylin levels in fasted and fed healthy volunteers

Range of baseline values for ProGuanylin and ProUroguanylin from healthy volunteers in fasting state

The concentration ranges for ProGuanylin and ProUroguanylin were determined in fasted healthy volunteers. For both proforms the distribution of the data and normality were determined and used to assess circulating concentrations of proforms in healthy volunteers which allowed for comparison with disease states in future studies.

From measured levels of both proforms in healthy volunteers, histograms were produced to assess the distribution of the data in fasting participants. The analysis was performed on the fasting state in order to remove meal-related variability. The data were tested for normality using a Shapiro-Wilk test and also tested for skewness and kurtosis (figure 5.2). ProGuanylin levels were normally distributed with a p-value of 0.69 in a Shapiro-Wilk normality test and a kurtosis of -0.08, whereas, ProUroguanylin levels were not normally distributed with a p-value < 0.01 and a skewness of 1.51.

The mean plasma ProGuanylin levels was 15249pg/ml (1230.95pmol/l) and the determined mean plasma ProUroguanylin concentration was 2594pg/ml (214.93pmol/l). Although it is

recommended to use at least 120 individuals to assess the definitive 95% confidence intervals for reference and to partition the volunteers according to age and gender (Institute, 2010), the 2.5th and 97.5th percentiles were calculated to give a table with expected values which includes 95% of values from the population comprising of 51 individuals (figure 5.2C).

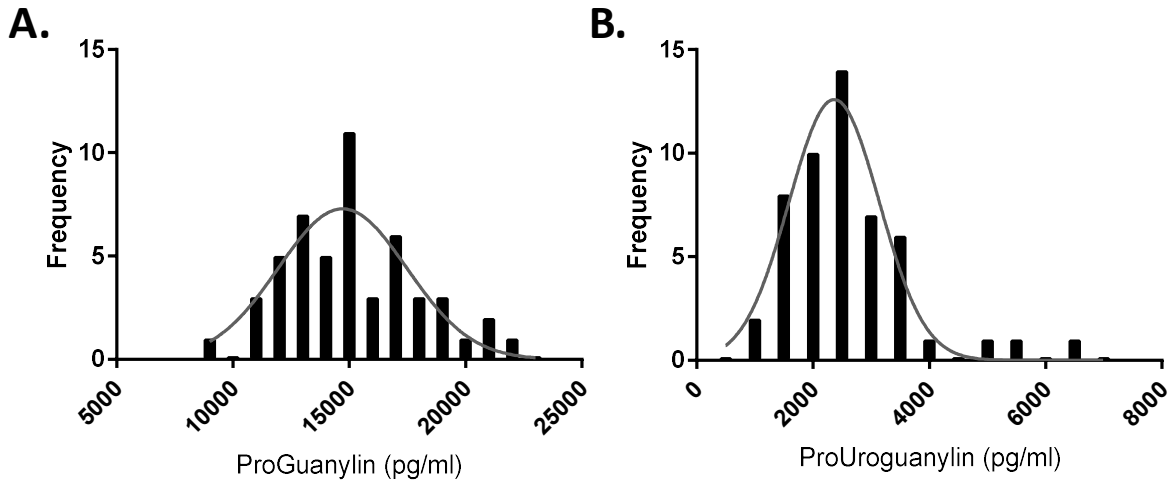

C.

	ProGuanylin	ProUroguanylin
Skewness	0.37	1.51
Kurtosis	-0.08	3.89
Shapiro-Wilk test	p=0.69	p<0.01
LRL	11104	1135
Median	15029	2395
URL	20554	5186

Figure 5.2: A. and B. Assessment of data distribution and normality for ProGuanylin and ProUroguanylin. n=51 healthy volunteers in fasting conditions. Assessment of Skewness and kurtosis and Shapiro-Wilk test are summarised in table **C.** which includes the expected values using the lower reference limit (LRL; 2.5th percentile), median and upper reference limit (URL; 97.5th percentile).

ProGuanylin and ProUroguanylin levels in response to oral glucose or liquid meal in healthy volunteers

Guanylin and uroguanylin have been postulated as candidate effector molecules within the GI-renal natriuretic axis and, consequently, gut transit (Romi, Cohen, Landau, Alkrinawi, Yerushalmi, Hershkovitz, Newman-Heiman, Garry R. Cutting, *et al.*, 2012). One proposed mechanism for these actions is the regulated secretion of ProGuanylin and ProUroguanylin from cells lining the proximal intestine following oral ingestion of a salt load.

The newly developed assay allowed the measurement of proforms in the circulation in fed healthy volunteers. Research subjects were recruited, and blood samples were collected

under the supervision of Dr Claire Meek. The baseline characteristics of the participants are presented in table 5.1.

Characteristic	Healthy volunteers for OGTT 50 mg	Healthy volunteers for OGTT 75 mg	Healthy Volunteers for Liquid meal	Volunteers for fasting study	Volunteers with Total Gastrectomy	Volunteers with small bowel transplant	Volunteers with Neuro-endocrine tumour	Volunteers with different osmolality levels
Gender	4F7M	8F4M	15F13M	6F7M	3F8M	5F1M	3F7M	22F13M 21U
Age (years at enrolment)	29.6 (6.9)	27.2 (4.6)	32.3 (11.6)	29.7 (5.9)	36.1 (8.1)	41.7 (15.0)	adults (18-60)	33.8 (11.5) for 35 patients
Body Mass index kg/m^2	25.0 (3.9)	25.2 (4.0)	25.2 (4.1)	25.0 (3.2)	22.1 (2.2)	20.3 (2.9)	N/A	25.6 (4.7)
Amount of time post operation	N/A	N/A	N/A	N/A	2.9 (2)	4.7 (5.2)	N/A	N/A
HbA1c mmol/mol	32.3 (2.6)	34.3 (3.0)	34.5 (3.3)	N/A	38.4 (6.2)	N/A	N/A	N/A

Table 5.1: Demographics of study volunteers. Characteristics are shown as mean (SD) for continuous variables and n's for categorical variables.

A pilot MSD experiment was performed on plasma samples taken from 3 subjects to determine the effect of 50g oral glucose on the plasma levels of ProGuanylin and ProUroguanylin at 15, 30, 45, 60, 90 and 120 minutes (figure 5.3).

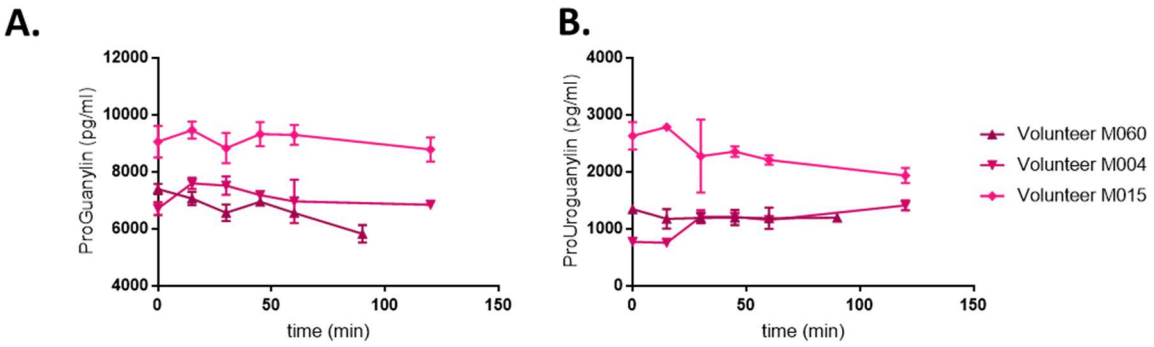

Figure 5.3: Effect of glucose intake on ProGuanylin and ProUroguanylin levels in healthy volunteers. ProGuanylin and ProUroguanylin were measured immediately before ingestion of 50g glucose and at 15, 30, 45, 60, 90 or 120 minutes in three healthy fasted volunteers. ProGuanylin (**A.**) and ProUroguanylin (**B.**) levels were measured in Lith Hep plasma samples using the MSD assay.

The data showed a negligible impact of oral glucose on the plasma concentrations of ProGuanylin and ProUroguanylin. However, volunteers following prophylactic total gastrectomy presented a noticeable change at 60 minutes following glucose challenge (data not shown). Subsequently, proforms were measured in Lith Hep plasma samples from healthy volunteers after ingestion of a liquid standardised meal test (11g of fat, 13g of protein as well as 50g of carbohydrate and 0.52g of salt), 50g or 75g glucose tolerance test at time 0 and after 60 minutes (figure 5.4). A small, but statistically significant, decrease in ProGuanylin was measured in the two oral glucose tolerance tests after 60 minutes compared with the time 0. No significant difference between plasma ProGuanylin concentrations was found after 60

minutes of ingestion of the liquid meal. ProUroguanylin plasma concentration was significantly higher (p value = 0.0379) 60 minutes following ingestion of the liquid meal. In contrast, 50g of oral glucose resulted in a significant decrease of ProUroguanylin (p value = 0.0186).

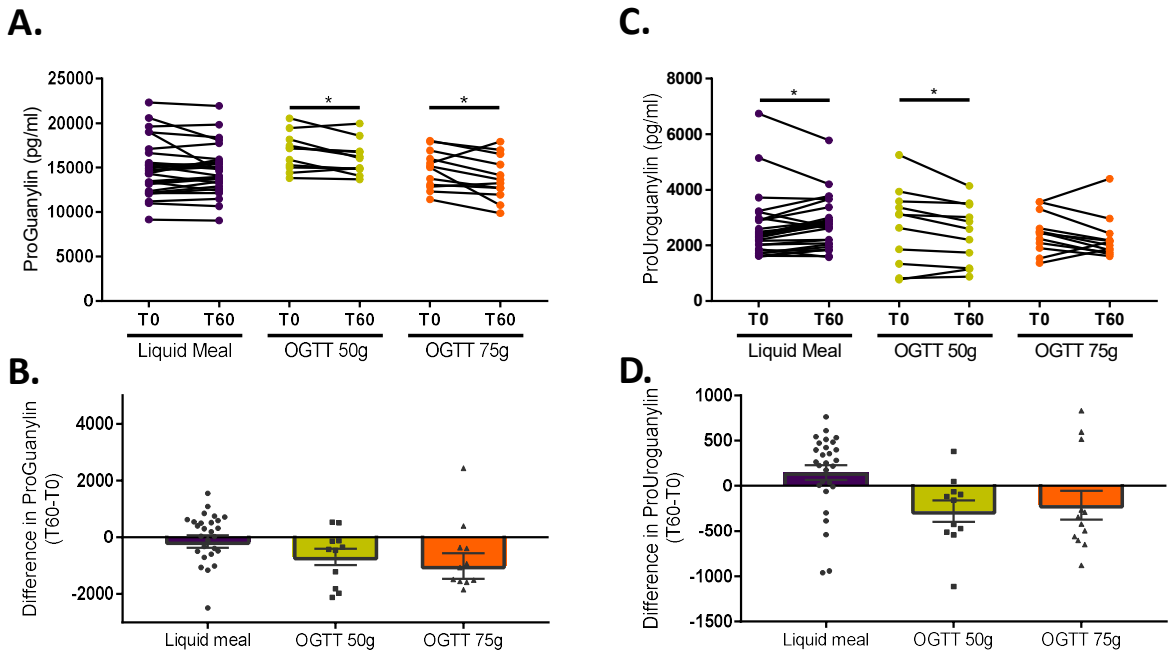

Figure 5.4: Effect of Liquid meal or glucose ingestion on ProGuanylin and ProUroguanylin levels in healthy volunteers. ProGuanylin and ProUroguanylin were measured immediately before and 60 minutes after ingestion of liquid meal, 50g glucose or 75g glucose in healthy fasted volunteers. ProGuanylin (**A.** and **B.**) and ProUroguanylin (**C.** and **D.**) levels were measured in Lith Hep plasma samples using the MSD assay on n=28 participants for Liquid meal ingestion, n=11 participants for 50mg glucose ingestion, and n=12 participants for 75mg glucose ingestion. In **B.** and **D.** Data are mean ± SEM. Statistical significance was assessed by paired t test for ProGuanylin and Wilcoxon test for ProUroguanylin. * indicates $p<0.05$.

The differences between 0 and 60 minutes were measured for both ProGuanylin and ProUroguanylin following the OGTT. A significant decrease in ProGuanylin levels were measured in both OGTT tests (p values = 0.0376 and 0.0464, for 50g and 75g glucose respectively) (figure 5.4A and B). A small but significant decrease in ProUroguanylin was measured for a 50mg OGTT only (p value = 0.0186) (figure 5.4C and D). In response to the liquid meal, ProUroguanylin levels significantly increased 60 minutes following ingestion, however no changes in Proguanylin levels were detected.

Effect of fasting on ProGuanylin and ProUroguanylin levels in healthy volunteers

A study coordinated by Prof. Jørgen Jensen (University of Copenhagen) determined gut hormone levels of healthy volunteers during a 7-day fast. The baseline characteristics of the

participants are listed in table 5.1. ProGuanylin and ProUroguanylin levels were measured on plasma samples from these subjects to determine the effect of a prolonged fast on ProGuanylin and ProUroguanylin plasma levels (figure 5.5).

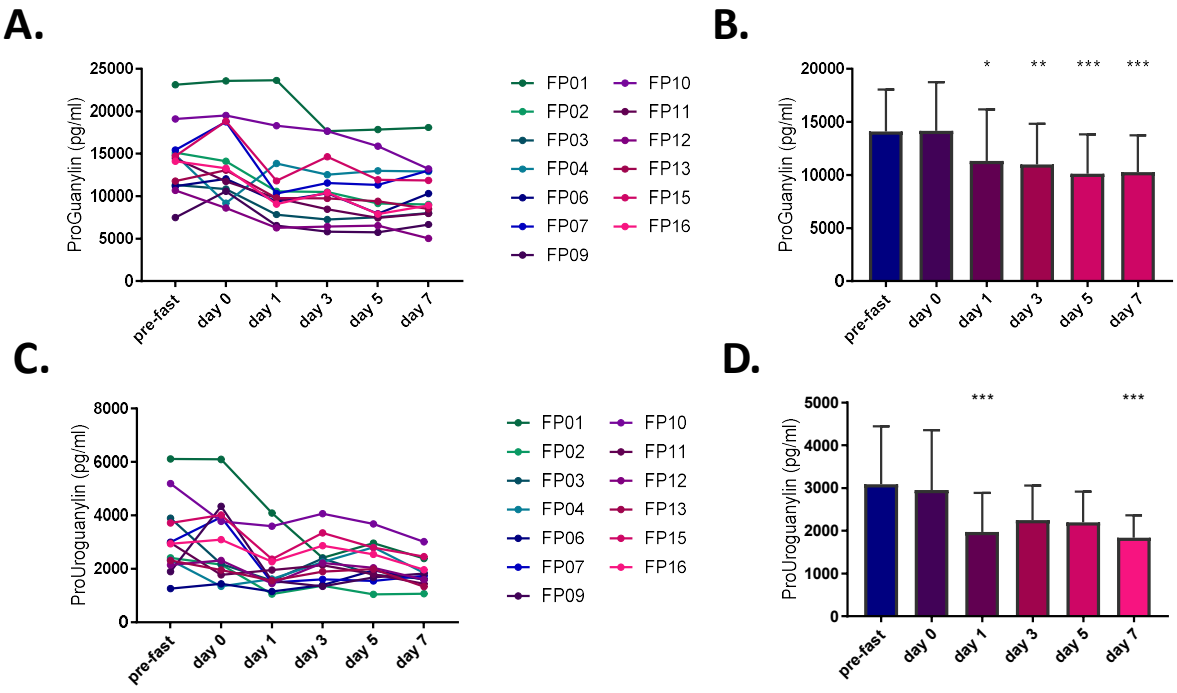

Figure 5.5: Effect of 7 days of fasting on ProGuanylin and ProUroguanylin levels in healthy volunteers. 13 healthy volunteers fasted for 7 days and ProGuanylin (**A.** and **B.**) and ProUroguanylin (**C.** and **D.**) levels were measured pre-fast and on day 0, 1, 3, 5 and 7 in Lith Hep plasma samples using the MSD assay. In **B.** and **D.** Data are mean ± SD. Statistical significance was assessed by Friedman with a post-hoc Dunn's test against the pre-fast condition. *** indicates p<0.001, ** indicates p<0.01, * indicates p<0.05.

ProGuanylin and ProUroguanylin levels were decreased significantly when compared to pre-fast levels. Furthermore, levels of both hormones continued to decrease during fast with hormone levels on day 7 approximately 50% less than levels measured at the start of the fast. These findings may be explained by mucosal atrophy with a diminution of epithelial proliferation, cells and in consequence proforms. Another hypothesis would be that the gut is trying to maximise absorption of salt and water during the fast and therefore does not secrete the proforms. To test this effect determining the luminal concentrations in future experiments may help to investigate this possibility.

Professor Jensen's research team also conducted a 50g OGTT assay on the volunteers before and after a 7-day fast and we measured levels of gut hormones, including ProGuanylin and ProUroguanylin (figure 5.6). Similar to previous results, the OGTT assay on the volunteers before fasting showed a similar trend for both ProGuanylin and ProUroguanylin (figure 5.4):

the levels of both proforms significantly decreased 60 minutes following glucose ingestion. However, after a 7-day fast, glucose ingestion did not provoke a decrease in the levels of the proforms.

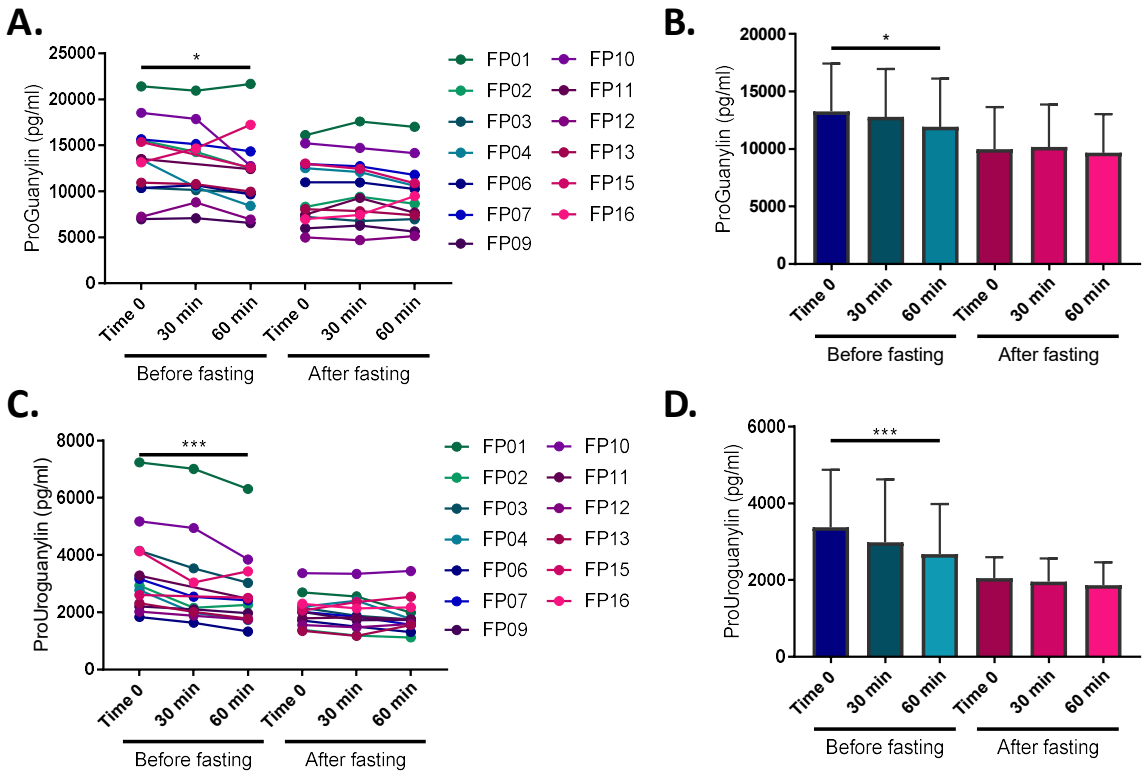

Figure 5.6: Effect of glucose intake after 7 days of fasting on ProGuanylin and ProUroguanylin levels in healthy volunteers. 13 healthy volunteers completed a 50g OGTT before and after a 7 day fast. ProGuanylin (**A.** and **B.**) and ProUroguanylin (**C.** and **D.**) levels were measured immediately before ingestion of 50mg glucose, and after 30 and 60 minutes in Lith Hep plasma samples using the MSD assay. In **B.** and **D.** Data are mean ± SD. Statistical significance was assessed by paired t test for ProGuanylin and Wilcoxon test for ProUroguanylin. *** indicates p<0.001, * indicates p<0.05.

5.2.3 ProGuanylin and ProUroguanylin levels in volunteers with metastatic midgut neuroendocrine tumours and carcinoid syndrome

In 1995, Kuhn *et al.* published a study on volunteers with Crohn's disease, ulcerative colitis and neuroendocrine tumours (NETs) (Kuhn *et al.*, 1995). The majority of the NET patients had carcinoid tumours and, consequently, chronic diarrhoea. Interestingly, greater than 60% of subjects had elevated plasma guanylin concentrations assessed with their in house radioimmunoassay.

Dr Ben Challis (Institute of Metabolic Science, University of Cambridge) collected samples from subjects with neuroendocrine tumours who were treatment naïve or receiving therapy with either octreotide (30mg) or lanreotide (60mg). The baseline characteristics of the subjects are

listed in table 5.1. ProGuanylin and ProUroguanylin levels were determined in these subjects in an attempt to observe possible differences in proforms concentrations similar to the previously described differences in active hormones (figure 5.7). Serum and plasma Lith Hep samples were collected and were compared to either serum or plasma Lith Hep samples from healthy participants. A previous experiment had shown that serum, plasma Lith Hep and plasma EDTA gave different interindividual concentrations of the proforms (data not shown). This result was also observed by Biovendor (www.biovendor.com). Therefore, plasma and serum samples were compared separately.

Preliminary data from samples isolated from subjects with neuroendocrine tumours showed a statistically significant increase in ProGuanylin levels in both serum and plasma Lith Hep. One outlier and one slightly elevated sample, in combination with a sample size of n=4, might explain this significance. ProUroguanylin levels in participants with neuroendocrine tumours did not present a significant difference with the healthy volunteers. However, the participant with extremely high levels of ProGuanylin also expressed extremely high levels of ProUroguanylin.

Subjects with neuroendocrine tumours treated with either octreotide or lanreotide did not have significantly increased ProGuanylin levels compared with control subjects. This result concurs with Kuhn's hypothesis that guanylin plasma levels in some patients could be normalised by an octreotide treatment but in order to verify this data, more participants would be required (Kuhn *et al.*, 1995).

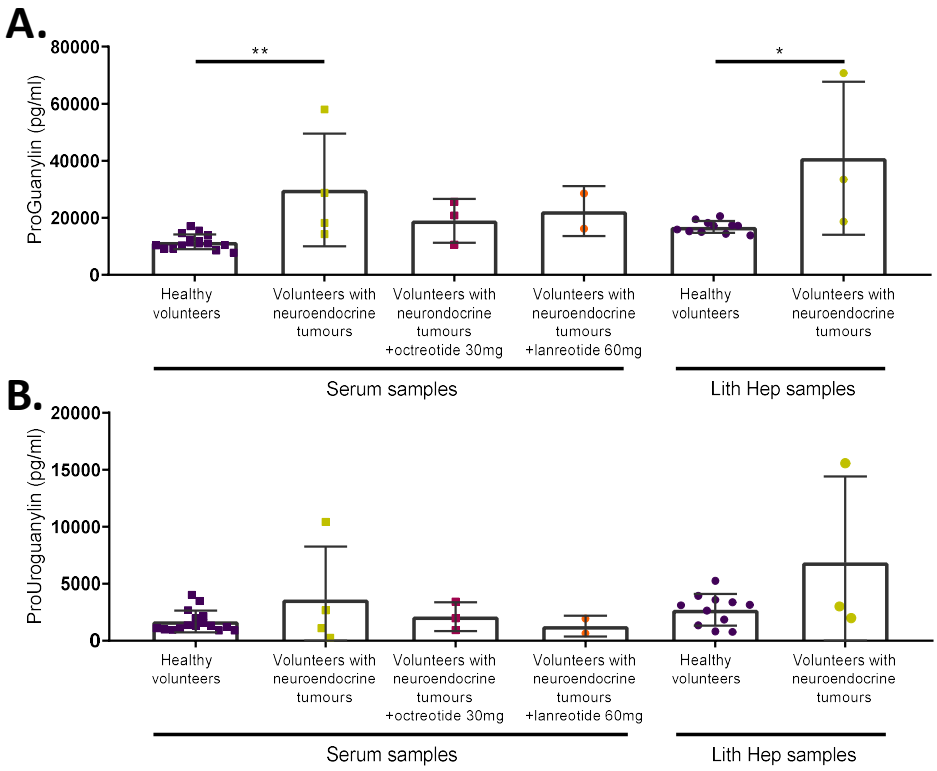

Figure 5.7: ProGuanylin and ProUroguanylin levels in healthy volunteers and volunteers with neuroendocrine tumours with and without treatment. ProGuanylin (**A.**) and ProUroguanylin (**B.**) levels were measured in fasted volunteers in serum or Lith Hep plasma samples using the MSD assay. Five volunteers with neuroendocrine tumours were under 30mg octreotide or 60mg lanreotide treatment. Data are mean ± SD. Statistical significance was assessed by Mann-Whitney test. ** indicates $p<0.01$ and * indicates $p<0.05$.

5.2.4 ProGuanylin and ProUroguanylin levels in subjects with severe gastrointestinal dysfunction

Recently, guanylin and uroguanylin have been proposed as signalling peptides in the regulation of energy balance through their effects on the brain (Valentino *et al.*, 2011; Begg *et al.*, 2014; Cintia Folgueira *et al.*, 2016). Work performed on obese subjects showed a decrease in uroguanylin levels in plasma and biopsy tissues of female adolescent volunteers compared to healthy participants (Di Guglielmo, Perdue, *et al.*, 2018; Di Guglielmo, Tonb, *et al.*, 2018).

Gut hormone profile is altered following bariatric surgery (Jacobsen *et al.*, 2012). Recently, mRNA expression of the guanylin peptides was measured in human subjects pre- and post-Roux-en-Y gastric bypass-surgery with transcripts levels for both *GUCA2A* and *GUCA2B* significantly upregulated in enteroendocrine cells (Fernandez-Cachon *et al.*, 2018).

In similarly themed research studies, the Gribble and Reimann lab have investigated the effect of Roux-en-Y bypass surgery on gut hormone profile and, opportunistically, it was possible to

access Lith Hep plasma and serum from subjects with severe gastrointestinal dysfunction. The baseline characteristics of the subjects are presented in table 5.1.

In the first study, a 50g OGTT study was completed on otherwise healthy volunteers that underwent a prophylactic total gastrectomy (due to the presence of a gastric cancer predisposing E-cadherin mutation); and ProGuanylin and ProUroguanylin levels were measured in Lith Hep plasma samples before and after 60 minutes of the OGTT (figure 5.8). In the fasting state, volunteers with prophylactic total gastrectomy had statistically higher levels of both ProGuanylin and ProUroguanylin. The means of the ProGuanylin and ProUroguanylin levels are 1.5 and 2-fold higher respectively in the participants with total gastrectomy. After 60 minutes post-OGTT, ProUroguanylin showed a statistically significant decrease when compared to baseline as previously observed in healthy volunteers. ProGuanylin, on the contrary, did not show any decrease as seen for healthy volunteers.

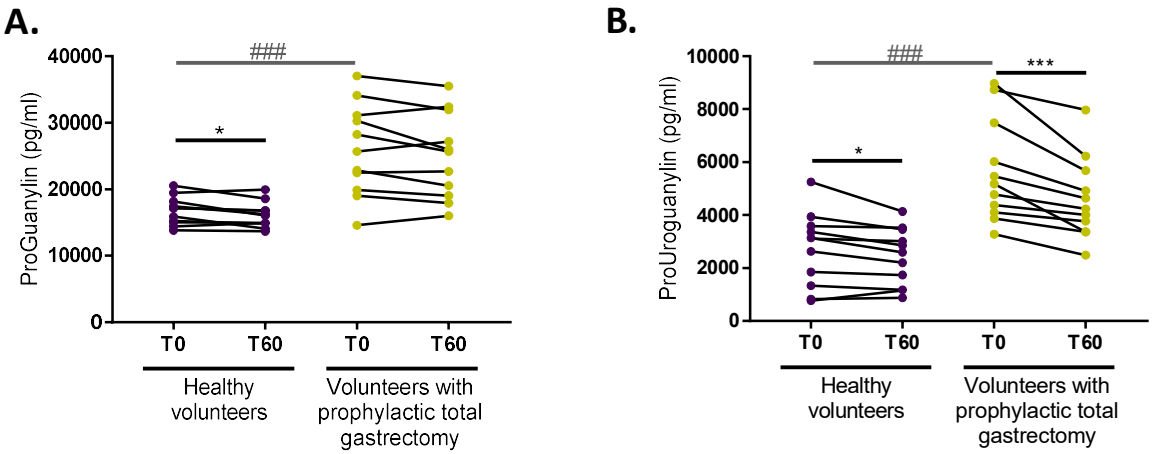

Figure 5.8: Effect of glucose ingestion on ProGuanylin and ProUroguanylin levels in healthy volunteers and volunteers with prophylactic total gastrectomy. 50g glucose was ingested at time 0, immediately after baseline blood samples were taken. ProGuanylin (**A.**) and ProUroguanylin (**B.**) levels were measured at time 0 and time 60 minutes in Lith Hep plasma samples using the MSD assay on n=11 healthy fasted volunteers and n=11 volunteers with prophylactic total gastrectomy. Statistical significance was assessed by paired t test when compared in between timepoints for ProGuanylin results or Wilcoxon test for ProUroguanylin. *** indicates $p<0.001$ and * indicates $p<0.05$. Statistical significance was assessed by Mann-Whitney test when compared in between volunteers' groups. ### indicates $p<0.001$

Other volunteers with extreme gut conditions were studied. ProGuanylin and ProUroguanylin levels were measured in serum samples from fasted subjects who had undergone small bowel transplants for a number of different clinical indications, and healthy volunteers (figure 5.9). The baseline characteristics of the participants are listed in table 5.1. ProGuanylin and ProUroguanylin levels were significantly higher in participants with small bowel transplants compared to healthy volunteers. However, these results must be interpreted with some

caution as participants that had a small bowel transplants did not all undergo the same operation. For example, some participants had both small intestine and colon transplanted, another had liver, stomach, pancreas, small bowel to native colon transplanted, whilst a third subject underwent a combined liver, pancreas and small bowel transplant

One subject of particular interest was M053 from whom a blood sample was collected following removal of the small and large intestine but prior to bowel transplantation. The serum sample did not contain any measurable levels of ProGuanylin or ProUroguanylin thereby demonstrating that the gut is the predominant source of these peptides in human blood (data not shown).

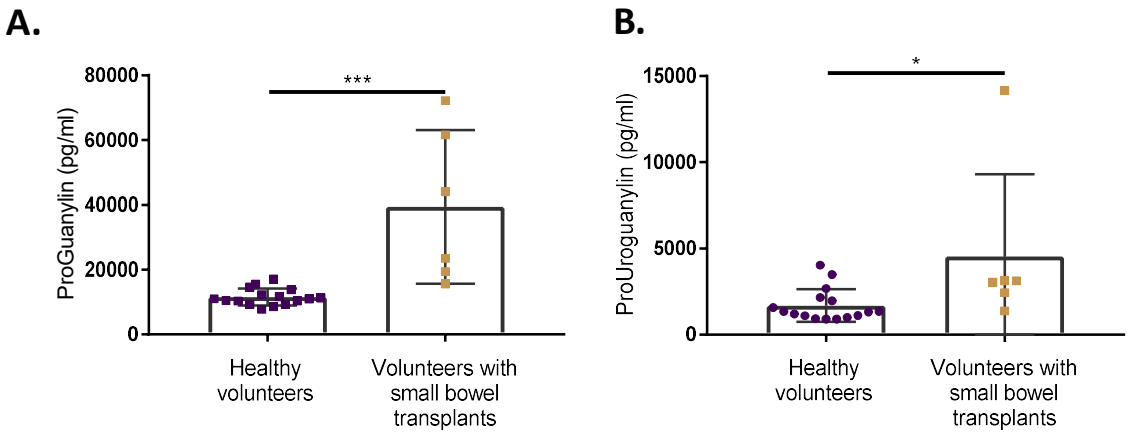

Figure 5.9: ProGuanylin and ProUroguanylin levels in healthy volunteers and volunteers with small bowel transplants. ProGuanylin (**A.**) and ProUroguanylin (**B.**) levels were measured in fasted volunteers in serum samples using the MSD assay. Data are mean ± SD. Statistical significance was assessed by Mann-Whitney test. *** indicates $p<0.001$ and * indicates $p<0.05$.

The role of ProGuanylin and ProUroguanylin in sodium homeostasis, and their potential effects on kidney function was previously studied by Kinoshita and colleagues. These investigators demonstrated that guanylin levels were increased in patients with impaired renal function (Kinoshita, Nakazato, *et al.*, 1997), and plasma uroguanylin levels were higher in subjects with chronic glomerulonephritis and hypertension (Kinoshita, Nakazato, *et al.*, 1997) as well as with chronic kidney disease (Kinoshita, Fujimoto, *et al.*, 1997).

To investigate whether plasma levels of guanylin-related peptides corrected with osmolality, samples from unselected volunteers with a range of osmolality levels were obtained from Dr Claire Meek. A summary of the data is presented in figure 5.10.

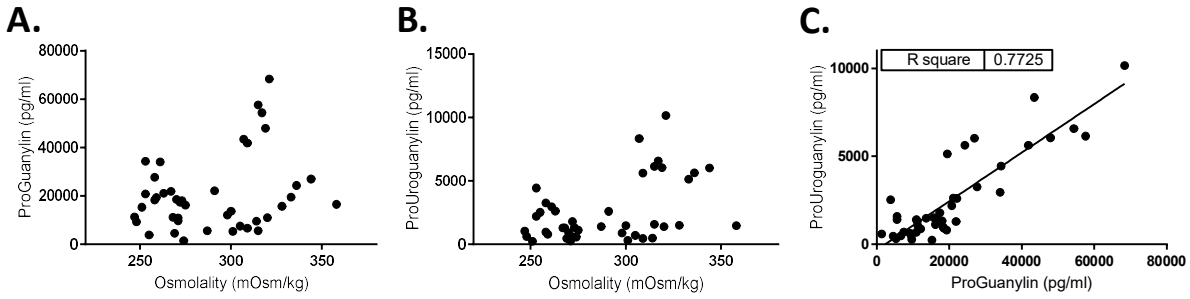

Figure 5.10: ProGuanylin and ProUroguanylin levels in unselected volunteers with a range of different osmolality levels. ProGuanylin (**A.**) and ProUroguanylin (**B.**) levels were measured in fasted volunteers in serum samples using the MSD assay. In (**C.**) levels of ProGuanylin and ProUroguanylin were plotted against each other and the linear regression was calculated.

Levels of ProGuanylin and ProUroguanylin did not show a correlation with osmolality levels, however a strong correlation was reached between the levels of ProGuanylin and ProUroguanylin with a coefficient of determination R^2 of 0.77. A caveat of this experiment was the use of unselected volunteers who had a range of different chronic or acute conditions with abnormal osmolality. The osmolality originating from chronic or acute conditions which might have differing results and would have to be divided into different categories to see a potential correlation with proforms' levels.

5.3 Discussion

5.3.1 Validation of the MSD assay on human serum samples

The MSD assay, previously described in chapter 3, was used to measure ProGuanylin and ProUroguanylin in human serum samples. This assay was compared with the commercial kit provided by Biovendor. The MSD assay presented a broader dynamic range of prohormone detection and was more sensitive at detecting lower levels of proforms compared to the competitor assay (Cf. chapter 3). Both proform MSD assays showed a strong correlation with the Biovendor kits when measuring proform levels from the same human plasma samples, but the values detected by the MSD assay were higher than the one detected by the ELISA. However, the MSD assay was able to detect and measure the provided Biovendor standards and their assessed concentrations were matching the expected values in the case of the ProUroguanylin. ProGuanylin provided by the Biovendor was, however, overestimated by a factor of 1.7. The Biovendor assay was able to detect the proforms values but the measured concentrations did not match as closely as the expected values from the MSD standards and all concentrations were underestimated. Finally, the MSD assays were easier to use in terms of incubation time and dilutions inter-assays when measuring both proforms compared with the competitor assays.

The quality of the MSD assay and binding to the correct target was further supported when tested on a human serum sample from a participant who underwent a total small and large intestine resection prior to transplantation. The sampling of the serum was performed post-removal of the small and large bowels but pre-transplant. This unique sample did not present any detectable levels of proforms and therefore provides two important insights into the MSD assay and fundamental aspects of guanylin peptide biology. Firstly, the MSD assay did not present false positive/non-specific binding in plasma Lith Hep samples and therefore the MSD assay does not overestimate the proforms in plasma Lith Hep. Secondly, the lack of proforms in this sample, correlating to a lack of gut in the volunteer, established the digestive system as the predominant source of circulation ProGuanylin and ProUroguanylin in humans.

The assay was performed on human samples and provided baseline values for ProGuanylin and ProUroguanylin in participants in a fasting state. These ranges provide the opportunity to assess circulating concentrations of the proforms in various diseases states. A limitation of the ranges' assessment was the limited number of patients that were used to establish them. The

International Federation for Clinical Chemistry (IFCC) and the Clinical and Laboratory Standards Institute (CLSI) recommends the use of 120 participants to assess the confidence intervals for reference limits which would allow the partition of the individuals according to gender or age. While the literature did not provide an insight into the expected concentrations of ProGuanylin and ProUroguanylin, the company providing both kits, Biovendor, did provide some information about the concentrations that should be expected as they tested their assay in different human samples. Whereas the Biovendor kits were performed on unselected donors and therefore do not represent a fasting or postprandial state nor a healthy or diseased state, the data showed a reasonable consistency with what was measured with the MSD assay in terms of order of magnitude. For ProGuanylin, the Biovendor kit measured 11400pg/ml when the MSD assay established a fasting concentration at 15249pg/ml. For ProUroguanylin, the Biovendor kit measured 1381pg/ml when the MSD assay established a fasting concentration of 2594pg/ml. This discrepancy could be caused by an underestimation of the levels in the ELISA kit.

Looking at the circulating levels of proforms in the blood has a potential caveat. The circulation levels do not reflect the autocrine or paracrine effect of the proforms in the gut lumen and therefore will not necessarily reflect the biological activity of these peptides. However, blood samples are the most readily available sample collected and is easy to test, thus making the establishment of reference ranges in blood samples critical to the usefulness of the developed assay.

5.3.2 Effects of standardised liquid meal and glucose on ProGuanylin and ProUroguanylin secretion

This work demonstrated that standardised liquid meal and glucose tolerance tests did not elicit a strong physiological response in plasma ProGuanylin and ProUroguanylin. A first pilot study allowed the measurement of those levels over a period of 2 hours and showed that a 60 minutes time point might measure a difference with baseline. Whereas the standardised liquid meal provoked an increase in ProUroguanylin, the oral glucose test had a decreasing effect on both ProGuanylin and ProUroguanylin. The standardised liquid meal consisted of a 230ml bottle of ensure plus, a balanced nutritional supplement containing 11g of fat, 13g of protein as well as 50g of carbohydrate and 0.52g of salt which would modify the physiological response on plasma ProGuanylin and ProUroguanylin levels when compared to an oral glucose

intake. A caveat of this study is the inability to measure the posited active version of the peptides. For instance, the decrease in ProGuanylin and ProUroguanylin levels could be caused by the action of proteases that elicit the action of guanylin peptides onto the Guanylate Cyclase-C receptor. Therefore, a decrease of proforms levels might be a sign of utilisation of the proforms.

In participants who fasted over 7 days, levels of proforms were decreased over the course of the study to half of the original concentration. An interesting finding of this study was the lack of physiological response in proforms plasma after a 50g OGTT assay after 7days of fasting, as it was originally the case.

5.3.3 Insight from patients with extreme gut conditions

Oral glucose tolerance tests were performed on participants that received a total gastrectomy. The levels of ProGuanylin and ProUroguanylin in a fasting state were extremely high with means 1.5 to 2-fold higher when compared to healthy participants. It was in accordance to a study showing that *GUCA2A* and *GUCA2B* transcripts were increased in participants that undertook a Roux-en-Y gastric bypass (Fernandez-Cachon *et al.*, 2018). Levels of proforms were measured again 60 minutes after 50mg OGTT. While ProGuanylin did not present a significant decrease as it was previously the case in healthy participants, ProUroguanylin levels decreased significantly when compared to time 0. A potential explanation is that the lack of stomach might result in a more dramatic and immediate glucose effect on the small intestine's response. ProUroguanylin is thought to be mostly expressed in the small intestine compared to the colon and the reverse was shown about ProGuanylin according to the literature (Qian *et al.*, 2000; Ikpa *et al.*, 2016) and would explain the apparent decrease in ProUroguanylin in total gastrectomy participants after 60 minutes. The reasons why ProGuanylin levels do not decrease over time after 50g OGTT are unclear and might have required measurements of hormones over a longer time period and might require further studies.

5.3.4 Use of the calculated expected values of proforms to diagnose diseases

Guanylin was mentioned as a potential marker for carcinoid tumours (Kuhn *et al.*, 1995). Levels of proforms were measured in patients before and after octreotide or lanreotide treatment. A significant increase in ProGuanylin only was measured in the small panel of samples. When treated with octreotide or lanreotide, no statistical significance was measured between the healthy volunteers and the volunteers with adenocarcinoma. Both treatments

are long-acting analogue of somatostatin. They inhibit gut hormone release and could explain the lower levels of ProGuanylin in blood.

However only 2 out of 4 samples (from the panel of serum sample) and 2 out of 3 samples (from the Lith Hep plasma) did present levels that were considered above the calculated upper reference limits. Also, the number of subjects was small, and more measurements needs to be performed on a substantial panel of individuals in order to confirm the preliminary data. If new results confirmed a reliable and significant difference in ProGuanylin levels when compared to healthy volunteers, the measurement of ProGuanylin could serve as a useful biomarker in the diagnosis and monitoring of patients with neuroendocrine tumours.

Another potential application of the measurement of the proforms as a biomarker would be on the potential implication of the guanylin peptides in colorectal cancer. Guanylin and Uroguanylin were shown to be the most commonly lost gene in colorectal cancer. More than 85% of 300 tumour samples presented a loss in *GUCA2A* and *GUCA2B* when compared to adjacent healthy tissues (Wilson *et al.*, 2014). A hypothesis suggested by Shailubai *et al.* was that the silencing of the receptor by the lack of guanylin peptides would result in colorectal cancer (Kunwar Shailubhai *et al.*, 2000). One of the arguments supporting this theory is the observed obesity-induced colorectal cancer driven by the loss of guanylin in a mouse model (Lin *et al.*, 2016).

5.3.5 Conclusions

In conclusion, the MSD assays were validated in human samples and managed to find levels of proforms that were correlating with the Biovendor kits. The advantages of the MSD assays include a broader dynamic range and is more user-friendly as undiluted samples can be used.

Assays were used to measure baseline levels of proforms and gave interesting preliminary results from a variety of human clinical samples. These assays will be able to provide insights to the physiological roles of proforms in human health states as well as a diagnostic tool in case the guanylin peptides become biomarkers.

Chapter 6: The effect of salt and gut stimuli on the secretion of ProGuanylin and ProUroguanylin

6.1 Introduction

The role of the guanylin peptides in the gastrointestinal tract became of interest when intraluminal guanylin and uroguanylin were shown to activate the GC-C receptor localised in the brush border membrane of enterocytes. Guanylin peptides are thought to be released into the intestinal lumen after the ingestion of high oral salt intake as well as on the basolateral side of the epithelium as it was detected in the circulation and in the urine (Kinoshita, Fujimoto, *et al.*, 1997; Kinoshita *et al.*, 1999). This theory was supported by a study performed in rat showing that sodium chloride oral intake increased mRNA expression of guanylin and uroguanylin in the intestine after 4hrs and the mRNA expression plateaued after 8hrs (Carrithers *et al.*, 2002). The lack of a high-throughput assay slowed down the understanding of the mechanisms of secretion of guanylin and uroguanylin. Such assay being now developed (cf. chapter 3), it allowed the investigation of the effect of salt, gut or vagal stimuli in different secretion models.

6.1.1 Models of interest to study the secretion of proforms

Caco-2/TC7 cell line as a secretion assay model

The Caco-2 cell line is a human intestinal cell line established from colonic adenocarcinoma in 1977 (Fogh, Wright and Loveless, 1977). When most of the cell lines required differentiation via synthetic or biological factors supplementation, Caco-2 upon confluence can undergo polarisation and differentiation to give rise to mature enterocytes upon confluence (Pinto *et al.*, 1983). Even though this cell line was originated from colonic adenocarcinoma, specific morphological and functional properties of the absorptive small bowel enterocytes as well as the colonocytes were displayed such as α_1-AT surfactant-like particle, a 55kDa protein only found in small intestine (Engle, Goetz and Alpers, 1998; Xie, Shao and Alpers, 1999; Sambuy *et al.*, 2005). Caco-2 cell monolayers have been extensively used for metabolism study (Béaslas *et al.*, 2008) and drug transport analysis (Artursson, Palm and Luthman, 2001).

In an attempt to make the Caco-2 cell line more homogenous, several subclones, such as Caco-2/15 (Beaulieu and Quaroni, 1991), Caco-2/BBE (Peterson and Mooseker, 1992) and Caco-2/TC7 (Caro *et al.*, 1995), were generated from the parental Caco2/ATCC cell line. The TC7 cell

line, originated from a Caco-2 wild type at late passage, demonstrated tighter junctions and reproducibility inter-experiments (Zucco *et al.*, 2005). Another advantage of the use of TC7 cell line is the quicker differentiation period of those cells compared to the standard Caco-2. Fourteen days of culture was enough to reach the same permeability characteristics when 21 days minimum were necessary for the use of the Caco-2 cell line (Zeller *et al.*, 2015). Finally, ProGuanylin and ProUroguanylin mRNA expression could be detected and protein and proforms production was measurable with the newly developed MSD assay, allowing their use as a secretion model.

Human intestinal organoids as a secretion assay model

The identification of the small intestine and colon stem cells by Barker *et al.* at the bottom of the crypts allowed the potential of three-dimensional, long-term and self-sufficient cultures, called organoids (Barker *et al.*, 2007). The Lgr5 marker was identified as a marker for adult stem cells. Stem cells lineage tracing acknowledged their differentiation into all intestinal epithelial cells.

The same group developed crypt villous organoids from either single Lgr5+ stem cells or isolated crypts (Sato *et al.*, 2009). They developed a culture media allowing the organoids to develop into budding structures, consisting of a central lumen with bourgeoning crypt structures and villus domain toward the centre of the 3D structure (figure 6.1).

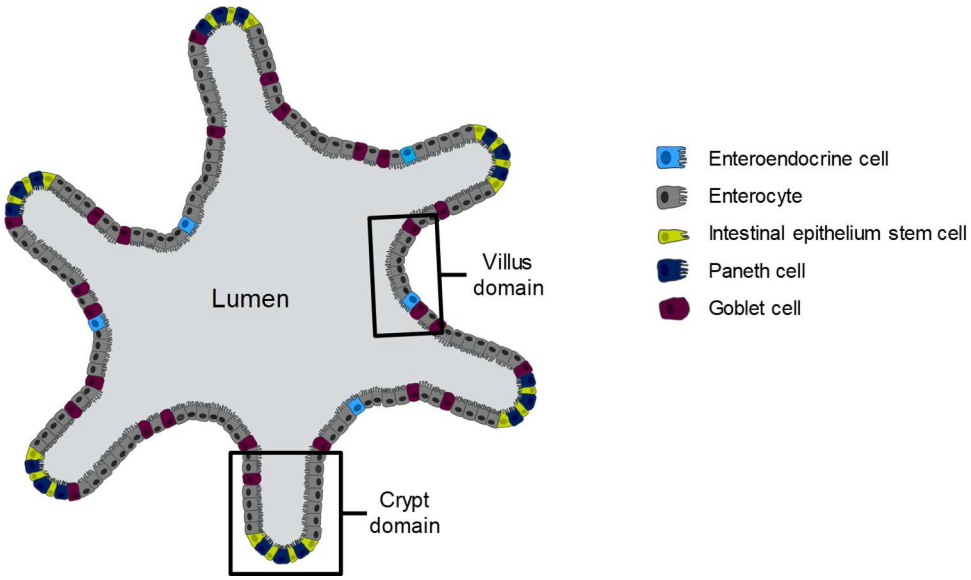

Figure 6.1: Schematic representation of an intestinal organoid. Figure adapted from Roeselers *et al.*, 2013.

New advances on protocols enabled the culture of human organoids from isolated human crypts. They are kept in an undifferentiated state by the addition of Wnt protein and can be

differentiated by its removal (Jung *et al.*, 2011; Sato *et al.*, 2011). Gastrointestinal organoids were successfully validated as a tool to assess hormone secretion to different stimuli (Petersen *et al.*, 2014; Zietek *et al.*, 2015; Goldspink *et al.*, 2018a) and when differentiated, they expressed, produced and secreted some guanylin and uroguanylin.

Air-Liquid Interface monolayer cultures on transwells

Transwells are permeable supports that provide access to both sides of a cell monolayer and allow to study side-specific stimulation and look at the results of secretion on both sides of the membrane. Transwells have been extensively used with Caco-2 cell lines in order to look at drug absorption across the intestinal epithelium as cells do not polarise and differentiate as well on glass/plastic (Artursson and Karlsson, 1991; Miret, Abrahamse and Groene, 2004).

Emergence of human organoids as a tool provides the opportunity to have readily available human intestinal epithelium material. Caco-2 cell lines harbouring cancerous mutations (for instance APC mutations) and not accurately representing any intestine part could therefore be replaced by organoids. A study compared the development and characterisation of mouse intestinal monolayer in transwells from organoids and compared gene expression of the differentiated cultures to corresponding tissues as well as trans-epithelial electrical resistance (TEER) (Kozuka *et al.*, 2017).

In an attempt to improve even further morphological and functional properties of the organoids monolayer, as well as oxygen supply, air-liquid interface (ALI) cultures were developed for gastric cultures (Ootani *et al.*, 2000; Yokoyama *et al.*, 2007). More recently, research was performed on the structural and functional differentiation of intestinal porcine epithelial cells in ALI cultures that showed an improved columnar shape and cell volume (Nossol *et al.*, 2011). Successful ALI cultures were established from human colonic organoids (Usui *et al.*, 2018) and intestinal ALI cultures established from stem cells presented crypt/villous configuration and typical epithelial cell markers of Paneth, goblet, and enteroendocrine cells (Wang *et al.*, 2015; Yamamoto *et al.*, 2016).

Ussing chamber

Ussing chamber is a device allowing the measurement of ions, nutrients, and drugs transport across various epithelial tissues. The method and apparatus were developed by Hans H. Ussing to understand the active transport of ions across frog skin. The technique principle relies on

the separation of the apical and basal part of an epithelium in two chambers containing the same Ringer solution and measure the short-circuit current as an indicator of net ion transport taking place across the epithelium. Since then, the Ussing chamber system evolved little but has been applied to the understanding of the mouse intestine (Clarke, 2009).

Ussing chamber is now a common tool to investigate the apical or basolateral response to stimuli (Brighton *et al.*, 2015; Pais *et al.*, 2016). However, Ussing chamber studies were mainly performed on animals, but studies by Collins *et al.*, and McDermott *et al.* also used mounted human colonic epithelia obtained during surgery (Collins *et al.*, 2009; McDermott *et al.*, 2015).

6.1.2 Sodium chloride role on the secretion of the guanylin peptides

Some previous studies tried to look at the implication of guanylin and uroguanylin on the gastrointestinal-renal natriuretic axis and the implication of an oral salt load on their secretion.

In a study performed in rat, a high salt diet correlated with higher levels of uroguanylin in urinary excretion when compared to a lower salt diet (0.08% Vs 4% NaCl). Interestingly plasma levels did not increase (Fukae *et al.*, 2002). A study from the same year supported by a study showing that sodium chloride oral intake increased mRNA expression of *Guca2a* and *Guca2b* in the intestine (Carrithers *et al.*, 2002). A similar method showed in rats that levels of *Guca2b* transcripts were increased after 4hrs of feeding with 7% NaCl in chow diet (Carrithers *et al.*, 2002). Finally, a study by Kinoshita and colleagues highlighted the physiological role of high salt diet on uroguanylin levels in a human study. Urinary excretion and blood levels of healthy participants were measured over 24hrs and uroguanylin levels were higher in participants on a high salt diet (10g/day) compared to volunteers on low salt diet (7g/day) (Kinoshita, Fujimoto, *et al.*, 1997).

The role of sodium on acute guanylin secretion has been investigated as well. A perfused small intestines rat model was used to look at the response of different salt and mannitol concentrations. Mannitol is used as a control to match the osmolarity levels of the solution without interacting with the cell as NaCl would. Kita *et al.* showed that a 200mM salt loading led to a 3-fold increase in guanylin with an effect lasting over 60 minutes. Such increase was not detected for uroguanylin in this model. However, a caveat of this study was that increasing concentration of mannitol also increased the guanylin release (Kita *et al.*, 1999). Finally, another study evaluated the guanylin protein and mRNA expression in colon of rats that

received low, normal or high salt diet (0.08%, 0.47%, 1.65% net NaCl concentration) for a week. Guanylin production was reduced by 30% in animals on low salt diet (Li *et al.*, 1996).

6.1.3 Other mediators implicated in the secretion of the guanylin peptides

Other stimuli of the guanylin and uroguanylin secretion were studied, but only in rat models. A study by Martin *et al.*, looked at the regulation of ProGuanylin by neuronal mediators that are implicated in intestinal ion regulation and water transport (Martin *et al.*, 1999). Carbachol, a cholinergic agonist and potent parasympathetic agent (Shiroma and Costa, 2015), triggered a 7-fold increase of ProGuanylin release on both sides of the mucosa in an Ussing chamber experiment on rat colonic mucosa. Other neuronal mediators NO and VIP did not affect the release of ProGuanylin. The use of cGMP mimetic (8-bromo-cGMP), a downstream signalling effector of the guanylin peptides and product of the GC-C receptor, increased the release of ProGuanylin as well. In this study however, measurement of ProGuanylin levels was performed using an ELISA with an antibody specific to the C-terminal (the active part of guanylin) and having a 100-fold lower affinity than for the smaller peptide. This low affinity can be an important problem as the proforms could dissociate from the antibody during one of the wash step leading to miscalculation of the levels of ProGuanylin (Martin *et al.*, 1999).

Those results were corroborated with an experiment using isolated perfused rat colon where cholinergic regulation was studied with carbachol and bethanecol, both muscarinic agonist. Luminal guanylin release displayed a 6-fold increase in presence of carbachol or bethanecol. Similarly, in perfused rat colon, forksolin and the neuropeptide bombesin have also been identified as potential stimuli of guanylin release (Moro *et al.*, 2000).

6.1.4 Project aims

Using Caco-2/TC7 cell line, human organoids, ALI cultures and Ussing chamber in combination with the MSD assays, the aims were to:

a) Investigate the secretion of ProGuanylin and ProUroguanylin in response to standard vagal and gut stimuli as well as previously described stimuli.
b) Study the secretion of ProGuanylin and ProUroguanylin in response to salt.
c) Explore the site-directed secretion of ProGuanylin and ProUroguanylin using Ussing chambers.

To address those aims, the secretion of ProGuanylin and ProUroguanylin in response to salt, gut or vagal mediators was investigated performing secretion assays on different culture models: TC7 cell line, human organoids, ALI cultures on transwells and Ussing chambers.

Duodenal and colonic human organoid lines were generated from human tissues using a modified protocol from Sato et al. Organoids were maintained in an undifferentiated state with a high concentration of Wnt-3a and differentiated when needed for 7-10 days through the removal of growth factors in media as described in section 2.8.2. ProGuanylin and ProUroguanylin secretion were performed on organoids differentiated for 7-10 days and on 9-day old confluent TC7 cells using test agents dissolved in basal media. Secretion assays were performed according to methods described in 2.8.3. Total protein levels in cell lysate of organoids were measured by BCA assay (See 2.8.4) while transcripts levels of TC7 were measured by qPCR after RNA extraction and reverse transcription (See 2.10).

Ussing chamber studies were performed on human tissue biopsies obtained through Addenbrooke's hospital tissue bank program from patients undergoing partial colectomy. Stripped epithelia were mounted in an Ussing chamber and samples were taken from both apical and basolateral compartments at 15, 45 and 90 minutes. At 45 minutes forskolin/IBMX was added bilaterally as described in section 2.9.

ProGuanylin and ProUroguanylin levels were measured in the newly developed MSD assay with methods described in sections 2.7.2 and toxicity of the test agents was evaluated by LDH assay (See 2.11).

6.2 Results

6.2.1 Proforms are not accumulated in the cells but secreted in the media in TC7 model

Pilot experiments were performed on TC7 cells to measure the levels of proforms in the supernatant as well as in the lysis samples. Early time points (30 minutes, 1hr and 2hrs) were tested in standard HEPES-buffered saline solution (138 buffer) but levels were too low to be measured in the MSD assays (data not shown). Concentrations of both proforms were in the detection range and in the linear part of the standard curves after 4hrs of secretion. In order to perform 4hrs, 8hrs or 24hrs secretion experiments and keep cells alive, standard growing media were used as basal media and stimuli were added to it. Consequently, the second pilot experiment was performed on TC7 cells and levels of proforms were measured after 4, 8 and 24 hrs for 2 conditions: basal media and media complemented with 10µM Forskolin and IBMX in cell lysates and supernatants (figure 6.2).

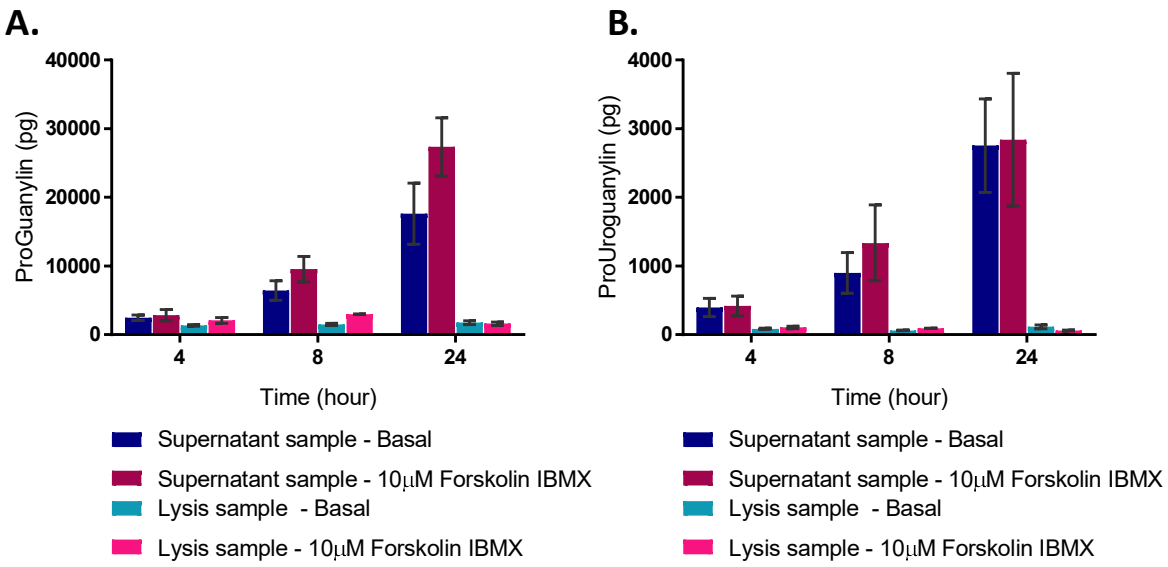

Figure 6.2: Measurement of ProGuanylin and ProUroguanylin levels in TC7 cells supernatant and cell lysis over 24 hours. TC7 cells were incubated with standard growing media with/without 10µM Forskolin/IBMX. Supernatant and cell lysis were collected after 4hrs, 8hrs and 24hrs incubation and ProGuanylin (**A.**) and ProUroguanylin (**B.**) levels were measured using the MSD assay. Data are mean ± SD, n=6 (two wells from each of 3 independent experiments).

A control experiment was performed in which proforms were spiked in DMEM media as well as in lysis buffer and measured in the MSD assays (data not shown). Percentage recoveries were above 95% in both the DMEM and the lysis media and it was concluded that the antibody pairs were able to measure proforms in the DMEM media and lysis buffer. Levels of proforms increased over time and a well of TC7 cells was enough to release 20-30ng of ProGuanylin and

3ng of ProUroguanylin in the supernatant over 24hrs. While proforms levels were accumulating in the supernatant, their levels stayed unchanged in cell lysates over the 3 different time points indicating that cells did not change their proform production during the experiment. The low but constant levels of proforms in the cell lysates suggest a minimal storage in the TC7 cells. Therefore, rather than a direct regulation of the secretion of the proforms already stored in the cells, it is the rate of production of the prohormone (RNA levels, translation machinery or RNA stability) which might be affecting the amount secreted into the media.

From this pilot experiment, it was decided to look at the protein levels of ProGuanylin and ProUroguanylin in the supernatant and at the transcript levels in the cell lysates after stimulus to correlate different release levels to possible changes in prohormone expression after 4hrs and 24hrs application of a potential stimulus.

6.2.2 Effect of gut stimuli on the secretion of proforms

We investigated the proforms release using this approach in response to previously described stimuli like bombesin and carbachol and other products known to stimuli intestinal cells such as peptones, a protein digest product activating pathways sensitive to amino acids and peptides (CASR, GPR93 (Choi *et al.*, 2007; Pais, Gribble and Reimann, 2016)), the secondary bile acid TDCA (activating TGR5 (Brighton *et al.*, 2015)), forskolin, in conjunction with IBMX, (inducing high levels of cAMP (Simpson *et al.*, 2007; Alasbahi and Melzig, 2012)), or PMA, a stimulator of protein kinase C (PKC) (Castagna *et al.*, 1982; Parker *et al.*, 2009).

6.2.2.1 Use of Caco-2/TC7 cell line

Using the pilot experiment results TC7 cells were in incubated for 4hrs and 24hrs with the aforementioned stimuli. Protein levels of ProGuanylin were measured using the MSD assay and concentrations were normalised to the basal condition (figures 6.3A and B). At the 4hrs incubation time point, 10μM forskolin/IBMX was the only condition that increased the release of ProGuanylin. The *GUCA2A* transcript levels were measured on the extracted RNA by RT-qPCR (figure 6.3C) and only forskolin/IBMX showed a significant increase in expression of the proform ProGuanylin in media.

After 24hrs peptone along with forskolin/IBMX increased ProGuanylin levels ($p<0.001$) whereas PMA decreased levels. On the other hand ProGuanylin levels were decreased in the

presence of PMA when compared to the basal condition (p<0.01). Transcript analysis at 24hrs showed changes in *GUCA2A* expression when stimulated with peptone (figure 6.3D).

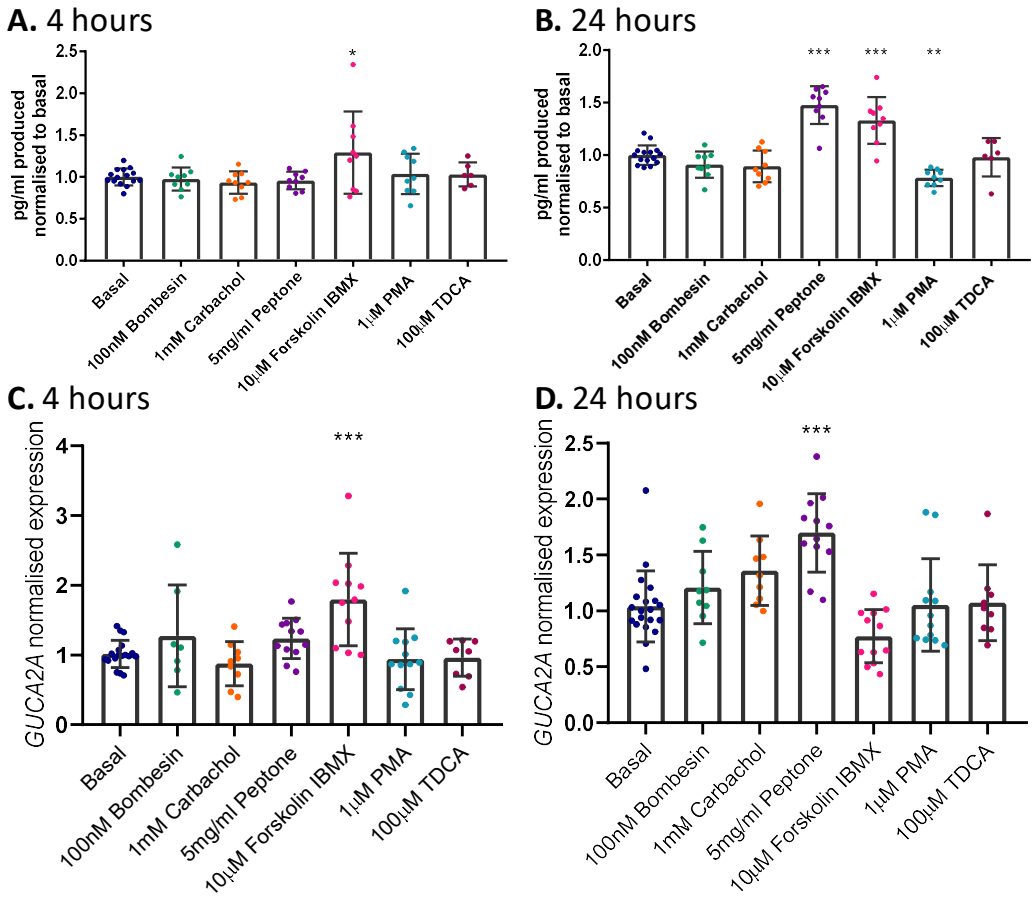

Figure 6.3: Effect of gut stimuli on ProGuanylin secretion on TC7 cultures. TC7 cells were incubated with standard growing media with 100nM bombesin, 1mM carbachol, 5mg/ml peptone, 10μM forskolin/10μM IBMX, 1μM PMA, or 100μM TDCA. ProGuanylin levels were measured after 4hrs incubation **(A.)** and after 24hrs incubation **(B.)** using the MSD assay. The measured concentrations were normalised to the mean basal value. The relative expression of mRNA for *GUCA2A* (Guanylin) was measured after 4hrs incubation **(C.)** and 24hrs incubation **(D.)** with stimuli. The relative expression to *ACTB* (beta-actin) is represented as $2^{(-\Delta CT)}$.
In **(A.)** and **(B.)** data are mean ± SD, n=9 (from 3 independent experiments). In **(C.)** and **(D.)** data are geometric mean ± SD. Statistical significance was assessed by one-way ANOVA with a post-hoc Dunnett's test. *** indicates p<0.001, ** indicates p<0.01, * indicates p<0.05.

ProUroguanylin levels were measured using the same supernatant: after 4hrs and 24hrs with stimulus. After 4hrs incubation, only a slight decrease in ProUroguanylin was noticed in presence of PMA and none of the transcript levels presented a significant difference when compared to the basal level (figures 6.4A and C). A 24hrs incubation displayed similar results with only PMA having a detrimental effect on the ProUroguanylin levels (figure 6.4B). Only the forskolin/IBMX condition presented a slight but significant decrease in *GUCA2B* transcript levels when compared to basal condition.

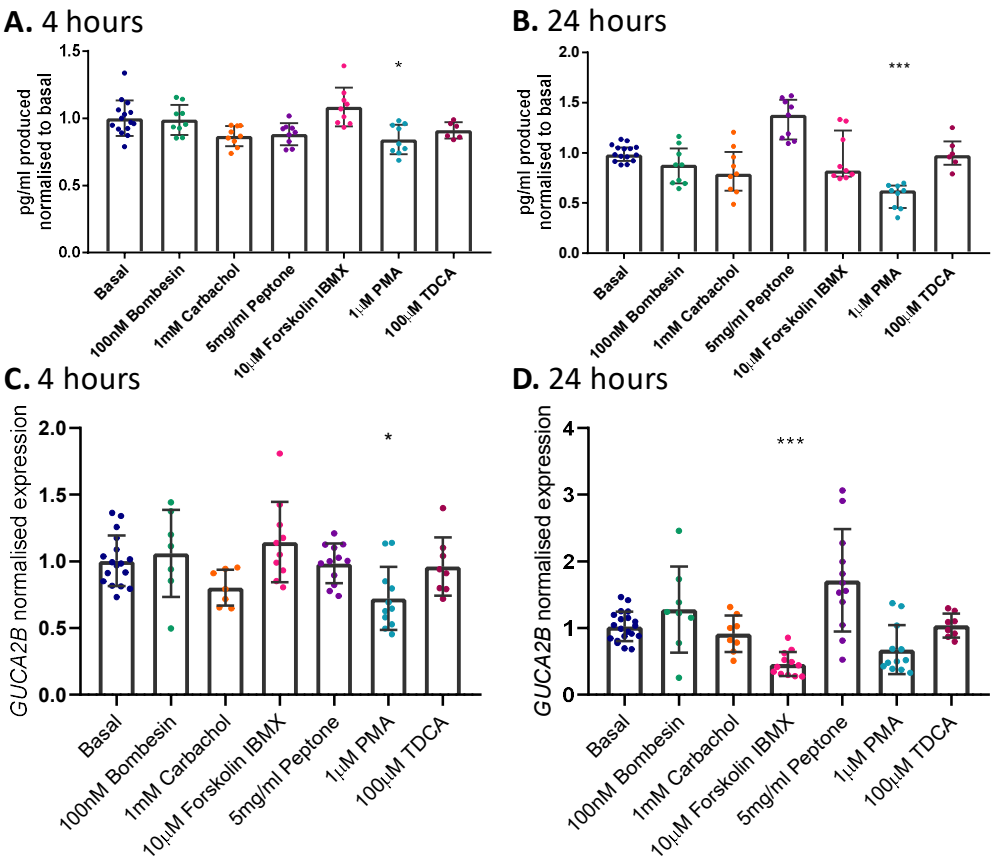

Figure 6.4: Effect of gut stimuli on ProUroguanylin secretion on TC7 cultures. TC7 cells were incubated with standard growing media with 100nM Bombesin, 1mM Carbachol, 5mg/ml Peptone, 10µM Forskolin/IBMX, 1µM PMA, or 100µM TDCA. ProUroguanylin levels were measured after 4hrs incubation **(A.)** and after 24hrs incubation **(B.)** using the MSD assay. The measured concentrations were normalised to the mean basal value. The relative expression of mRNA for *GUCA2B* (Uroguanylin) was measured after 4hrs incubation **(C.)** and 24hrs incubation **(D.)** with stimuli. The relative expression to *ACTB* (beta-actin) is represented as $2^{(-\Delta CT)}$.
Data are median and interquartile ranges, n=9 (from 3 independent experiments). Statistical significance was assessed by Kruskal-Wallis with a post-hoc Dunn's test. *** indicates p<0.001, ** indicates p<0.01, * indicates p<0.05.

PMA toxicity on the TC7 cell line

When compared to basal secretion, levels of proforms were decreased after 24hrs and this result could be explained either by an inhibiting effect of PMA on the cells or a toxic effect leading to cell death. Toxicity of the PMA was therefore investigated on the TC7 cells after 24hrs using a Lactate Dehydrogenase (LDH) cytotoxicity assay. LDH is a marker of osmotic lysis or cytotoxicity and the LDH cytotoxicity assay is a colorimetric assay which measures and quantify the release of LDH in the media (Korzeniewski and Callewaert, 1983).

Toxicity effect of PMA on the TC7 cells was measured after 24hrs of exposure (figure 6.5). Cells presented a higher percentage of cell death after exposure to PMA compared to the basal

condition. The toxicity of PMA provoked cell death and could explain the decrease in proforms secretion in the media and gene expression observed for both hormones.

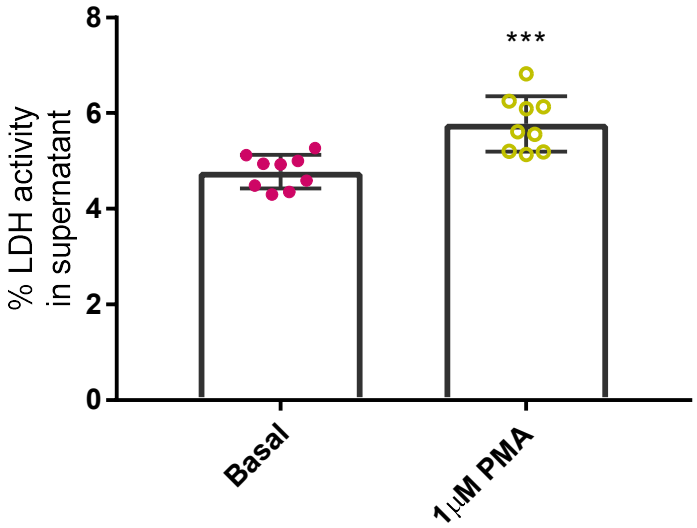

Figure 6.5: Toxicity effect of PMA on TC7 cultures. TC7 cells were incubated with standard growing media with 1µM PMA. LDH activity was measured in supernatant and cell lysate after 24hrs incubation using the LDH assay. Levels of LDH activity in supernatant were normalised to the total LDH activity per well (supernatant and cell lysate).
Data are mean ± SD, n=9 (from 3 independent experiments). Statistical significance was assessed by unpaired t-test. *** indicates p<0.001.

6.2.2.2 Use of human organoid

Assessment of the differentiation period to use organoids for secretion

Human organoids are a relatively new tool to study the effect of stimuli on secretion (Zietek *et al.*, 2015; Goldspink *et al.*, 2017). Human organoids were maintained in an undifferentiated state in WENR media. To differentiate the organoids, Wnt3a is removed from the media. As early indication showed that the guanylin peptides are produced in mature enterocytes and goblet cells, monitoring the differentiation of the organoids was necessary to perform secretion assay while knowing the cells were able to express ProGuanylin and ProUroguanylin. To control that organoids were sufficiently differentiated, *GUCA2A* and *GUCA2B* expression was measured in organoids over a 12 days period (figure 6.6). After 12 days, the organoids have changed morphology and were not used for secretion.

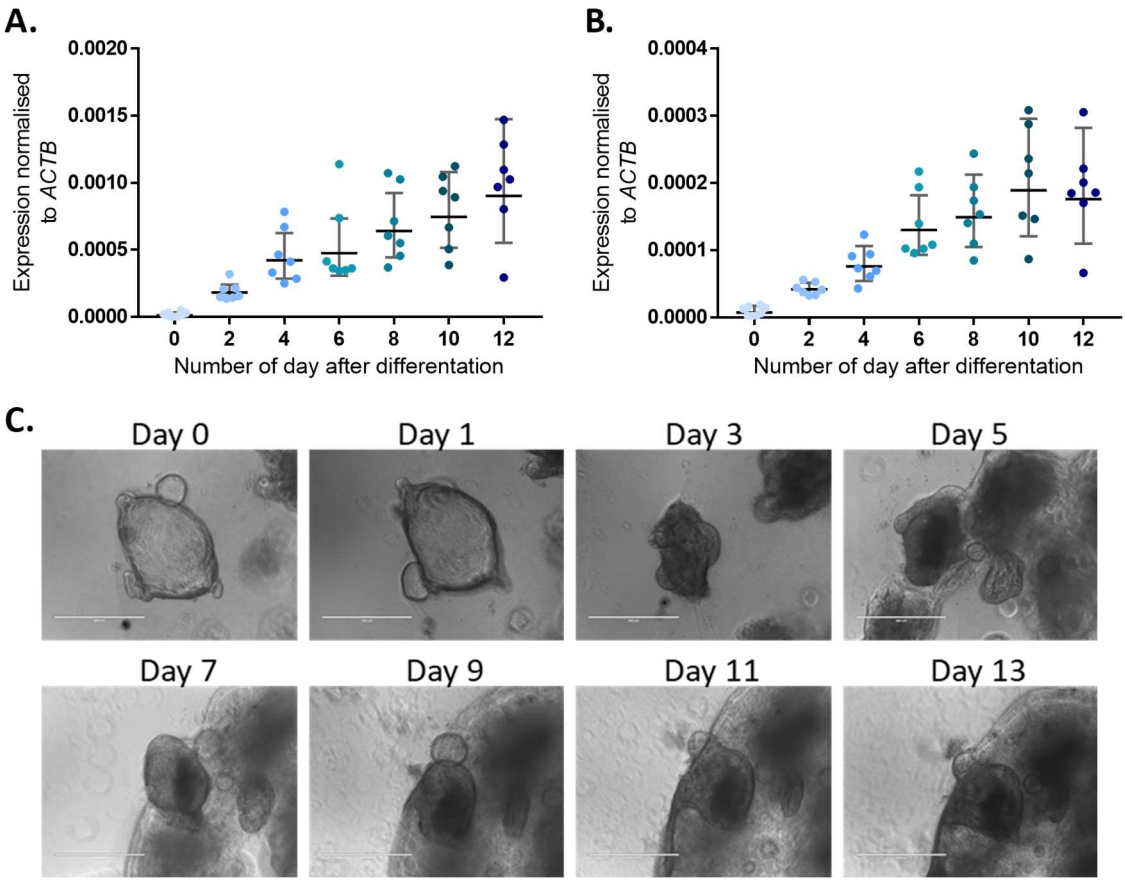

Figure 6.6: Effect of differentiation media on mRNA expression and visual aspect of human duodenum organoids. Undifferentiated human duodenum organoids were incubated with differentiation media over a 12 days course. Every other day, mRNA was extracted and the expression levels of *GUCA2A* (Guanylin) **(A.)** and *GUCA2B* (Uroguanylin) **(B.)** were measured by qPCR. Data is represented as relative expression to *ACTB* (beta-actin) using the $2^{(-\Delta CT)}$ method. Data are geometric mean ± SD, n=7 wells (two or three wells from each of 3 independent experiments). **(C.)** Phase contrast images of human duodenum organoid over 13 days of differentiation.

GUCA2A and *GUCA2B* were undetected in the undifferentiated duodenal organoids and transcripts levels increased over time during differentiation. After 8 days of differentiation, the transcripts levels plateaued, and it was decided to perform the secretion between 8 and 10 days of differentiation. Similar results were found in human colonic organoids.

Secretion and transcription levels with previously described stimuli on human organoids

Human colonic and duodenal organoids were used to study the secretion of ProGuanylin and ProUroguanylin in response to bombesin, carbachol, peptone, forskolin/IBMX, PMA, TDCA and aldosterone. Aldosterone was tested on organoids due to its role on the mineralocorticoid receptor, regulating electrolyte balance in the circulation. The receptor is not expressed by TC7 cells and therefore aldosterone as a stimulus was not investigated on the TC7 cells. After differentiating the organoids for 8-10 days, cells were used for secretion. A pilot experiment

was performed on 2D organoid cultures and 3D organoid cultures on basal media over 24hrs and levels of proforms were higher in MSD assays on 3D organoid cultures after 24hrs (data not shown). Secretion were started after washing wells three times with differentiation media. Stimuli were diluted in differentiation media and supernatant was collected after 24hrs. Proforms were measured using the MSD assay developed in chapter 3. The concentrations were normalised to the total protein levels (measured by BCA) to correct inconsistencies of organoid sizes and organoids density between splitting.

Normalisations of the measured ProGuanylin and ProUroguanylin levels after 24hrs incubation in duodenum and colon are summarised in figure 6.7 and figure 6.8 respectively. As expected, undifferentiated organoids did not secrete the proforms and were in accordance with the measured mRNA levels (figures 6.6A and B). ProUroguanylin levels were low to undetectable in the duodenum organoids but quantifiable in colonic samples.

Levels secreted of ProGuanylin and ProUroguanylin (in colon) were not altered by any stimuli except PMA which had a significant inhibiting effect on the secretion of ProGuanylin in duodenum and a trend in colon. ProUroguanylin levels appeared also to be decreased by PMA in the colonic organoid.

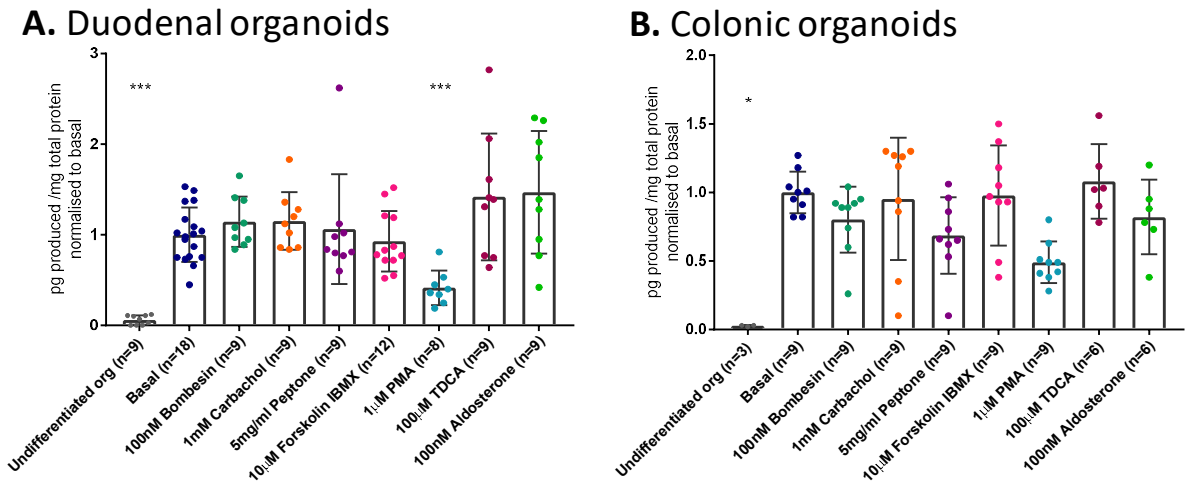

Figure 6.7: Effect of different stimuli on ProGuanylin secretion on human differentiated organoids. (A.) Duodenal human organoids and **(B.)** Colonic human organoids were incubated with differentiation media supplemented with 100nM bombesin, 1mM carbachol, 5mg/ml peptone, 10µM forskolin/IBMX, 1µM PMA, 100µM TDCA or 100nM aldosterone. ProGuanylin levels were measured after 24hrs incubation using the MSD assay. Data normalised to total protein content and to the mean basal value.
Duodenal and colonic organoids lines were established from a single human donor each. Data are mean ± SD, n=6-18 (from 3 independent experiments). Statistical significance was assessed by one-way ANOVA with a post-hoc Dunnett's test. *** indicates $p<0.001$, * indicates $p<0.05$.

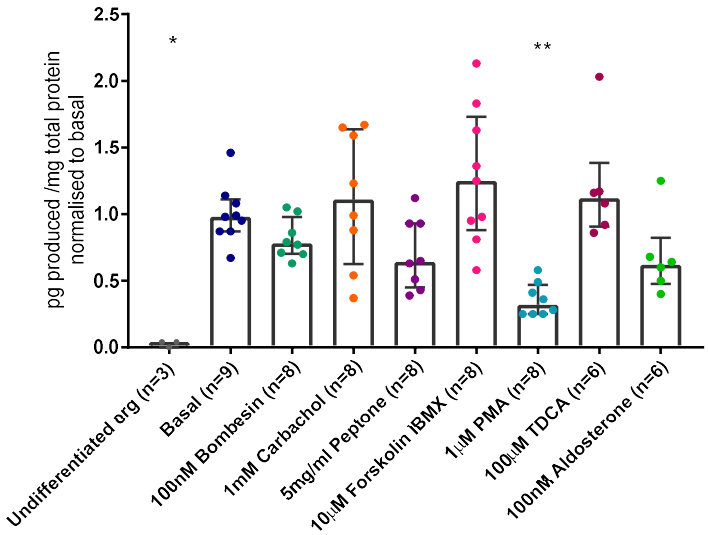

Figure 6.8: Effect of stimuli on ProUroguanylin secretion on human differentiated colonic organoids. Colonic human organoids were incubated with differentiation media supplemented with 100nM Bombesin, 1mM Carbachol, 5mg/ml Peptone, 10µM Forskolin/IBMX, 1µM PMA, 100µM TDCA or 100nM Aldosterone. ProUroguanylin levels were measured after 24hrs incubation using the MSD assay. Data normalised to total protein content and to the mean basal value.
The colonic organoid line was established from a single human donor. Data are median and interquartile ranges, n=3-9 (from 3 independent experiments). Statistical significance was assessed by Kruskal-Wallis with a post-hoc Dunn's test. ** indicates $p<0.01$ and * indicates $p<0.05$.

6.2.2.3 Summary

Two models were used to look at the effect of gut stimuli on proforms secretion and results are summarised in the table 6.1. Bombesin and carbachol which were described in the literature as stimulating secretion of guanylin did not present any effect on the proforms secretion in both the TC7 cell line and duodenal and colonic organoid model.

Standard gut stimuli action on the proform release and transcript levels of the guanylin peptides was investigated using the 2 models. Peptones presented a low but significant effect on the protein secretion of ProGuanylin after 24hrs. A similar effect was noticed for forskolin/IBMX as a stimulus, displaying higher levels of ProGuanylin proteins after 4hrs and 24hrs. PMA had a consistent adverse effect on the cells (either organoids or TC7) when used for over 24hrs and could be explained by the toxic effect of the drug over such period of time. Bile Acid TDCA and mineralocorticoid receptor activator aldosterone did not modify the secretion of proforms.

A.

ProGuanylin mRNA and protein levels	100nM Bombesin	1mM Carbachol	5mg/ml Peptone	10µM Forskolin IBMX	1µM PMA	100µM TDCA	100nM Aldosterone
TC7 4H protein levels	nc	nc	nc	+	nc	nc	nc
TC7 4H mRNA levels	nc	nc	nc	+	nc	nc	nc
TC7 24H protein levels	nc	nc	+	+	-	nc	nc
TC7 24H mRNA levels	nc	nc	+	nc	nc	nc	nc
Duodenum Organoids 24H protein levels	nc	nc	nc	nc	nc	nc	nc
Colon Organoids 24H protein levels	nc	nc	nc	nc	nc	nc	nc

B.

ProUroguanylin mRNA and protein levels	100nM Bombesin	1mM Carbachol	5mg/ml Peptone	10µM Forskolin IBMX	1µM PMA	100µM TDCA	100nM Aldosterone
TC7 4H protein levels	nc	-	nc	nc	-	nc	nc
TC7 4H mRNA levels	nc	nc	nc	nc	-	nc	nc
TC7 24H protein levels	nc	nc	+	nc	-	nc	nc
TC7 24H mRNA levels	nc	nc	nc	-	-	nc	nc
Duodenum Organoids 24H protein levels	nc	nc	nc	nc	nc	nc	nc
Colon Organoids 24H protein levels	nc	nc	nc	nc	-	nc	nc

Table 6.1: Summary of the effects of stimuli on proforms secretion and mRNA levels using different in vitro models. Protein and mRNA levels of ProGuanylin (**A.**) and ProUroguanylin (**B.**) were measured at 4hrs and 24hrs after stimulation with 100nM bombesin, 1mM carbachol, 5mg/ml peptone, 10µM forskolin/IBMX, 1µM PMA, 100µM TDCA or 100nM aldosterone in a TC7 cell secretion assay. Proteins levels were only measured after 24hrs secretion when using human organoids as a model. NA indicates not applicable. nc indicates no change. – or + indicates significant decreased or increased levels compared to the basal condition.

6.2.3 Effect of salt levels on the secretion of proforms

Studies have shown the importance of the guanylin peptides (Cf. 6.1.2) in response to salt intake. Protein expression and transcripts levels of ProGuanylin and ProUroguanylin were studied in response to salt stimulus in the secretion models.

6.2.3.1 Use of TC7 cell line

Salt toxicity on the TC7 cell line

To control which salt concentrations could be used on the ProGuanylin and ProUroguanylin secretion assay, a LDH cytotoxicity assay study was performed on the TC7 cells with a range of different NaCl and Mannitol concentrations. Mannitol was used as a control to match the osmolarity levels of the solution without being able to interact with the cell as NaCl would. TC7 cultures were incubated with concentrations ranging from 50mM to 150mM of NaCl or 100mM to 300mM mannitol on top of the salt already contained in DMEM. LDH assay was performed after 4hrs and 24hrs incubation time with the salt or mannitol concentrations (figure 6.9).

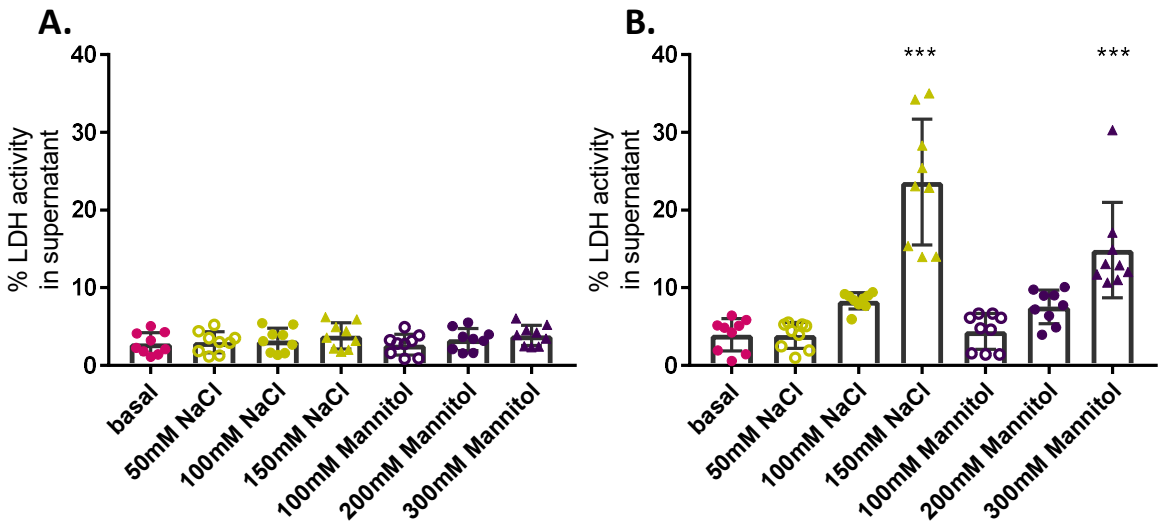

Figure 6.9: Toxicity effect of NaCl and Mannitol on TC7 cultures. TC7 cells were incubated with standard growing media complemented with 50mM NaCl, 100mM NaCl, 150mM NaCl, 100mM mannitol, 200mM mannitol or 300mM mannitol. LDH activity was measured using a colorimetric assay (Pierce) in supernatants and lysed cells after 4hrs incubation **(A.)** and after 24hrs incubation **(B.)** as per manufacturer's instructions and expressed as a percentage of total LDH.
Data are mean ± SD, n=9 (from 3 independent experiments). Statistical significance was assessed by one-way ANOVA with a post-hoc Dunnett's test. *** indicates $p<0.001$.

A 4hrs incubation with concentrations ranging from 50mM to 150mM of NaCl or 100mM to 300mM mannitol did not present any effect on the cell death when compared to basal. After 24hrs, high concentrations of NaCl and mannitol did impact on the cytolysis of the TC7 cells. A concentration of 100mM NaCl (200mM mannitol) presented 10% of LDH activity or doubled the LDH activity compared to basal levels. A concentration of 150mM NaCl and 300mM mannitol had a 25% and 15% LDH activity respectively. In conclusion, concentration of 100mM NaCl or 200mM mannitol were decided as the highest concentration to use on secretion assay on TC7, with the knowledge that a 24hrs incubation slightly affects cell viability.

Protein expression and transcription levels with elevated levels of salt on TC7 cell line

Concentrations of salt ranging from 10mM to 100mM were incubated for 4hrs and 24hrs on TC7 cells. Mannitol concentrations of 100mM and 200mM were used as osmolarity control. Levels of ProGuanylin were measured using the MSD assay (figures 6.10A and B) as well as *GUCA2A* transcript levels by qPCR (figures 6.10C and D). An identical protocol was applied for ProUroguanylin levels (figures 6.11A and B) and *GUCA2B* transcripts levels (figures 6.11C and D).

A first look at the data showed that after 4hrs and 24hrs incubation, TC7 stimulated with NaCl had similar levels of ProGuanylin and ProUroguanylin as TC7 stimulated with the control

mannitol. Therefore, osmolarity may affect total protein release and the observed decreasing levels of proforms might be due to cytotoxicity.

A 4hrs incubation on salt decreased both ProGuanylin and ProUroguanylin levels in the supernatant for salt and mannitol concentrations above 10mM and 50mM respectively. Transcript levels were also decreased for *GUCA2A* but not significant for *GUCA2B* after 4 hours when compared to the basal.

After 24hrs incubation, ProGuanylin protein levels were not significantly different anymore for the 10mM and 50mM NaCl concentration when compared to basal (figure 6.10). However, the protein levels of ProGuanylin under 100mM NaCl stimulus were lower but might be attributed to cytotoxicity as previously seen in cytotoxicity assay. *GUCA2A* transcript levels were raised significantly after 24hrs when the 50mM NaCl concentration was used as stimuli. The equivalent mannitol concentration did not increase significantly the *GUCA2A* levels. A discrepancy exists between the secreted protein levels of high salt concentrations being identical to the ones from basal condition after 24hrs, when they were significantly decreased after 4hrs, attesting of 2 effects imposed by the salt. The first effect decreasing the levels of protein and transcript would be due to the change in osmolarity. The second effect would be salt-dependent increasing the transcript levels and readjusting the levels of ProGuanylin to basal levels after 24hrs. In order to produce the same amount of proforms after 24hrs than what is present in the basal, cells might have to adapt themselves to the high salt concentration after 24hrs either in transcription rate as well as potential translation rate or secretion rate. Indeed, a potential explanation would be a mechanism of compensation of the translation rate.

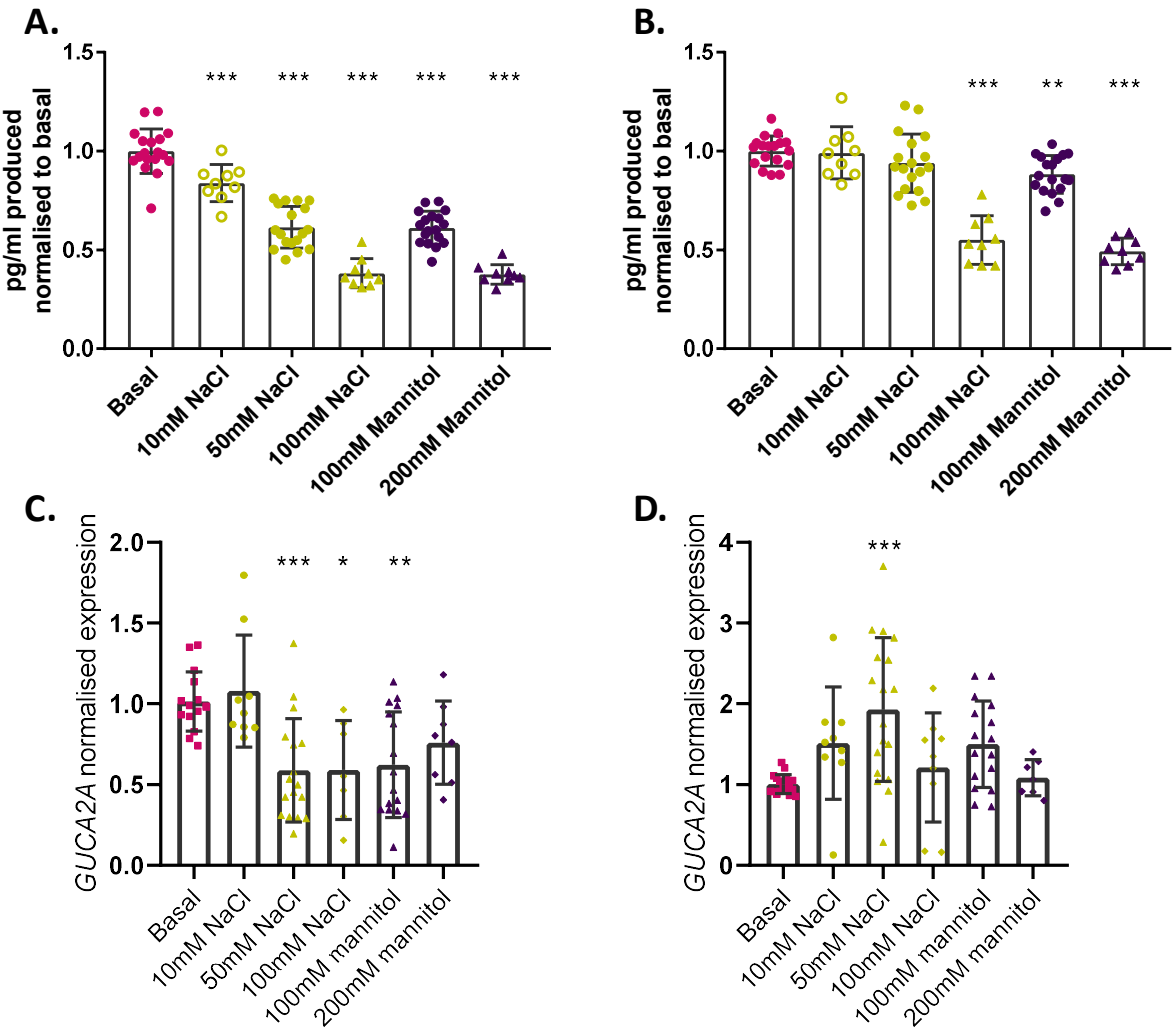

Figure 6.10: Effect of salt on ProGuanylin secretion and mRNA expression on TC7 cultures. TC7 cells were incubated with standard growing media complemented with 10mM NaCl, 50mM NaCl, 100mM NaCl, 100mM mannitol or 200mM mannitol. ProGuanylin levels were measured after 4hrs incubation **(A.)** and after 24hrs incubation **(B.)** using the MSD assay. The measured concentrations were normalised to the mean basal value. The relative expression of mRNA for *GUCA2A* (Guanylin) was measured after 4hrs incubation **(C.)** and 24hrs incubation **(D.)** with stimuli. The relative expression to *ACTB* (beta-actin) is represented as $2^{(-\Delta CT)}$.
In **(A.)** and **(B.)** data are mean ± SD, n=9 (from 3 independent experiments). In **(C.)** and **(D.)** data are geometric mean ± SD. n=9 (from 3 independent experiments). Statistical significance was assessed by one-way ANOVA with a post-hoc Dunnett's test against the basal condition. *** indicates $p<0.001$, ** indicates $p<0.01$.

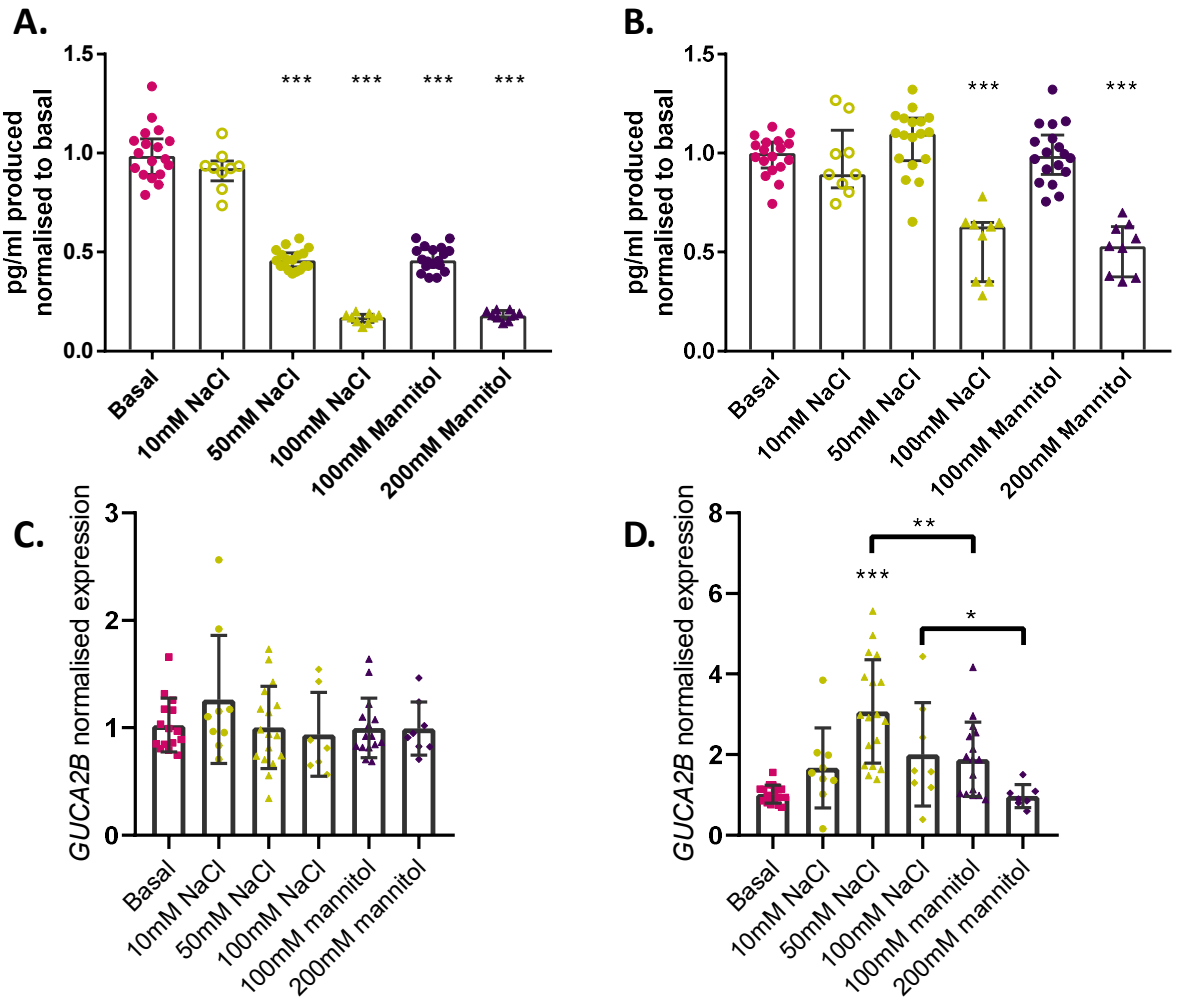

Figure 6.11: Effect of salt on ProUroguanylin secretion and mRNA expression on TC7 cultures. TC7 cells were incubated with standard growing media complemented with 10mM NaCl, 50mM NaCl, 100mM NaCl, 100mM mannitol or 200mM mannitol. ProUroguanylin levels were measured after 4hrs incubation **(A.)** and after 24hrs incubation **(B.)** using the MSD assay. The measured concentrations were normalised to the mean basal value. The relative expression of mRNA for *GUCA2B* (Uroguanylin) was measured after 4hrs incubation **(C.)** and 24hrs incubation **(D.)** with stimuli. The relative expression to *ACTB* (beta-actin) is represented as $2^{(-\Delta CT)}$.
Data are median and interquartile ranges, n=9 (from 3 independent experiments). Statistical significance between conditions was assessed by Kruskal-Wallis test with a post-hoc Dunn's test against the basal condition. *** indicates p<0.001, ** indicates p<0.01. In **(D.)**, Mann-Whitney test was performed between NaCl and mannitol conditions. # indicates p<0.05.

Similarly, after 24hrs incubation ProUroguanylin protein levels under 100mM NaCl stimulus were significantly lower compared to basal but matched levels in the osmolarity controlled samples, indicating a potential effect of cytotoxicity at high osmolarity. Also, ProUroguanylin protein release after 24hrs incubation with 10mM and 50mM NaCl stimuli were not significantly different compared to basal (figure 6.11). *GUCA2B* transcript levels did not present significant difference after 24hrs for 10mM NaCl salt concentration, however transcripts levels were significantly higher in the case of salt concentration above 50mM NaCl. A Mann-Whitney test indicated a significant difference between ProUroguanylin levels

between salt and the corresponding mannitol concentration. This control showed that the effect was due to the NaCl concentration and not the osmolarity levels. However, the mRNA levels are difficult to translate to the protein levels as the 50mM NaCl concentration did not present a significant difference compared to basal.

6.2.3.2 Use of human organoid lines

Human organoids were used to study the secretion of ProGuanylin and ProUroguanylin in response to salt stimuli. Human organoids coming from duodenum and colon were differentiated for 8-10 days before being used in a secretion assay. Secretion were started after washing wells three times with differentiation media containing the stimuli (salt and mannitol) after which organoids were incubated for 24hrs. The MSD assays measured ProGuanylin and ProUroguanylin in supernatant after 24hrs. Proforms levels were normalised to the total protein levels (measured by BCA) to normalise according to organoid sizes and organoid densities between splits. Secretion were performed on both human duodenum and colon organoids and ProGuanylin levels are summarized on figure 6.12.

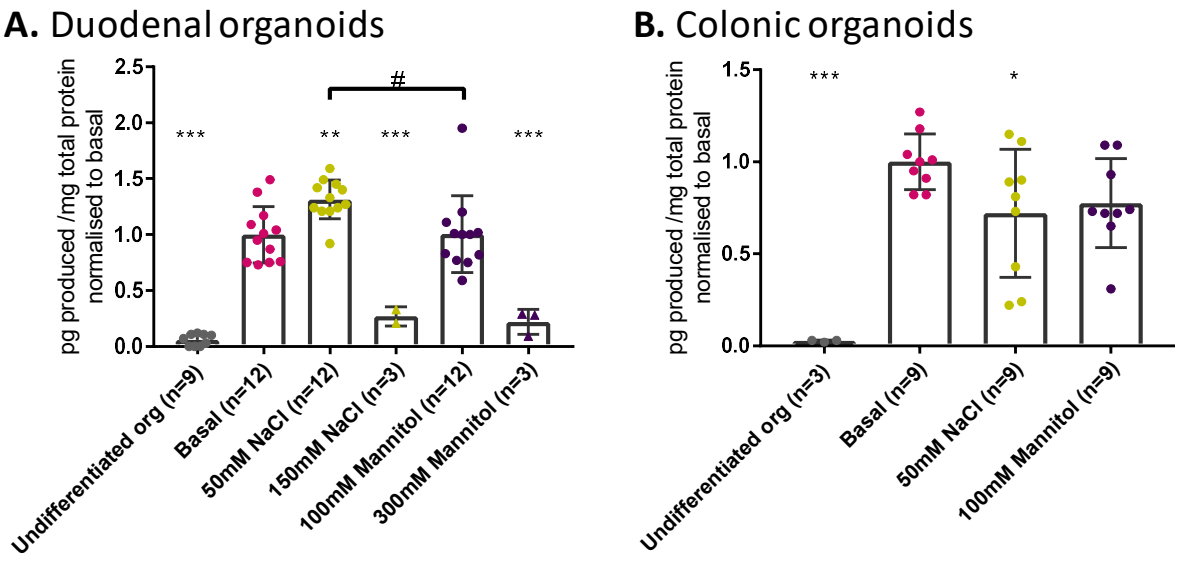

Figure 6.12: Effect of Salt stimuli on ProGuanylin secretion on human organoids. (A.) Duodenal human organoids and **(B.)** Colonic human organoids were incubated with differentiation media supplemented with 50mM NaCl, 150mM NaCl, 100mM mannitol or 300mM mannitol. Duodenal and colonic organoids lines were established from a single human donor each. ProGuanylin levels were measured after 24hrs incubation using the MSD assay. Data normalised to total protein content and to the mean basal value.
Data are mean ± SD, n=3-18 (from 3 independent experiments). Statistical significance was assessed by one-way ANOVA with a post-hoc Dunnett's test. *** indicates $p<0.001$, ** indicates $p<0.01$, * indicates $p<0.05$. In **(A.)** Unpaired t test was performed between NaCl and mannitol conditions. # indicates $p<0.05$.

ProGuanylin levels were also measured on undifferentiated organoids. Those organoids were split at the same time as the ones used for the experiment but were kept in an undifferentiated state using Wnt3a in the media. A 24hrs secretion was performed on the undifferentiated organoids using Wnt3a media instead of differentiation media. Levels were significantly decreased compared to the basal level of differentiated organoids and were below the linear range of detection in both organoid systems.

Concentrations of 50mM and 150mM NaCl and equivalent mannitol osmolarity control conditions were used on the duodenum organoids (figure 6.12A). The highest salt concentration gave a low response in ProGuanylin compared to the basal levels but this might be explained by toxic effects of such concentration similar to what was seen with TC7 cells. Only a triplicate was performed at such concentration and the experiment was not repeated. Using 50mM NaCl concentration as stimuli, did not provoke cell death and the supernatants were analysed in the same fashion. A 24hrs time point showed a significant increase in ProGuanylin compared to the basal condition. When the 50mM NaCl condition was compared to the 100mM mannitol, samples were also significantly different ($p<0.05$) attesting that the increase in ProGuanylin was not due to osmolarity increase. In colon organoids, ProGuanylin did not follow the same trend and a 50mM concentration induced a small but significant decrease in ProGuanylin release (figure 6.12B).

On the same experiments, ProUroguanylin levels were measured using the MSD assay (figure 6.13). A first look at the data demonstrated that ProUroguanylin levels were really low compared to the ProGuanylin levels. Therefore all 3 repeated experiments performed in duodenum did not display strong enough concentrations to interpolate the detected values to the linear range of standard concentration. In conclusion, the secretion experiment on duodenum did not provide any information on salt effect on ProUroguanylin secretion.

Surprisingly, ProUroguanylin levels were detectable in the colon organoid experiment when it is thought to be less expressed in comparison to the duodenum (figure 6.13). No significant difference was measured between basal and the salt/mannitol conditions.

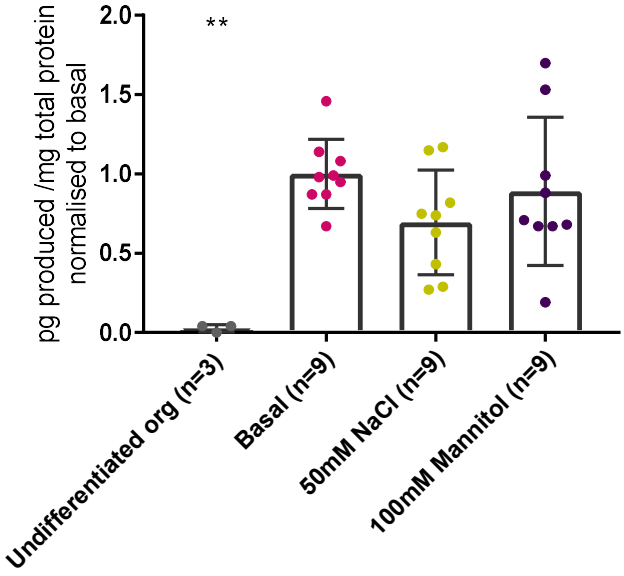

Figure 6.13: Effect of Salt stimuli on ProUroguanylin secretion on human colonic organoids. Colonic human organoids were incubated with differentiation media supplemented with 50mM NaCl or 100mM mannitol. ProUroguanylin levels were measured after 24hrs incubation using the MSD assay. The measured concentrations were normalised to the total protein per well and to the mean basal value. The colonic organoid line was established from a single human donor each Data are mean ± SD, n=3-9 (from 3 independent experiments). Statistical significance was assessed by Kruskal-Wallis test with a post-hoc Dunn's test. ** indicates $p<0.01$.

6.2.3.3 Use of ALI cultures on transwells as preliminary examination

The use of human organoids as a monolayer in transwells has been described in the literature as a new way to reproduce similar gene expression to normal tissues. These culture models showed suitable for studying the paracrine and endocrine secretory functions of different segments of mouse as well as human intestinal tract (Kozuka *et al.*, 2017). Air-Liquid Interface (ALI) monolayer culture model presented crypt/villous structures and typical epithelial cell markers of Paneth, goblet, and enteroendocrine cells (Wang *et al.*, 2015).

A first pilot experiment was designed using the transwells with human duodenum ALI cultures. Fourteen-day old ALI cultures were pre-incubated for 20 minutes with standard secretion 138 buffer, or buffer with identical osmolarity but free from sodium or chloride. Proforms levels were measured using the MSD assays on both apical and basal side. While proforms were not detectable in the basolateral side, ProGuanylin levels measured in the apical side. This interesting result suggests that proforms are preferentially secreted into the lumen. Proforms amounts were normalised to total protein (from the cell lysis) and summarised in figure 6.14. From this pilot study, ProGuanylin secretions in buffer without sodium or without chloride did not have significant difference with secretions performed in the standard 138 buffer.

ProUroguanylin levels were too low in all conditions to be detected by the MSD assay. This result was not surprising because ProUroguanylin levels were below the detection limit in conventionally cultured and differentiated duodenal organoids (figures 6.8A and 6.13A).

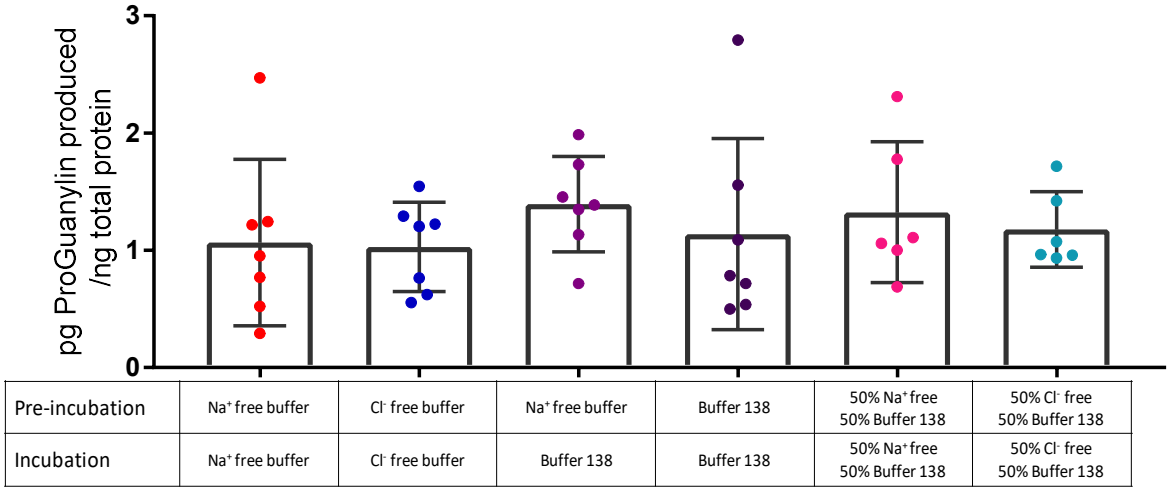

Pre-incubation	Na^+ free buffer	Cl^- free buffer	Na^+ free buffer	Buffer 138	50% Na^+ free 50% Buffer 138	50% Cl^- free 50% Buffer 138
Incubation	Na^+ free buffer	Cl^- free buffer	Buffer 138	Buffer 138	50% Na^+ free 50% Buffer 138	50% Cl^- free 50% Buffer 138

Figure 6.14: Effect of Salt stimuli on ProGuanylin secretion on human duodenal ALI cultures in transwells. Duodenal human transwells were incubated with standard buffer 138, Sodium-free buffer 138, Chloride-free buffer 138 or a mixture of standard buffer with sodium or chloride free buffer. ProGuanylin levels were measured after 4hrs incubation using the MSD assay. Data are mean ± SD, n=6-7 wells (from at least 3 independent experiments).

6.2.3.4 Summary

Three models were used to look at the effect of salt on secretion of proforms and results are summarised in the table 6.2.

The TC7 cell line model was useful to look at protein levels as well as transcript levels in response to salt and mannitol stimuli. Levels ranging from 10mM to 100mM NaCl presented an inhibitory effect on the secretion of proforms and on the transcription after 4hrs incubation. A similar reduction in proforms and transcripts was found using an osmolarity control, mannitol, as stimulus. Therefore, the osmolarity instead of the salt might be affecting the levels of ProGuanylin and ProUroguanylin. After 24hrs incubation, salt concentration above 100mM had a toxic effect on the cells. For 50mM salt concentration, ProGuanylin and ProUroguanylin levels were equal to the one found in the basal secretion with an increase in *GUCA2A* and *GUCA2B* transcript levels after 24hrs incubation.

A.

ProGuanylin mRNA and protein levels					
	10mM NaCl	50mM NaCl	100mM Mannitol	100mM NaCl	200mM Mannito
TC7 4H protein levels	-	-	-	-	-
TC7 4H mRNA levels	nc	-	-	-	nc
TC7 24H protein levels	nc	nc	-	-	-
TC7 24H mRNA levels	nc	+	nc	nc	nc
Duodenum Organoids 24H protein levels	N/A	+	nc	-	-
Colon Organoids 24H protein levels	N/A	-	nc	nc	nc

B.

ProUroguanylin mRNA and protein results					
	10mM NaCl	50mM NaCl	100mM Mannitol	100mM NaCl	200mM Mannito
TC7 4H protein levels	nc	-	-	-	-
TC7 4H mRNA levels	nc	nc	nc	nc	nc
TC7 24H protein levels	nc	nc	nc	-	-
TC7 24H mRNA levels	nc	+	nc	+	nc
Duodenum Organoids 24H protein levels	N/A	nc	nc	nc	nc
Colon Organoids 24H protein levels	N/A	nc	nc	nc	nc

Table 6.2: Summary of the effects of gut stimuli on proforms secretion and mRNA levels using different in vitro models. Protein and mRNA levels of ProGuanylin (A.) and ProUroguanylin (B.) were measured at 4hrs and 24hrs after stimulation with NaCl or Mannitol in the TC7 cell line model. Proteins levels were only measured after 24hrs secretion when using human organoids as a model. NA indicates not applicable. nc indicates no change. – or + indicates significant decreased or increased level compared to the basal condition.

6.2.4 Preliminary data on the secretion using Ussing chambers

J. Rievaj performed preliminary experiment on human colonic mucosa that were isolated after surgery and mounted in Ussing chamber. Colons were mounted on the Ussing chambers and equilibrated for 20 minutes in Ringer solution. During pre-treatment, a sample was removed from both chambers and 10mM glucose final concentration was added to the media. After 30 minutes, another aliquot was removed and 10µM forskolin/IBMX was added before the last time point at 90 minutes. MSD assays were performed on samples from both apical and basal chambers and ProGuanylin and ProUroguanylin concentrations are summarised in figure 6.15.

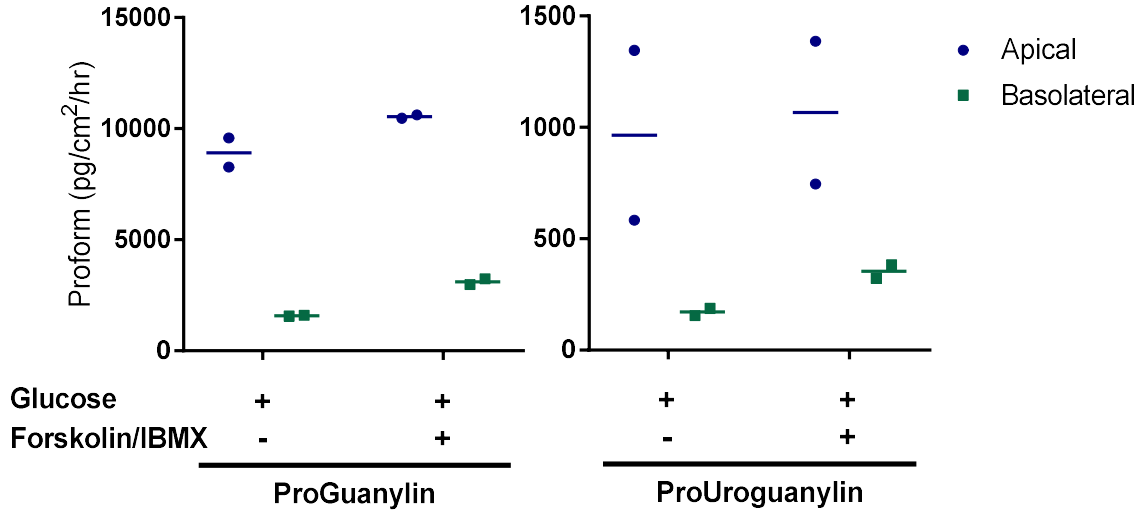

Figure 6.15: Preliminary data on secretion of ProGuanylin and ProUroguanylin by Ussing chamber. Proforms were measured on both the apical and basolateral side. Data are mean, from 2 independent experiments.

A first interesting result was the levels of ProGuanylin in comparison to the levels of ProUroguanylin. In both tissues, the levels or ProGuanylin are ~10-fold higher than those of ProUroguanylin. In addition, the preliminary data showed that both ProGuanylin and ProUroguanylin were secreted mainly at the apical side. The apical compartment presented an amount 4 to 6-fold higher in ProGuanylin and ProUroguanylin compared to the basolateral compartment, confirming also the results found on the ALI model. ProGuanylin, in accordance with Martin *et al.*'s results, presents site-directed secretion (Martin *et al.*, 1999); and this site-directed secretion could be extended to ProUroguanylin as well.

6.3 Discussion

6.3.1 An unconventional secretion of ProGuanylin and ProUroguanylin

Interestingly, measurement of proforms through time in the TC7 model did not present accumulation in the cell lysate and levels found in the supernatant were much higher than in the lysates. Consequently, there is no accumulation of the proforms in the lysate and proforms are directly secreted by the cells and it was therefore unlikely that acute secretion of the peptides could be increased. Gene expression, translation machinery, RNA stability, protein turnover would be the parameters affecting the protein secretion in media. To look at some of those parameters, proforms were measured only in supernatants and cells were used to extract RNA and look at transcript levels.

An unconventional aspect of the secretion of both proforms was the site-directed secretion in the luminal as well as in the basolateral side. However, apical levels were much higher than basolateral levels in the ALI and Ussing chambers models. Whilst this is in accordance with the only available study performed on the subject by Martin *et al.*, 1999, we cannot exclude the simple explanation of selective apical secretion with some leak into the basolateral compartment; however, proforms were also detectable in human plasma suggesting that either this leak is also present in vivo or some basolateral secretion does take place. Basolateral prohormone detection is thus unlikely a result of a compromised barrier function in the experimental setups. Future work could address this further, including the identification of signals resulting in preferential apical secretion.

6.3.2 Secretion models in contradiction with the literature on the effect of NaCl on proforms secretion

Several models were used to look at the secretion response to salt and other stimuli: TC7 cell line, human organoids, and ALI cultures.

ProGuanylin and ProUroguanylin transcript levels in TC7 cells were affected by moderately elevated salt concentration and the protein levels under stimuli differed between the 4hrs and 24hrs timepoints when compared to the basal levels. The concentration above 50mM NaCl presented a toxic effect and won't be discussed further. Salt and mannitol decreased proforms release as well as transcript levels during the first 4hrs of incubation, but no difference could

be found after 24hrs of incubation for the protein levels. Osmolarity might affect either the transcription rate, and potentially the translation rate or the secretion of the proforms in the supernatant but after 4hrs incubation, cells could adapt to the salt concentration: increasing the transcription rate, they would produce proforms to match the basal levels.

Incubation of duodenum organoids in presence of 50mM salt presented a small but significant 1.3-fold increase in ProGuanylin secretion. This modification was also significantly different to the levels of ProGuanylin secreted in presence of osmolarity-matching mannitol. The salt concentration on colon organoids however did have an inhibitory effect on the ProGuanylin levels. These results are mainly in contradiction with the literature. Kita *et al.* and Li *et al.* both showed in perfused rat colons that guanylin in circulation increased in response to salt (Li *et al.*, 1996; Kita *et al.*, 1999). However, both studies were measuring guanylin on the basolateral side of the cell membrane whereas the secretion models used only allowed a measurement of the proforms summing up basolateral and apical secretion. Another caveat of the secretion performed in this chapter was the fact that levels of active guanylin peptides could not be measured. Potentially, ProGuanylin could be cleaved when secreted from the cells and therefore would not have been accounted in the measurement. On the other hand, the protein cleavage could happen as well in the basal levels and therefore the normalisation should account for the potential loss of protein.

Similarly, ProUroguanylin secretion in response of salt concentration did not corroborate the literature. None of the models used showed a positive effect on the ProUroguanylin levels but showed an increase in transcript levels. A similar caveat mentioned previously would be the potential processing of ProUroguanylin into the active form or the fact that levels in the circulation might not be directly regulated by secretion from epithelial cells.

It was hypothesised that the lack of response to salt was due to its presence in the media which would make the cells already expressing and secreting proforms at the maximum of their capacity. When ALI cultures were used, a different experimental set up was considered because of concerns on the salt concentration already present in the differentiation or DMEM media. The TC7 cells media already contained 110.34mM of NaCl (Gibco High Glucose DMEM) and the differentiation media contained 120.61mM of NaCl. Those concentrations of salt might already be in excess and affect the secretion of ProGuanylin and ProUroguanylin, to the point that cells reached their maximum protein expression and secretion capacity. Therefore,

work on ALI duodenal cultures was performed with standard secretion 138 buffer with/without sodium and with/without chloride. The result of this work did not show any difference on the apical secretion of ProGuanylin when using standard 138 buffer when compared to buffer without sodium or without chloride. More work could be performed on ALI cultures with matching concentration of salt to what was used previously in the organoids and TC7 cell line.

The discrepancy in results about salt or gut stimuli effect on proforms secretion could be due to the difference in models but also the difference in species that were looked at. Most experiments were performed on rats, when the study performed in this chapter only focused on human models. In a human study, 15 volunteers were controlled for their response to acute intravenous versus oral sodium load. They did not find a difference in NaCl excretion nor changes in ProGuanylin concentrations in response to either oral versus intravenous (IV) sodium administration over 6hrs but observed a decrease in ProUroguanylin concentration in response to both oral and IV sodium (Preston *et al.*, 2012).

6.3.3 2 Secretion models did not find a consensus on stimulus for the secretion of proforms

ProGuanylin and ProUroguanylin expression in the presence of other stimuli did not present a strong correlation with the literature either. Forskolin, previously identified as a stimulus for guanylin secretion (Moro *et al.*, 2000), was the only stimulus in which the TC7 cell line model reproduced literature reports. Significant increase in secretion over 4hrs and 24hrs were measured when compared to basal and difference in transcript levels were detected. Peptone was the only other gut stimulus that presented a positive effect on the secretion of ProGuanylin in the TC7 cell line model after 24hrs only. Bombesin and carbachol which were mentioned as stimuli (Martin *et al.*, 1999; Moro *et al.*, 2000), did not show any positive effect on the secretion of both proforms using both TC7 cell line and human organoids. A caveat of the experimental design from this chapter is that only one concentration was used to trigger a secretion of proforms. A range of higher concentrations of each stimulus could have ensured that the tested stimuli did not have an effect.

From the models used no real consensus for potential stimuli was achieved. A possible conclusion from these results is that both proforms are secreted by the intestine in a constant rate and that yet to be determined signals might modify this rate.

6.3.4 Limitations and advantages of the used secretion assay models

Several secretion assay models were used in this chapter and all present advantages and limitations. While the TC7 cell line model is potentially the most high-throughput and cheapest one, it represents an enterocyte-like system. Originally from colonic adenocarcinoma, cells contain cancerous mutations, and even though this cell line was isolated from the colon, it does not represent an intestine segment in particular as it expresses markers for both small intestine and colon (Engle, Goetz and Alpers, 1998; Sun *et al.*, 2008). Studies have mainly used Caco-2 cell monolayers grown on transwells (culture inserts). This standard protocol allows the polarisation of the cells after 21 days for the standard Caco-2 cell line and 14 days with the TC7 cell line. In this chapter, TC7 cells were plated directly at the bottom of 24 well plates. The lack of evidence that cells do have apical and basolateral sides in these cultures might affect the polarity and differentiation of the monolayer and prevent the display of physiological response to stimulus. However, the expression of guanylin peptides was investigated with the measurement of *GUCA2A* and *GUCA2B* transcript levels in the cell line and 7 days post splitting already showed measurable levels of transcripts levels (data not shown).

Duodenal and colonic organoids on the other hand keep polarity between basal and apical part. However, a limitation of this system is the apical membrane facing the inside of the organoids. Therefore, the organoids will contain dead cells and mucus inside the organoids. The presentation of the basal part of the cells on the outside of the organoid is a limitation in this chapter as the general idea of the salt or gut stimuli is that it comes from the lumen and secretion should be at the apical side. Methods were developed to convert organoids into monolayers cultures, but characterisation of these cultures has been limited (VanDussen *et al.*, 2015; Kozuka *et al.*, 2017; Goldspink *et al.*, 2018b). The 2D cultures from human organoids were investigated as part of this chapter. Secretion on organoids plated in 2D culture on 2% Matrigel coated 48-well plates presented lower levels of ProGuanylin and ProUroguanylin than 3D cultures that were measured in parallel. As the levels of ProGuanylin and ProUroguanylin from 3D organoid cultures were quite low after 24hrs, with ProUroguanylin not even detected in human duodenal organoids, it was decided to perform secretion on 3D cultures.

2D cultures were investigated again but this time using ALI cultures with transwells. Even though human colonic organoids showed stronger levels of proforms detected by MSD assays, the use of duodenal organoid for the ALI cultures was decided based on the duodenal organoids growing faster and their differentiation easier than the colonic organoids and the fact that the duodenum is more likely to see changes in nutrients whereas the colon is most of the time in presence of bacterial products. The use of standard secretion buffer, prevented the experiment to run for 24hrs. Therefore, only ProGuanylin was detected in the MSD assays and only in the apical side of the transwells. The preliminary experiment highlighted other limitations of this experiment in term of costs and low-throughput of the experiment. Transwells are expensive and come on top of an already costly organoid model due to matrigel/BME and drugs necessary to organoid growth.

The Ussing chamber technique provides a really relevant short-term representation of a human organ that enables measurement of transport and stimulus response of a complete polarised intestinal epithelium. However, limitations of this technique are important in terms of low-throughput as well as need of fresh human tissues. The dissection should be performed as soon as possible but sometimes the reception of the colectomy can be delayed and is consequently detrimental to the tissue integrity. Moreover, not all tissues survive that long.

6.3.5 Future work

The main work performed in this chapter was performed using TC7 cell lines and 2 different human organoid lines, one originating from duodenum and one originating from colon. Both organoids and TC7 cell line are relatively high-throughput methods but results showed that nothing really stimulate strongly the secretion of ProGuanylin and ProUroguanylin on the apical side of the epithelium.

Preliminary results on Ussing chambers exhibiting detectable levels of both ProGuanylin and ProUroguanylin in 2 human colon tissues are encouraging. ALI cultures from human duodenual organoids showed secretion of ProGuanylin to detectable levels on the apical side. The Gribble/Reimann lab has now created and banked several lines of human organoids covering the different sections of the small and large intestine. Using these other organoid lines in ALI cultures that potentially express more ProGuanylin and ProUroguanylin is of interest for more secretion assays with specific stimuli. The use of differentiation media

instead of secretion 138 buffer, would allow longer secretion that might be necessary to detect the proforms in ALI cultures.

Both ALI cultures and Ussing chambers are low-throughput therefore selecting carefully which experiments will be performed on them is necessary. From this results chapter, the rare stimulus that showed a possible impact on the secretion of the proforms were a 50mM NaCl concentration, forskolin/IBMX and peptone and would have the priority on the future experiments. Effect of neuronal mediators carbachol, bethanecol, bombesin, NO and VIP were looked at in previous rats' studies (Martin *et al.*, 1999; Moro *et al.*, 2000). While carbachol, bethanecol and bombesin showed an effect on the secretion of ProGuanylin, NO and VIP did not. The discrepancy with the lack of response to stimulus in this chapter might be species dependent as well as concentration dependent (as only one concentration was tested in this chapter). More research on the role of the vagal system in human is necessary with the use of human models.

Finally, the Gribble/Reimann lab developed techniques to study gut hormones secretion from primary cultures of either murine or human primary cultures (Habib *et al.*, 2013; Psichas *et al.*, 2017). This technique could be used to look at secretion of both proforms in human tissues.

Chapter 7: Identification and characterisation of guanylin-expressing cells

7.1 Introduction

7.1.1 Tissue distribution and cellular localisation of guanylin-related peptides

The specific cell types that express guanylin and uroguanylin, both within and outside the gastrointestinal tract, remains uncertain. Data from early research studies suggested that the guanylin-related peptides play a critical role in the gut's response to an oral salt load through communication with the kidneys in the so-called gut-renal axis. Therefore, it was speculated that gastrointestinal tract and kidneys were the main organs expressing guanylin peptides (Potthast *et al.*, 2001). Following identification of the receptor for guanylin and uroguanylin, many researchers, using a number of different methodologies, reported peptide expression across a number of different tissues. Miyazato and colleagues found in rats uroguanylin transcripts in the lung, pancreas and stomach by Northern-blot and qRT-PCR (Miyazato *et al.*, 1996). Kulaksiz confirmed the presence of guanylin peptides in pancreas and salivary glands of rats with ambiguous immunohistochemistry (Kulaksiz, Rausch, *et al.*, 2001; Kulaksiz, Schmid, *et al.*, 2001; Kulaksiz *et al.*, 2004). Miyazato's group subsequently identified uroguanylin in the pancreatic islet β cells in rats (Nakazato *et al.*, 1998). In the opossum, *Guca2a* transcripts were found in the brain (Fan *et al.*, 1997), and reproductive organs, (Fan *et al.*, 1997; Jaleel *et al.*, 2002). Finally, Schwabe revealed that in both the rat and opossum guanylin related peptides were expressed within the liver (epithelial cells of the bile duct), and gallbladder (Schwabe and Cetin, 2012). All the mentioned papers presented data obtained through a number of different experimental methods, all of which have their limitations. For example, northern blot analysis presents risk of mRNA degradation as well as low sensitivity. Therefore, validating and reproducing the current data that exists for the tissue distribution of guanylin-related peptides are required with alternative and more advanced techniques. In the human protein atlas database (www.proteinatlas.org), protein expression for guanylin is reported to occur within the gastrointestinal tract as well as low levels in glandular cells of the appendix. Low mRNA expression for *GUCA2A* was found in the stomach, cerebral cortex, smooth muscle, and gallbladder. No protein expression was reported for uroguanylin, but mRNA expression was detected in stomach and GI tract, as well as low level expression within gallbladder, liver and smooth muscle.

Early studies suggested that based on the hormonal function proposed for guanylin peptides, enteroendocrine cells were the likely source of these peptides. Indeed, a few studies have demonstrated enteroendocrine cells as a possible source of uroguanylin in the duodenum, and Kokrashvili and colleagues presented immunohistochemical data that demonstrated co-staining of uroguanylin with GFP specific antibodies in Trpm5 gene reporter mice. However, Trpm5 is considered a marker for both enteroendocrine cells and tuft cells (Kokrashvili *et al.*, 2009). Enterochromaffin cells were also shown to express guanylin in guinea pigs, and, in rats, this cell type was also shown to express uroguanylin, based on studies reported by Cetin and Perkins, respectively (Cetin *et al.*, 1994; Perkins, Goy and Li, 1997). Other cells from the secretory lineage have been convincingly found as a source of guanylin peptides. Goblet cells were identified as a source of peptides, and these findings were more recently confirmed by Rubio and Ikpa (Li *et al.*, 1995; Rubio, 2012; Ikpa *et al.*, 2016). Paneth cells have been shown to secrete guanylin in rat (de Sauvage *et al.*, 1992; Whitaker, Witte, *et al.*, 1997) and Paneth-like cells in colon express *Guca2a* and *Guca2b* transcripts as detected by a sensitive *in situ* hybridization method called RNAscope (Ikpa *et al.*, 2016). This method also detected tuft cells as a potential source of *Guca2a* and *Guca2b* transcripts in accordance with Kokrashvili's finding in duodenum. Finally, this sensitive method found guanylin peptide present in most of the enterocytes in mice (Ikpa *et al.*, 2016).

7.1.2 Use of mass spectrometry as a translational model between species

Considerable work has been performed on rodents to understand and characterise the expression of guanylin and uroguanylin expressing cells using different approaches, including immunohistochemistry and techniques that assess gene expression (*in situ* hybridization, Northern blot). However, when referring to the currently available human data, a lack of data exists regarding the characterisation of guanylin peptides expressing cells. So far only clinically-based assumptions exist regarding the cellular basis for guanylin secretion; and few published about their localisation in the GI tract (Kuhn *et al.*, 1994, 1995; Kinoshita, Fujimoto, *et al.*, 1997; Kulaksiz, Rausch, *et al.*, 2001).

Recently, members of our research group have used transcriptomic and peptidomic profiling to draw a comparison between human and murine enteroendocrine cells (Roberts *et al.*, 2018) and precisely analyse gut hormone distribution along the GI tract. Their work aimed at translating the knowledge from mouse to human at RNA and peptides levels.

While the distribution of the guanylin and uroguanylin along the rostro-caudal axis of the GI tract has been studied through gene expression in mice (Ikpa *et al.*, 2016) and in rat (Qian *et al.*, 2000), with uroguanylin being more expressed proximally and guanylin distally, no comparison has been performed with human tissue. Moreover, gene expression does not necessarily reflect protein levels and a phenotype cannot be based only on transcript levels. On the other hand, mass spectrometry is an approach that detects and identifies unambiguously peptides in a biosample. For example, Drs Geoff Roberts and Pierre Larraufie from the Gribble/Reimann lab have looked at mouse and human intestinal homogenates allowing them to identify and quantify gut hormones along the GI tract in human and mouse (Roberts *et al.*, 2018). Through collaboration with them, it was possible to assess and compare the distribution of guanylin and uroguanylin peptides along the GI tract in mouse and humans.

7.1.3 Generation of a guanylin-reporter transgenic mouse

In order to establish the cellular source of guanylin and uroguanylin and due to a lack of reliable antibodies, an alternative approach had to be used. To this end, a transgenic reporter mouse model expressing a fluorescent protein in cells expressing guanylin or uroguanylin is a methodology that does not require specific antibodies or probes for guanylin and uroguanylin.

Two new mouse models were designed by cloning the reporter Venus sequence into the coding sequence of *Guca2a* or *Guca2b* in a bacterial artificial chromosome (BAC) and integrating this sequence in the mouse genome. The Venus sequence codes for an enhanced yellow fluorescent protein (EYFP) which was developed by Nagai *et al.* who introduced 5 mutations into the already-characterised EYFP (Nagai *et al.*, 2002). These new mutations improved the protein maturation and folding of the Venus variant, increased its brightness and reduced its environmental sensitivity (Rekas *et al.*, 2002).

The recombination using BAC vectors was first described by Yang *et al.* as an alternative to manipulation of large genomic DNA by yeast artificial chromosome (YAC) (Yang, Model and Heintz, 1997). By replacing the *Guca2a* (or *Guca2b*) sequence with the Venus sequence from its starting codon to its stop codon, the promoter sequence as well as most transcription unit is conserved in the BAC vector. As the location of regulatory elements of transcriptions are usually unknown, continuous experience by Gong substantiated that 50kb of genomic region flanking both 5' and 3' ends of the reporter gene in the BAC would lead to 85% of successful transgene expression in different transgenic lines (Gong *et al.*, 2003). Therefore, the choice of

BAC vector among those containing the gene of interest is essential to achieve proper regulation of the reporter genes and thus its cell specific expression.

Founder mice for the Guanylin-Venus construct were backcrossed with C57Bl6 and positive Guanylin-Venus offspring were found to have fluorescence in *Guca2a*-expressing cells. The fluorescence allowed immunohistochemistry using validated antibody against the Venus protein as well as detection and sorting of live cells to identify the guanylin-expressing cell type.

7.1.4 Project Aims

The overall objective of this chapter is to identify and characterise the guanylin and uroguanylin cells population. Using Mass Spectrometry on human and mouse samples, FACS analysis and transcriptomic on new mouse models guanylin-Venus and uroguanylin-Venus mouse model, the specific aims were to:

d) Characterise guanylin peptides along the GI tract in human and mice
e) Generate guanylin-Venus and uroguanylin-Venus mouse models
f) Characterise the mouse models and looking for guanylin expression along the rostro-caudal axis of the GI tract and the crypt-villus axis
g) Identify the guanylin and uroguanylin expressing intestinal cell types

In order to establish the tissue distribution and cellular localisation of guanylin peptides, reporter gene mice models were generated (see section 2.13). The reporter Venus sequence was cloned into the coding sequence of the guanylin or uroguanylin gene of a BAC vector. The codons of the guanylin peptides genes were replaced by a fluorescent gene -Venus- into the BAC vectors using Red/Et recombination. After confirmation of the correct positioning of the Venus gene sequence, DNA was purified and microinjected in mice ova according to the methods described in section 2.13.

To assess the expression of the guanylin peptides and the Venus fluorescent marker along the gut axis and the crypt-villi axis, tissues were immunostained for specific cell markers and/or GFP as described in section 2.14 and 2.15 for whole mounted tissues. Using the new Guca2a-Venus mouse model, primary murine intestinal single cell suspensions from different regions

along the GI tract were generated and then sorted using FACS into Venus-positive and Venus-negative populations (See section 2.16). RNA was then extracted from these samples and used for both quantitative RT-PCR and bulk RNA sequencing (see methods described on section 2.10 and 2.17).

Finally, in order to measure guanylin peptides levels along the gastrointestinal tract, peptides were extracted from human and murine tissue by homogenisation in 80% ACN. The peptides were analysed using a Thermo Fisher Ultimate 3000 nano-LC system coupled to a Q exactive Plus Orbitrap mass spectrometer and the analysis was performed using nano-flow-based separation according to methods described in 2.12.

7.2 Results

7.2.1 Generation of the transgenic mice

Two transgenic mice models were designed to study, separately, the guanylin-expressing cells and the uroguanylin-expressing cells. The murine models were generated by recombination to express the Venus fluorescent protein under the control of the guanylin or uroguanylin promoter.

Guanylin and uroguanylin are both present on the murine chromosome 4 but for the purposes of construct generation, two different BAC vectors were used for each gene: RP23-104G3 and RP23-440N21 respectively. Both sequences were removed starting from the start codon in exon 1 and finishing at the stop codon of exon 3 (figure 7.1). The guanylin gene was initially deleted and replaced by the counter-selection cassette rpsL-neo before exchanging it for the Venus sequence using, each time, the Red/ET recombination technology. This method was successful in the generation of the Guanylin-Venus construct; however, it was unsuccessful in the generation of the Uroguanylin-Venus construct when removing the counter-selection cassette. While the 3 codons encoding for uroguanylin were quickly replaced by the counter-selection cassette rpsL-neo, the removal of the cassette proved challenging. When the removal of the rpsL-neo cassette should have made the BAC vector kanamycin sensitive, numerous colonies were growing on kanamycin plates. Another method was applied to create the construct.

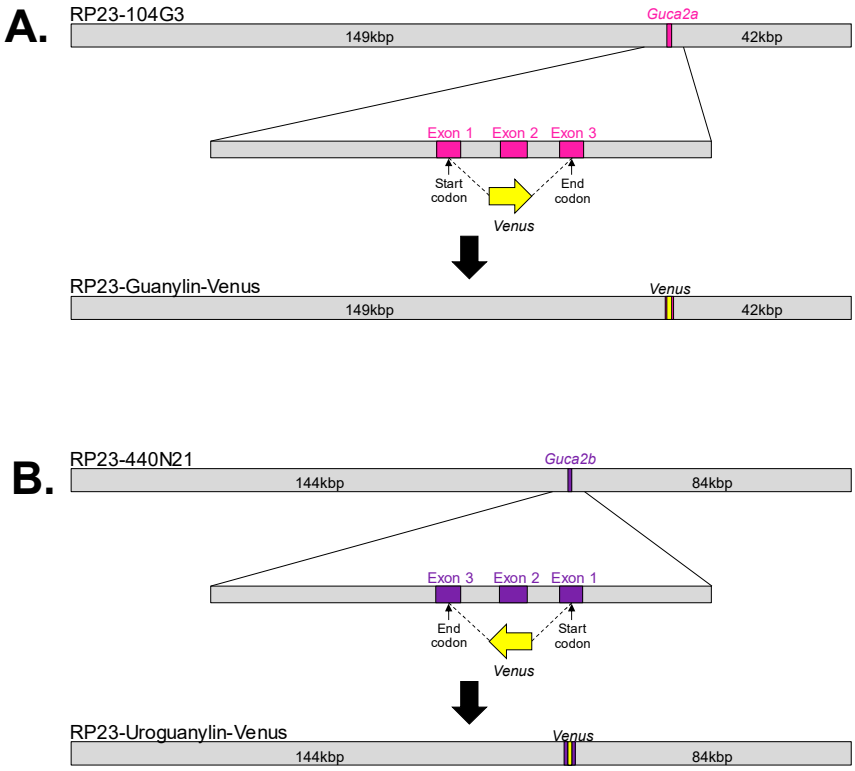

Figure 7.1: Schematics represent the insert of the BAC RP23-104G3 and replacement of the *Guca2a* coding region (1-3) with *Venus* in (**A.**) and the insert of the BAC RP23-440N21 and replacement of the *Guca2b* coding region (1-3) with *Venus* in (**B.**).

In the first instance the uroguanylin sequence was replaced by a PCR construct containing both a counter-selection cassette rpsL-Tet fused to the Venus sequence using the Red/ET recombination technology. Once the rpsL-Tet-Venus construct was recombined in the BAC vector, the counter-selection cassette was removed using a single stranded oligonucleotide of 119bp consisting only of homology arms for the Venus sequence and the uroguanylin promoter.

Positive recombinants of Guanylin-Venus and Uroguanylin-Venus constructs were screened by PCR. The location of the Venus sequence in the different BAC vectors was controlled by sequencing using the oligonucleotides FSD045-FSD076 for the Guanylin-Venus construct and FSD110-127 (cf. appendix 2) for the Uroguanylin-Venus construct (data not shown). Finally, the final constructs and intermediates were controlled by enzyme restriction DNA fingerprint (figures 7.2 and 7.3). The DNA finger print experiments presented the expected pattern of enzyme-restricted DNA bands for both the Guanylin-Venus construct and Uroguanylin-Venus construct. Differences between the starting, intermediate and final constructs were detectable and are highlighted in blue in the DNA gel pictures (figures 7.2 and 7.3).

A.

Cleavage products using XhoI			
1	2	3	4
49827	49827	49827	49827
45920	45920	45920	45920
22458	22458	22458	22458
17207	17207	17207	17207
16738	16738	16738	16738
11356	11356	11356	11356
7681	7681	7681	7681
7237	7237	7237	7237
6795	6795	6795	6795
6734	6734	6734	6734
5800	5800	5800	5800
5453	5453	5453	5453
4761	4761	4761	4761
		4432	
4153	4153	4153	4153
3919	3919	3919	3919
	3789		
3737	3737	3737	3737
3256	3256	3256	3256
2445			***2445***
2415	2415	2415	2415
128	128	128	128
95	95	95	95

B.

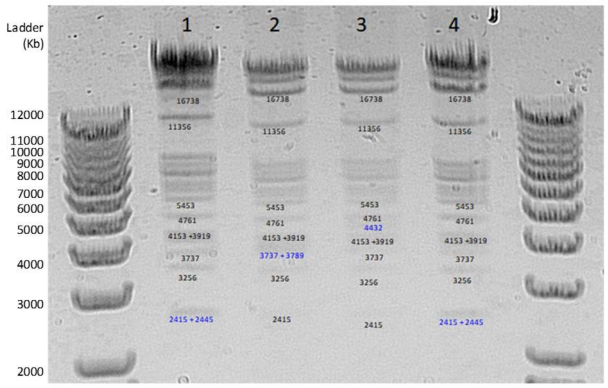

Figure 7.2: Quality control of the BAC vector recombination for the construct Uroguanylin-Venus by DNA fingerprint. Four BAC vectors were subjected to enzyme restriction to control the recombination: 1/ Modified RP23-440N21 Uroguanylin-Venus purified DNA for microinjection, 2/ Unmodified RP23-440N21 miniprep, 3/ Modified RP23-440N21 Uroguanylin-RpsL/Tet-Venus, 4/ Modified RP23-440N21 Uroguanylin-Venus miniprep. **A.** Table summarising the different cleavage products using XhoI as restriction enzyme. The expected changes are bolded and italicised. **B.** DNA gel picture of the 4 different DNA constructs following enzyme restriction. In blue are the expected changes in cleavage products between the unmodified and modified BAC vectors.

A.

Cleavage products using ZraI			
1	2	3	4
52277	52277	52277	52277
44792	44792	44792	44792
36869	36869	36869	36869
29152	29152	29152	29152
12094	***12899***	***12693***	***12094***
8778	8778	8778	8778
5870	5870	5870	5870
2352	2352	2352	2352

B.

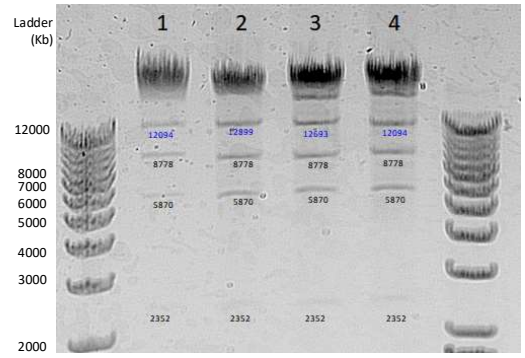

C.

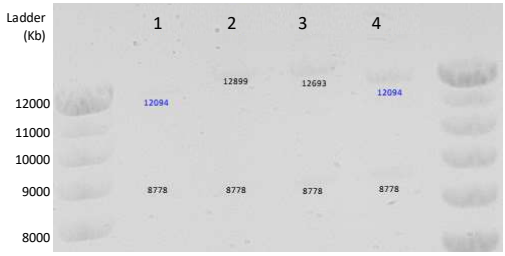

Figure 7.3: Quality control of the BAC vector recombination for the construct Guanylin-Venus by DNA fingerprint. Four BAC vectors were subjected to enzyme restriction to control the recombination: 1/ Modified RP23-104G3 Guanylin-Venus purified DNA for microinjection, 2/ Unmodified RP23-104G3 miniprep, 3/ Modified RP23-104G3 Guanylin-RpsL/Neo, 4/ Modified RP23-104G3 Guanylin-Venus miniprep. (**A.**) Table summarising the different cleavage products using ZraI as restriction enzyme. The expected changes are bolded and italicised. In (**B.**) and (**C.**) DNA gel pictures of the 4 different DNA constructs following enzyme restriction after 4hrs and 16hrs running on a gel. In blue are the expected changes in cleavage products between the unmodified and modified BAC vectors.

The BAC DNA constructs were purified using a commercial kit (Qiagen) and the purified DNA was microinjected into ova derived from C57Bl6/CBA F1 parents and resulting embryos were implanted in pseudopregnant females. Isolated DNA from the pups was screened for the

transgene using a pair of oligonucleotides specific to the Venus transgene (GFPF1 and GFPF2, cf. appendix 2). The first injection failed and none of the mice pups harboured the transgene. In a second attempt, two Guanylin-Venus pups (#26 and #28) were positive (figure 7.4) and presented a band of the 442bp expected size. A fainter band was also present in the Uroguanylin-Venus mouse pup #2. Several PCR attempts using different set of primers did not corroborate the integration of the entire transgene in the pup #2 (data not shown). Confirmation PCRs were performed alongside the mouse pup #2 for the Guanylin-Venus founders #26 and #28 and presented strong bands at the expected size (data not shown). A third attempt to microinject the Uroguanylin-Venus BAC vector was unsuccessful and it was decided to focus only on the guanylin-Venus line.

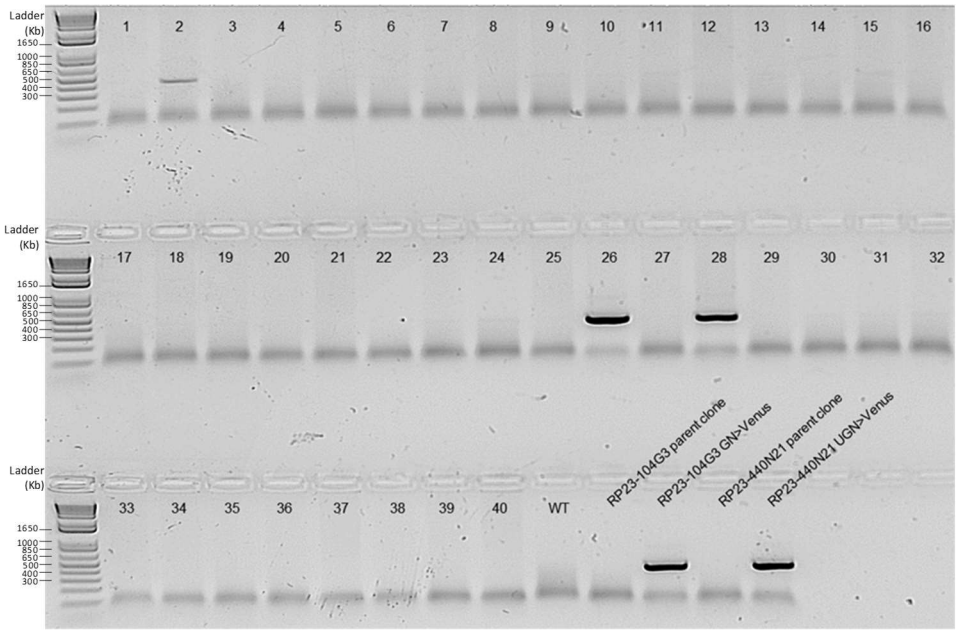

Figure 7.4: PCR screening of the mice ear biopsies. 40 mice pups where screened in order to assess the potential presence of the Venus transgene. Mice pups 1-22 were screened for the integration of the Uroguanylin-Venus transgene and mice pups 23-40 were screened for the integration of the Guanylin-Venus transgene. The expected size of the PCR product is 442bp and is specific to the Venus gene. The modified and unmodified BAC vectors were used as PCR controls.

Once the founders reached sexual maturity they were backcrossed against a C57Bl6 background. Whereas the female founder #26 passed the transgene to its offspring, the male founder #28 did not. Every effort made to transfer the transgene to the next generation failed from this founder. The positive offspring of the founder #26 have been so far backcrossed for 6 generations and most mice used for characterisation of the mouse model thus still harbour some CBA-background; this was considered of little relevance as it seems reasonable to assume similar expression profiles in C57Bl6 and CBA.

7.2.2 Mapping out the Guanylin-expressing cells along the murine gut axis using the mouse model

Cells expressing *Guca2a* should also express *Venus* in this model. To identify cells that express Venus, duodenal, jejunal, ileal and colonic sections of the Guanylin-Venus mice were immune-stained for GFP. Frequency and distribution of GFP-positive cells varied along the intestinal axis (figure 7.5). Jejunum and ileum presented a similar staining pattern where positive cells were mainly present at the top of the villi (white arrow). Some fainter staining was also present in the crypt (yellow arrow). The colon presented high levels of marker expression at the surface epithelium at the top of the crypt. These first observations brought some light on the potential nature of the guanylin-expressing cells, indicating that guanylin-expressing cells might be mature enterocytes. Unexpectedly the duodenum presented a different immunostaining pattern with scarce cells that were not positioned toward the tip of the villi.

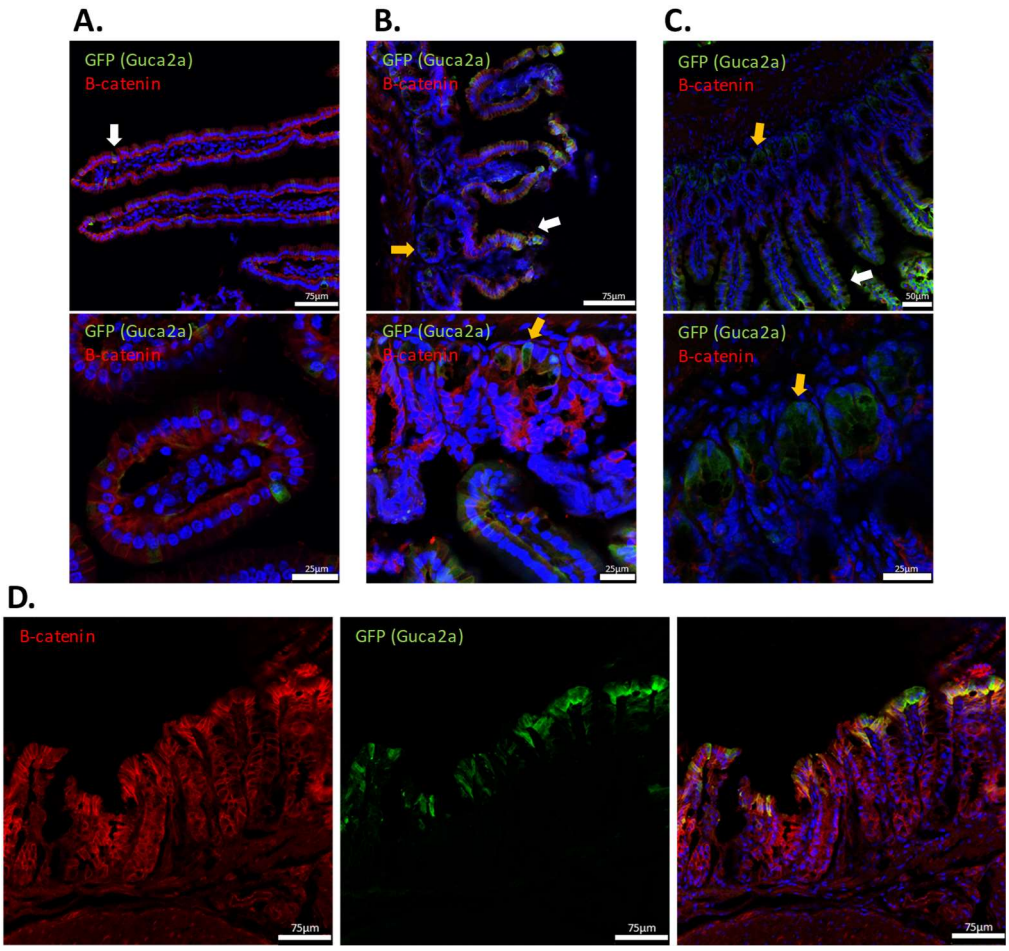

Figure 7.5: Presence of guanylin cells in the gut. Gut tissues from Guanylin-Venus mice (n=2) were assessed by immunohistochemistry. All sections were stained for GFP (green), β-catenin (red) and DNA (Hoechst; blue) (**A.**) Representative villi sections from duodenum. (**B.**) Representative villi (top and bottom) and crypt (bottom) section from the jejunum. (**C.**) Representative villi (top) and crypt (bottom) section from the ileum. (**D.**) Representative colonic section stained.

Coexpression of the reporter with guanylin in this mouse model was investigated by quantifying the RNA expression of *Venus* and *Guca2a* in the Venus-positive and -negative cells of the GI tract. Epithelial cells were dissociated to single cells with EDTA and were FACS sorted (figure 7.6). Epithelial cells from each tissue were separated and collected in two subpopulations: highly fluorescent and non-fluorescent population.

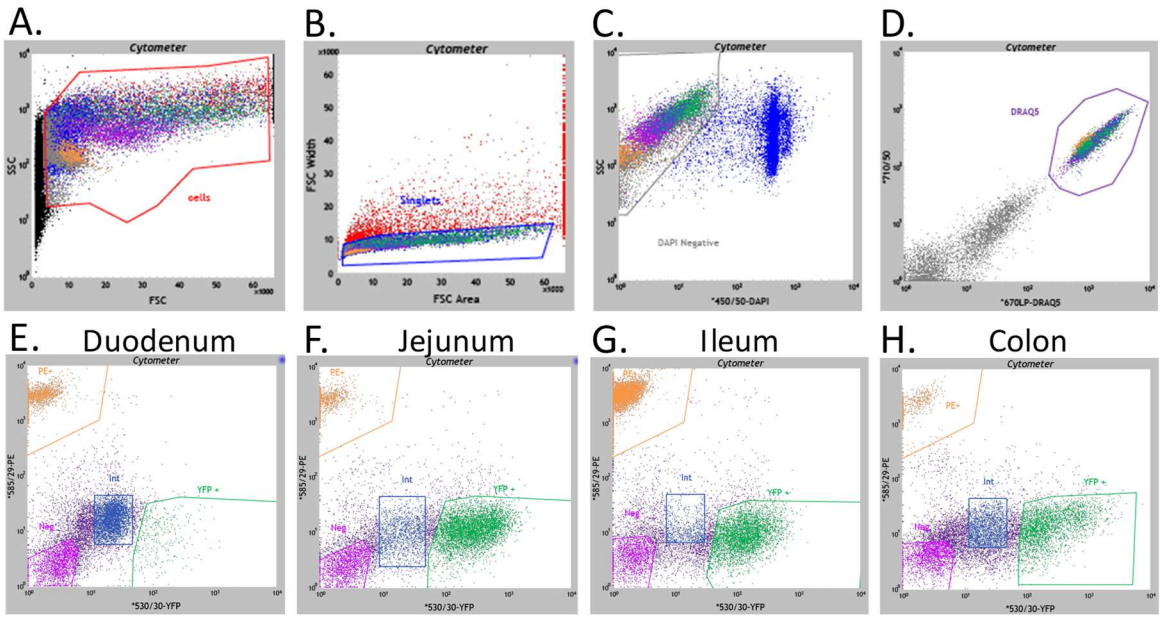

Figure 7.6: Gating procedures for FACS isolation of gut Guanylin-Venus positive epithelial cells. Representative plots illustrating the similar gating strategy for sorting positive Guanylin-Venus cells from mice duodenum, jejunum, ileum and colon. (**A.**) Cells were initially gated by size using forward and side scatter to exclude cell debris. (**B.**) Doublets and larger aggregates were excluded using pulse width. (**C.**) Dead cells were excluded using DAPI staining. (**D.**) Live cell-shape remains were removed by DRAQ5 staining. Cells were sorted and collected into a positive (YFP+) population with high green fluorescence and non-fluorescent negative cells (Neg) population in the duodenum (**E.**), jejunum (**F.**), ileum (**G.**) and colon (**H.**). Immune cells (CD45 positive) were excluded from the sort

RNAs of all subpopulation were purified and reverse transcribed before controlling the expression of guanylin, uroguanylin and Venus by qPCR (figure 7.7). The subpopulations with high fluorescence expressed higher levels of *Guca2a*, *Guca2b* and *Venus* in all tissues, and statistical significance was reached in the jejunum and in the colon. The statistical significance for the duodenum and ileum components was not reached due to important standard deviation between mice samples and the low sample numbers. It was still possible to conclude that a clear difference was demonstrated between positive and negative subpopulations. Finally, the strong correlation between *Venus* positive cells and *Guca2a* positive cells concluded that the sorting strategy worked and is validating the gene reporter mouse model.

Guanylin positive subpopulations presented statistically significant higher expression of G*uca2b* compared to the subpopulation. This result is valid across the 4 tissues but levels of expression of *Guca2b* are particularly high in the duodenum and in the jejunum (figure 7.7).

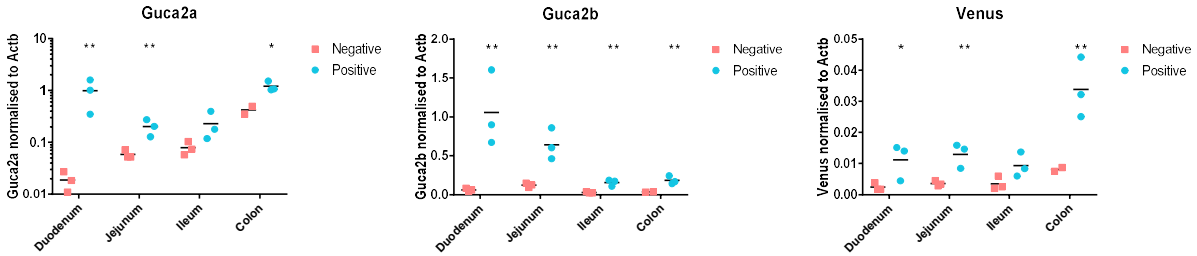

Figure 7.7: Analysis by qPCR of separated populations for each tissue for *Guca2a*, *Guca2b* or *Venus* expression. Data are mean, n=3 mice. Statistical significance was assessed by t test. * indicates p<0.05, ** indicates p<0.01.

Levels of *Guca2a* are particularly high in the positive cells of the duodenum when normalised to *Actb* and are contrasting with the levels of *Venus*. This discrepancy is not uniform across the 4 different tissues for reasons which remain uncertain.

The number of cells expressing the Venus marker was measured when performing the cell sorts and it presented a great disparity in the number of positive cells (figure 7.8). In the duodenum, the percentage of positive cells represented 2.5%. It drastically increased to 49.8% in the jejunum, 30.5% and 21.1% in the ileum and colon respectively. In the regions where positive cells are rare, positive cells had higher *Guca2a* expression levels. We can hypothesise that the different levels of *Guca2a* expression detected in the different tissues (figure 7.7) and the difference in percentage of positive cells are due to different populations of cells.

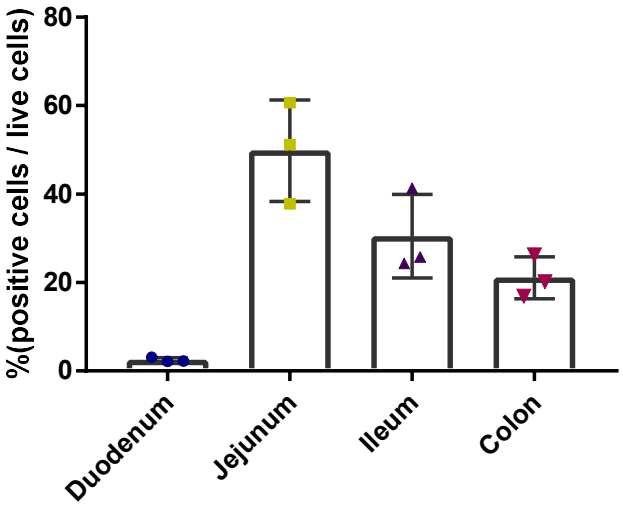

Figure 7.8: Percentage of positive Guanylin-Venus cells present in each intestinal tissue. Mouse duodenum, jejunum, ileum and colon tissues were sorted by FACS and the percentage of positive Guanylin-Venus cells were plotted. Data are mean ± SD, n=3.

To explore further the disparity of cell localisation throughout the gut, an immunostaining of the complete GI tract was performed using an adapted method that was developed by Winton and Ponder, 1990. Whole mounted duodenum, jejunum, ileum and colon were stained for GFP and tissues were scanned using Zeiss Axioscan Z1 slidescanner. Most of the villi and crypts were stained in the tissue, making impossible to analyse the staining with a quantitative approach due to the villi hiding one another on the slide (figure 7.9). However, nuances in the brightness per tissue were apparent. Most of the duodenum parts that were scanned present a dimmed fluorescence compared to the jejunum and ileum parts. On the contrary of the rectum, the colonic invaginations in the proximal and mid distal colon parts presented bright fluorescence.

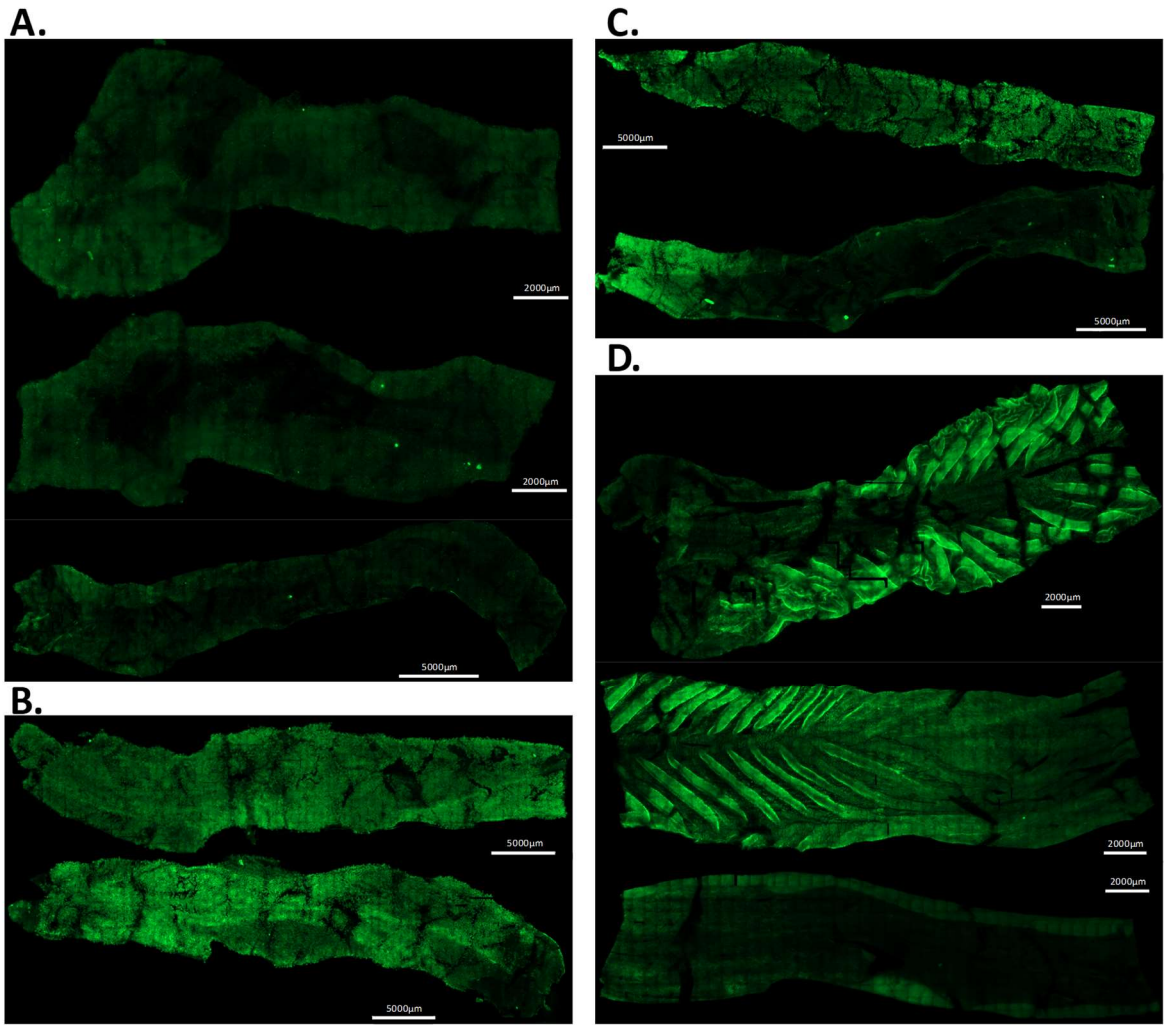

Figure 7.9: Immunohistochemistry on the whole mounted gut tissue. Whole mounted gut tissues from Guanylin-Venus mice were stained for GFP (green). All sections were stained for GFP (green) and a tile-scan of the duodenum (**A.**), jejunum (**B.**), ileum (**C.**) and colon-rectum (**D.**) was performed. The tissues had to be cut in several pieces and presented from left to right in order of section from duodenum to colon.

7.2.3 Measuring guanylin peptides in the murine gut axis using mass spectrometry

mRNA levels do not necessarily reflect protein levels and transcriptome analysis cannot be used as a strict correlation to a phenotype (Vogel and Marcotte, 2012; Edfors *et al.*, 2016; Silva and Vogel, 2016). Post-transcriptional regulations -such as translation, protein stability and protein modification- all play a role in the discrepancy between RNA levels and protein levels. To investigate the protein phenotype, transcriptomic data must be correlated to proteomic/peptidomic data analysis.

It was possible to tackle the peptidomic challenge thanks to the work of Pierre Larraufie and Geoff Roberts from the Gribble and Reimann's lab who looked at peptide levels along the GI tract by mass spectrometry in mouse and human samples (Roberts *et al.*, 2018). Briefly, samples were homogenised, and protein extracted. Peptides were separated from proteins by precipitating proteins with 80% Acetonitrile in water. Samples were extracted using a solid-phase extraction plate. After resuspending the peptides in 0.1% v/v Formic acid, samples were reduced/alkylated to perform a peptidomic analysis. Extracted peptides were analysed using a high flow rate based LC/MS-MS which was previously described (Kay *et al.*, 2017).

ProGuanylin derived peptides were detected in the 10 different regions analysed by LC-MS/MS by Peaks 8.0 against the mouse Swissprot databases. Peptides were later searched in the 10 different regions –from the duodenum to the rectum- using the Quantitation tool of Excalibur software (figure 7.10B). ProGuanylin derived peptides 22-49 and 60-116 were the peptides described previously in chapter 4. Including peptide 60-90, these peptides were detected at the highest quantity. Quantification for each peptide draw an interesting representation of the localisation of the peptides production through the GI tract. ProGuanylin derived peptides are barely detectable in homogenates from the proximal duodenum. Their expression is linearly increasing through the small intestine where the MS response peaks in the ileum and distal ileum. The proximal colon presents high levels of ProGuanylin derived peptides 22-49 and 60-116 which decline drastically to low or no detectable levels in the rectum. These results correlate with the immunohistochemistry data (figures 7.5 and 7.9) and show an increasing staining from proximal to distal small intestine and low-level staining in the rectum.

The mass spectrometry data for the ProGuanylin derived peptide 60-90 presented a different pattern of expression compared to the peptide 60-116 in the colon. The peptide expression

was really low in the colon and a hypothesis explaining this discrepancy could be a difference of peptide processing in the colon and in the small intestine.

Only one ProUroguanylin derived peptide was found by LC-MS/MS in all mice homogenates using Peaks 8.0 against the mouse Swissprot databases. This peptide 93-106 was searched using the Quantitation tool of Excalibur software in the 10 different regions. The peak areas measured for this peptide were low in all samples and the peptide was not detectable in the colon and rectum (figure 7.10C).

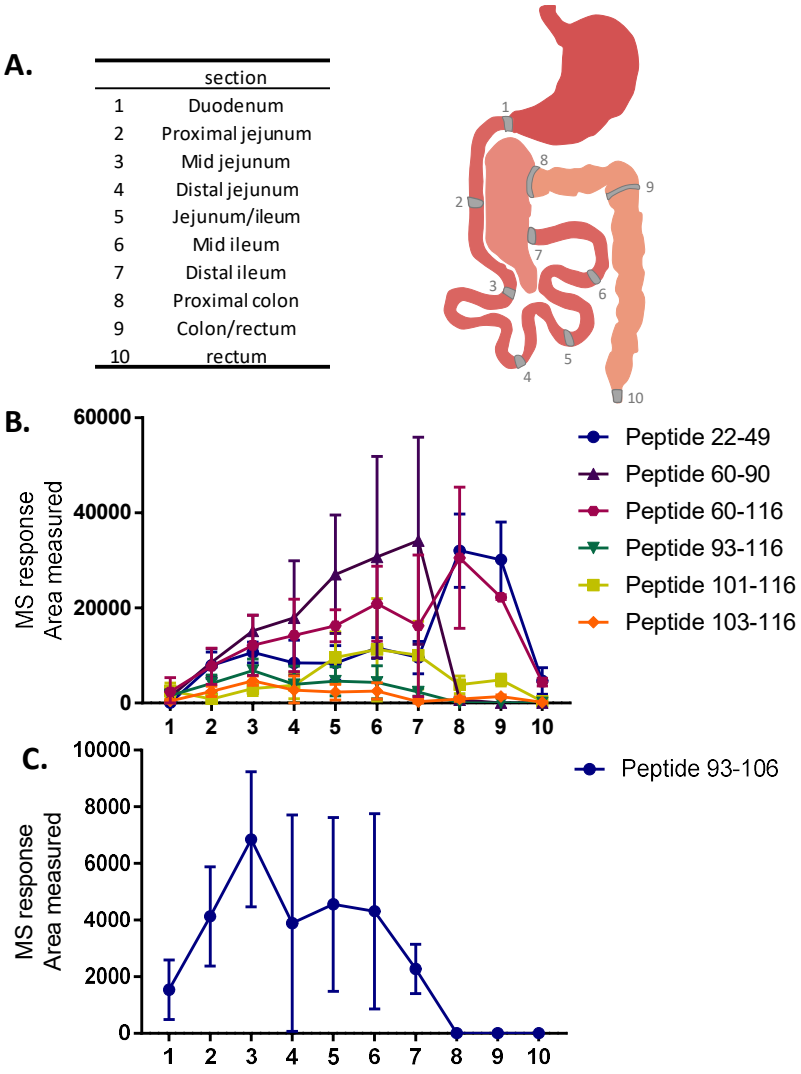

Figure 7.10: Guanylin and uroguanylin peptides presence in homogenates of mouse gut tissues. Ten different mice section were homogenized (**A.**). Peptides fragments of GUC2A (guanylin) were detected in several regions of the mouse guts (**B.**) Only one peptide fragment of GUC2B (uroguanylin) was found in the mouse (**C.**). The average quantification (peak area) from 4 mice is represented for each region. Data are mean ± SD, n=4.

7.2.4 Similitude of guanylin-expressing cells in human tissue

A similar experiment was performed in human samples to confirm the pattern of peptides localisation by mass spectrometry. Human samples were biopsies from the stomach (n=7) the duodenum (n=9), jejunum (n=2), ileum (n=5), caecum (n=1), ascending colon (n=3), sigmoid colon (n=6) and rectum (n=3). Human mucosas were treated in a similar method but were analysed using nano-flow based separation and electrospray approaches on a Thermo Fisher Ultimate 3000 19 nano LC system coupled to a Q Exactive Plus Orbitrap mass spectrometer (ThermoScientific). Downstream analysis was performed using Peaks 8.0 software against the human Swissprot database as described in Roberts' paper (Roberts *et al.*, 2018).

In a peptidomic analysis, only 2 ProGuanylin derived peptides could be detected and recognised on Peaks 8.0 in human samples: peptides 22-49 and 100-115 (as described in chapter 4). These peptides were later searched in the 8 different regions using the Quantitation tool of Excalibur software (figure 7.11). The result in human samples presented a higher disparity in MS response implicating high standard deviation. The highest expression levels of ProGuanylin derived peptides were found in the jejunum and in the sigmoid colon. An interesting difference to note, when comparing with the mouse result, was the presence of ProGuanylin derived peptides in the rectum and in the duodenum. Ileum, caecum and ascending colon presented overall the lowest levels of peptides. Finally, barely any peptides were measured in the stomach.

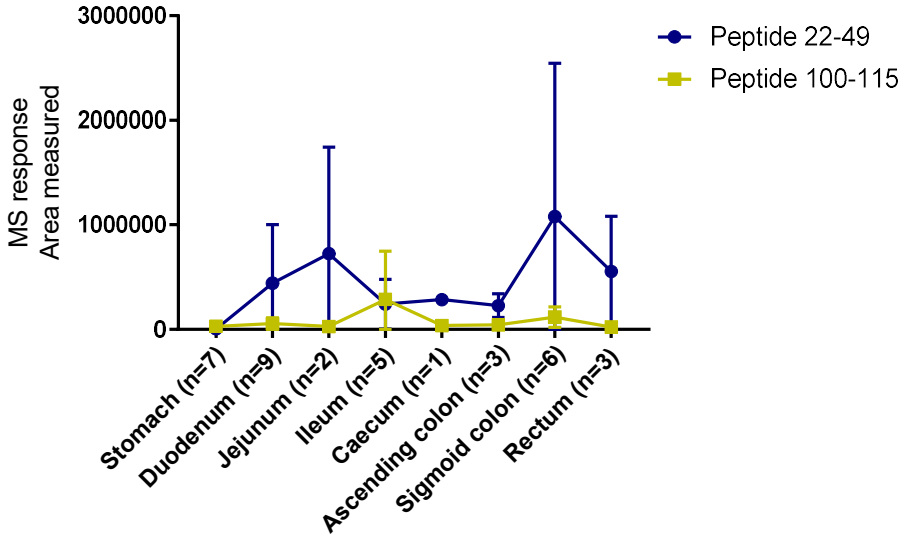

Figure 7.11: Guanylin peptides presence in human homogenates of gut tissues. Peptides fragments of ProGuanylin were detected in several regions of the human guts and the average quantification (peak area) from the different tissue is represented for each region. Data are mean ± SD.

7.2.5 Guanylin-producing cell types in the GI tract

Transcriptomic profiling of Guca2a-expressing cells

To determine the identity of the fluorescent cells in the small and large intestine, Venus-positive and non-fluorescent control cell population were isolated from Guanylin-Venus mice. RNAs were extracted using Qiagen RNEasy micro plus kit. Their quality was measured by calculation of the RIN (RNA integrity number), a user-independent algorithm calculating RNA quality (Schroeder *et al.*, 2006). The 24 samples (2 subpopulations of 4 tissues for 3 replicate mice) RIN were of high quality, averaging 9.6. Libraries were generated from these samples using the Takara's SMARTer Pico V2 kit protocol, starting from 10ng of RNA. Libraries were sequenced at CRUK Cambridge on the Illumina HiSeq SE50 platform. The average total number of reads in each sample was 32.3 million with an average of 21.4 million mapping the mouse genome GRCm38 using STAR (Dobin *et al.*, 2013). The average mapping efficiency was 66.4 % (lowest 46.6 %), showing a very good sequencing depth.

The Principal-component analysis (PCA) of the 4 tissues subpopulation transcriptomes showed a clear separation of the positive and negative subpopulation as well as a distinct clustering per tissue and group, which was a comforting result on the quality of the RNA-sequencing (figure 7.12).

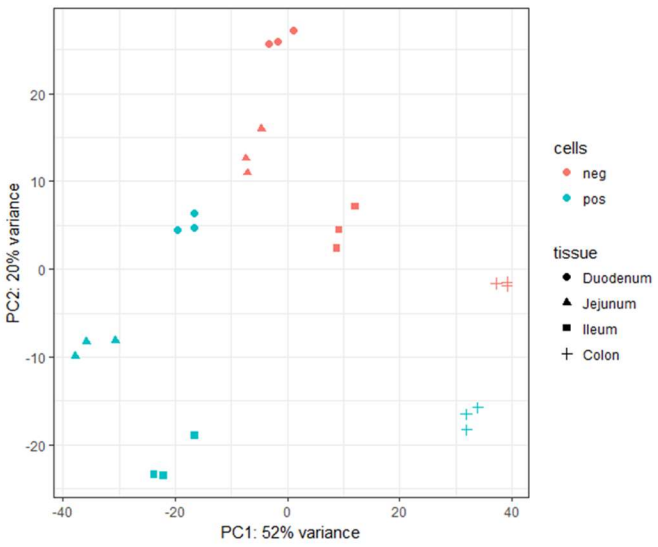

Figure 7.12: Principal-Component analysis (PCA) of the transcriptomes of the 4 tissues (duodenum, jejunum, ileum and colon) subpopulations. Non-coding and mitochondrial genes were excluded. In blue are the Venus-positive subpopulations and in red are the negative control population for the 4 tissues.

In these results the PC1 would explain the variance in the tissue whereas the PC2 would explain the variance in the positive and negative subpopulation. A heatmap of the absolute expression of the top 100 most differentially expressed coding genes is shown on figure 7.13 as determined by using a negative binomial model (DESeq2). The heatmap highlighted *Guca2a* as one of the top differently expressed genes between negative and positive cells, as expected. The presence of *Guca2b* in the top 100 most differentially expressed coding genes was consistent with the positive vs. negative cells qPCR results (figure 7.7). Cell specific markers are highly represented in the top 100 DE genes, giving indications about the *Guca2a*-producing cell identity. Goblet cell markers (*Fcgbp*, *Muc2*, *Tff3*) were significantly enriched in the Venus-positive cells across the 4 tissues. Paneth cell markers (*Spdef*, and some defensin genes *Defa24*, *Defa22*, *Defa21*, *Defa29*, *Defa27*) appear significantly enriched in all tissues but the colon, consistently with the fact that Paneth cells are not present in the colon. Finally, enteroendocrine cell markers (*Gip*, *Cck*, *Sst*) were significantly depleted in the Venus-Positive cells.

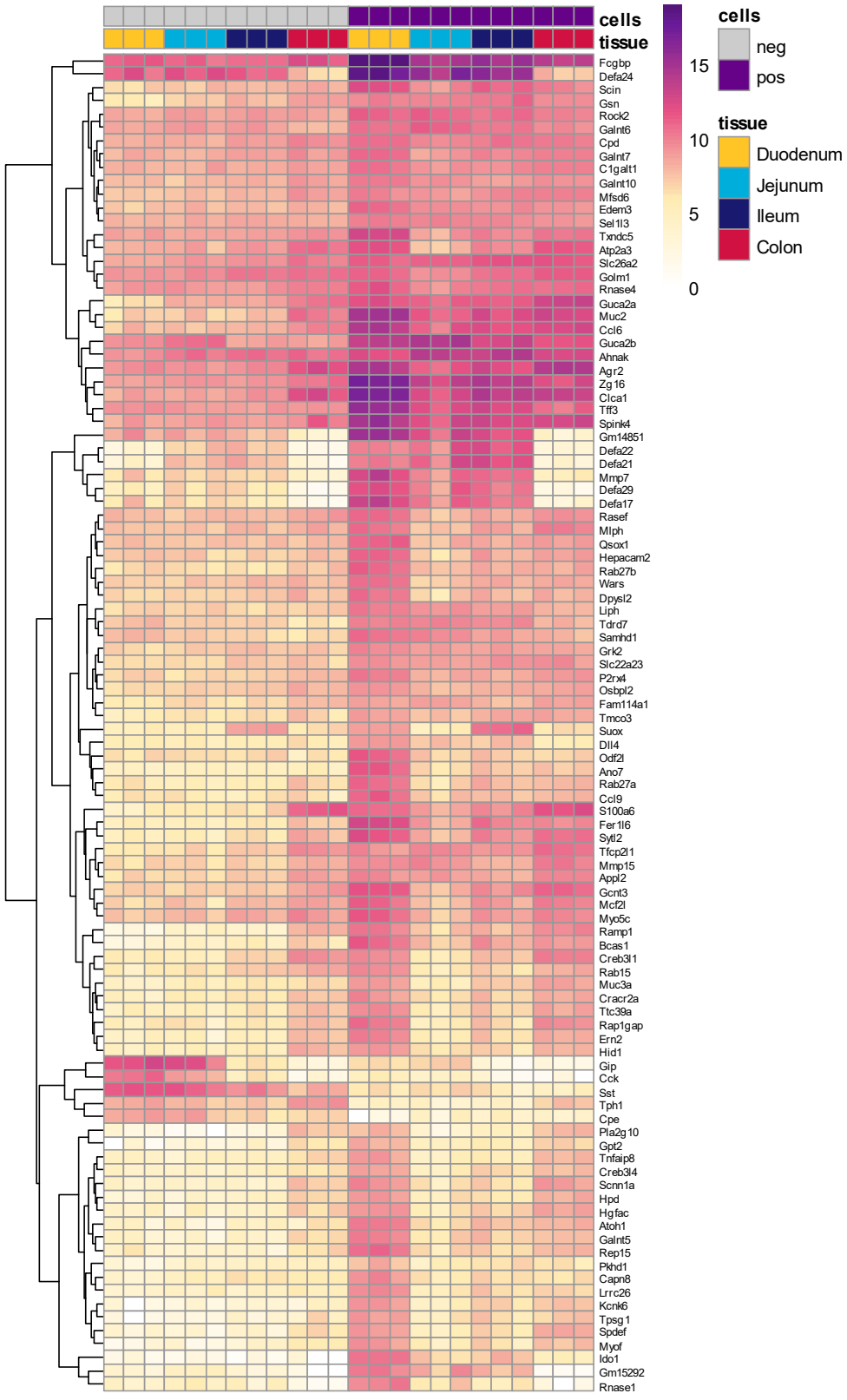

Figure 7.13: Heatmap showing the top 100 most differentially expressed genes between positive and negative cells found during RNA-sequencing of FACS-isolated cell populations from three Guanylin-Venus mice GI tract. Non-coding and mitochondrial genes were excluded. Values are log10 (normalised read counts using DEseq2). Genes are grouped via hierarchical clustering based on Euclidean distance and complete linkage. The heatmap was generated with the assistance of P. Larraufie.

To confirm what cell types are the *Guca2a*-expressing cells, single genes were singled out of the RNA sequencing analysis. Figure 7.14 presents the gene of interest *Guca2a*, *Guca2b* and the guanylate-cyclase C receptor gene: *Gucy2c*. These results agreed with the previous qPCR results (figure 7.7) that found higher levels of *Guca2a* in the duodenum and in the colon and higher levels of *Guca2b* in the duodenum and jejunum compared with the negative population. The low levels of *Guca2b* in the negative population would suggest that both guanylin and uroguanylin could be expressed by common cell-populations.

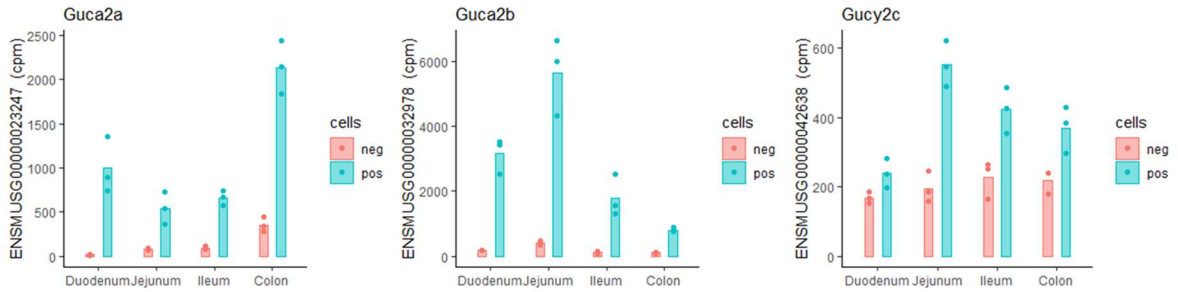

Figure 7.14: Gene expression levels of *Guca2a*, *Guca2b* and *Gucy2c* assessed by RNA-sequencing on cell sorted positive and negative subpopulations of Guanylin-Venus mice.

The RNA-sequencing results of specific secretory cell markers of enteroendocrine cells, goblet cells, Paneth cells and tuft cells were looked at and qPCR were performed on some of the markers (figures 7.15 and 7.16). As mentioned, markers of enteroendocrine cells were depleted in the *Guca2a*-positive subpopulations (*Cck*, and *ChgA*) as well as enterochromaffin cells (*Tph1*). The qPCR presented a similar trend with depletion of *Gcg* and *Pyy* in the *Guca2a*-enriched population. *Cck* and *Gip* were also depleted in the duodenum and jejunum of *Guca2a*-enriched subpopulations but their levels too low for detection in the ileum and colon even in the negative population. This result is not surprising as GIP-expressing cells are the enteroendocrine K-cells predominantly found in the proximal small intestine (Buchan *et al.*, 1978).

Paneth cell marker *Lyz1* is highly expressed in the guanylin-expressing cell subpopulation suggesting a potential guanylin-producing cell type. *Sox9,* however, seems depleted in all tissues (except duodenum for which non enriched). *Sox9* is expressed specifically in stem cells, progenitor cells, tuft cells and in early-differentiated Paneth cells (Bastide *et al.*, 2007). On the other hand, the expression of *Defa22*, regarded as a differentiated Paneth cell marker (Wang *et al.*, 2011), is dramatically increased in the guanylin-producing cells. Those results support

the differentiated Paneth cell as a subgroup of guanylin-expressing cells in duodenum, jejunum and ileum.

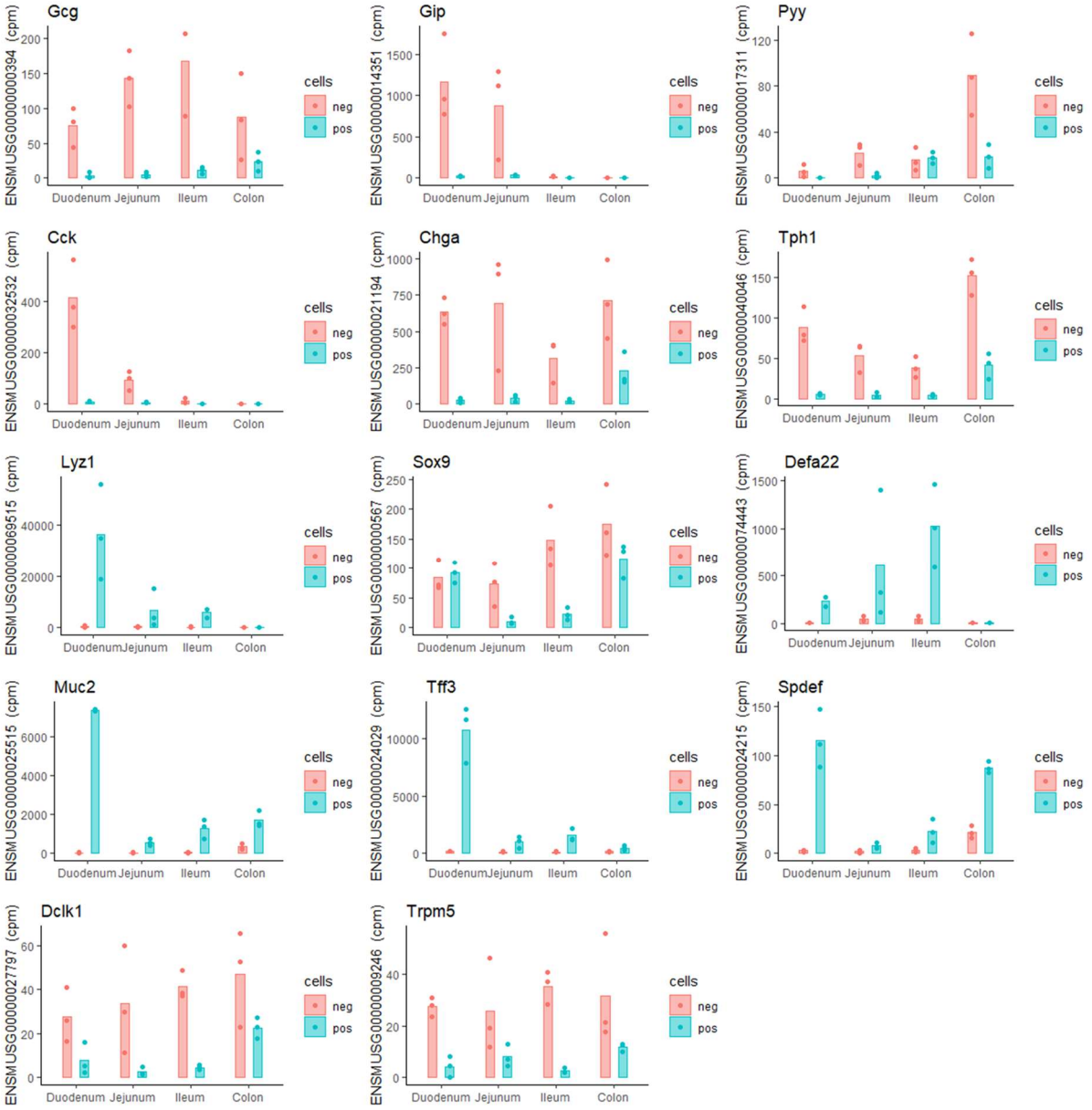

Figure 7.15: Gene expression levels of secretory cell markers assessed by RNA-sequencing on cell-sorted Venus-positive and negative control subpopulations of Guanylin-Venus mice. Markers for enteroendocrine cells (*Gcg*, *Gip*, *Pyy*, *Cck*, *Chga*, *Tph1*), Paneth cells (*Lyz1*, *Sox9*, *Defa22*), goblet cells (*Muc2*, *Tff3, Spdef*), and tuft cells (*Dclk1*, *Trpm5*) were checked for both negative (red) and positive (blue) subpopulation. Data are mean, n=3 mice.

Goblet cell markers (*Muc2*, *Tff3*, *Spdef*) are highly expressed in the guanylin-enriched subpopulations of the duodenum and colon, and *Muc2* is still significantly increased in the jejunum ($p<0.01$) when looking at the qPCR results. (Figures 7.15 and 7.16). Goblet cells are

therefore a second main population of guanylin-expressing cells in duodenum and colon and probably an additional source of guanylin in the jejunum and ileum.

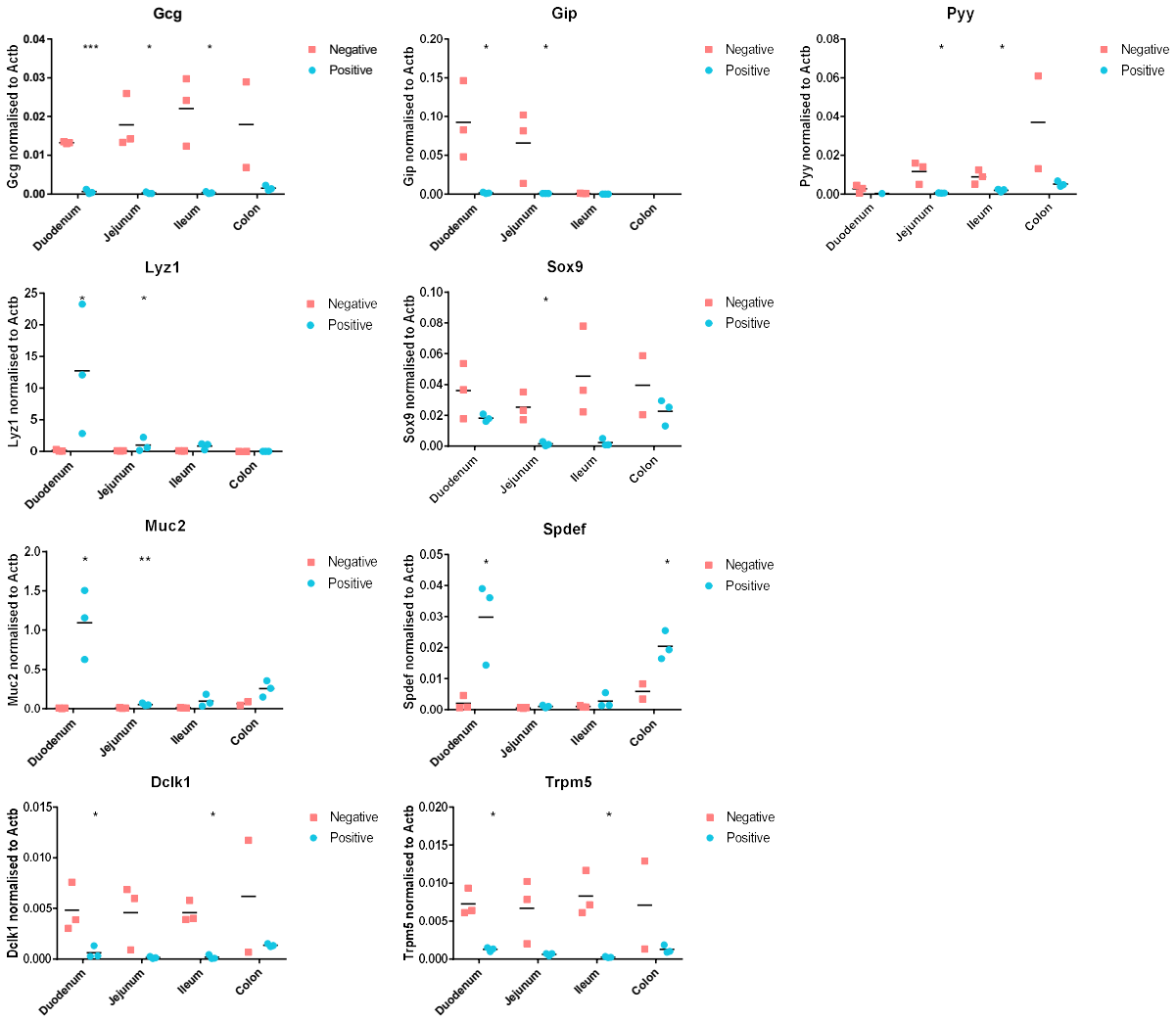

Figure 7.16: Gene expression levels of secretory cell markers measured by qPCR on cell-sorted Venus-positive and negative control subpopulations of Guanylin-Venus mice. Markers for enteroendocrine cells (*Gcg*, *Gip*, *Pyy*), Paneth cells (*Lyz1*, *Sox9*), goblet cells (*Muc2*, *Spdef*), and tuft cells (*Dclk1*, *Trpm5*) were checked for both negative (red) and positive (blue) subpopulation. Data are mean, n=3 mice. Statistical significance was assessed by paired t test in between subpopulations. *** indicates p<0.001, ** indicates p<0.01 and * indicates p<0.05.

Finally, the tuft cell markers presented depleted transcript levels compared to the negative control subpopulation. This last result is contradictory to previous reports that used *in situ* hybridization by RNAscope and suggested that tuft cells were a potential cell type expressing guanylin and uroguanylin (Ikpa *et al.*, 2016).

Previously shown immunohistochemistry (figure 7.5), highlighted the fact that jejunum and ileum had a huge number of Venus positive cells along the villi, leading to the assumption that mature enterocytes might be a source of guanylin. Enterocyte cell markers (*Vil1*, *Elf3* and

Pmepa1) presented a strong enrichment in guanylin-expressing cells in the jejunum and ileum but not in the duodenum (figure 7.17). Statistically significant qPCR results showed corroborating results (figure 7.18) identifying enterocyte cells as the main source of guanylin in jejunum and ileum.

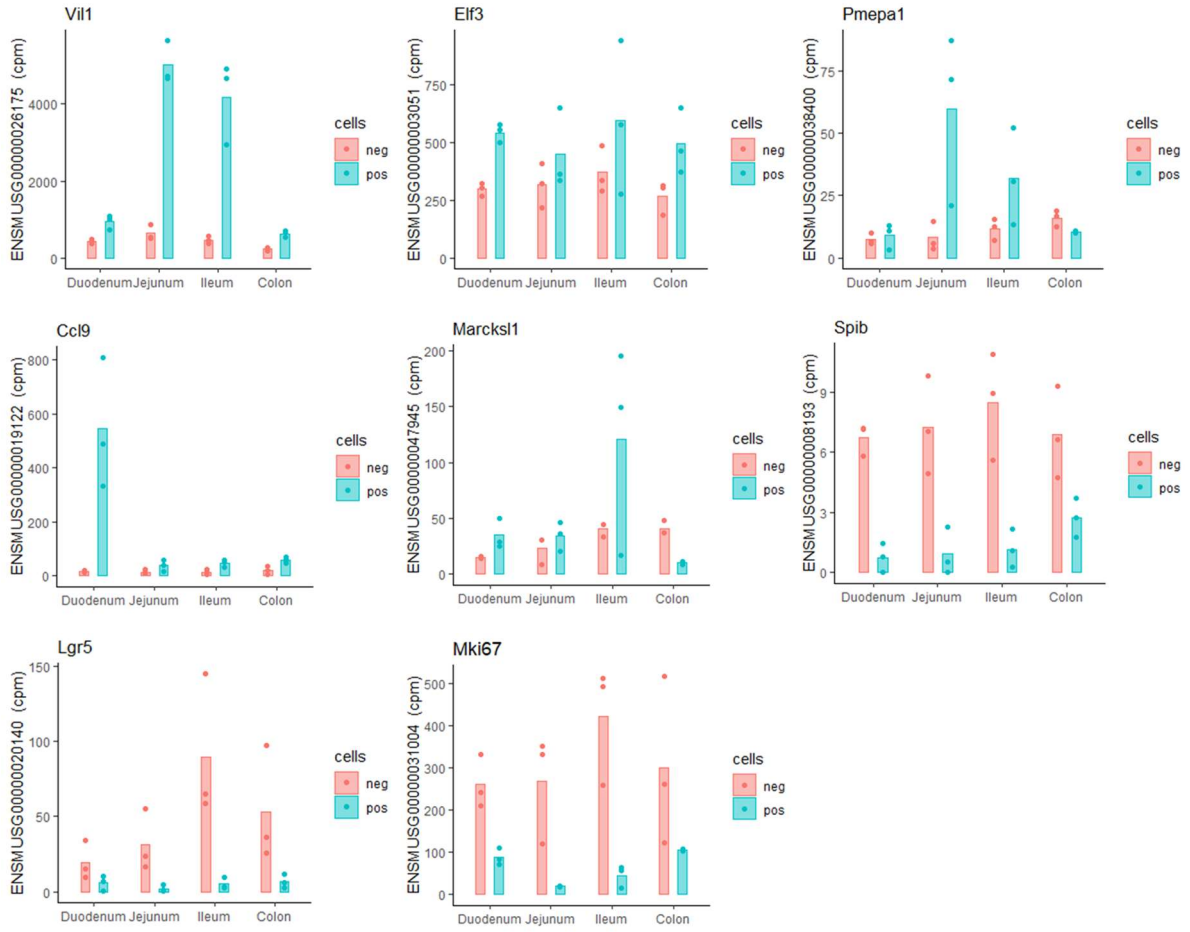

Figure 7.17: Gene expression levels of non-secretory cell markers assessed by RNA-sequencing on cell-sorted Venus-positive and negative control subpopulations of Guanylin-Venus mice. Markers for enterocytes cells (*Vil1*, *Elf3*, *Pmepa1*), M cells (*Ccl9*, *Marcksl1*, *SpiB*) and stem cells (*Lgr5*) as well as a marker for proliferative cells (Mki67) were checked for both negative (red) and positive (blue) subpopulation. Data are mean, n=3 mice.

Lgr5 stem cell's marker showed a reduction in transcripts in the *Guca2a*-enriched subpopulations compared to the negative control subpopulations. *Mki67* marker for proliferative cells presented a reduction as well in transcripts in guanylin-positive cells.

M cells are a poorly defined lineage of intestinal epithelial cells that initiate mucosal immune responses by uptake of luminal antigens (Neutra, Frey and Kraehenbuhl, 1996). Several M cells markers were described in the literature (Kanaya *et al.*, 2012) and looked at in the RNA-sequencing data: *Ccl9*, *Marcksl1*, *SpiB*, *Gp2* and *Anxa5*. While *SpiB*, and *Anxa* presented low

cpm values (0-30cpm) in both negative and positive subpopulations (data not shown for *Anxa5*), *Ccl9* presented a significant increase in the guanylin-positive subpopulation in the duodenum whereas *Marcksl1* was significantly increased in the ileum. Finally, the fully differentiated M cells marker *Gp2* was not detected in our subpopulations. The disparity in results might be due to markers appearing at different stages in the differentiation of M cells. *Marcksl1* appears at the early stage of the differentiation whereas *Ccl9* appears only in the last differentiation stage (Ohno, 2016). The discrepancy of *Gp2* not being detected by RNAseq while being a marker of late differentiation is so far unexplained. M cells are also present in follicle-associated epithelium (FAE) which could have been removed during the preparation of the cell sort.

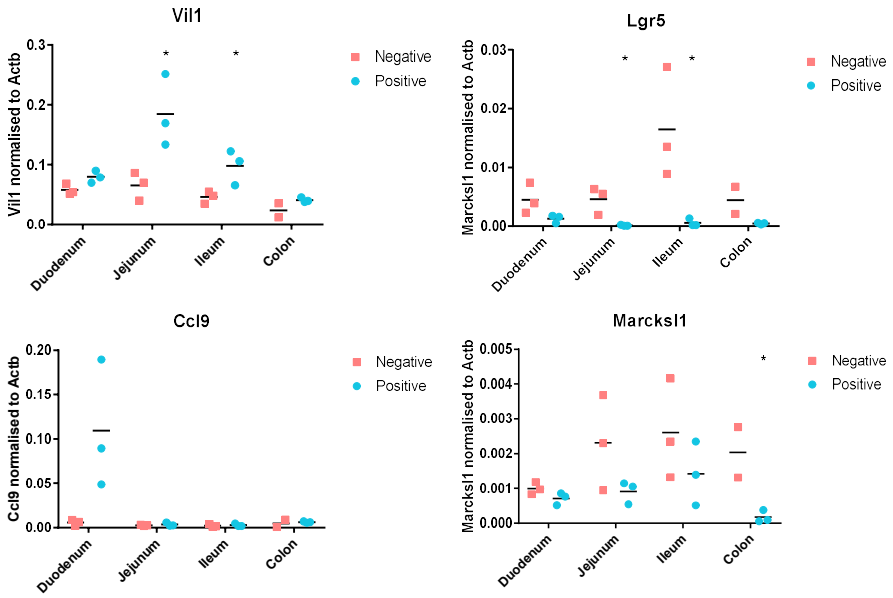

Figure 7.18: Gene expression levels of non-secretory cell markers measured by qPCR on cell-sorted Venus-positive and negative control subpopulations of Guanylin-Venus mice. Markers for enterocytes cells (*Vil1*), stem cells (*Lgr5*), and M cells (*Ccl9, Marcksl1*) were checked for both negative (red) and positive (blue) subpopulation. Data are mean, n=3 mice. Statistical significance was assessed by paired t test in between subpopulations. * indicates $p<0.05$.

Validation of guanylin-expressing cells by Immunohistochemistry

RNA-sequencing data suggested there may be some overlap between Paneth cells and the fluorescent cells in Guanylin-Venus mice. Sections of small intestine and colon were stained using antibodies raised against GFP and lysozyme. Double-positive staining of GFP and lysozyme was present at the bottom of the crypt when staining duodenum, jejunum and ileum sections (figure 7.19). 69.7% of Paneth cells were also positive for GFP in the duodenum. No staining was found in the colon with an antibody against lysozyme as expected.

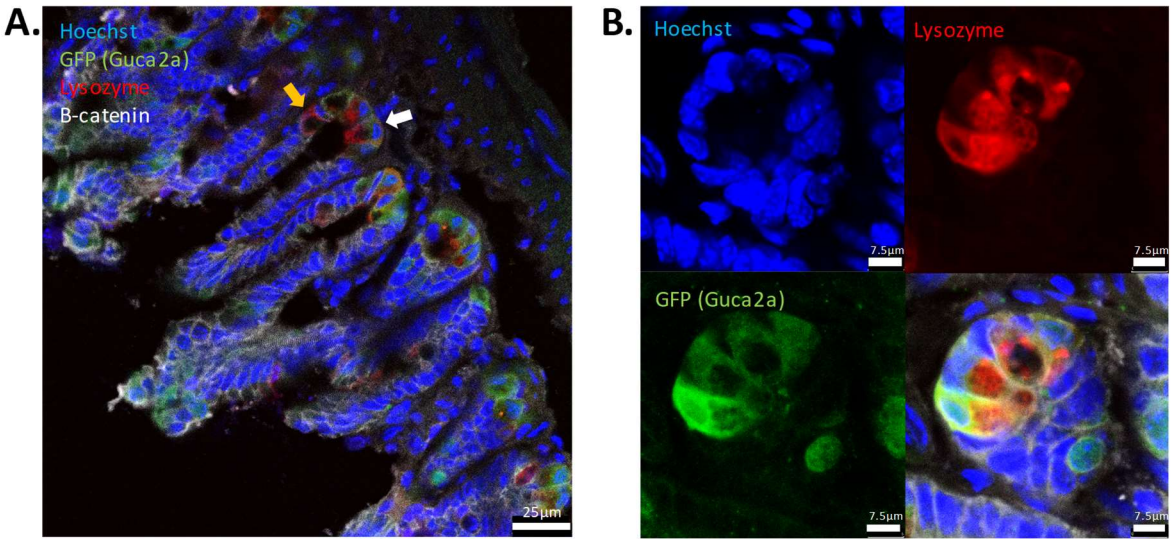

Figure 7.19: Triple staining of guanylin cells with Paneth cells marker.
Immunohistochemistry sections of jejunum (**A.**) and duodenum (**B.**) were stained for GFP (green), lysozyme (red), β-catenin (white) and Hoechst (blue). The white arrow highlights a double-stained cell. The yellow arrow highlights a cell that is not a double positive cell.

RNA-sequencing data also suggested that goblet cell markers were expressed in the fluorescent cells of the Guanylin-Venus mice. Sections of duodenum, jejunum, ileum and colon were stained using antibodies raised against GFP and Muc2 (figure 7.20). Double-positive staining was identified for all tissues with some difference in between them. In jejunum and ileum, double positive staining was less common, and figure 7.20B presents staining of a goblet cell that does not co-stain for Venus but is surrounded by Venus-positive cells. In the duodenum (figures 7.20B, C and D) however, double-positive staining represented 51% of goblet cells and 53% of the GFP staining was co-stained with muc2.

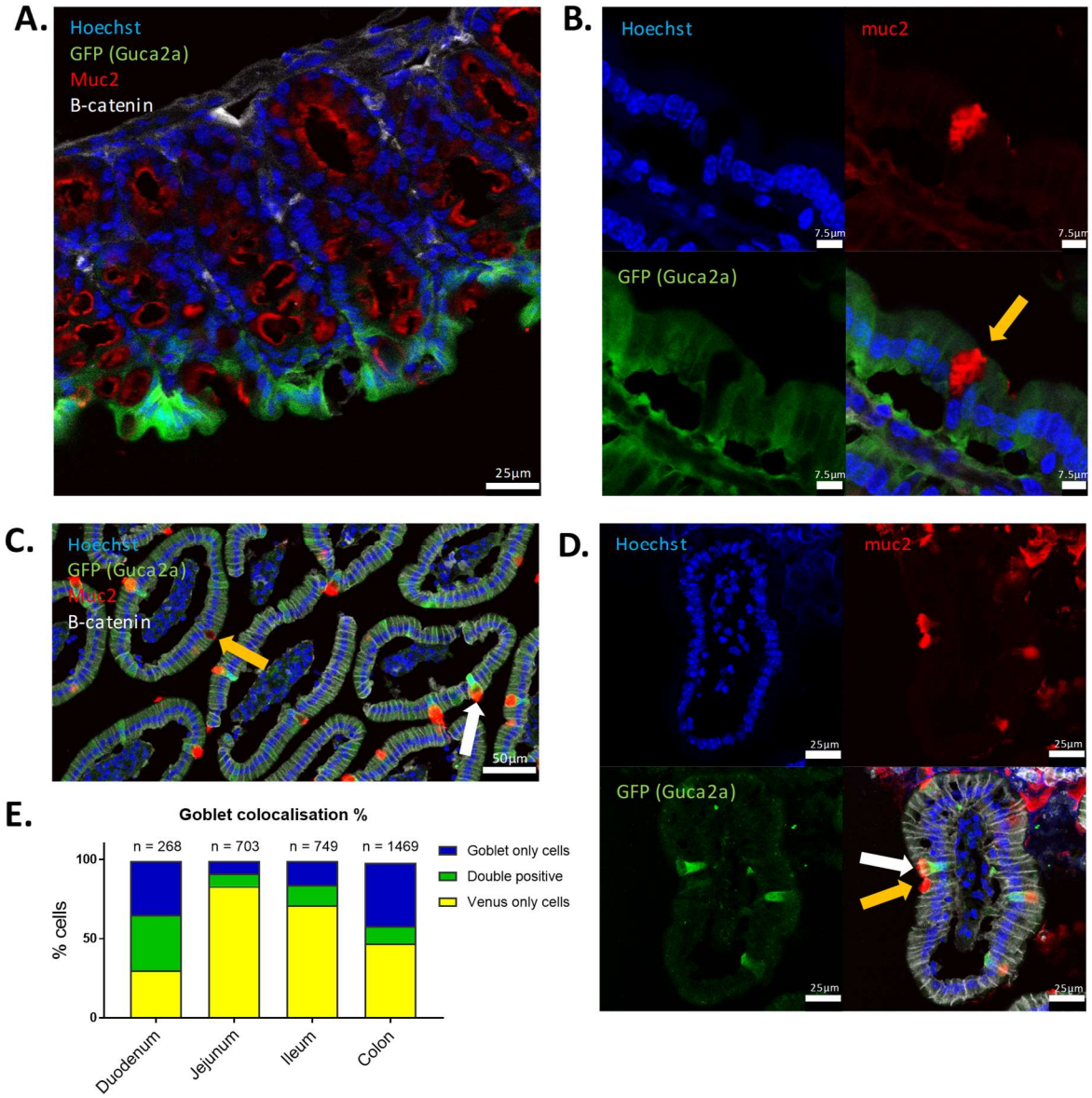

Figure 7.20: Triple staining of guanylin cells with goblet cells marker. Immunohistochemistry sections of colon (**A.**), jejunum (**B.**), and duodenum (**C.** and **D.**) were stained for GFP (green), muc2 (red), β-catenin (white) and Hoechst (blue). (**E.**) Muc2 and GFP double positive cells were counted and compared to single positive cells in duodenum, jejunum, ileum an colon sections. White arrows highlight a double-stained cell. Yellow arrows highlight cells that are not double positive.

These results support the previous RNA-sequencing data highlighting gene expression markers for Paneth cells and goblet cells in the duodenum. Jejunum and ileum showed GFP positive cells co-staining with Paneth cells in the crypt. In jejunum and ileum's villi, the GFP was essentially present in enterocytes (figure 7.5), with the odd goblet cells. Goblet-rich colon displayed a co-staining of GFP-cells with goblet cells marker muc2. Potential other GFP-positive cells could be mature colonocytes.

7.2.6 Guanylin-producing cells in stomach and kidneys

Uroguanylin was shown in the past to be present in the collecting ducts and distal tubules of the kidneys (Nakazato *et al.*, 1998; Fujimoto *et al.*, 2000). Another group looked at the uroguanylin and guanylin mRNA distribution along the mouse nephron and claimed that qPCR analysis showed guanylin expression in the collecting ducts (Potthast *et al.*, 2001). In a similar fashion, qPCRs were used in the past to detect mRNA for guanylin and uroguanylin mRNA in stomach (London *et al.*, 1997). The Guanylin-Venus mouse is a good tool to study the potential expression of guanylin in different tissues, however a pilot data showed no evidence of Guanylin-Venus staining in kidneys nor in stomach. (Figure 7.21).

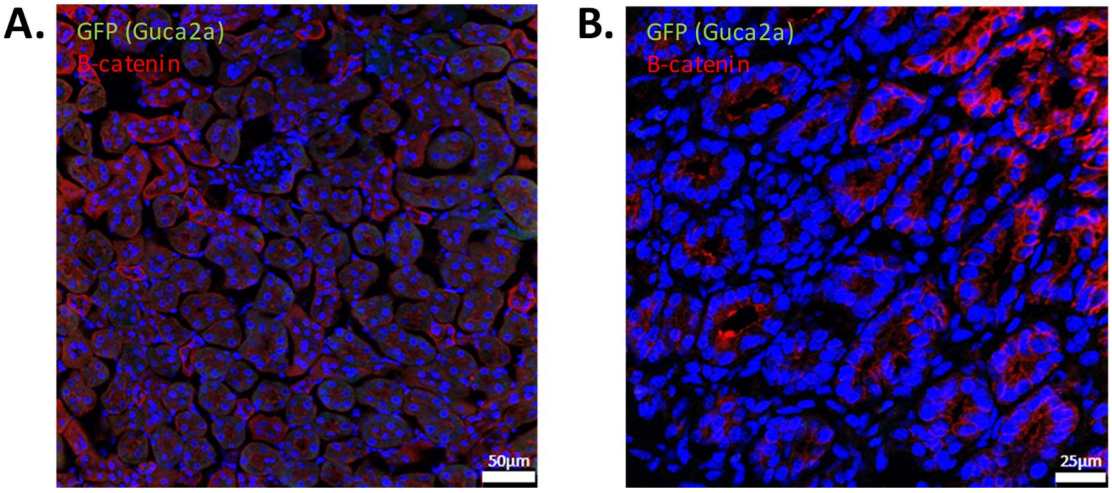

Figure 7.21: Absence of guanylin in kidney and stomach sections. Kidney (**A.**) and stomach (**B.**) sections from Guanylin-Venus mouse were assessed by immunohistochemistry. All sections were stained for GFP (green), β-catenin (red) and Hoechst (blue).

7.2.7 Insight from the RNA-sequencing on the guanylin-expressing cells per tissue

Guanylin expressing cells were previously analysed without distinction between tissues. However, a look at the different cell marker genes showed a great disparity between tissues. To look at the difference of genes enrichment per tissue, 4 heatmaps were generated to compare enriched population per tissues (figure 7.22). Tissues showed all distinct maps and each top 50 enriched genes presented few of the cell markers that were already described. The duodenum heatmap highlights the gene enrichment of goblet and Paneth cell markers *Fcgbp*, *Tff3*, *Muc2*, *Spdef* in the *Guca2a*-positive subpopulation. Both jejunum and ileum heatmaps displayed the enterocyte cell marker *Vil1* in the top 50 enriched genes, and the ileum heatmap also presented some goblet cell markers (*Fcgbp* and *Muc2*).

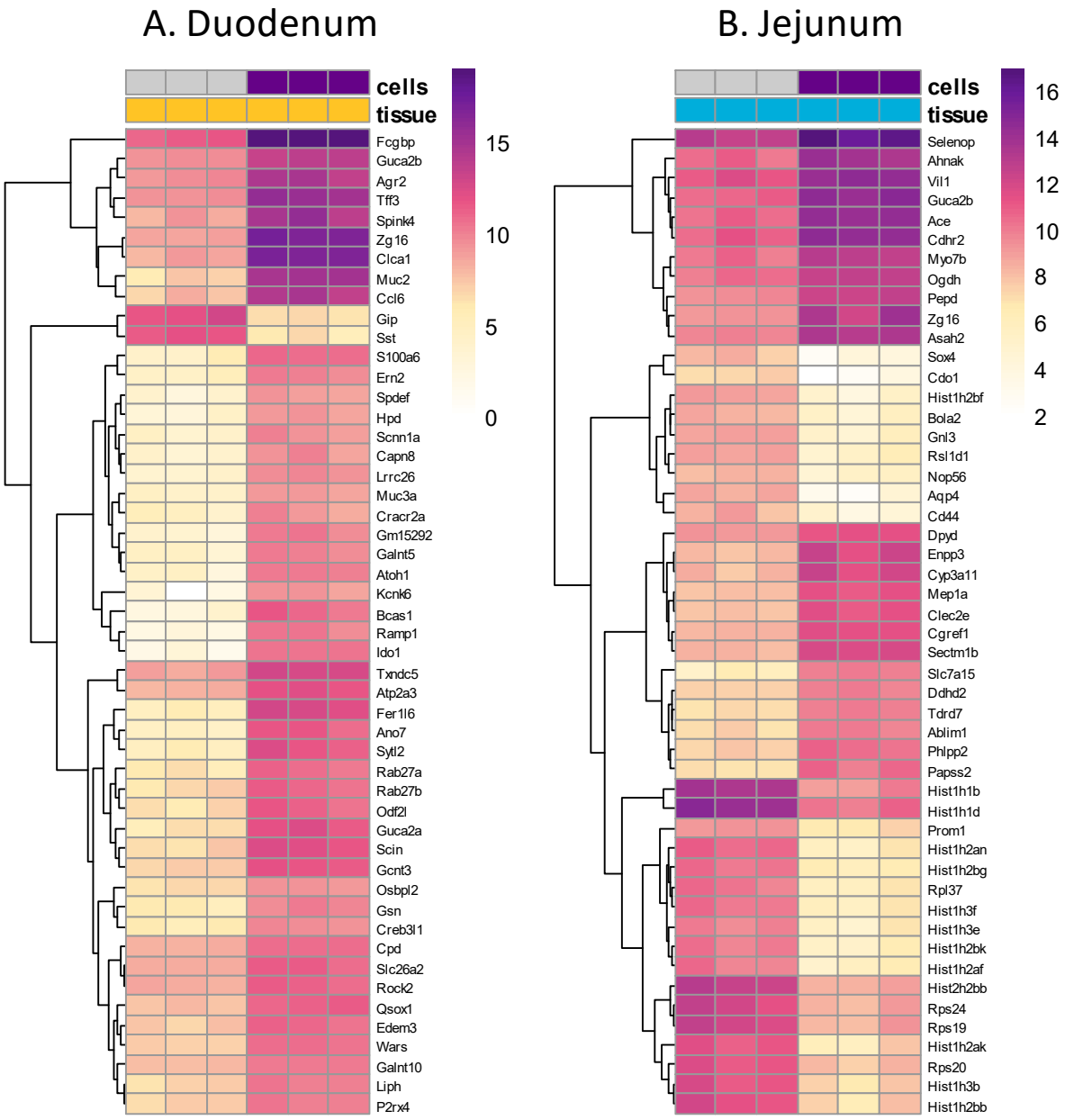

Figure 7.22: Heatmaps showing the top 50 most differentially expressed genes found for the duodenum (A), jejunum (B), ileum (C) and colon (D) from RNA-sequencing of FACS-isolated cell populations from three Guanylin-Venus mice. Non-coding and mitochondrial genes were excluded. Values are log10 (normalised read counts using DEseq2). Genes are grouped via hierarchical clustering based on Euclidean distance and complete linkage. Heatmaps were generated with the assistance of P. Larraufie.

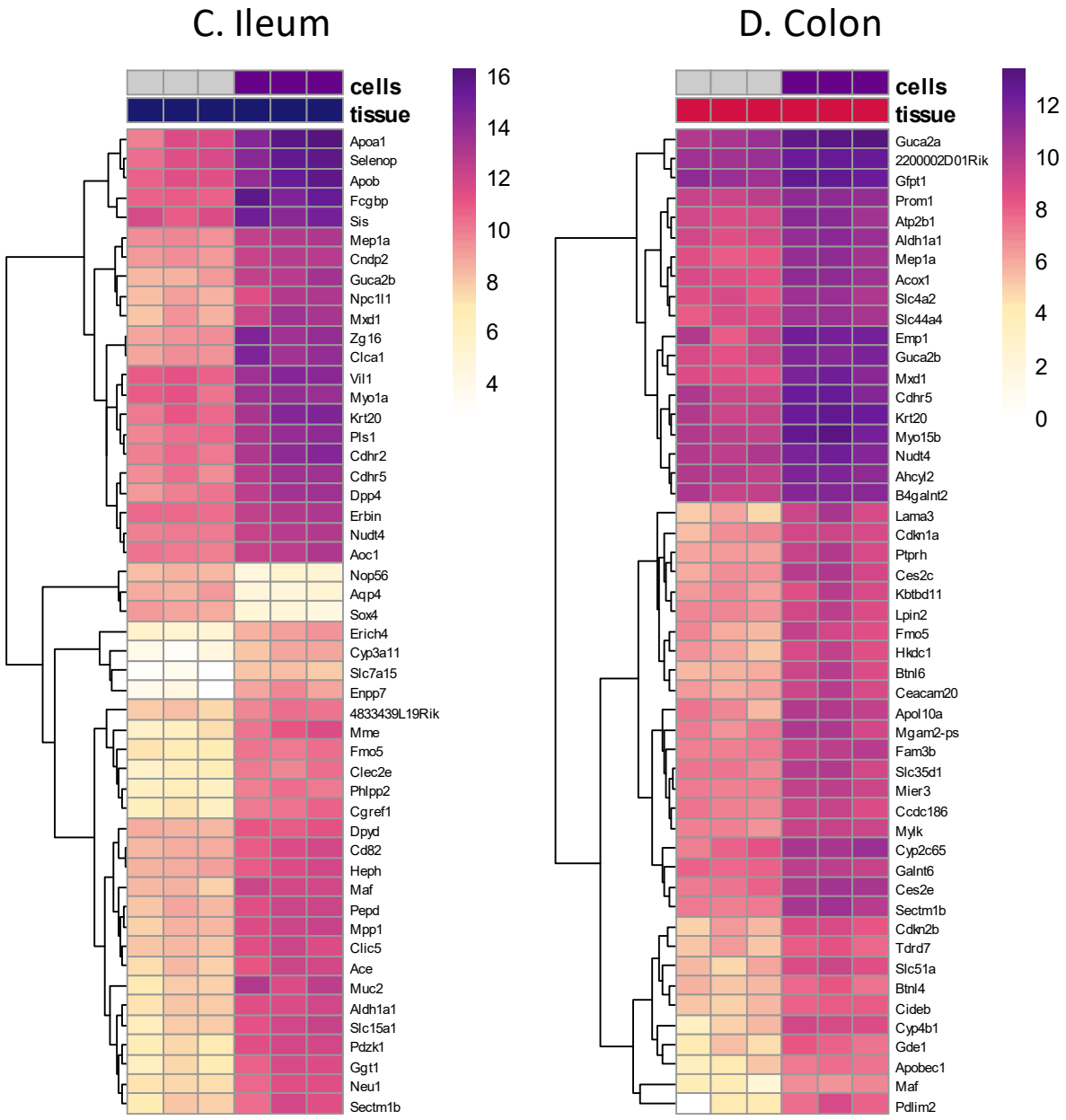

End of figure 7.22.

Several ribosomal family genes and histone family genes were highly depleted in the guanylin-positive subpopulation (figure 7.22B). Jejunum's guanylin-positive subpopulation being mainly mature enterocytes, a decrease in division or secretion from this subpopulation would explain this trend.

Finally, the uroguanylin gene *Guca2b* is in the top 50 differentially expressed genes across the 4 heatmaps providing further evidence that guanylin-producing cells are producing uroguanylin as well.

To represent how many positively-enriched genes overlapped between tissues, Venn diagrams were used (figure 7.23). The duodenum had 1575 positively-enriched genes in total, the jejunum 3077 genes, the ileum 2811 and the colon 1419 positively-enriched genes. 515 positively-enriched genes were common to all 4 tissues. When looking specifically to the small intestine overlap, jejunum and ileum had a high number of shared enriched genes with 2339 (888+1451) genes overlapping. On the contrary the duodenum only shared 1006 (888+118) positively-enriched genes in common with either the jejunum or the ileum; result which agrees with the jejunum and ileum having similar guanylin-expressing cell types.

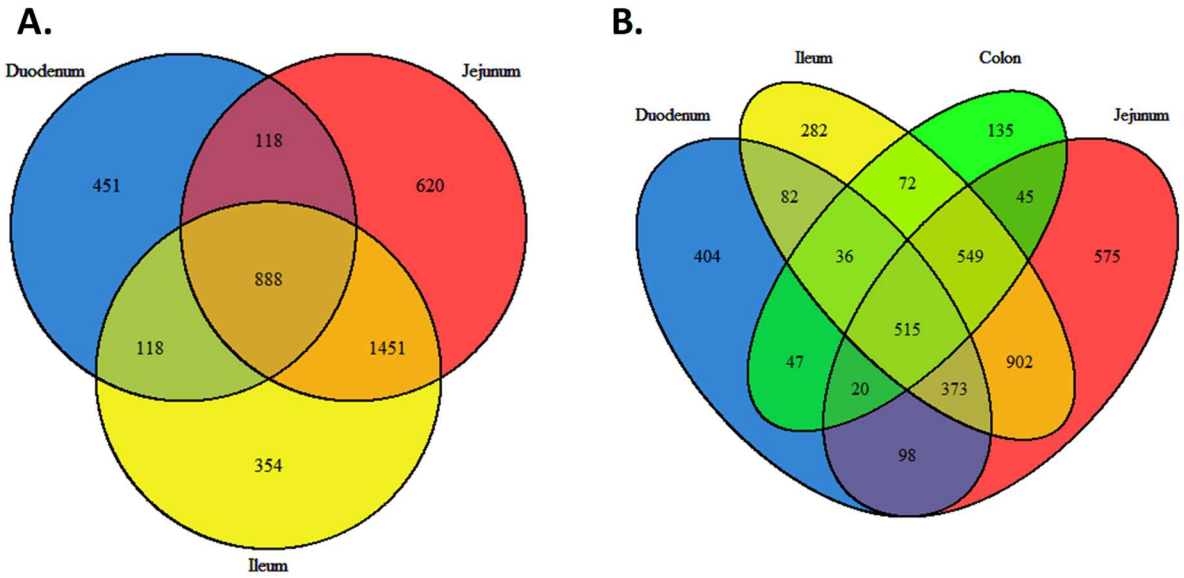

Figure 7.23: Venn diagrams summarising the overlap of positively-enriched genes in the guanylin-positive cell subpopulation. In **A.** duodenum, jejunum and ileum were compared in a 3 sets Venn diagram. Colon positively-enriched genes were added in the 4 sets Venn diagram **B.** Positively enriched genes were selected for a p-adjusted value <0.05.

A gene ontology (GO) analysis was performed using GOseq on the positively enriched genes. It is used to highlight biological processes and was used on the positively enriched genes of the 4 tissues. The summary of the 4 tissues Gene Ontology (GO) is shown in appendix 5. Sixty gene categories came out of the analysis with 1/6 of them related to the defence against bacteria, linking the enriched genes to the defensive role of Paneth cells that secrete antimicrobial peptides and proteins in the mucus layer. Few of the gene ontology functions emphasised on the glycosylation of protein which was connecting the enriched genes to the production of mucin by the goblet cells.

7.3 Discussion

7.3.1 Generation of the Guanylin-Venus and Uroguanylin-Venus transgenic mice

While this chapter focused on the generation and characterisation of a Guanylin-Venus mouse model, a Uroguanylin-Venus mouse model was attempted to be developed in parallel. The generation of both mouse models was performed by cloning Venus into the *Guca2a* or *Guca2b* coding sequence in a BAC vector. Vectors were microinjected into mice ova which were reimplanted into pseudo-pregnant mice. Random integration of the modified BAC vector into the DNA from the mice ova is supposed to express the gene reporter when the native *Guca2a* or *Guca2b* was also expressed. The generation of both the Guanylin-Venus and the Uroguanylin-Venus BAC vectors was performed using Red/ET recombination technology between linear double stranded DNA and the BAC vector. The pRed/ET system encodes for the phage λ homologous recombination system. It includes 3 components: 5' to 3' exonuclease, annealing protein Beta, and inhibitor of *E. coli* exonuclease and recombination complex, Gamma. After breaking the double-stranded DNA, the exonuclease degrades the 5' end of the broken sites and the Beta component protects the remaining 3' single strand before recombination (Shizuya *et al.*, 1992; Murphy, 1998; Wang *et al.*, 2006).

This system was a success in facilitating Guanylin-Venus BAC vector recombination, but it was not successful for the Uroguanylin-Venus BAC vector recombination. Therefore, a new recombination method was designed by replacing the uroguanylin gene with an rspL-Tet counter-selection cassette fused to the Venus sequence in the BAC vector. The removal of the counter-selection cassette was done with a second round of recombination using a single-stranded DNA oligonucleotide. The use of single-stranded DNA oligonucleotides was identified as a more efficient method to perform recombination in *E. coli* chromosomal targets (Ellis *et al.*, 2001; Costantino and Court, 2003) or BAC vectors (Swaminathan *et al.*, 2000) compared to the standard recombination on double-stranded DNA. This recombination method requires only the Beta compound of the λ homologous recombination system due to the complex formed by dsDNA and the Beta compound being resistant to single-stranded DNase. It also promotes the annealing to complementary single-stranded DNA (Costantino and Court, 2003).

When the constructs were completed and quality controlled, they were microinjected into one-day old ova and reimplanted in pseudopregnant females. Two Guanylin-Venus founders were identified following the second microinjection but a third attempt to make uroguanylin

founders was unsuccessful. Due to the cost of each microinjection campaign, and time constraint for the project, the decision was made not to proceed with the generation of a Uroguanylin-Venus mouse model. However, one potential way to overcome the failed microinjection would have been by linearizing the BAC vector, which can make the recombination more efficient. However, to microinject linearised BAC vectors, larger needle openings and lower injection pressures will have to be applied to minimize the easy shearing of the BAC vector (Liu *et al.*, 2013).

Fortunately, one of the two Guanylin-Venus founders managed to pass the transgene to its offspring. According to the Mendelian ratio, 50% of the progenies should contain the transgene if the transgene is integrated in one chromosome in a cell from the germline. An explanation to the second founder not transmitting the transgene would be that it was a mosaic mouse with the transgene not present in the germ cells (Haruyama, Cho and Kulkarni, 2009). This is not an uncommon problem; microinjection is performed on a day old fertilized eggs which should still be at a 1 cell stage, but the recombination can happen at a later stage and integrate the DNA into a non-germline cell.

7.3.2 Guanylin tissue and cellular localisation in the GI tract

The development of a new transgenic mouse model expressing Venus under the guanylin promoter is the strongest surrogate for the lack of specific antibodies to guanylin and the limitation of *in situ* hybridization.

Guanylin and uroguanylin have long been described as two hormones having a differential expression along the GI tract with *Guca2b* mainly expressed in the proximal small intestine and *Guca2a* mainly expressed in the distal small intestine and the colon (Qian *et al.*, 2000; Ikpa *et al.*, 2016). The pattern of *Guca2a* expression in the mouse model is overall agreeing with the published data, it is important to emphasize that the highest percentage of Venus-positive cells compared to the total epithelial cells was found in the jejunum, followed by the ileum and the colon. While jejunum and ileum guanylin-expressing cells were the most abundant ones, the guanylin-expressing cells from these tissues displayed the lowest gene expression in average compared to positive cells coming from the duodenum or the colon. This is potentially caused by higher *Guca2a* expression in the goblet cells and Paneth cells compared to the expression in enterocytes. Therefore, a bulk RNA-sequencing would reduce the apparent

expression of *Guca2a*, as the expression counts would be diluted by the heterogeneity of the cell population.

Despite previous studies suggesting that guanylin is barely expressed in the duodenum and highly expressed in the colon, both peptidomic analysis and immunohistochemistry showed that guanylin was expressed to detectable levels in the duodenum and guanylin levels were low to absent in the rectum. Finally, the human data presented an overall high expression in jejunum for guanylin. Uroguanylin peptides were not detected in human homogenates.

Conflicting literature describes guanylin and uroguanylin expression pattern along the crypt-villus axis. Early *in situ* hybridization indicated uroguanylin primarily localised to the intestinal villi whereas guanylin was reported in both crypts and villi in the small intestine as well as in the colonic surface epithelium (Whitaker, Witte, *et al.*, 1997). However, an improved *in situ* hybridization method, RNAscope, also detected guanylin and uroguanylin at the base of the colonic crypt in Paneth-like cells (Ikpa *et al.*, 2016). This last result is in contradiction with the immunohistochemistry performed on the mouse model which agrees with guanylin being present on the superficial epithelium only. Despite not having a Uroguanylin-Venus mouse model, data from the RNA-sequencing on the Guanylin-Venus mouse model informed us about the localisation of uroguanylin. *Guca2b* gene expression was statistically significantly higher in positive cells compared to negative cells in the colon concluding that guanylin-expressing cells do express *Guca2b*. By deduction, uroguanylin-expressing cells should be present in the surface epithelium of the colon and not at the bottom of the crypt where Paneth-like cells were described.

Guanylin-expressing cell types vary between tissues as revealed by the analysis of cell type markers by RNA-sequencing and qPCR. Markers for stem cells, enteroendocrine cells and tuft cells were depleted in the Guanylin-Venus subpopulation across the 4 tissues. This is in contradiction with early literature showing guanylin expression in enterochromaffin cells in guinea pig (Cetin *et al.*, 1994) and human (Fernandez-Cachon *et al.*, 2018) and uroguanylin in enterochromaffin cells in rat (Perkins, Goy and Li, 1997). The data reported here is supported by results from other researchers who found other cell types from the secretory and absorptive lineages as the main source for guanylin peptide expression. While groups only distinguished Paneth cells in mouse (de Sauvage *et al.*, 1992; Whitaker, Witte, *et al.*, 1997), several groups localised guanylin in goblet cells (Cohen *et al.*, 1995; Li *et al.*, 1995; Rubio,

2012). More recent work on the localisation of guanylin peptides showed that goblet cells and Paneth cells in small intestine express them as well as tuft cells and enterocytes (Ikpa *et al.*, 2016). The RNAscope technique used for this study highlighted similar regional differences existing along the small and large intestine that was found with the transgenic mouse model described in this chapter. RNA-sequencing data in the duodenum, identified goblet cells and mature (only) Paneth cells as the main sources of guanylin. Enterocyte markers presented a low but significant increase in the guanylin-enriched cells. Their RNAscope experiment agreed with goblet and Paneth cells but found tuft cells as well expressing guanylin and uroguanylin in the duodenum. In another study, cells were found in mouse duodenum that co-stained with uroguanylin (but not guanylin) with Trpm5 concluding that tuft cells (or enteroendocrine cells) in the duodenum do express uroguanylin (Kokrashvili *et al.*, 2009). Tuft cells being a relatively rare cell population, the RNA-sequencing method would not be able to detect *Guca2b* transcripts in the negative population. In conclusion, it is not possible to corroborate or disprove the presence of uroguanylin in tuft cells with our data. In the jejunum and ileum, RNA-sequencing and immunohistochemistry data concurred with their study agreeing that enterocytes are the main cell-type expressing guanylin peptides in the villi, though crypts are still expressing guanylin through Paneth cells and goblet cells. In the colon, goblet cells and enterocytes expressed guanylin according to the RNA-sequencing and immunohistochemistry data, however Ikpa's data indicated Paneth-like cells as the main source. While the lack of gene markers for Paneth-like cells cannot disprove such theory, the Guanylin-Venus immunostaining only stained the top of the crypt in the surface epithelium.

7.3.3 Guanylin peptides support the defence mechanisms of secretory lineage cells

Across the GI tract and more specifically in the duodenum and colon, one of guanylin's predominant sites of cellular expression occurs within Paneth cells. Paneth cells release secretory granules when exposed to bacterial antigens. Those granules contain antimicrobial peptides and compounds (α-defensins, CRS peptides, Lysozyme C, sPLA2, REG3 α, ANG4) that have either Gram-positive or Gram-negative antibacterial activities (Bevins and Salzman, 2011) and these molecules are thought to shape the microbiota composition (Salzman *et al.*, 2010). Guanylin and uroguanylin's receptor GC-C when activated results in cGMP conversion. cGMP will activate a variety of effector proteins such as phosphodiesterases, protein kinases (PKGII and PKA) and ion channels thereby stimulating CFTR channels resulting in an osmotic

imbalance leading to water release in the GI tract (Guba *et al.*, 1996). Secretion of fluid into the duodenum contributes to the nutrient transit through the small intestine and water secretion in the colon shapes the stool formation and consistency and therefore intestinal transit (Jarmuz *et al.*, 2015). An interesting theory proposed by de Sauvage hypothesized that antimicrobial defence mechanism of Paneth cells could be supported by the action on the liquid content by the guanylin peptides (de Sauvage *et al.*, 1992). This theory is supported by the Gene Ontology analysis performed on the RNA-sequencing. Genes enriched in guanylin expressing cells showed implications in the defence response to bacterium with 1/6 of the GO functions related to this area.

A similar theory could also be applied to the function of goblet cells. Goblet cells are responsible for the production and maintenance of the protective mucus on the epithelium by synthesizing and secreting glycoproteins called mucins (Specian and Oliver, 1991). From the RNA-sequencing data, out of the 60 gene functions that were enriched in the gene ontology analysis of the differently expressed genes enriched in the positively-enriched guanylin-expressing cells, 4 functions were related to protein glycosylation. In conclusion, in addition to finding markers of goblet cells, these cells express a higher proportion of genes corresponding to the cell type function of goblet cells. Finally, two independent groups show that mucin and guanylin secretion are driven by cholinergic stimulation (Phillips, 1992; Martin *et al.*, 1999).

7.3.4 Summary

In conclusion, here I describe the successful generation of a new transgenic mouse model that enables accurate localisation of the cells that express guanylin. The recombination of the fluorescent marker was performed by modifying a BAC vector that contained *Guca2a*. The Guanylin-Venus mice possessed a transgene that directly transcribed the yellow fluorescent protein Venus under the control of the *Guca2a* promoter. An advantage of the use of BAC vectors for recombination is their cargo carrying capacity. Furthermore, BACs are more likely to contain all the regulatory elements required to replicate the endogenous gene expression pattern of the gene of interest.

This new transgenic mouse model helped defined the localisation of guanylin-expressing cells on the rostro-caudal axis of the small and large intestine and along the crypt-villous axis of each intestinal section (or crypt-surface axes in the case of the colon). RNA-sequencing data

analysis allowed the identification of guanylin-expressing cell types. Major cell types found to express guanylin and include goblet cells, Paneth cells and enterocytes with different patterns of expression depending on the intestinal tissue analysed. Expression in M cells will have to be confirmed through specific immunostaining around the FAE.

This work allowed to address similar conclusions on uroguanylin-expressing cells to some extent. It is indeed possible to assume that the negative control cells from the cell sort were not producing uroguanylin through careful interrogation of the RNA-sequencing data; later confirmed by the qPCR data performed on negative control and guanylin-expressing cells. However, at this stage it is not possible to conclude on the cellular subpopulations among the guanylin-expressing cells that also express *Guca2b*. Alternative methods will be required to obtain these data.

Pilot studies did not show any evidence of *Guca2a*-fluorescence in stomach nor in kidneys. Investigations of adrenal glands and reproductive systems should be performed to corroborate (or not) already published literature.

7.3.5 Future work

The objective of the work described in this chapter was to identify the guanylin-expressing cell types in a transgenic mouse model. However, one caveat of a mouse model is its translatability to human physiology. For instance, published data on other rodents such as rats and guinea pigs did not show guanylin expression in the villus (Cetin *et al.*, 1994; Perkins, Goy and Li, 1997) suggesting species differences in peptide expression might exist. Raising monoclonal antibodies against human guanylin and uroguanylin was the way I employed to perform immunohistochemistry on human samples. Unfortunately, the pilot study performed on human tissues, were not successful. Due to time constraint, an optimised version of the immunohistochemistry protocol on human samples was not executed.

The transgenic mouse model described in this chapter provides new opportunities to understand and characterise the cellular expression of guanylin. In future studies, the use of Guanylin-Venus mouse organoids combined to time-lapse microscopy could be used to control in a new and elegant way the gene expression modification under stimuli. Fluorescence could be measured overtime in Guanylin-Venus organoids in presence or absence of stimuli.

A field of research that received much excitement recently, pertains to the role of guanylin and uroguanylin on satiety and energy expenditure (Valentino *et al.*, 2011; Cintia Folgueira *et al.*, 2016). Some clinical data converging with my own results showed that obese volunteers were reported to have lower levels of guanylin and uroguanylin, and volunteers that underwent Roux-en-Y gastric by-pass surgery had increased plasma levels of prohormones (A Rodríguez *et al.*, 2016). An interesting use of the Guanylin-Venus mouse would be to look at the effect of high fat, restricted food intake or standard chow diet on the expression of guanylin and uroguanylin in mouse and their circulating levels. The mouse model would provide an insight of the effect of different food intake on the guanylin transcript levels.

Guanylin and uroguanylin role in the crypt-villous proliferation and their role in colon carcinoma cells have received some interest from different groups. *Guca2a* gene expression was markedly down-regulated in adenocarcinomas of the colon (Cohen, Hawkins and Witte, 1998) and guanylin and uroguanylin mRNA levels are reduced in polyps and adenocarcinomas of human colon relative to levels from normal colon mucosa from the same patients (Kunwar Shailubhai *et al.*, 2000). Alongside the research on guanylin peptides, new cancer related mouse models were generated. Tetteh generated for instance an inducible colon-specific Cre enzyme mouse model for colon cancer research that initiates the colon cancer and represent its progression (Tetteh *et al.*, 2016). A potential mouse line could be generated by crossing Tetteh's mouse line with the Guanylin-Venus mouse. Such line would be useful to directly look at the expression of guanylin in colonic carcinogenic tissues and assess their roles.

Chapter 8: Discussion

8.1 Summary

The overall aim of this thesis was to characterise the localisation and secretion of the guanylin peptides and their proforms, ProGuanylin and ProUroguanylin, in mouse and humans. To achieve this goal, several research tools were developed. Firstly, novel high-throughput monoclonal antibody-based immunoassays were developed to characterise the levels of the proforms in serum and plasma collected from healthy volunteers and across a number of physiological and pathophysiological states. These immunoassays were also utilised to measure the level of protein expression on samples originating from different secretion assay models. In parallel to the attempted development of antibodies against the historically known active peptides, mass spectrometry analysis was used on both human and mouse tissues and biological samples in order to measure the levels of endogenous active peptides. This technique shed light on the endogenous sequence of the guanylin peptides present in those samples. Finally, a novel guanylin transgenic reporter mouse model was generated and used to identify and characterise guanylin-expressing cells in the gastrointestinal tract.

8.2 Antibodies against human ProGuanylin and ProUroguanylin, a new tool for investigation

In chapter 3, new monoclonal antibodies for ProGuanylin and ProUroguanylin were identified through a hybridoma process. State of the art technologies allowed the characterisation of newly isolated monoclonal antibody pairs that were used subsequently to develop extremely sensitive immunoassays with high dynamic range. The ability of these immunoassays to detect ProGuanylin and ProUroguanylin was confirmed using different human blood samples (serum, plasma Lith Hep, and plasma EDTA). The assay was compared with the commercially available ELISA and presented higher range of detection as well as an improved user-friendly property.

The assay proved useful to measure proforms levels in healthy volunteers that underwent oral glucose tolerance tests as well as a standardised liquid meal test. As it was demonstrated in the past that salt intake elicits a physiological response in the expression of guanylin peptides in rat (Carrithers *et al.*, 2002) as well as in humans (Kinoshita, Nakazato, *et al.*, 1997), release of the proforms in response to the standardised liquid meal was expected. However, these expectations were not fulfilled as no strong physiological release of ProGuanylin and

ProUroguanylin was detected in human plasma following food and glucose intake in healthy participants. However, levels of ProGuanylin and ProUroguanylin did differ between fasted and fed participants in healthy and diseased states (subjects with neuroendocrine tumours, participants that had a prophylactic total gastrectomy, or a small bowel transplants). Proforms were also increased in subject who previously underwent Roux-en-Y gastric bypass compared to standard participants. This was corroborated in a recent publication highlighting an increase in *GUCA2A* and *GUCA2B* transcripts after gastric bypass surgery (Fernandez-Cachon *et al.*, 2018). However, the significance of these findings requires further investigation.

Immunoassays were able to accurately measure ProGuanylin and ProUroguanylin levels in various pre-clinical gastrointestinal human models including the TC7 cell line, organoids and Ussing chamber's supplemented with Ringer buffer. Therefore, the expression of the proforms was measured in these different secretion assay models. Salt concentration, gut hormones and vagal stimuli were all screened to assess their effect, if any, on the secretion of the proforms. Previously reported studies proposed NaCl to be a potent regulator of the secretion of guanylin peptides in rats (Li *et al.*, 1996; Kinoshita, Nakazato, *et al.*, 1997; Kita *et al.*, 1999; Carrithers *et al.*, 2002; Fukae *et al.*, 2002). The results generated in the human studies described herein, however, did not support a critical role for NaCl concentration on the secretion of ProGuanylin or ProUroguanylin. Similarly, vagal and other enteroendocrine secretory stimuli did not present any noticeable effects in the different models studied.

Other secretion models would need to be used to better understand the regulatory effects of vagal and gut hormones as well as gut lumen nutrient content on ProGuanylin and ProUroguanylin secretion and the range of buffer used over the course of the thesis (Ringer solution, plasma and serum sample, PBS and DMEM-based cell media) testify about the versatility of the use of the immunoassays. Additional experiments could be performed on more complex model systems that may better represent human physiology. However, in the interests of time and resource available these were not pursued further. Secretion on Ussing chambers, air-liquid interface or primary cultures of small/large intestine in association with the immunoassays are established and validated research tools routinely used in the Gribble/Reimann laboratory to assess the role of potential stimuli (Pais *et al.*, 2016; Larraufie *et al.*, 2018). However, these experiments are not high-throughput and depend critically on the availability and healthiness of tissues.

The use of the newly developed monoclonal antibodies is not restricted to immunoassays. The high affinity antibodies could be utilised for immunohistochemistry of human tissues or Western blots. Whilst the utility of the antibodies as immunohistochemical reagents for the study of human tissues, was briefly explored, due to the inability to develop a robust methodology this was not explored further during my PhD.

The physiological role of ProGuanylin and ProUroguanylin could be investigated in different tissues by using the antibodies to block the proforms from activating the GC-C receptor. However, this study would require the antibody panel to be cross-reactive for a rodent species and involve further characterisation of the panel of antibodies to show that the antibody is functional (blocking the access of the peptide to the receptor).

8.3 Redefining the active guanylin peptides

Currently, mass spectrometry and peptidomic analysis are increasingly being employed in attempt to improve our understanding of the bioactive peptide products that are processed from larger prohormone peptides (Kay *et al.*, 2017), as well as the tissue distribution of these hormones (Roberts *et al.*, 2018). The development of such methods in the Gribble/Reimann laboratory has allowed me to make an unexpected but significant discovery in the guanylin peptides field. Previous studies have postulated that the bioactive guanylin peptide is defined by the last 15 amino acids of the C-terminal sequence of the GUCA2A protein sequence (Mark G Currie *et al.*, 1992). While Currie *et al.* questions the possibility of a different N-terminal end of the sequence, the scientific community accepted the sequence. The method using acetonitrile to extract all peptides from different biological sources such as tissue homogenates, blood, ileal secretion or intestinal content, highlighted the absence in all samples of the 15 amino acid guanylin peptide. The highly sensitive LC-MS/MS method identified peptides that were present in abundance across the different biological specimens. In mouse, one identified peptide of interest is guanylin 60-116, a peptide that encompasses the C-terminal sequence considered as essential for activating the GC-C receptor. In human serum samples this peptide was not identified via peptidomic analysis, but a proteomic approach supported the potential existence of a similarly sized peptide, however it was too long to be fully characterised via LC-MS/MS with acetonitrile-based precipitation of larger proteins.

Going forward, further studies are required to clearly ascertain the amino acid sequence of the human peptide and confirm that both murine and human versions of this larger peptide are functional and able to activate the GC-C receptor. It is so far believed that the 15 amino acid version of the guanylin peptide is more potent in basic conditions (Hamra *et al.*, 1997) and is highly susceptible to degradation via endoproteases (Hamra *et al.*, 1996). The longer version of the guanylin peptide might present different physicochemical properties that will need to be assessed to understand their physiology along the gastrointestinal tract. Uroguanylin peptide was in most samples undetectable.

8.4 Identifying sites of guanylin peptides expression

During the course of my PhD, I successfully developed a transgenic reporter mouse in which the Venus fluorescent protein was expressed under the guanylin promoter, thereby allowing me to identify and characterise guanylin-expressing cells. To date, assessment of the sites of guanylin expression has been debated with much discordance in the literature. Therefore, to improve our understanding of the physiological, and potentially pathological roles of the guanylin peptides detailed knowledge regarding their sites of expression and action is required. The transgenic reporter mouse clearly demonstrated that goblet cells and Paneth cells were the main cell-type expressing guanylin in the duodenum. In the jejunum and ileum, the main cell-type expressing guanylin are enterocytes as well as goblet and Paneth cells. Finally, colonocytes and goblet cells were the only cell types expressing *Guca2a* transcripts in the large intestine. The development of the reporter mouse model for guanylin-expressing cells gave some clues about the potential site of expression of uroguanylin as well. RNAseq and qPCR showed that uroguanylin transcripts were significantly expressed in guanylin expressing cells, suggesting that guanylin-expressing cells express uroguanylin as well. However smaller cellular populations (such as tuft cells or Paneth-like cells) would not be picked up in the guanylin-expressing cells and therefore further work is required to completely delineate the anatomical location(s) of uroguanylin expressing cells.

At the beginning of my thesis, understanding how guanylin expression and cellular secretion is regulated under different physiological states was an unanswered question. The transgenic reporter Guanylin-Venus mouse line has been used to address some aspects of this question. However, a number of questions regarding the physiological regulation of ProGuanylin derived peptides remains to be answered.

8.5 Potential future uses for the Guanylin-Venus mouse model

TC7 cell lines and human organoids provided limited results to understand which stimuli regulate the secretion of guanylin and uroguanylin. The Gribble/Reimann laboratory recently acquired new technology that will enable time-lapse microscopy of organoids or 2D cultures to be undertaken. This powerful instrument, in association with organoids or 2D cultures made of the Venus-reporter mouse small or large intestine, may be used to examine guanylin expression over time. For example, organoids could be cultured with salt, vagal or gut stimuli to determine whether such treatments increase the number of Venus expressing cells or increase the fluorescence in differentiated cells. This method would only rely on the endogenous reporter and not on antibodies thereby allowing real time expression to be determined.

One study showed that *Guca2a* expression was reduced in mice fed on HF or HC diets (Lin *et al.*). Similarly, in the human colon, guanylin mRNA levels were inversely proportional to BMI in morbidly obese patients (Lin *et al.*). Finally, other studies have shown that uroguanylin levels are lower in obese adolescent and adult participants when compared to healthy participants (A. Rodríguez *et al.*, 2016; Di Guglielmo, Perdue, *et al.*, 2018; Di Guglielmo, Tonb, *et al.*, 2018). The reporter mouse model is a perfect tool to look at the modification of transcript levels in mouse that would be fed on HF or HC diets and compare it to a standard diet.

The long-term effect of salt on guanylin and uroguanylin expression can also be studied using the transgenic model. Previous investigators have shown that a low salt diet reduced guanylin mRNA and peptide expression in the rat distal colon (Li *et al.*, 1996), while high salt intake over 4 days significantly increased the expression of guanylin mRNA in the duodenum and jejunum (Carrithers *et al.*, 2002). Similar dietary intervention studies could be undertaken with the Guanylin-Venus transgenic mice.

The intersectional role of guanylin and uroguanylin on obesity and colorectal cancer has been the recent focus of attention within the field (Lin *et al.*, 2010b). Guanylin gene expression was lost in human colonic adenocarcinoma (Cohen, Hawkins and Witte, 1998), and uroguanylin transcript levels were found to be decreased in human colonic polyps (Kunwar Shailubhai *et al.*, 2000). Mouse models are widely used to study cancer progression and disease

mechanisms. To study topical colon cancer, an inducible colon-specific Cre enzyme mouse model that initiates colon cancer and replicate its progression has been generated (Tetteh *et al.*, 2016). Additionally, a mouse model displaying hyperproliferation induced by nutritional stress diet was conceived and could be of interest in the case of the potential intersectional role of guanylin and uroguanylin (Newmark, Lipkin and Maheshwari, 1990). Generation of a mouse line crossing the guanylin reporter mouse with those colorectal cancer specific mouse models would shed light on the potential role of the guanylin peptides on colorectal cancer.

8.5 Conclusion

George Box (1919-2013), statistician, once mentioned that "all models are wrong, but some are useful". This could not relate more to the work provided to contribute to the basic knowledge of the localisation and secretion of the guanylin peptides. It is hoped that the finding presented in this thesis will spur on further characterisation of the mouse cell types and understanding of the signals delivered to secrete either guanylin or uroguanylin. Further work is required on some of these findings in humans, which is already underway with the development of antibodies against both targets. It will be exciting to see whether these findings can be applied to the discovery of new treatments for conditions including colorectal cancer or obesity.

References

Al-Majali, A. M. *et al.* (2007) 'Interaction of Escherichia coli heat-stable enterotoxin (STa) with its putative receptor on the intestinal tract of newborn kids', *FEMS Immunology and Medical Microbiology*, 49(1), pp. 35–40. doi: 10.1111/j.1574-695X.2006.00167.x.

Alasbahi, R. H. and Melzig, M. F. (2012) 'Forskolin and derivatives as tools for studying the role of cAMP.', *Die Pharmazie*, 67(1), pp. 5–13.

Arden, K. C. *et al.* (1995) 'Localization of the human B-type natriuretic peptide precursor (NPPB) gene to chromosome 1p36', *Genomics*. Academic Press, 26(2), pp. 385–389. doi: 10.1016/0888-7543(95)80225-B.

Artavanis-Tsakonas, S., Rand, M. D. and Lake, R. J. (1999) 'Notch signaling: cell fate control and signal integration in development.', *Science (New York, N.Y.)*. American Association for the Advancement of Science, 284(5415), pp. 770–6. doi: 10.1126/SCIENCE.284.5415.770.

Artursson, P. and Karlsson, J. (1991) 'Correlation between oral drug absorption in humans and apparent drug permeability coefficients in human intestinal epithelial (Caco-2) cells', *Biochemical and Biophysical Research Communications*. Academic Press, 175(3), pp. 880–885. doi: 10.1016/0006-291X(91)91647-U.

Artursson, P., Palm, K. and Luthman, K. (2001) 'Caco-2 monolayers in experimental and theoretical predictions of drug transport.', *Advanced drug delivery reviews*, 46(1–3), pp. 27–43.

Bäckhed, F. *et al.* (2005) 'Host-bacterial mutualism in the human intestine.', *Science (New York, N.Y.)*. American Association for the Advancement of Science, 307(5717), pp. 1915–20. doi: 10.1126/science.1104816.

Baggio, L. L. and Drucker, D. J. (2007) 'Biology of Incretins: GLP-1 and GIP', *Gastroenterology*, 132(6), pp. 2131–2157. doi: 10.1053/j.gastro.2007.03.054.

Bak, M. J. *et al.* (2014) 'Specificity and sensitivity of commercially available assays for glucagon-like peptide-1 (GLP-1): implications for GLP-1 measurements in clinical studies.', *Diabetes, obesity & metabolism*, 16(11), pp. 1155–64. doi: 10.1111/dom.12352.

Barderas, R. *et al.* (2008) 'Affinity maturation of antibodies assisted by *in silico* modeling', *Proceedings of the National Academy of Sciences*, 105(26), pp. 9029–9034. doi: 10.1073/pnas.0801221105.

Barker, N. *et al.* (2007) 'Identification of stem cells in small intestine and colon by marker gene Lgr5', *Nature*. Nature Publishing Group, 449(7165), pp. 1003–1007. doi: 10.1038/nature06196.

Barker, N. (2014) 'Adult intestinal stem cells: critical drivers of epithelial homeostasis and regeneration', *Nature Reviews Molecular Cell Biology*. Nature Publishing Group, 15(1), pp. 19–33. doi: 10.1038/nrm3721.

Barker, N. and Clevers, H. (2010) 'Leucine-Rich Repeat-Containing G-Protein-Coupled Receptors as Markers of Adult Stem Cells', *Gastroenterology*, 138(5), pp. 1681–1696. doi: 10.1053/j.gastro.2010.03.002.

Barker, N., van de Wetering, M. and Clevers, H. (2008) 'The intestinal stem cell.', *Genes & development*. Cold Spring Harbor Laboratory Press, 22(14), pp. 1856–64. doi: 10.1101/gad.1674008.

Bastide, P. *et al.* (2007) 'Sox9 regulates cell proliferation and is required for Paneth cell differentiation in the intestinal epithelium', *The Journal of Cell Biology*, 178(4), pp. 635–648. doi: 10.1083/jcb.200704152.

Basu, N. and Visweswariah, S. S. (2010) 'Defying the stereotype: Non-canonical roles of the peptide hormones guanylin and uroguanylin', *Frontiers in Endocrinology*, 2(JUN), pp. 1–5. doi: 10.3389/fendo.2011.00014.

Bäumler, A. J. and Sperandio, V. (2016) 'Interactions between the microbiota and pathogenic bacteria in the gut', *Nature*, 535(7610), pp. 85–93. doi: 10.1038/nature18849.

Béaslas, O. *et al.* (2008) 'Transcriptome response of enterocytes to dietary lipids: impact on cell architecture, signaling, and metabolism genes.', *American journal of physiology. Gastrointestinal and liver physiology*, 295(5), pp. G942-52. doi: 10.1152/ajpgi.90237.2008.

Beaulieu, J. F. and Quaroni, A. (1991) 'Clonal analysis of sucrase-isomaltase expression in the human colon adenocarcinoma Caco-2 cells.', *The Biochemical journal*, 280 (Pt 3), pp. 599–608.

Begg, D. P. *et al.* (2014) 'Effect of guanylate cyclase-C activity on energy and glucose homeostasis', *Diabetes*, 63(11), pp. 3798–3804. doi: 10.2337/db14-0160.

Bertram, J. S. (2000) 'The molecular biology of cancer', *Molecular Aspects of Medicine*. Pergamon, 21(6), pp. 167–223. doi: 10.1016/S0098-2997(00)00007-8.

den Besten, G. *et al.* (2013) 'The role of short-chain fatty acids in the interplay between diet, gut microbiota, and host energy metabolism', *Journal of Lipid Research*, 54(9), pp. 2325–2340. doi: 10.1194/jlr.R036012.

Bevins, C. L. and Salzman, N. H. (2011) 'Paneth cells, antimicrobial peptides and maintenance of intestinal homeostasis', *Nature Reviews Microbiology*. Nature Publishing Group, 9(5), pp. 356–368. doi: 10.1038/nrmicro2546.

Bezençon, C. *et al.* (2008) 'Murine intestinal cells expressing Trpm5 are mostly brush cells and express markers of neuronal and inflammatory cells.', *The Journal of comparative neurology*, 509(5), pp. 514–25. doi: 10.1002/cne.21768.

Bezencon, C., le Coutre, J. and Damak, S. (2007) 'Taste-Signaling Proteins Are Coexpressed in Solitary Intestinal Epithelial Cells', *Chemical Senses*, 32(1), pp. 41–49. doi: 10.1093/chemse/bjl034.

Biagi, E. *et al.* (2013) 'Ageing and gut microbes: Perspectives for health maintenance and longevity', *Pharmacological Research*, 69(1), pp. 11–20. doi: 10.1016/j.phrs.2012.10.005.

Biggs, E. K. *et al.* (2018) 'Development and characterisation of a novel glucagon like peptide-1 receptor antibody', *Diabetologia*. Springer Berlin Heidelberg, 61(3), pp. 711–721. doi: 10.1007/s00125-017-4491-0.

Billing, L. J. *et al.* (2018) 'Co-storage and release of insulin-like peptide-5, glucagon-like

peptide-1 and peptideYY from murine and human colonic enteroendocrine cells', *Molecular Metabolism*, 16, pp. 65–75. doi: 10.1016/j.molmet.2018.07.011.

Biswas, K. H. *et al.* (2009) 'The Evolution of Guanylyl Cyclases as Multidomain Proteins: Conserved Features of Kinase-Cyclase Domain Fusions', *Journal of Molecular Evolution*, 68(6), pp. 587–602. doi: 10.1007/s00239-009-9242-5.

Bjerknes, M. and Cheng, H. (1981) 'The stem-cell zone of the small intestinal epithelium. I. Evidence from paneth cells in the adult mouse', *American Journal of Anatomy*, 160(1), pp. 51–63. doi: 10.1002/aja.1001600105.

Bjerknes, M. and Cheng, H. (1999) 'Clonal analysis of mouse intestinal epithelial progenitors', *Gastroenterology*. Elsevier, 116(1), pp. 7–14. doi: 10.1016/S0016-5085(99)70222-2.

Bockman, D. E. and Cooper, M. D. (1973) 'Pinocytosis by epithelium associated with lymphoid follicles in the bursa of fabricius, appendix, and Peyer's patches. An electron microscopic study', *American Journal of Anatomy*, 136(4), pp. 455–477. doi: 10.1002/aja.1001360406.

Boder, E. T., Midelfort, K. S. and Wittrup, K. D. (2000) 'Directed evolution of antibody fragments with monovalent femtomolar antigen-binding affinity', *Proceedings of the National Academy of Sciences*, 97(20), pp. 10701–10705. doi: 10.1073/pnas.170297297.

Boder, E. T. and Wittrup, K. D. (1997) 'Yeast surface display for screening combinatorial polypeptide libraries', *Nature Biotechnology*, 15(6), pp. 553–557. doi: 10.1038/nbt0697-553.

Boron, W. F. and Boulpaep, E. L. (2016) *Medical physiology*.

Bown, R. L. *et al.* (1974) 'Effects of lactulose and other laxatives on ileal and colonic pH as measured by a radiotelemetry device.', *Gut*, 15(12), pp. 999–1004.

Brandtzaeg, P. *et al.* (2008) 'Terminology: nomenclature of mucosa-associated lymphoid tissue', *Mucosal Immunology*, 1(1), pp. 31–37. doi: 10.1038/mi.2007.9.

Brenner, D. M. *et al.* (2018) 'Efficacy, safety, and tolerability of plecanatide in patients with irritable bowel syndrome with constipation: results of two phase 3 randomized clinical trials', *The American Journal of Gastroenterology*, 113(5), pp. 735–745. doi: 10.1038/s41395-018-0026-7.

Brezinschek, H. P. *et al.* (1997) 'Analysis of the human VH gene repertoire. Differential effects of selection and somatic hypermutation on human peripheral CD5(+)/IgM+ and CD5(-)/IgM+ B cells.', *The Journal of clinical investigation*. American Society for Clinical Investigation, 99(10), pp. 2488–501. doi: 10.1172/JCI119433.

Brighton, C. A. *et al.* (2015) 'Bile Acids Trigger GLP-1 Release Predominantly by Accessing Basolaterally Located G Protein–Coupled Bile Acid Receptors', *Endocrinology*, 156(11), pp. 3961–3970. doi: 10.1210/en.2015-1321.

Buchan, A. M. *et al.* (1978) 'Electronimmunocytochemical evidence for the K cell localization of gastric inhibitory polypeptide (GIP) in man.', *Histochemistry*, 56(1), pp. 37–44.

Campbell, P. T. *et al.* (2015) 'Association between Body Mass Index and Mortality for Colorectal Cancer Survivors: Overall and by Tumor Molecular Phenotype', *Cancer Epidemiology Biomarkers & Prevention*, 24(8), pp. 1229–1238. doi: 10.1158/1055-9965.EPI-

15-0094.

Carey, R. M. (1978) 'Evidence for a splanchnic sodium input monitor regulating renal sodium excretion in man. Lack of dependence upon aldosterone.', *Circulation research*, 43(1), pp. 19–23. doi: 10.1161/01.RES.43.1.19.

Caro, I. *et al.* (1995) 'Characterisation of a newly isolated Caco-2 clone (TC-7), as a model of transport processes and biotransformation of drugs', *International Journal of Pharmaceutics*. Elsevier, 116(2), pp. 147–158. doi: 10.1016/0378-5173(94)00280-I.

Carrithers, S. L. *et al.* (1999) 'Renal effects of uroguanylin and guanylin in vivo', *Brazilian Journal of Medical and Biological Research*, 32(11), pp. 1337–1344. doi: 10.1590/S0100-879X1999001100003.

Carrithers, S. L. *et al.* (2002) 'Site-specific effects of dietary salt intake on guanylin and uroguanylin mRNA expression in rat intestine', *Regulatory Peptides*, 107(1–3), pp. 87–95. doi: 10.1016/S0167-0115(02)00069-1.

Carrithers, S. L. *et al.* (2004) 'Guanylin and uroguanylin induce natriuresis in mice lacking guanylyl cyclase-C receptor', *Kidney International*, 65(1), pp. 40–53. doi: 10.1111/j.1523-1755.2004.00375.x.

Castagna, M. *et al.* (1982) 'Direct activation of calcium-activated, phospholipid-dependent protein kinase by tumor-promoting phorbol esters.', *The Journal of biological chemistry*, 257(13), pp. 7847–51.

Cetin, Y. *et al.* (1994) 'Enterochromaffin cells of the digestive system: cellular source of guanylin, a guanylate cyclase-activating peptide.', *Proceedings of the National Academy of Sciences*, 91(8), pp. 2935–2939. doi: 10.1073/pnas.91.8.2935.

Chambers, E. E. *et al.* (2014) 'Multidimensional LC-MS/MS Enables Simultaneous Quantification of Intact Human Insulin and Five Recombinant Analogs in Human Plasma', *Analytical Chemistry*, 86(1), pp. 694–702. doi: 10.1021/ac403055d.

Chao, A. C. *et al.* (1994) 'Activation of intestinal CFTR Cl- channel by heat-stable enterotoxin and guanylin via cAMP-dependent protein kinase.', *The EMBO journal*, 13(5), pp. 1065–72.

Cheng, H. (1974) 'Origin, differentiation and renewal of the four main epithelial cell types in the mouse small intestine. IV. Paneth cells.', *The American journal of anatomy*, 141(4), pp. 521–35. doi: 10.1002/aja.1001410406.

Cheng, H. (1974) 'Origin, differentiation and renewal of the four main epithelial cell types in the mouse small intestine II. Mucous cells', *American Journal of Anatomy*, 141(4), pp. 481–501. doi: 10.1002/aja.1001410404.

Cheng, H. and Leblond, C. P. (1974a) 'Origin, differentiation and renewal of the four main epithelial cell types in the mouse small intestine I. Columnar cell', *American Journal of Anatomy*, 141(4), pp. 461–479. doi: 10.1002/aja.1001410403.

Cheng, H. and Leblond, C. P. (1974b) 'Origin, differentiation and renewal of the four main epithelial cell types in the mouse small intestine V. Unitarian theory of the origin of the four epithelial cell types', *American Journal of Anatomy*, 141(4), pp. 537–561. doi: 10.1002/aja.1001410407.

Choi, S. *et al.* (2007) 'GPR93 activation by protein hydrolysate induces CCK transcription and secretion in STC-1 cells', *American Journal of Physiology-Gastrointestinal and Liver Physiology*, 292(5), pp. G1366–G1375. doi: 10.1152/ajpgi.00516.2006.

Chowdhury, F., Williams, A. and Johnson, P. (2008) 'Validation and comparison of two multiplex technologies, Luminex ® and Mesoscale Discovery, for human cytokine profiling'. doi: 10.1016/j.jim.2008.10.002.

Chu, S. and Montrose, M. H. (1995) 'Extracellular pH regulation in microdomains of colonic crypts: effects of short-chain fatty acids.', *Proceedings of the National Academy of Sciences of the United States of America*, 92(8), pp. 3303–7.

Clackson, T. and Lowman, H. B. (2004) *Phage display : a practical approach*. Oxford University Press.

Clark, L. A. *et al.* (2006) 'Affinity enhancement of an in vivo matured therapeutic antibody using structure-based computational design', *Protein Science*, 15(5), pp. 949–960. doi: 10.1110/ps.052030506.

Clarke, L. L. (2009) 'A guide to Ussing chamber studies of mouse intestine.', *American journal of physiology. Gastrointestinal and liver physiology*. American Physiological Society, 296(6), pp. G1151-66. doi: 10.1152/ajpgi.90649.2008.

Clevers, H. (2013) 'The intestinal crypt, a prototype stem cell compartment', *Cell*. Elsevier Inc., 154(2), pp. 274–284. doi: 10.1016/j.cell.2013.07.004.

Clevers, H. C. and Bevins, C. L. (2013) 'Paneth Cells: Maestros of the Small Intestinal Crypts', *Annual Review of Physiology*. Annual Reviews , 75(1), pp. 289–311. doi: 10.1146/annurev-physiol-030212-183744.

Cockerham, R. E. *et al.* (2009) 'Functional Analysis of the Guanylyl Cyclase Type D Signaling System in the Olfactory Epithelium', *Annals of the New York Academy of Sciences*, 1170(1), pp. 173–176. doi: 10.1111/j.1749-6632.2009.04104.x.

Cohen, M. B. *et al.* (1988) *Age-related differences in receptors for Escherichia coli heat-stable enterotoxin in the small and large intestine of children*, *Gastroenterology*. doi: S0016508588000411 [pii].

Cohen, M. B. *et al.* (1995) *Immunohistochemical localization of guanylin in the rat small intestine and colon*, *Biochem Biophys Res Commun*. doi: S0006-291X(85)71571-9 [pii]\r10.1006/bbrc.1995.1571 [doi].

Cohen, M. B., Hawkins, J. A. and Witte, D. P. (1998) 'Guanylin mRNA expression in human intestine and colorectal adenocarcinoma.', *Laboratory investigation; a journal of technical methods and pathology*, 78(1), pp. 101–8.

Collins, D. *et al.* (2009) 'Cyclic AMP-mediated chloride secretion is induced by prostaglandin F2alpha in human isolated colon.', *British journal of pharmacology*. Wiley-Blackwell, 158(7), pp. 1771–6. doi: 10.1111/j.1476-5381.2009.00464.x.

Corsetti, M. and Tack, J. (2013) 'Linaclotide: A new drug for the treatment of chronic constipation and irritable bowel syndrome with constipation.', *United European gastroenterology journal*. SAGE Publications, 1(1), pp. 7–20. doi:

10.1177/2050640612474446.

Costantino, N. and Court, D. L. (2003) 'Enhanced levels of Red-mediated recombinants in mismatch repair mutants', *Proceedings of the National Academy of Sciences*, 100(26), pp. 15748–15753. doi: 10.1073/pnas.2434959100.

Cox, J. M. *et al.* (2016) 'Characterization and quantification of oxyntomodulin in human and rat plasma using high-resolution accurate mass LC–MS', *Bioanalysis*, 8(15), pp. 1579–1595. doi: 10.4155/bio-2016-0012.

Crosnier, C., Stamataki, D. and Lewis, J. (2006) 'Organizing cell renewal in the intestine: stem cells, signals and combinatorial control', *Nature Reviews Genetics*. Nature Publishing Group, 7(5), pp. 349–359. doi: 10.1038/nrg1840.

Cull, M. G. and Schatz, P. J. (2000) '[26] Biotinylation of proteins in vivo and in vitro using small peptide tags', *Applications of Chimeric Genes and Hybrid Proteins Part A: Gene Expression and Protein Purification*, Volume 326(1996), pp. 430–440. doi: http://dx.doi.org/10.1016/S0076-6879(00)26068-0.

Cunliffe, R. N. *et al.* (2001) 'Human defensin 5 is stored in precursor form in normal Paneth cells and is expressed by some villous epithelial cells and by metaplastic Paneth cells in the colon in inflammatory bowel disease.', *Gut*, 48(2), pp. 176–85.

Currie, M. G. *et al.* (1992) 'Guanylin: an endogenous activator of intestinal guanylate cyclase', *Proc Natl Acad Sci U S A*, 89(3), pp. 947–951. doi: 10.1073/pnas.89.3.947.

Currie, M. G. *et al.* (1992) *Guanylin: An endogenous activator of intestinal guanylate cyclase (intestine/cyclic GMP/heat-stable enterotoxin/diarrhea/peptide)*, *Pharmacology*.

Cuthbert, A. W. *et al.* (1994) 'Chloride secretion in response to guanylin in colonic epithelial from normal and transgenic cystic fibrosis mice.', *British journal of pharmacology*, 112(1), pp. 31–6.

Dabitao, D. *et al.* (2011) 'Multiplex measurement of proinflammatory cytokines in human serum: comparison of the Meso Scale Discovery electrochemiluminescence assay and the Cytometric Bead Array.', *Journal of immunological methods*. NIH Public Access, 372(1–2), pp. 71–7. doi: 10.1016/j.jim.2011.06.033.

Daniel, H. *et al.* (1985) 'Localization of acid microclimate along intestinal villi of rat jejunum.', *The American journal of physiology*, 248(3 Pt 1), pp. G293-8. doi: 10.1152/ajpgi.1985.248.3.G293.

Deneke, C. F. *et al.* (1983) *Attachment of Enterotoxigenic Escherichia coli to Human Intestinal Cells*, *Infection and immunity*.

Dobin, A. *et al.* (2013) 'STAR: ultrafast universal RNA-seq aligner', *Bioinformatics*, 29(1), pp. 15–21. doi: 10.1093/bioinformatics/bts635.

Dockray, G., Dimaline, R. and Varro, A. (2005) 'Gastrin: old hormone, new functions', *Pfl*[illegible]*gers Archiv - European Journal of Physiology*, 449(4), pp. 344–355. doi: 10.1007/s00424-004-1347-5.

Drucker, D. J. and Yusta, B. (2014) 'Physiology and Pharmacology of the Enteroendocrine

Hormone Glucagon-Like Peptide-2', *Annual Review of Physiology*, 76(1), pp. 561–583. doi: 10.1146/annurev-physiol-021113-170317.

Duda, T. and Sharma, R. K. (2009) 'Ca2+ -modulated ONE-GC odorant signal transduction', *FEBS Letters*, 583(8), pp. 1327–1330. doi: 10.1016/j.febslet.2009.03.036.

Dümmler, A., Lawrence, A.-M. and de Marco, A. (2005) 'Simplified screening for the detection of soluble fusion constructs expressed in E. coli using a modular set of vectors', *Microbial Cell Factories*. BioMed Central, 4(1), p. 34. doi: 10.1186/1475-2859-4-34.

Edfors, F. *et al.* (2016) 'Gene-specific correlation of RNA and protein levels in human cells and tissues.', *Molecular systems biology*. EMBO Press, 12(10), p. 883. doi: 10.15252/MSB.20167144.

Eggermont, E. (1996) 'Gastrointestinal manifestations in cystic fibrosis.', *European journal of gastroenterology & hepatology*, 8(8), pp. 731–8.

El-Serag, H. B., Olden, K. and Bjorkman, D. (2002) 'Health-related quality of life among persons with irritable bowel syndrome: a systematic review.', *Alimentary pharmacology & therapeutics*, 16(6), pp. 1171–85.

Elitsur, N. *et al.* (2006) 'The proximal convoluted tubule is a target for the uroguanylin-regulated natriuretic response.', *Journal of pediatric gastroenterology and nutrition*. Lippincott Williams & Wilkins, 43 Suppl 1(July), pp. S74-81. doi: 10.1097/01.mpg.0000228092.36089.7c.

Ellis, H. M. *et al.* (2001) 'High efficiency mutagenesis, repair, and engineering of chromosomal DNA using single-stranded oligonucleotides', *Proceedings of the National Academy of Sciences*, 98(12), pp. 6742–6746. doi: 10.1073/pnas.121164898.

Engelstoft, M. S. *et al.* (2008) 'A gut feeling for obesity: 7TM sensors on enteroendocrine cells.', *Cell metabolism*, 8(6), pp. 447–9. doi: 10.1016/j.cmet.2008.11.004.

Engle, M. J., Goetz, G. S. and Alpers, D. H. (1998) 'Caco-2 cells express a combination of colonocyte and enterocyte phenotypes', *Journal of Cellular Physiology*, 174(3), pp. 362–369. doi: 10.1002/(SICI)1097-4652(199803)174:3<362::AID-JCP10>3.0.CO;2-B.

Fahlgren, A. *et al.* (2003) 'Increased expression of antimicrobial peptides and lysozyme in colonic epithelial cells of patients with ulcerative colitis.', *Clinical and experimental immunology*. Wiley-Blackwell, 131(1), pp. 90–101. doi: 10.1046/J.1365-2249.2003.02035.X.

Fakhoury, K. *et al.* (1992) 'Meconium ileus in the absence of cystic fibrosis.', *Archives of disease in childhood*, 67(10 Spec No), pp. 1204–6.

Fan, X. *et al.* (1997) 'Signaling Pathways for Guanylin and Uroguanylin in the Digestive, Renal, Central Nervous, Reproductive, and Lymphoid Systems'.

Fernandez-Cachon, M. L. *et al.* (2018) 'Guanylin and uroguanylin mRNA expression is increased following Roux-en-Y gastric bypass, but guanylins do not play a significant role in body weight regulation and glycemic control', *Peptides*, 101(October 2017), pp. 32–43. doi: 10.1016/j.peptides.2017.12.024.

Field, B. C. T., Chaudhri, O. B. and Bloom, S. R. (2010) 'Bowels control brain: gut hormones and

obesity', *Nature Reviews Endocrinology*, 6(8), pp. 444–453. doi: 10.1038/nrendo.2010.93.

Field, M. *et al.* (1978) 'Heat-stable enterotoxin of Escherichia coli: in vitro effects on guanylate cyclase activity, cyclic GMP concentration, and ion transport in small intestine.', *Proceedings of the National Academy of Sciences of the United States of America*, 75(6), pp. 2800–4. doi: 10.1073/pnas.75.6.2800.

Fiskerstrand, T. *et al.* (2012) 'Familial Diarrhea Syndrome Caused by an Activating *GUCY2C* Mutation', *New England Journal of Medicine*, 366(17), pp. 1586–1595. doi: 10.1056/NEJMoa1110132.

van der Flier, L. G. and Clevers, H. (2009) 'Stem Cells, Self-Renewal, and Differentiation in the Intestinal Epithelium', *Annual Review of Physiology*, 71(1), pp. 241–260. doi: 10.1146/annurev.physiol.010908.163145.

Fodde, R. and Smits, R. (2001) 'Disease model: familial adenomatous polyposis.', *Trends in molecular medicine*, 7(8), pp. 369–73.

Fogh, J., Wright, W. C. and Loveless, J. D. (1977) 'Absence of HeLa cell contamination in 169 cell lines derived from human tumors.', *Journal of the National Cancer Institute*, 58(2), pp. 209–14.

Folgueira, C. *et al.* (2016) 'Uroguanylin action in the brain reduces weight gain in obese mice via different efferent autonomic pathways', *Diabetes*. doi: 10.2337/db15-0889.

Folgueira, C. *et al.* (2016) 'Uroguanylin levels in intestine and plasma are regulated by nutritional status in a leptin-dependent manner', *European Journal of Nutrition*, 55(2), pp. 529–536. doi: 10.1007/s00394-015-0869-2.

Forte, L. R. *et al.* (1992) 'Stimulation of intestinal Cl- transport by heat-stable enterotoxin: activation of cAMP-dependent protein kinase by cGMP', *American Journal of Physiology-Cell Physiology*, 263(3), pp. C607–C615. doi: 10.1152/ajpcell.1992.263.3.C607.

Forte, L. R. *et al.* (1993) 'Guanylin stimulation of Cl- secretion in human intestinal T84 cells via cyclic guanosine monophosphate.', *Journal of Clinical Investigation*, 91(6), pp. 2423–2428. doi: 10.1172/JCI116476.

Forte, L. R. (1999) 'Guanylin regulatory peptides: Structures, biological activities mediated by cyclic GMP and pathobiology', *Regulatory Peptides*, 81(1–3), pp. 25–39. doi: 10.1016/S0167-0115(99)00033-6.

Forte, L. R. *et al.* (1999) 'Lymphoguanylin: Cloning and characterization of a unique member of the guanylin peptide family', *Endocrinology*, 140(4), pp. 1800–1806. doi: 10.1210/en.140.4.1800.

Forte, L. R. (2004a) 'Uroguanylin and guanylin peptides: pharmacology and experimental therapeutics', *Pharmacology & Therapeutics*. Pergamon, 104(2), pp. 137–162. doi: 10.1016/J.PHARMTHERA.2004.08.007.

Forte, L. R. (2004b) 'Uroguanylin and guanylin peptides: Pharmacology and experimental therapeutics', *Pharmacology and Therapeutics*, 104(2), pp. 137–162. doi: 10.1016/j.pharmthera.2004.08.007.

Forte, L. R., Fan, X. and Hamra, F. K. (1996) 'Salt and water homeostasis: Uroguanylin is a circulating peptide hormone with natriuretic activity', *American Journal of Kidney Diseases*, 28(2), pp. 296–304. doi: 10.1016/S0272-6386(96)90318-2.

Fothergill, L. J. *et al.* (2017) 'Costorage of Enteroendocrine Hormones Evaluated at the Cell and Subcellular Levels in Male Mice', *Endocrinology*, 158(7), pp. 2113–2123. doi: 10.1210/en.2017-00243.

French, P. J. *et al.* (1995) 'Isotype-specific activation of cystic fibrosis transmembrane conductance regulator-chloride channels by cGMP-dependent protein kinase II.', *The Journal of biological chemistry*, 270(44), pp. 26626–31.

Frenzel, A., Schirrmann, T. and Hust, M. (2016) 'Phage display-derived human antibodies in clinical development and therapy', *mAbs*, 8(7), pp. 1177–1194. doi: 10.1080/19420862.2016.1212149.

Frey, A. *et al.* (1996) 'Role of the glycocalyx in regulating access of microparticles to apical plasma membranes of intestinal epithelial cells: implications for microbial attachment and oral vaccine targeting.', *The Journal of experimental medicine*, 184(3), pp. 1045–59.

Fujii, M. *et al.* (2015) 'Efficient genetic engineering of human intestinal organoids using electroporation', *Nature Protocols*. Nature Publishing Group, 10(10), pp. 1474–1485. doi: 10.1038/nprot.2015.088.

Fujimoto, S. *et al.* (2000) *Letter to the Editor Immunohistochemical Localization of Uroguanylin in the Human Kidney*, *Nephron*.

Fukae, H. *et al.* (2002) 'Changes in urinary levels and renal expression of uroguanylin on low or high salt diets in rats.', *Nephron*, 92(2), pp. 373–8. doi: 63311.

Furness, J. . (2000) 'Types of neurons in the enteric nervous system', *Journal of the Autonomic Nervous System*. Elsevier, 81(1–3), pp. 87–96. doi: 10.1016/S0165-1838(00)00127-2.

Gai, S. A. and Wittrup, K. D. (2007) 'Yeast surface display for protein engineering and characterization', *Current Opinion in Structural Biology*, 17(4), pp. 467–473. doi: 10.1016/j.sbi.2007.08.012.

Garabedian, E. M. *et al.* (1997) 'Examining the role of Paneth cells in the small intestine by lineage ablation in transgenic mice.', *The Journal of biological chemistry*. American Society for Biochemistry and Molecular Biology, 272(38), pp. 23729–40. doi: 10.1074/JBC.272.38.23729.

Garet, E. *et al.* (2010) 'Rapid isolation of single-chain antibodies by phage display technology directed against one of the most potent marine toxins: Palytoxin.', *Toxicon : official journal of the International Society on Toxinology*, 55(8), pp. 1519–26. doi: 10.1016/j.toxicon.2010.03.005.

Gerbe, F. *et al.* (2011) 'Distinct ATOH1 and Neurog3 requirements define tuft cells as a new secretory cell type in the intestinal epithelium.', *The Journal of cell biology*. Rockefeller University Press, 192(5), pp. 767–80. doi: 10.1083/jcb.201010127.

Gerbe, F. *et al.* (2016) 'Intestinal epithelial tuft cells initiate type 2 mucosal immunity to helminth parasites', *Nature*, 529(7585), pp. 226–230. doi: 10.1038/nature16527.

Gerbe, F., Legraverend, C. and Jay, P. (2012) 'The intestinal epithelium tuft cells: Specification and function', *Cellular and Molecular Life Sciences*, 69(17), pp. 2907–2917. doi: 10.1007/s00018-012-0984-7.

Gerritsen, J. *et al.* (2011) 'Intestinal microbiota in human health and disease: the impact of probiotics', *Genes & Nutrition*, 6(3), pp. 209–240. doi: 10.1007/s12263-011-0229-7.

Gibbons, A. V *et al.* (2013) 'Intestinal GUCY2C prevents TGF-β secretion coordinating desmoplasia and hyperproliferation in colorectal cancer.', *Cancer research*, 73(22), pp. 6654–66. doi: 10.1158/0008-5472.CAN-13-0887.

Gill, S. R. *et al.* (2006) 'Metagenomic Analysis of the Human Distal Gut Microbiome', *Science*, 312(5778), pp. 1355–1359. doi: 10.1126/science.1124234.

Glebov, O. K. *et al.* (2006) 'Gene expression patterns distinguish colonoscopically isolated human aberrant crypt foci from normal colonic mucosa', *Cancer Epidemiology Biomarkers and Prevention*, 15(11), pp. 2253–2262. doi: 10.1158/1055-9965.EPI-05-0694.

Goldspink, D. A. *et al.* (2017) 'Immuno-fluorescent Labeling of Microtubules and Centrosomal Proteins in Ex Vivo Intestinal Tissue and 3D In Vitro Intestinal Organoids', *J. Vis. Exp*, (130), p. 56662. doi: 10.3791/56662.

Goldspink, D. A. *et al.* (2018a) 'Mechanistic insights into the detection of free fatty and bile acids by ileal glucagon-like peptide-1 secreting cells', *Molecular Metabolism*, 7, pp. 90–101. doi: 10.1016/j.molmet.2017.11.005.

Goldspink, D. A. *et al.* (2018b) 'Mechanistic insights into the detection of free fatty and bile acids by ileal glucagon-like peptide-1 secreting cells', *Molecular Metabolism*. Elsevier, 7, pp. 90–101. doi: 10.1016/J.MOLMET.2017.11.005.

Gong, R. *et al.* (2011) 'Role for the Membrane Receptor Guanylyl Cyclase-C in Attention Deficiency and Hyperactive Behavior', *Science*, 333(6049), pp. 1642–1646. doi: 10.1126/science.1207675.

Gong, S. *et al.* (2003) 'A gene expression atlas of the central nervous system based on bacterial artificial chromosomes', *Nature*. Nature Publishing Group, 425(6961), pp. 917–925. doi: 10.1038/nature02033.

Gowan, S. M. *et al.* (2007) 'Application of Meso Scale Technology for the Measurement of Phosphoproteins in Human Tumor Xenografts', *ASSAY and Drug Development Technologies*, 5(3). doi: 10.1089/adt.2006.044.

Gowda, S. *et al.* (2010) 'Markers of renal function tests.', *North American journal of medical sciences*. Wolters Kluwer -- Medknow Publications, 2(4), pp. 170–3.

Gribble, F. M. and Reimann, F. (2016) 'Enteroendocrine Cells: Chemosensors in the Intestinal Epithelium', *Annual Review of Physiology*, 78(1), pp. 277–299. doi: 10.1146/annurev-physiol-021115-105439.

Grosse, J. *et al.* (2014) 'Insulin-like peptide 5 is an orexigenic gastrointestinal hormone.', *Proceedings of the National Academy of Sciences of the United States of America*, 111(30), pp. 11133–8. doi: 10.1073/pnas.1411413111.

Groves, M. A. and Nickson, A. A. (2012) 'Affinity Maturation of Phage Display Antibody Populations Using Ribosome Display', in. Springer, New York, NY, pp. 163–190. doi: 10.1007/978-1-61779-379-0_10.

Groves, M. A. and Osbourn, J. K. (2005) 'Applications of ribosome display to antibody drug discovery', *Expert Opinion on Biological Therapy*, 5(1), pp. 125–135. doi: 10.1517/14712598.5.1.125.

Guba, M. *et al.* (1996) 'Guanylin strongly stimulates rat duodenal HCO3- secretion: Proposed mechanism and comparison with other secretagogues', *Gastroenterology*. W.B. Saunders, 111(6), pp. 1558–1568. doi: 10.1016/S0016-5085(96)70018-5.

Di Guglielmo, M. D., Perdue, L., *et al.* (2018) 'Immunohistochemical Staining for Uroguanylin, a Satiety Hormone, is Decreased in Intestinal Tissue Specimens From Female Adolescents With Obesity', *Pediatric and Developmental Pathology*, 21(3), pp. 285–295. doi: 10.1177/1093526617722912.

Di Guglielmo, M. D., Tonb, D., *et al.* (2018) 'Pilot Study Measuring the Novel Satiety Hormone, Pro-Uroguanylin, in Adolescents with and Without Obesity', *Journal of Pediatric Gastroenterology and Nutrition*, 66(3), pp. 489–495. doi: 10.1097/MPG.0000000000001796.

Guyton, A. and Hall, J. (2016) *Medical Physiology, 13th Edition*.

Habib, A. M. *et al.* (2012) 'Overlap of Endocrine Hormone Expression in the Mouse Intestine Revealed by Transcriptional Profiling and Flow Cytometry', *Endocrinology*, 153(7), pp. 3054–3065. doi: 10.1210/en.2011-2170.

Habib, A. M. *et al.* (2013) 'Co-localisation and secretion of glucagon-like peptide 1 and peptide YY from primary cultured human L cells', *Diabetologia*. Springer-Verlag, 56(6), pp. 1413–1416. doi: 10.1007/s00125-013-2887-z.

Hamra, F. K. *et al.* (1993) 'Uroguanylin: structure and activity of a second endogenous peptide that stimulates intestinal guanylate cyclase.', *Proceedings of the National Academy of Sciences of the United States of America*, 90(22), pp. 10464–8. doi: 10.1073/pnas.90.22.10464.

Hamra, F. K. *et al.* (1996) *Prouroguanylin and proguanylin: purification from colon, structure, and modulation of bioactivity by proteases.*

Hamra, K. F. *et al.* (1997) *Regulation of intestinal uroguanylinguanylin receptor-mediated responses by mucosal acidity*.

Hanahan, D. and Weinberg, R. A. (2000) *The Hallmarks of Cancer Review evolve progressively from normalcy via a series of pre*, *Cell*.

Hanahan, D. and Weinberg, R. A. (2011) 'Hallmarks of cancer: The next generation', *Cell*. Elsevier Inc., 144(5), pp. 646–674. doi: 10.1016/j.cell.2011.02.013.

Hanes, J. *et al.* (2000) 'Picomolar affinity antibodies from a fully synthetic naive library selected and evolved by ribosome display', *Nature Biotechnology*. Nature Publishing Group, 18(12), pp. 1287–1292. doi: 10.1038/82407.

Hapfelmeier, S. *et al.* (2010) 'Reversible Microbial Colonization of Germ-Free Mice Reveals the Dynamics of IgA Immune Responses', *Science*, 328(5986), pp. 1705–1709. doi:

10.1126/science.1188454.

Haruyama, N., Cho, A. and Kulkarni, A. B. (2009) 'Overview: Engineering Transgenic Constructs and Mice', *Current Protocols in Cell Biology*, 42(1), p. 19.10.1-19.10.9. doi: 10.1002/0471143030.cb1910s42.

Hase, K. *et al.* (2009) 'Uptake through glycoprotein 2 of FimH(+) bacteria by M cells initiates mucosal immune response.', *Nature*, 462(7270), pp. 226–30. doi: 10.1038/nature08529.

Hass, N., Schwarzenbacher, K. and Breer, H. (2010) 'T1R3 is expressed in brush cells and ghrelin-producing cells of murine stomach', *Cell and Tissue Research*, 339(3), pp. 493–504. doi: 10.1007/s00441-009-0907-6.

Heath, J. (1996) 'Epithelial cell migration in the intestine', *Cell Biology International*, 20(2), pp. 139–146. doi: 10.1006/cbir.1996.0018.

Heidelbaugh, J. J. *et al.* (2015) 'The Spectrum of Constipation-Predominant Irritable Bowel Syndrome and Chronic Idiopathic Constipation: US Survey Assessing Symptoms, Care Seeking and Disease Burden', *The American Journal of Gastroenterology*, 110(4), pp. 580–587. doi: 10.1038/ajg.2015.67.

Herbert, D. R. *et al.* (2009) 'Intestinal epithelial cell secretion of RELM-β protects against gastrointestinal worm infection', *The Journal of Experimental Medicine*, 206(13), pp. 2947–2957. doi: 10.1084/jem.20091268.

Hess, R. *et al.* (1995) 'GCAP-II: Isolation and characterization of the circulating form of human uroguanylin', *FEBS Letters*, 374(1), pp. 34–38. doi: 10.1016/0014-5793(95)01075-P.

Hill, O. *et al.* (1995) *Analysis of the human guanylin gene and the processing and cellular localization of the peptide (gut hormone/guanylyl cyclase C/regulatory peptide/enterochromaffin cells/diarrhea)*, *Biochemistry*.

Hooper, L. V *et al.* (1999) 'A molecular sensor that allows a gut commensal to control its nutrient foundation in a competitive ecosystem.', *Proceedings of the National Academy of Sciences of the United States of America*. National Academy of Sciences, 96(17), pp. 9833–8.

Hoos, A. *et al.* (2001) 'High Ki-67 proliferative index predicts disease specific survival in patients with high-risk soft tissue sarcomas.', *Cancer*, 92(4), pp. 869–74.

Howitt, M. R. *et al.* (2016) 'Tuft cells, taste-chemosensory cells, orchestrate parasite type 2 immunity in the gut', *Science*, 351(6279), pp. 1329–1333. doi: 10.1126/science.aaf1648.

Hughes, J. M. *et al.* (1978) 'Role of cyclic GMP in the action of heat-stable enterotoxin of Escherichia coli.', *Nature*, 271(5647), pp. 755–6.

Husvéth, F. (2011) *Physiological and reproductional aspects of animal production*.

Ikpa, P. T. *et al.* (2016) 'Guanylin and uroguanylin are produced by mouse intestinal epithelial cells of columnar and secretory lineage', *Histochemistry and Cell Biology*. Springer Berlin Heidelberg, 146(4), pp. 445–455. doi: 10.1007/s00418-016-1453-4.

Institute, C. and L. S. (2010) *Defining, Establishing, and Verifying Reference Intervals in the Clinical Laboratory; Approved Guideline-Third Edition*.

Jacobsen, S. H. *et al.* (2012) 'Changes in Gastrointestinal Hormone Responses, Insulin Sensitivity, and Beta-Cell Function Within 2 Weeks After Gastric Bypass in Non-diabetic Subjects', *Obesity Surgery*, 22(7), pp. 1084–1096. doi: 10.1007/s11695-012-0621-4.

Jaleel, M. *et al.* (2002) 'Expression of the receptor guanylyl cyclase C and its ligands in reproductive tissues of the rat: a potential role for a novel signaling pathway in the epididymis.', *Biology of reproduction*, 67(6), pp. 1975–80.

Jarmuz, A. *et al.* (2015) 'Emerging treatments in Neurogastroenterology: Perspectives of guanylyl cyclase C agonists use in functional gastrointestinal disorders and inflammatory bowel diseases', *Neurogastroenterology and Motility*, 27(8), pp. 1057–1068. doi: 10.1111/nmo.12574.

Johansson, M. E. V. and Hansson, G. C. (2014) 'Is the Intestinal Goblet Cell a Major Immune Cell?', *Cell Host & Microbe*, 15(3), pp. 251–252. doi: 10.1016/j.chom.2014.02.014.

Johansson, M. E. V., Thomsson, K. A. and Hansson, G. C. (2009) 'Proteomic Analyses of the Two Mucus Layers of the Colon Barrier Reveal That Their Main Component, the Muc2 Mucin, Is Strongly Bound to the Fcgbp Protein', *Journal of Proteome Research*, 8(7), pp. 3549–3557. doi: 10.1021/pr9002504.

de Jonge, H. R. (1975) 'Properties of guanylate cyclase and levels of cyclic GMP in rat small intestinal villous and crypt cells', *FEBS Letters*. Wiley-Blackwell, 55(1–2), pp. 143–152. doi: 10.1016/0014-5793(75)80980-X.

Jorgensen, W. L. (2004) 'The many roles of computation in drug discovery.', *Science (New York, N.Y.)*. American Association for the Advancement of Science, 303(5665), pp. 1813–8. doi: 10.1126/science.1096361.

Jung, P. *et al.* (2011) 'Isolation and in vitro expansion of human colonic stem cells', *Nature Medicine*. Nature Publishing Group, 17(10), pp. 1225–1227. doi: 10.1038/nm.2470.

Kalinin, N. L., Ward, L. D. and Winzor, D. J. (1995) 'Effects of solute multivalence on the evaluation of binding constants by biosensor technology: studies with concanavalin A and interleukin-6 as partitioning proteins.', *Analytical biochemistry*, 228(2), pp. 238–44. doi: 10.1006/abio.1995.1345.

Kanaya, T. *et al.* (2012) 'The Ets transcription factor Spi-B is essential for the differentiation of intestinal microfold cells.', *Nature immunology*. NIH Public Access, 13(8), pp. 729–36. doi: 10.1038/ni.2352.

Kang, A. S., Jones, T. M. and Burton, D. R. (1991) *Antibody redesign by chain shuffling from random combinatorial immunoglobulin libraries (combinatorial Immunogobuln repertore/catalytlc antibodies)*, *Proc. Nati. Acad. Sci. USA*.

Karam, S. M. (1999) 'Lineage commitment and maturation of epithelial cells in the gut.', *Frontiers in bioscience : a journal and virtual library*, 4, pp. D286-98.

Karlsson, N. G. *et al.* (1996) 'Molecular characterization of the large heavily glycosylated domain glycopeptide from the rat small intestinal Muc2 mucin.', *Glycoconjugate journal*, 13(5), pp. 823–31.

Katz, J. P. *et al.* (2002) 'The zinc-finger transcription factor Klf4 is required for terminal

differentiation of goblet cells in the colon.', *Development (Cambridge, England)*, 129(11), pp. 2619–28.

Kaun, K. R. *et al.* (2007) 'Natural variation in food acquisition mediated via a Drosophila cGMP-dependent protein kinase.', *The Journal of experimental biology*, 210(Pt 20), pp. 3547–58. doi: 10.1242/jeb.006924.

Kay, R. G. *et al.* (2017) 'Liquid chromatography/mass spectrometry based detection and semi-quantitative analysis of INSL5 in human and murine tissues.', *Rapid communications in mass spectrometry : RCM*. Wiley-Blackwell, 31(23), pp. 1963–1973. doi: 10.1002/rcm.7978.

Kebarle, P. (2000) 'A brief overview of the present status of the mechanisms involved in electrospray mass spectrometry', *Journal of Mass Spectrometry*, 35(7), pp. 804–817. doi: 10.1002/1096-9888(200007)35:7<804::AID-JMS22>3.0.CO;2-Q.

Kim, G. W. *et al.* (2016) 'Calorie-induced ER stress suppresses uroguanylin satiety signaling in diet-induced obesity', *Nutrition & Diabetes*, 6(5), p. e211. doi: 10.1038/nutd.2016.18.

Kim, Y. S. and Ho, S. B. (2010) 'Intestinal Goblet Cells and Mucins in Health and Disease: Recent Insights and Progress', *Current Gastroenterology Reports*, 12(5), pp. 319–330. doi: 10.1007/s11894-010-0131-2.

Kinoshita, H., Nakazato, M., *et al.* (1997) *Increased plasma guanylin levels in patients with impaired renal function*, *Clin Nephrol*.

Kinoshita, H., Fujimoto, S., *et al.* (1997) 'Urine and plasma levels of uroguanylin and its molecular forms in renal diseases.', *Kidney international*, 52(4), pp. 1028–34. doi: 10.1038/ki.1997.424.

Kinoshita, H. *et al.* (1999) 'Plasma and urine levels of uroguanylin, a new natriuretic peptide, in nephrotic syndrome', *Nephron*, 81(2), pp. 160–164. doi: 10.1159/000045272.

Kita, T. *et al.* (1994) 'Characterization of human uroguanylin: a member of the guanylin peptide family.', *The American journal of physiology*, 266(2 Pt 2), pp. F342-8. Available at: http://www.ncbi.nlm.nih.gov/pubmed/8141334.

Kita, T. *et al.* (1999) 'Marked increase of guanylin secretion in response to salt loading in the rat small intestine', *Am J Physiol*, 277(5 Pt 1), pp. G960-6.

Klaenhammer, T. R. (1993) 'Genetics of bacteriocins produced by lactic acid bacteria.', *FEMS microbiology reviews*, 12(1–3), pp. 39–85.

Köhler, G. and Milstein, C. (1975) 'Continuous cultures of fused cells secreting antibody of predefined specificity', *Nature*. Nature Publishing Group, 256(5517), pp. 495–497. doi: 10.1038/256495a0.

Kokrashvili, Z. *et al.* (2009) 'Release of Endogenous Opioids From Duodenal Enteroendocrine Cells Requires Trpm5'. doi: 10.1053/j.gastro.2009.02.070.

Koloski, N. A., Talley, N. J. and Boyce, P. M. (2000) 'The impact of functional gastrointestinal disorders on quality of life', *The American Journal of Gastroenterology*. Nature Publishing Group, 95(1), pp. 67–71. doi: 10.1111/j.1572-0241.2000.01735.x.

Korzeniewski, C. and Callewaert, D. M. (1983) 'An enzyme-release assay for natural

cytotoxicity.', *Journal of immunological methods*, 64(3), pp. 313–20.

Kozuka, K. *et al.* (2017) 'Development and Characterization of a Human and Mouse Intestinal Epithelial Cell Monolayer Platform.', *Stem cell reports*. Elsevier, 9(6), pp. 1976–1990. doi: 10.1016/j.stemcr.2017.10.013.

Krause', W. J. *et al.* (1994) 'Distribution of heat-stable enterotoxin/guanylin receptors in the intestinal tract of man and other mammals', *J Anat*, 184 (Pt 2, pp. 407–417.

Kuhn, M. *et al.* (1993) 'The circulating bioactive form of human guanylin is a high molecular weight peptide (10.3 kDa).', *FEBS letters*, 318(2), pp. 205–9.

Kuhn, M. *et al.* (1994) 'Radioimmunoassay for circulating human guanylin.', *FEBS letters*, 341(2–3), pp. 218–22.

Kuhn, M. *et al.* (1995) 'Circulating and tissue guanylin immunoreactivity in intestinal secretory diarrhoea', *European Journal of Clinical Investigation*, 25(12), pp. 899–905. doi: 10.1111/j.1365-2362.1995.tb01964.x.

Kulaksiz, H., Rausch, U., *et al.* (2001) 'Guanylin and uroguanylin in the parotid and submandibular glands: potential intrinsic regulators of electrolyte secretion in salivary glands.', *Histochemistry and cell biology*, 115(6), pp. 527–33.

Kulaksiz, H., Schmid, A., *et al.* (2001) 'Guanylin in the human pancreas: a novel luminocrine regulatory pathway of electrolyte secretion via cGMP and CFTR in the ductal system.', *Histochemistry and cell biology*, 115(2), pp. 131–45.

Kulaksiz, H. *et al.* (2004) 'Guanylin regulates chloride secretion in the human gallbladder via the bile fluid', *Gastroenterology*. W.B. Saunders, 126(3), pp. 732–740. doi: 10.1053/J.GASTRO.2003.11.053.

Kunwar Shailubhai *et al.* (2000) 'Uroguanylin Treatment Suppresses Polyp Formation in the Apc Min / ⁄. Mouse and Induces Apoptosis in Human Colon Adenocarcinoma Cells via Cyclic GMP', *Cancer research*, 60, pp. 5151–5157.

Larraufie, P. *et al.* (2018) 'SCFAs strongly stimulate PYY production in human enteroendocrine cells', *Scientific Reports*, 8(1), p. 74. doi: 10.1038/s41598-017-18259-0.

Lauber, T. *et al.* (2002) 'Native and recombinant proguanylin feature identical biophysical properties and are monomeric in solution', *Biochemistry*, 41(49), pp. 14602–14612. doi: 10.1021/bi026434j.

Lauber, T. *et al.* (2003) 'Solution structure of human proguanylin: The role of a hormone prosequence', *Journal of Biological Chemistry*, 278(26), pp. 24118–24124. doi: 10.1074/jbc.M300370200.

Lee, A. S. (2005) 'The ER chaperone and signaling regulator GRP78/BiP as a monitor of endoplasmic reticulum stress', *Methods*, 35(4), pp. 373–381. doi: 10.1016/j.ymeth.2004.10.010.

Leinders-Zufall, T. *et al.* (2007) 'Contribution of the receptor guanylyl cyclase GC-D to chemosensory function in the olfactory epithelium', *Proceedings of the National Academy of Sciences*, 104(36), pp. 14507–14512. doi: 10.1073/pnas.0704965104.

Lennane, R. J. *et al.* (1975) *A comparison of natriuresis after oral and intravenous sodium loading in sodium-depleted man: evidence for a gastrointestinal or portal monitor of sodium intake.*, *Clinical science and molecular medicine*.

Li, L. T. *et al.* (2015) 'Ki67 is a promising molecular target in the diagnosis of cancer (Review)', *Molecular Medicine Reports*. Spandidos Publications, 11(3), pp. 1566–1572. doi: 10.3892/mmr.2014.2914.

Li, P., Schulz, S., *et al.* (2007) 'Guanylyl Cyclase C Suppresses Intestinal Tumorigenesis by Restricting Proliferation and Maintaining Genomic Integrity', *Gastroenterology*, 133(2), pp. 599–607. doi: 10.1053/j.gastro.2007.05.052.

Li, P., Lin, J. E., *et al.* (2007) 'Homeostatic Control of the Crypt-Villus Axis by the Bacterial Enterotoxin Receptor Guanylyl Cyclase C Restricts the Proliferating Compartment in Intestine', *The American Journal of Pathology*. Elsevier, 171(6), pp. 1847–1858. doi: 10.2353/AJPATH.2007.070198.

Li, Z. *et al.* (1995) 'Guanylin, an endogenous ligand for C-type guanylate cyclase, is produced by goblet cells in the rat intestine', *Gastroenterology*, 109(6), pp. 1863–1875. doi: 10.1016/0016-5085(95)90753-X.

Li, Z. *et al.* (1996) 'Low salt intake down-regulates the guanylin signaling pathway in rat distal colon', *Gastroenterology*, 111(6), pp. 1714–1721. doi: 10.1016/S0016-5085(96)70037-9.

Li, Z. *et al.* (1997) *Purification, cDNA sequence, and tissue distribution of rat uroguanylin*, *Regulatory Peptides*.

Liddle, R. A. (1997) 'Cholecystokinin cells', *Annual Review of Physiology*, 59(1), pp. 221–242. doi: 10.1146/annurev.physiol.59.1.221.

Lin, J. E. *et al.* (2010a) 'The Hormone Receptor GUCY2C Suppresses Intestinal Tumor Formation by Inhibiting AKT Signaling', *Gastroenterology*. Elsevier Inc., 138(1), pp. 241–254. doi: 10.1053/j.gastro.2009.08.064.

Lin, J. E. *et al.* (2010b) 'The Hormone Receptor GUCY2C Suppresses Intestinal Tumor Formation by Inhibiting AKT Signaling', *Gastroenterology*, 138(1), pp. 241–254. doi: 10.1053/j.gastro.2009.08.064.

Lin, J. E. *et al.* (2016) 'Obesity-induced colorectal cancer is driven by caloric silencing of the guanylin-GUCY2C paracrine signaling axis', *Cancer Research*, 76(2), pp. 339–346. doi: 10.1158/0008-5472.CAN-15-1467-T.

Liu, C. *et al.* (2013) 'Pronuclear microinjection and oviduct transfer procedures for transgenic mouse production', *Methods in Molecular Biology*. doi: 10.1007/978-1-60327-369-5_10.

Liu, P. *et al.* (2011) 'Transient receptor potential channel type M5 is essential for fat taste.', *The Journal of neuroscience : the official journal of the Society for Neuroscience*. NIH Public Access, 31(23), pp. 8634–42. doi: 10.1523/JNEUROSCI.6273-10.2011.

Lloyd, C. *et al.* (2008) 'Modelling the human immune response: performance of a 1011 human antibody repertoire against a broad panel of therapeutically relevant antigens', *Protein Engineering Design and Selection*. Oxford University Press, 22(3), pp. 159–168. doi: 10.1093/protein/gzn058.

London, R. M. *et al.* (1997) *Signal transduction pathways via guanylin and uroguanylin in stomach and intestine*.

London, R. M. *et al.* (1999) 'Structure and activity of OK-GC: a kidney receptor guanylate cyclase activated by guanylin peptides.', *The American journal of physiology*, 276(6 Pt 2), pp. F882-91.

Lorenz, J. N. *et al.* (2003) 'Uroguanylin knockout mice have increased blood pressure and impaired natriuretic response to enteral NaCl load', *Journal of Clinical Investigation*, 112(8), pp. 1244–1254. doi: 10.1172/JCI200318743.

Lovell, R. M. and Ford, A. C. (2012) 'Global Prevalence of and Risk Factors for Irritable Bowel Syndrome: A Meta-analysis', *Clinical Gastroenterology and Hepatology*, 10(7), p. 712–721.e4. doi: 10.1016/j.cgh.2012.02.029.

Lowe, J. S. and Anderson, P. G. (2015) *Stevens & Lowe's human histology*.

Lu, V. B., Gribble, F. M. and Reimann, F. (2018) 'Free Fatty Acid Receptors in Enteroendocrine Cells', *Endocrinology*, 159(7), pp. 2826–2835. doi: 10.1210/en.2018-00261.

Magert, H.-J. *et al.* (1998) 'Uroguanylin: Gene structure, expression, processing as a peptide hormone, and co-storage with somatostatin in gastrointestinal D-cells', *Regulatory Peptides*, 73(3), pp. 165–176. doi: 10.1016/S0167-0115(97)01078-1.

Martin, S. *et al.* (1999) 'Regulated, side-directed secretion of proguanylin from isolated rat colonic mucosa', *Endocrinology*, 140(11), pp. 5022–5029. doi: 10.1210/endo.140.11.7103.

Maury, J. *et al.* (1995) 'The filamentous brush border glycocalyx, a mucin-like marker of enterocyte hyper-polarization.', *European journal of biochemistry*, 228(2), pp. 323–31.

May, C. L. and Kaestner, K. H. (2010) 'Gut endocrine cell development', *Molecular and Cellular Endocrinology*. Elsevier, 323(1), pp. 70–75. doi: 10.1016/J.MCE.2009.12.009.

McCafferty, J. *et al.* (1990) 'Phage antibodies: filamentous phage displaying antibody variable domains.', *Nature*, 348(6301), pp. 552–4. doi: 10.1038/348552a0.

McDermott, F. D. *et al.* (2015) 'Gnotobiotic Human Colon *Ex Vivo*', *Gastroenterology Research*, 8(5), pp. 247–252. doi: 10.14740/gr675w.

Meek, C. L. *et al.* (2016) 'The effect of encapsulated glutamine on gut peptide secretion in human volunteers', *Peptides*, 77, pp. 38–46. doi: 10.1016/j.peptides.2015.10.008.

Mellitzer, G. *et al.* (2010) 'Loss of enteroendocrine cells in mice alters lipid absorption and glucose homeostasis and impairs postnatal survival', *Journal of Clinical Investigation*, 120(5), pp. 1708–1721. doi: 10.1172/JCI40794.

Meyer-Hoffert, U. *et al.* (2008) 'Secreted enteric antimicrobial activity localises to the mucus surface layer', *Gut*, 57(6), pp. 764–771. doi: 10.1136/gut.2007.141481.

Miller, H. *et al.* (2007) 'Intestinal M cells: the fallible sentinels?', *World journal of gastroenterology*, 13(10), pp. 1477–86.

Miret, S., Abrahamse, L. and Groene, E. M. de (2004) 'Comparison of in Vitro Models for the Prediction of Compound Absorption across the Human Intestinal Mucosa', *Journal of*

Biomolecular Screening. Sage PublicationsSage CA: Thousand Oaks, CA, 9(7), pp. 598–606. doi: 10.1177/1087057104267162.

Miyazato, M. *et al.* (1996) *Cloning and Characterization of a cDNA Encoding a Precursor for Human Uroguanylin*.

von Moltke, J. *et al.* (2016) 'Tuft-cell-derived IL-25 regulates an intestinal ILC2–epithelial response circuit', *Nature*, 529(7585), pp. 221–225. doi: 10.1038/nature16161.

von Moltke, J. (2018) 'Intestinal Tuft Cells', *Physiology of the Gastrointestinal Tract*. Academic Press, pp. 721–733. doi: 10.1016/B978-0-12-809954-4.00031-1.

Mooseker, M. S. (1985) 'Organization, Chemistry, and Assembly of the Cytoskeletal Apparatus of the Intestinal Brush Border', *Annual Review of Cell Biology*, 1(1), pp. 209–241. doi: 10.1146/annurev.cb.01.110185.001233.

Mori-Akiyama, Y. *et al.* (2007) 'SOX9 is required for the differentiation of paneth cells in the intestinal epithelium.', *Gastroenterology*, 133(2), pp. 539–46. doi: 10.1053/j.gastro.2007.05.020.

Moro, F. *et al.* (2000) 'Release of guanylin immunoreactivity from the isolated vascularly perfused rat colon', *Endocrinology*, 141(7), pp. 2594–2599. doi: 10.1210/en.141.7.2594.

Morton, T. A., Myszka, D. G. and Chaiken, I. M. (1995) 'Interpreting Complex Binding Kinetics from Optical Biosensors: A Comparison of Analysis by Linearization, the Integrated Rate Equation, and Numerical Integration', *Analytical Biochemistry*. Academic Press, 227(1), pp. 176–185. doi: 10.1006/ABIO.1995.1268.

Moss, N. G. *et al.* (2008) 'Uroguanylin, an intestinal natriuretic peptide, is delivered to the kidney as an unprocessed propeptide.', *Endocrinology*. The Endocrine Society, 149(9), pp. 4486–98. doi: 10.1210/en.2007-1725.

Mowat, A. M. and Agace, W. W. (2014) 'Regional specialization within the intestinal immune system', *Nature Reviews Immunology*, 14(10), pp. 667–685. doi: 10.1038/nri3738.

Muller-Loennies, S. *et al.* (2000) 'Characterization of high affinity monoclonal antibodies specific for chlamydial lipopolysaccharide', *Glycobiology*. Oxford University Press, 10(2), pp. 121–130. doi: 10.1093/glycob/10.2.121.

Müller, T. *et al.* (2015) 'Congenital secretory diarrhoea caused by activating germline mutations in GUCY2C.', *Gut*, 3, p. gutjnl-2015-309441-. doi: 10.1136/gutjnl-2015-309441.

Murphy, K. C. (1998) 'Use of bacteriophage lambda recombination functions to promote gene replacement in Escherichia coli.', *Journal of bacteriology*. American Society for Microbiology, 180(8), pp. 2063–71.

Murphy, K. G. and Bloom, S. R. (2006) 'Gut hormones and the regulation of energy homeostasis', *Nature*, 444(7121), pp. 854–859. doi: 10.1038/nature05484.

Nagai, T. *et al.* (2002) *A variant of yellow fluorescent protein with fast and efficient maturation for cell-biological applications*.

Nakazato, M. *et al.* (1998) 'Tissue distribution, cellular source, and structural analysis of rat immunoreactive uroguanylin', *Endocrinology*, 139(12), pp. 5247–5254. doi:

10.1210/endo.139.12.6347.

Nandi, A., Bhandari, R. and Visweswariah, S. S. (1997) 'Epitope conservation and immunohistochemical localization of the guanylin/stable toxin peptide receptor, guanylyl cyclase C', *Journal of Cellular Biochemistry*, 66(4), pp. 500–511. doi: 10.1002/(SICI)1097-4644(19970915)66:4<500::AID-JCB9>3.0.CO;2-P.

Natividad, J. M. M. and Verdu, E. F. (2013) 'Modulation of intestinal barrier by intestinal microbiota: Pathological and therapeutic implications', *Pharmacological Research*, 69(1), pp. 42–51. doi: 10.1016/j.phrs.2012.10.007.

Neish, A. S. (2009) 'Microbes in Gastrointestinal Health and Disease', *Gastroenterology*, 136(1), pp. 65–80. doi: 10.1053/j.gastro.2008.10.080.

Neutra, M. R., Frey, A. and Kraehenbuhl, J.-P. (1996) 'Epithelial M Cells: Gateways for Mucosal Infection and Immunization', *Cell*. Cell Press, 86(3), pp. 345–348. doi: 10.1016/S0092-8674(00)80106-3.

Newmark, H. L., Lipkin, M. and Maheshwari, N. (1990) 'Colonic hyperplasia and hyperproliferation induced by a nutritional stress diet with four components of Western-style diet.', *Journal of the National Cancer Institute*, 82(6), pp. 491–6.

Nicholson, J. K. and Wilson, I. D. (2003) 'Understanding "Global" Systems Biology: Metabonomics and the Continuum of Metabolism', *Nature Reviews Drug Discovery*, 2(8), pp. 668–676. doi: 10.1038/nrd1157.

Noah, T. K., Donahue, B. and Shroyer, N. F. (2011) 'Intestinal development and differentiation', *Experimental Cell Research*. Elsevier Inc., 317(19), pp. 2702–2710. doi: 10.1016/j.yexcr.2011.09.006.

Nokihara, K. *et al.* (1997) 'Synthesis, solution structure, binding activity, and cGMP activation of human guanylin and its disulfide isomer.', *Regulatory peptides*, 70(2–3), pp. 111–20.

Nossol, C. *et al.* (2011) 'Air–liquid interface cultures enhance the oxygen supply and trigger the structural and functional differentiation of intestinal porcine epithelial cells (IPEC)', *Histochemistry and Cell Biology*. Springer-Verlag, 136(1), pp. 103–115. doi: 10.1007/s00418-011-0826-y.

Notterman, D. a *et al.* (2001) 'Transcriptional gene expression profiles of colorectal adenoma, adenocarcinoma, and normal tissue examined by oligonucleotide arrays', *Cancer Res.*, 61, pp. 3124–3130.

O'Shannessy, D. J. and Winzor, D. J. (1996) 'Interpretation of Deviations from Pseudo-First-Order Kinetic Behavior in the Characterization of Ligand Binding by Biosensor Technology', *Analytical Biochemistry*. Academic Press, 236(2), pp. 275–283. doi: 10.1006/ABIO.1996.0167.

Ogawa, Y. *et al.* (1994) 'Molecular Cloning and Chromosomal Assignment of the Mouse C-Type Natriuretic Peptide (CNP) Gene (Nppc): Comparison with the Human CNP Gene (NPPC)', *Genomics*. Academic Press, 24(2), pp. 383–387. doi: 10.1006/GENO.1994.1633.

Ohno, H. (2016) 'Intestinal M cells.', *Journal of biochemistry*. Oxford University Press, 159(2), pp. 151–60. doi: 10.1093/jb/mvv121.

Okoh, A. and Osode, A. (2008) *Enterotoxigenic Escherichia coli (ETEC): a recurring decimal in infants' and travelers' diarrhea. - PubMed - NCBI*, *Rev Environ Health*.

Ootani, A. *et al.* (2000) 'An Air–Liquid Interface Promotes the Differentiation of Gastric Surface Mucous Cells (GSM06) in Culture', *Biochemical and Biophysical Research Communications*. Academic Press, 271(3), pp. 741–746. doi: 10.1006/BBRC.2000.2673.

Van Op den bosch, J. *et al.* (2009) 'The role(s) of somatostatin, structurally related peptides and somatostatin receptors in the gastrointestinal tract: a review', *Regulatory Peptides*, 156(1–3), pp. 1–8. doi: 10.1016/j.regpep.2009.04.003.

Ouellette, A. J. (no date) 'Paneth cells and innate mucosal immunity'. doi: 10.1097/MOG.0b013e32833dccde.

Owen, R. L. and Jones, A. L. (1974a) 'Epithelial cell specialization within human Peyer's patches: an ultrastructural study of intestinal lymphoid follicles.', *Gastroenterology*, 66(2), pp. 189–203.

Owen, R. L. and Jones, A. L. (1974b) 'Epithelial cell specialization within human Peyer's patches: an ultrastructural study of intestinal lymphoid follicles.', *Gastroenterology*, 66(2), pp. 189–203.

Pais, R. *et al.* (2016) 'Angiotensin II Type 1 Receptor-Dependent GLP-1 and PYY Secretion in Mice and Humans', *Endocrinology*, 157(10), pp. 3821–3831. doi: 10.1210/en.2016-1384.

Pais, R., Gribble, F. M. and Reimann, F. (2016) 'Stimulation of incretin secreting cells', *Therapeutic Advances in Endocrinology and Metabolism*, 7(1), pp. 24–42. doi: 10.1177/2042018815618177.

Parker, H. E. *et al.* (2009) 'Nutrient-dependent secretion of glucose-dependent insulinotropic polypeptide from primary murine K cells', *Diabetologia*, 52(2), pp. 289–298. doi: 10.1007/s00125-008-1202-x.

Parker, H. E., Gribble, F. M. and Reimann, F. (2014) 'The role of gut endocrine cells in control of metabolism and appetite.', *Experimental physiology*, 99(9), pp. 1116–20. doi: 10.1113/expphysiol.2014.079764.

Pearse, A. G. *et al.* (1970) 'The endocrine polypeptide cells of the human stomach, duodenum, and jejunum.', *Gut*, 11(8), pp. 649–58.

Pelaseyed, T. *et al.* (2014) 'The mucus and mucins of the goblet cells and enterocytes provide the first defense line of the gastrointestinal tract and interact with the immune system', *Immunological Reviews*, 260(1), pp. 8–20. doi: 10.1111/imr.12182.

Percival-Alwyn, J. L. *et al.* (2015) 'Generation of potent mouse monoclonal antibodies to self-proteins using T-cell epitope "tags"', *mAbs*, 7(1), pp. 129–137. doi: 10.4161/19420862.2014.985489.

Perkins, A., Goy, M. F. and Li, Z. (1997) 'Uroguanylin is expressed by enterochromaffin cells in the rat gastrointestinal tract', *Gastroenterology*, 113(3), pp. 1007–1014. doi: 10.1016/S0016-5085(97)70198-7.

Petersen, N. *et al.* (2014) 'Generation of L cells in mouse and human small intestine

organoids.', *Diabetes*. American Diabetes Association, 63(2), pp. 410–20. doi: 10.2337/db13-0991.

Peterson, D. A. *et al.* (2007) 'IgA response to symbiotic bacteria as a mediator of gut homeostasis.', *Cell host & microbe*, 2(5), pp. 328–39. doi: 10.1016/j.chom.2007.09.013.

Peterson, M. D. and Mooseker, M. S. (1992) 'Characterization of the enterocyte-like brush border cytoskeleton of the C2BBe clones of the human intestinal cell line, Caco-2.', *Journal of cell science*, 102 (Pt 3), pp. 581–600.

Phillips, T. E. (1992) *Both crypt and villus intestinal goblet cells secrete mucin in response to cholinergic stimulation*.

Pinto, D. *et al.* (2003) 'Canonical Wnt signals are essential for homeostasis of the intestinal epithelium', *Genes & Development*, 17(14), pp. 1709–1713. doi: 10.1101/gad.267103.

Pinto, M. *et al.* (1983) 'Enterocyte-like differentiation and polarization of the human-colon carcinoma cell-line Caco-2 in culture'.

Pitari, G. M. *et al.* (2001) 'Guanylyl cyclase C agonists regulate progression through the cell cycle of human colon carcinoma cells.', *Proceedings of the National Academy of Sciences of the United States of America*, 98(14), pp. 7846–7851. doi: 10.1073/pnas.141124698.

Pitari, G. M. *et al.* (2003) 'Bacterial enterotoxins are associated with resistance to colon cancer', *Proc Natl Acad Sci U S A*, 100(5), pp. 2695–2699. doi: 10.1073/pnas.0434905100.

Potten, C. S., Booth, C. and Pritchard, D. M. (1997) 'The intestinal epithelial stem cell: the mucosal governor.', *International journal of experimental pathology*, 78(4), pp. 219–43.

Potthast, R. *et al.* (2001) *High Salt Intake Increases Uroguanylin Expression in Mouse Kidney*.

Preston, R. A. *et al.* (2012) 'Sodium challenge does not support an acute gastrointestinal–renal natriuretic signaling axis in humans', *Kidney International*. Nature Publishing Group, 82(12), pp. 1313–1320. doi: 10.1038/ki.2012.269.

Psichas, A. *et al.* (2017) 'Mixed Primary Cultures of Murine Small Intestine Intended for the Study of Gut Hormone Secretion and Live Cell Imaging of Enteroendocrine Cells', *J. Vis. Exp*, (122), p. 55687. doi: 10.3791/55687.

Qian, X. *et al.* (2000) 'Expression of GC-C, a Receptor-Guanylate Cyclase, and Its Endogenous Ligands Uroguanylin and Guanylin along the Rostrocaudal Axis of the Intestine [1]', *Endocrinology*. Oxford University Press, 141(9), pp. 3210–3224. doi: 10.1210/endo.141.9.7644.

Qian, X. *et al.* (2008) 'Circulating Prouroguanylin Is Processed to Its Active Natriuretic Form Exclusively within the Renal Tubules', *Endocrinology*. Oxford University Press, 149(9), pp. 4499–4509. doi: 10.1210/en.2007-1724.

Qian, X. *et al.* (2011) 'The rat kidney contains high levels of prouroguanylin (the uroguanylin precursor) but does not express GC-C (the enteric uroguanylin receptor).', *American journal of physiology. Renal physiology*, 300(2), pp. F561-73. doi: 10.1152/ajprenal.00282.2010.

Rahbi, H. *et al.* (2012) 'The uroguanylin system and human disease', *Clinical Science*, 123(12), pp. 659–668. doi: 10.1042/CS20120021.

Ramare, F. *et al.* (1993) 'Trypsin-dependent production of an antibacterial substance by a human Peptostreptococcus strain in gnotobiotic rats and in vitro.', *Applied and environmental microbiology*, 59(9), pp. 2876–83.

Rekas, A. *et al.* (2002) 'Crystal Structure of Venus, a Yellow Fluorescent Protein with Improved Maturation and Reduced Environmental Sensitivity* Downloaded from', *THE JOURNAL OF BIOLOGICAL CHEMISTRY*. JBC Papers in Press, 277(52), pp. 50573–50578. doi: 10.1074/jbc.M209524200.

Renehan, A. G., Zwahlen, M. and Egger, M. (2015) 'Adiposity and cancer risk: new mechanistic insights from epidemiology', *Nature Reviews Cancer*. Nature Publishing Group, 15(8), pp. 484–498. doi: 10.1038/nrc3967.

Riechmann, L. and Weill, M. (1993) 'Phage display and selection of a site-directed randomized single-chain antibody Fv fragment for its affinity improvement.', *Biochemistry*, 32(34), pp. 8848–55.

Riley, M. A. and Wertz, J. E. (2002) 'Bacteriocin diversity: ecological and evolutionary perspectives.', *Biochimie*, 84(5–6), pp. 357–64.

Roberts, G. P. *et al.* (2018) 'Comparison of human and murine enteroendocrine cells by transcriptomic and peptidomic profiling', *bioRxiv*. Cold Spring Harbor Laboratory, p. 374579. doi: 10.1101/374579.

Robey, R. B. and Hay, N. (2009) 'Is Akt the "Warburg kinase"?-Akt-energy metabolism interactions and oncogenesis.', *Seminars in cancer biology*. NIH Public Access, 19(1), pp. 25–31. doi: 10.1016/j.semcancer.2008.11.010.

Rodríguez-Piñeiro, A. M. *et al.* (2013) 'Studies of mucus in mouse stomach, small intestine, and colon. II. Gastrointestinal mucus proteome reveals Muc2 and Muc5ac accompanied by a set of core proteins', *American Journal of Physiology-Gastrointestinal and Liver Physiology*, 305(5), pp. G348–G356. doi: 10.1152/ajpgi.00047.2013.

Rodríguez, A. *et al.* (2016) 'Guanylin and uroguanylin stimulate lipolysis in human visceral adipocytes', *International Journal of Obesity*, 40(9), pp. 1405–1415. doi: 10.1038/ijo.2016.66.

Rodríguez, A. *et al.* (2016) 'Guanylin and uroguanylin stimulate lipolysis in human visceral adipocytes', *International Journal of Obesity*, 40, pp. 1405–1415. doi: 10.1038/ijo.2016.66.

Roeselers, G. *et al.* (2013) 'Ex vivo systems to study host–microbiota interactions in the gastrointestinal tract', *Best Practice & Research Clinical Gastroenterology*. Baillière Tindall, 27(1), pp. 101–113. doi: 10.1016/J.BPG.2013.03.018.

Romi, H., Cohen, I., Landau, D., Alkrinawi, S., Yerushalmi, B., Hershkovitz, R., Newman-Heiman, N., Cutting, G. R., *et al.* (2012) 'Meconium ileus caused by mutations in GUCY2C, encoding the CFTR-activating guanylate cyclase 2C', *American Journal of Human Genetics*. The American Society of Human Genetics, 90(5), pp. 893–899. doi: 10.1016/j.ajhg.2012.03.022.

Romi, H., Cohen, I., Landau, D., Alkrinawi, S., Yerushalmi, B., Hershkovitz, R., Newman-Heiman, N., Cutting, G. R., *et al.* (2012) 'Meconium Ileus Caused by Mutations in GUCY2C, Encoding the CFTR-Activating Guanylate Cyclase 2C', *The American Journal of Human Genetics*, 90(5), pp. 893–899. doi: 10.1016/j.ajhg.2012.03.022.

Rosenblatt, J., Raff, M. C. and Cramer, L. P. (2001) 'An epithelial cell destined for apoptosis signals its neighbors to extrude it by an actin- and myosin-dependent mechanism.', *Current biology : CB*, 11(23), pp. 1847–57.

Rosenstein, B. J. and Langbaum, T. S. (1980) 'Incidence of meconium abnormalities in newborn infants with cystic fibrosis.', *American journal of diseases of children (1960)*, 134(1), pp. 72–3.

Rubio, C. A. (2012) 'Paneth cells and goblet cells express the neuroendocrine peptide synaptophysin. I- normal duodenal mucosa', *In Vivo*, 26(1), pp. 135–138. doi: 26/1/135 [pii].

Salzman, N. H. *et al.* (2010) 'Enteric defensins are essential regulators of intestinal microbial ecology.', *Nature immunology*, 11(1), pp. 76–83. doi: 10.1038/ni.1825.

Sambuy, Y. *et al.* (2005) 'The Caco-2 cell line as a model of the intestinal barrier: in£uence of cell and culture-related factors on Caco-2 cell functional characteristics', *Cell Biology and Toxicology*. Springer, 21(1), pp. 1–26. doi: 10.1007/s10565-005-0085-6.

Sato, T. *et al.* (2009) 'Single Lgr5 stem cells build crypt-villus structures in vitro without a mesenchymal niche', *Nature*. Nature Publishing Group, 459(7244), pp. 262–265. doi: 10.1038/nature07935.

Sato, T. *et al.* (2011) 'Paneth cells constitute the niche for Lgr5 stem cells in intestinal crypts', *Nature*, 469(7330), pp. 415–418. doi: 10.1038/nature09637.

de Sauvage, F. J. *et al.* (1992) 'Precursor structure, expression, and tissue distribution of human guanylin.', *Proceedings of the National Academy of Sciences of the United States of America*. National Academy of Sciences, 89(19), pp. 9089–93. doi: 10.1073/PNAS.89.19.9089.

Scarpellini, E. *et al.* (2015) 'The human gut microbiota and virome: Potential therapeutic implications', *Digestive and Liver Disease*, 47(12), pp. 1007–1012. doi: 10.1016/j.dld.2015.07.008.

Scarpignato, C. and Blandizzi, C. (2014) 'Editorial: adequate management may reduce the colorectal cancer risk associated with constipation', *Alimentary Pharmacology & Therapeutics*. Wiley/Blackwell (10.1111), 40(5), pp. 562–564. doi: 10.1111/apt.12851.

Schauer, D. B. (1997) 'Indigenous microflora: Paving the way for pathogens?', *Current biology : CB*. Elsevier, 7(2), pp. R75-7. doi: 10.1016/S0960-9822(06)00040-6.

Schier, R., Bye, J., *et al.* (1996) 'Isolation of High-affinity Monomeric Human Anti-c-erbB-2 Single chain Fv Using Affinity-driven Selection', *Journal of Molecular Biology*. Academic Press, 255(1), pp. 28–43. doi: 10.1006/JMBI.1996.0004.

Schier, R., McCall, A., *et al.* (1996) 'Isolation of Picomolar Affinity Anti-c-erbB-2 Single-chain Fv by Molecular Evolution of the Complementarity Determining Regions in the Center of the Antibody Binding Site', *Journal of Molecular Biology*, 263(4), pp. 551–567. doi: 10.1006/jmbi.1996.0598.

Schonhoff, S. E., Giel-Moloney, M. and Leiter, A. B. (2004) 'Minireview: Development and Differentiation of Gut Endocrine Cells', *Endocrinology*, 145(6), pp. 2639–2644. doi: 10.1210/en.2004-0051.

Schroeder, A. *et al.* (2006) 'The RIN: an RNA integrity number for assigning integrity values to

RNA measurements', *BMC Molecular Biology*. BioMed Central, 7(1), p. 3. doi: 10.1186/1471-2199-7-3.

Schulz, A. *et al.* (1999) *Role of the prosequence of guanylin*. doi: 10.1110/ps.8.9.1850.

Schulz, S. *et al.* (1990) 'Guanylyl cyclase is a heat-stable enterotoxin receptor.', *Cell*, 63(5), pp. 941–8.

Schulz, S. (1999) 'Targeted Gene Disruption in the Development of Mouse Models to Elucidate the Role of Receptor Guanylyl Cyclase Signaling Pathways in Physiological Function', *Methods*. Academic Press, 19(4), pp. 551–558. doi: 10.1006/METH.1999.0897.

Schulz, S. *et al.* (2006) 'A validated quantitative assay to detect occult micrometastases by reverse transcriptase-polymerase chain reaction of guanylyl cyclase C in patients with colorectal cancer', *Clinical Cancer Research*, 12(15), pp. 4545–4552. doi: 10.1158/1078-0432.CCR-06-0865.

Schulz, S., Chrisman, T. D. and Garbers, D. L. (1992) *Cloning and expression of guanylin. Its existence in various mammalian tissues. - PubMed - NCBI*, *J Biol Chem.*

Schwabe, K. and Cetin, Y. (2012) 'Guanylin and functional coupling proteins in the hepatobiliary system of rat and guinea pig', *Histochemistry and Cell Biology*, 137(5), pp. 589–597. doi: 10.1007/s00418-012-0927-2.

Sciaky, D., Kosiba, J. L. and Cohen, M. B. (1994) 'Genomic sequence of the murine guanylin gene.', *Genomics*, 24(3), pp. 583–7. doi: 10.1006/geno.1994.1670.

Semenza, G. (1986) 'Anchoring and Biosynthesis of Stalked Brush Border Membrane Proteins: Glycosidases and Peptidases of Enterocytes and Renal Tubuli', *Annual Review of Cell Biology*. Annual Reviews 4139 El Camino Way, P.O. Box 10139, Palo Alto, CA 94303-0139, USA , 2(1), pp. 255–307. doi: 10.1146/annurev.cb.02.110186.001351.

Servin, A. L. (2004) 'Antagonistic activities of lactobacilli and bifidobacteria against microbial pathogens', *FEMS Microbiology Reviews*. Oxford University Press, 28(4), pp. 405–440. doi: 10.1016/j.femsre.2004.01.003.

Shah, E. D., Kim, H. M. and Schoenfeld, P. (2018) 'Efficacy and Tolerability of Guanylate Cyclase-C Agonists for Irritable Bowel Syndrome with Constipation and Chronic Idiopathic Constipation: A Systematic Review and Meta-Analysis', *The American Journal of Gastroenterology*. Nature Publishing Group, 113(3), pp. 329–338. doi: 10.1038/ajg.2017.495.

Shiroma, L. O. and Costa, V. P. (2015) 'Parasympathomimetics', *Glaucoma*. W.B. Saunders, pp. 577–582. doi: 10.1016/B978-0-7020-5193-7.00056-X.

Shizuya, H. *et al.* (1992) 'Cloning and stable maintenance of 300-kilobase-pair fragments of human DNA in Escherichia coli using an F-factor-based vector.', *Proceedings of the National Academy of Sciences of the United States of America*. National Academy of Sciences, 89(18), pp. 8794–7. doi: 10.1073/pnas.89.18.8794.

Shoshkes-Carmel, M. *et al.* (2018) 'Subepithelial telocytes are an important source of Wnts that supports intestinal crypts', *Nature*, 557(7704), pp. 242–246. doi: 10.1038/s41586-018-0084-4.

Shroyer, N. F. *et al.* (2005) 'Gfi1 functions downstream of Math1 to control intestinal secretory cell subtype allocation and differentiation.', *Genes & development*. Cold Spring Harbor Laboratory Press, 19(20), pp. 2412–7. doi: 10.1101/gad.1353905.

Silva, G. M. and Vogel, C. (2016) 'Quantifying gene expression: the importance of being subtle.', *Molecular systems biology*. EMBO Press, 12(10), p. 885. doi: 10.15252/MSB.20167325.

Simpson, A. K. *et al.* (2007) 'Cyclic AMP triggers glucagon-like peptide-1 secretion from the GLUTag enteroendocrine cell line', *Diabetologia*, 50(10), pp. 2181–2189. doi: 10.1007/s00125-007-0750-9.

Sindic, A. *et al.* (2013) 'Current understanding of guanylin peptides actions.', *ISRN nephrology*. Hindawi Publishing Corporation ISRN Nephrology, 2013, p. 813648. doi: 10.5402/2013/813648.

Sjölund, K. *et al.* (1983) 'Endocrine cells in human intestine: an immunocytochemical study.', *Gastroenterology*, 85(5), pp. 1120–30.

Smith, A. *et al.* (2015) 'Meconium ileus in a Lebanese family secondary to mutations in the GUCY2C gene.', *European journal of human genetics : EJHG*. Nature Publishing Group, 23(7), pp. 990–992. doi: 10.1038/ejhg.2014.236.

Smith, G. P. (1985) 'Filamentous fusion phage: novel expression vectors that display cloned antigens on the virion surface.', *Science (New York, N.Y.)*. American Association for the Advancement of Science, 228(4705), pp. 1315–7. doi: 10.1126/SCIENCE.4001944.

Snoeck, V., Goddeeris, B. and Cox, E. (2005) 'The role of enterocytes in the intestinal barrier function and antigen uptake', *Microbes and Infection*. Elsevier Masson, 7(7–8), pp. 997–1004. doi: 10.1016/J.MICINF.2005.04.003.

Sonnenberg, A. and Müller, A. D. (1993) 'Constipation and cathartics as risk factors of colorectal cancer: a meta-analysis.', *Pharmacology*. Karger Publishers, 47 Suppl 1(Suppl. 1), pp. 224–33. doi: 10.1159/000139862.

Specian, R. D. and Oliver, M. G. (1991) 'Functional biology of intestinal goblet cells.', *The American journal of physiology*. American Physiological Society Bethesda, MD , 260(2 Pt 1), pp. C183-93. doi: 10.1152/ajpcell.1991.260.2.C183.

Srikanth, C. V and McCormick, B. A. (2008) 'Interactions of the intestinal epithelium with the pathogen and the indigenous microbiota: a three-way crosstalk.', *Interdisciplinary perspectives on infectious diseases*. Hindawi Limited, 2008, p. 626827. doi: 10.1155/2008/626827.

Stappenbeck, T. S. (2009) 'Paneth Cell Development, Differentiation, and Function: New Molecular Cues', *Gastroenterology*, 137(1), pp. 30–33. doi: 10.1053/j.gastro.2009.05.013.

Steinbrecher, K. A. *et al.* (2000) 'Expression of Guanylin Is Downregulated in Mouse and Human Intestinal Adenomas', *Biochemical and Biophysical Research Communications*, 273(1), pp. 225–230. doi: 10.1006/bbrc.2000.2917.

Steinbrecher, K. A. *et al.* (2002) 'Targeted inactivation of the mouse guanylin gene results in altered dynamics of colonic epithelial proliferation', *American Journal of Pathology*, 161(6),

pp. 2169–2178. doi: 10.1016/S0002-9440(10)64494-X.

Steinhelper, M. E. (1993) 'Structure, expression, and genomic mapping of the mouse natriuretic peptide type-B gene.', *Circulation Research*, 72(5), pp. 984–992. doi: 10.1161/01.RES.72.5.984.

Sun, H. *et al.* (2008) 'The Caco-2 cell monolayer: usefulness and limitations', *Expert Opinion on Drug Metabolism & Toxicology*. Taylor & Francis, 4(4), pp. 395–411. doi: 10.1517/17425255.4.4.395.

Sun, S. X. *et al.* (2011) 'Impact of Chronic Constipation on Health-Related Quality of Life, Work Productivity, and Healthcare Resource Use: An Analysis of the National Health and Wellness Survey', *Digestive Diseases and Sciences*. Springer US, 56(9), pp. 2688–2695. doi: 10.1007/s10620-011-1639-5.

Sun, Y. *et al.* (2016) 'Combining Yeast Display and Competitive FACS to Select Rare Hapten-Specific Clones from Recombinant Antibody Libraries.', *Analytical chemistry*. American Chemical Society, 88(18), pp. 9181–9. doi: 10.1021/acs.analchem.6b02334.

Swaminathan, S. *et al.* (2000) 'Rapid engineering of bacterial artificial chromosomes using oligonucleotides', *genesis*. Wiley-Blackwell, 29(1), pp. 14–21. doi: 10.1002/1526-968X(200101)29:1

Takahashi, N. *et al.* (2008) 'IL-17 produced by Paneth cells drives TNF-induced shock.', *The Journal of experimental medicine*. Rockefeller University Press, 205(8), pp. 1755–61. doi: 10.1084/jem.20080588.

Taupin, D. and Podolsky, D. K. (2003) 'Erratum: Trefoil factors: initiators of mucosal healing', *Nature Reviews Molecular Cell Biology*, 4(9), pp. 721–732. doi: 10.1038/nrm1203.

Tetteh, P. W. *et al.* (2016) 'Generation of an inducible colon-specific Cre enzyme mouse line for colon cancer research.', *Proceedings of the National Academy of Sciences of the United States of America*. National Academy of Sciences, 113(42), pp. 11859–11864. doi: 10.1073/pnas.1614057113.

Thakkar, S. *et al.* (2014) 'Affinity improvement of a therapeutic antibody to methamphetamine and amphetamine through structure-based antibody engineering.', *Scientific reports*. Nature Publishing Group, 4, p. 3673. doi: 10.1038/srep03673.

Tolhurst, G. *et al.* (2012) 'Short-Chain Fatty Acids Stimulate Glucagon-Like Peptide-1 Secretion via the G-Protein-Coupled Receptor FFAR2', *Diabetes*, 61(2), pp. 364–371. doi: 10.2337/db11-1019.

Toriano, R. *et al.* (2011) 'Uroguanylin Regulates Net Fluid Secretion via the NHE2 Isoform of the Na/H+ Exchanger in an Intestinal Cellular Model', *Cellular Physiology and Biochemistry*, 28(4), pp. 733–742. doi: 10.1159/000335767.

Tsubouchi, S. and Leblond, C. P. (1979) 'Migration and turnover of entero-endocrine and caveolated cells in the epithelium of the descending colon, as shown by radioautography after continuous infusion of3H-thymidine into mice', *American Journal of Anatomy*, 156(4), pp. 431–451. doi: 10.1002/aja.1001560403.

Usui, T. *et al.* (2018) 'Preparation of Human Primary Colon Tissue-Derived Organoid Using Air

Liquid Interface Culture', in *Current Protocols in Toxicology*. Hoboken, NJ, USA: John Wiley & Sons, Inc., p. 22.6.1-22.6.7. doi: 10.1002/cptx.40.

Vaandrager, A. B. *et al.* (2000) 'Differential role of cyclic GMP-dependent protein kinase II in ion transport in murine small intestine and colon.', *Gastroenterology*, 118(1), pp. 108–14.

Vaandrager, A. B. (2002) 'Structure and function of the heat-stable enterotoxin receptor/guanylyl cyclase C.', *Molecular and cellular biochemistry*, 230(1–2), pp. 73–83.

Vaandrager, A. B., Bot, A. G. and De Jonge, H. R. (1997) 'Guanosine 3',5'-cyclic monophosphate-dependent protein kinase II mediates heat-stable enterotoxin-provoked chloride secretion in rat intestine.', *Gastroenterology*, 112(2), pp. 437–43.

Valentino, M. A. *et al.* (2011) 'A uroguanylin-GUCY2C endocrine axis regulates feeding in mice', *Journal of Clinical Investigation*, 121(9), pp. 3578–3588. doi: 10.1172/JCI57925.

VanDussen, K. L. *et al.* (2015) 'Development of an enhanced human gastrointestinal epithelial culture system to facilitate patient-based assays', *Gut*, 64(6), pp. 911–920. doi: 10.1136/gutjnl-2013-306651.

Vaughan, T. J. *et al.* (1996) 'Human antibodies with sub-nanomolar affinities isolated from a large non-immunized phage display library.', *Nature biotechnology*, 14(3), pp. 309–14. doi: 10.1038/nbt0396-309.

Vaughan, T. J. *et al.* (1996) 'Human Antibodies With Sub-Nanomolar Affinities Isolated From A Large Non-Immunized Phage Display Library', *Nature Biotechnology*, 14(3), pp. 309–314. doi: 10.1038/nbt0396-309.

Vereecke, L., Beyaert, R. and van Loo, G. (2011) 'Enterocyte death and intestinal barrier maintenance in homeostasis and disease', *Trends in Molecular Medicine*. Elsevier Current Trends, 17(10), pp. 584–593. doi: 10.1016/J.MOLMED.2011.05.011.

Vesentini, S. *et al.* (2010) *Mechanisms of Polymyxin B Endotoxin Removal from Extracorporeal Blood Flow: Molecular Interactions Sepsis is a generalized infection of an organism with presence of bacteria in the blood flow (bacteremia). Recently, in parallel to clinical and research*, *Therapy. Contrib Nephrol. Basel, Karger*.

Vogel, C. and Marcotte, E. M. (2012) *Insights into the regulation of protein abundance from proteomic and transcriptomic analyses*. doi: 10.1038/nrg3185.

Wang, D. *et al.* (2011) 'Paneth cell marker expression in intestinal villi and colon crypts characterizes dietary induced risk for mouse sporadic intestinal cancer.', *Proceedings of the National Academy of Sciences of the United States of America*. National Academy of Sciences, 108(25), pp. 10272–7. doi: 10.1073/pnas.1017668108.

Wang, J. *et al.* (2006) 'An improved recombineering approach by adding RecA to lambda Red recombination.', *Molecular biotechnology*, 32(1), pp. 43–53.

Wang, X. *et al.* (2015) 'Cloning and variation of ground state intestinal stem cells', *Nature*. Nature Publishing Group, 522(7555), pp. 173–178. doi: 10.1038/nature14484.

Wang, X. Z. *et al.* (1996) 'Signals from the stressed endoplasmic reticulum induce C/EBP-homologous protein (CHOP/GADD153).', *Molecular and cellular biology*, 16(8), pp. 4273–80.

Warburg, O. (1956) 'On the Origin of Cancer Cells', *Science*, 123(3191), pp. 309–314. doi: 10.1126/science.123.3191.309.

Ward, P. S. and Thompson, C. B. (2012) 'Metabolic reprogramming: a cancer hallmark even warburg did not anticipate.', *Cancer cell*. NIH Public Access, 21(3), pp. 297–308. doi: 10.1016/j.ccr.2012.02.014.

Weinberg, D. S. *et al.* (2017) 'Bioactivity of Oral Linaclotide in Human Colorectum for Cancer Chemoprevention.', *Cancer prevention research (Philadelphia, Pa.)*. American Association for Cancer Research, 10(6), pp. 345–354. doi: 10.1158/1940-6207.CAPR-16-0286.

Whitaker, T. L., Steinbrecher, K. A., *et al.* (1997) 'The uroguanylin gene (Guca1b) is linked to guanylin (Guca2) on mouse chromosome 4.', *Genomics*, 45(2), pp. 348–54. doi: 10.1006/geno.1997.4942.

Whitaker, T. L., Witte, D. P., *et al.* (1997) 'Uroguanylin and guanylin: distinct but overlapping patterns of messenger RNA expression in mouse intestine', *Gastroenterology*, 113(3), pp. 1000–1006. doi: 10.1016/S0016-5085(97)70197-5.

Wiegand, R. C. *et al.* (1992) 'Human guanylin: cDNA isolation, structure, and activity.', *FEBS letters*, 311(2), pp. 150–4.

Wiegand, R. C., Kato, J. and Currie, M. G. (1992) 'Rat guanylin cDNA: characterization of the precursor of an endogenous activator of intestinal guanylate cyclase.', *Biochemical and biophysical research communications*, 185(3), pp. 812–7.

Wilson, C. *et al.* (2014) 'The paracrine hormone for the GUCY2C tumor suppressor, guanylin, is universally lost in colorectal cancer', *Cancer Epidemiology Biomarkers and Prevention*, 23(11), pp. 2328–2337. doi: 10.1158/1055-9965.EPI-14-0440.

Winton, D. J. and Ponder, B. A. (1990) 'Stem-cell organization in mouse small intestine.', *Proceedings. Biological sciences*. The Royal Society, 241(1300), pp. 13–8. doi: 10.1098/rspb.1990.0059.

Woods, S. C. (2009) 'The Control of Food Intake: Behavioral versus Molecular Perspectives', *Cell Metabolism*, 9(6), pp. 489–498. doi: 10.1016/j.cmet.2009.04.007.

Xie, Q. M., Shao, J. S. and Alpers, D. H. (1999) 'Rat intestinal alpha1-antitrypsin secretion is regulated by triacylglycerol feeding.', *The American journal of physiology*, 276(6 Pt 1), pp. G1452-60.

Yamaguchi, H. *et al.* (1995) 'Two Novel Rat Guanylin Molecules, Guanylin-94 and Guanylin-16, Do Not Increase Cyclic GMP Production in T84 Cells', *Biochemical and Biophysical Research Communications*. Academic Press, 214(3), pp. 1204–1210. doi: 10.1006/BBRC.1995.2414.

Yamamoto, Y. *et al.* (2016) 'Mutational spectrum of Barrett's stem cells suggests paths to initiation of a precancerous lesion.', *Nature communications*, 7, p. 10380. doi: 10.1038/ncomms10380.

Yan, K. S. *et al.* (2012) 'The intestinal stem cell markers Bmi1 and Lgr5 identify two functionally distinct populations', *Proceedings of the National Academy of Sciences*, 109(2), pp. 466–471. doi: 10.1073/pnas.1118857109.

Yang-Feng, T. L. *et al.* (1985) 'The pronatriodilatin gene is located on the distal short arm of human chromosome 1 and on mouse chromosome 4.', *American journal of human genetics*, 37(6), pp. 1117–28.

Yang, K. *et al.* (1997) 'A mouse model of human familial adenomatous polyposis.', *The Journal of experimental zoology*, 277(3), pp. 245–54.

Yang, Q. *et al.* (2001) 'Requirement of Math1 for Secretory Cell Lineage Commitment in the Mouse Intestine', *Science*, 294(5549), pp. 2155–2158. doi: 10.1126/science.1065718.

Yang, W. P. *et al.* (1995) 'CDR walking mutagenesis for the affinity maturation of a potent human anti-HIV-1 antibody into the picomolar range.', *Journal of molecular biology*, 254(3), pp. 392–403. A

Yang, X. W., Model, P. and Heintz, N. (1997) 'Homologous recombination based modification in esherichia coli and germline transmission in transgenic mice of a bacterial artificial chromsome', *Nature Biotechnology*, 15(9), pp. 859–865. doi: 10.1038/nbt0997-859.

Yilmaz, Ö. H. *et al.* (2012) 'mTORC1 in the Paneth cell niche couples intestinal stem-cell function to calorie intake', *Nature*, 486(7404), pp. 490–495. doi: 10.1038/nature11163.

Yokoyama, F. *et al.* (2007) 'Differentiation of gastric surface mucous cells (GSM06) induced by air–liquid interface is regulated partly through mitogen-activated protein kinase pathway', *Journal of Gastroenterology and Hepatology*, 22(12), pp. 2310–2315. doi: 10.1111/j.1440-1746.2006.04729.x.

You, Y. jai *et al.* (2008) 'Insulin, cGMP, and TGF-beta Signals Regulate Food Intake and Quiescence in C. elegans: A Model for Satiety', *Cell Metabolism*, 7(3), pp. 249–257. doi: 10.1016/j.cmet.2008.01.005.

Yuge, S. *et al.* (2003) 'A novel guanylin family (guanylin, uroguanylin, and renoguanylin) in eels: Possible osmoregulatory hormones in intestine and kidney', *Journal of Biological Chemistry*. doi: 10.1074/jbc.M303111200.

Zeller, P. *et al.* (2015) 'Multiparametric temporal analysis of the Caco-2/TC7 demonstrated functional and differentiated monolayers as early as 14 days of culture', *European Journal of Pharmaceutical Sciences*. Elsevier B.V., 72, pp. 1–11. doi: 10.1016/j.ejps.2015.02.013.

Zemlin, M. *et al.* (2003) 'Expressed murine and human CDR-H3 intervals of equal length exhibit distinct repertoires that differ in their amino acid composition and predicted range of structures.', *Journal of molecular biology*, 334(4), pp. 733–49.

Zhang, L. (1997) 'Gene Expression Profiles in Normal and Cancer Cells', *Science*, 276(5316), pp. 1268–1272. doi: 10.1126/science.276.5316.1268.

Zhang, X. and Oglesbee, M. (2003) 'Use of surface plasmon resonance for the measurement of low affinity binding interactions between HSP72 and measles virus nucleocapsid protein', *Biological Procedures Online*, 5(1), pp. 170–181. doi: 10.1251/bpo59.

Zietek, T. *et al.* (2015) 'Intestinal organoids for assessing nutrient transport, sensing and incretin secretion', *Scientific Reports*. Nature Publishing Group, 5(1), p. 16831. doi: 10.1038/srep16831.

Zucco, F. *et al.* (2005) 'An inter-laboratory study to evaluate the effects of medium composition on the differentiation and barrier function of Caco-2 cell lines.', *Alternatives to laboratory animals : ATLA*, 33(6), pp. 603–18.

Appendices

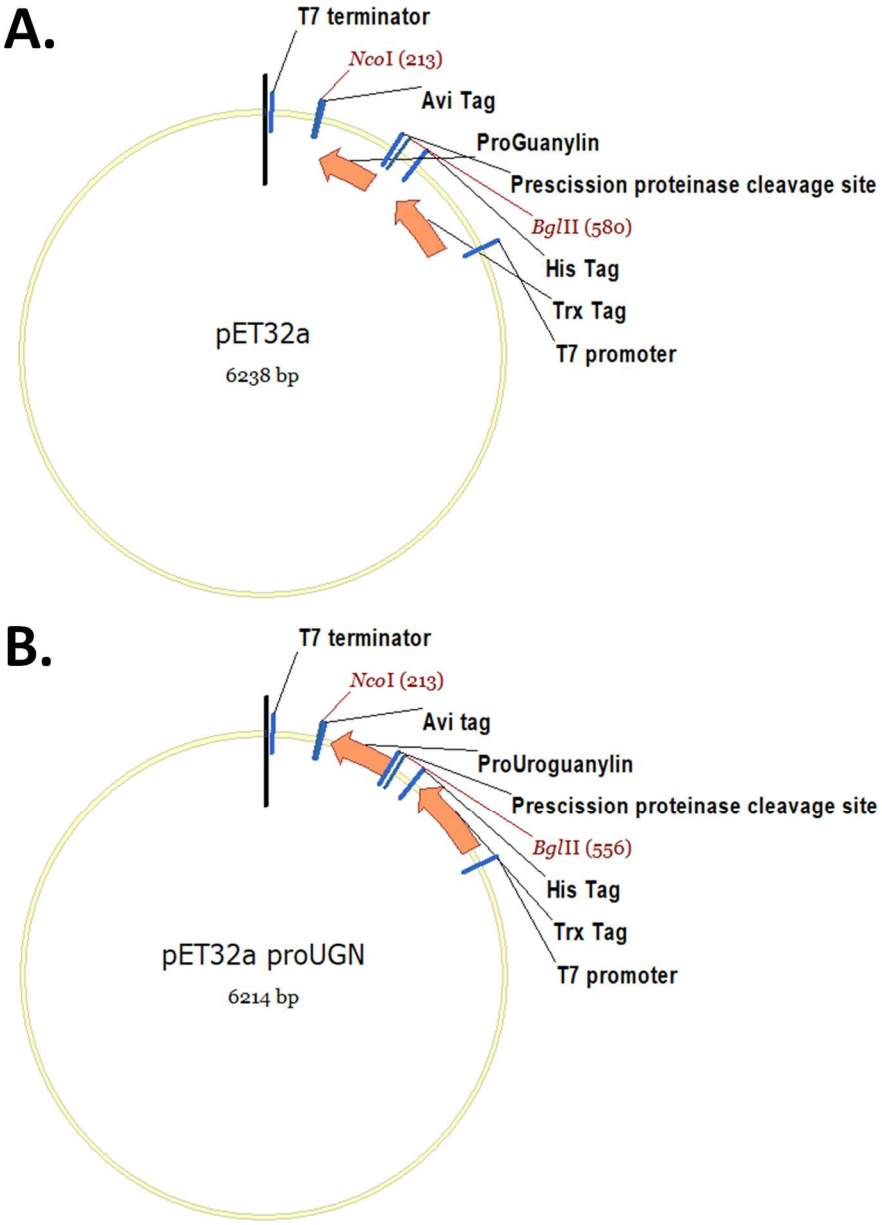

Appendix 1: Plasmid maps of ProGuanylin in pET32a (A.) and ProUroguanylin in pET32a (B.).

Primer	Purpose	Sequence (5'-3')
Oligo (dC)	Forward primer for V_H and V_L	CCCCCCCCCCCCCCCCCCCCCCCC
IgG77R	Reverse primer for mouse V_H	TARCCYTTGACMAGGCATCC
KconsR	Reverse primer for mouse V_L	CGTTCACTGCCATCAATC
pUC19 reverse	Amplify the scfv for Phage sequencing	AGCGGATAACAATTTCACACAGG
fdtetseq	Amplify the scfv for Phage sequencing	GTCGTCTTTCCAGACGTTAGT
PCR L-link	Sequencing the phage	GGCGGAGGTGGCTCTGGCGGT
mycseq10	Sequencing the phage	CTCTTCTGAGATGAGTTTTTG
MycRestore	Ribosome display	ATTCAGATCCTCTTCTGAGATGAG
SDCAT-CG	Ribosome display	AGACCACAACGGTTTCCCTCTAGAAATAATTTTGTTTAACTTTAAGAAGGAG ATATATCCATGGCCCAGGTGCAGC
geneIIIfor2	Ribosome display	CCGTCACCGACTTGAGCC
MycgeneIIIshortadapt	Ribosome display	ATCTCAGAAGAGGATCTGAATGGTGGCGGCTCCGGTTCCGGTGAT
T7te	Ribosome display	GTAGCACCATTACCATTAGCAAG
T7B	Ribosome display	ATACGAAATTAATACGACTCACTATAGGGAGACCACAACGG
T6te	Ribosome display	CCGCACACCAGTAAGGTGTGCGGTATCACCAGTAGCACCATTACCATTAGCA AG
SDCAT-CC	Ribosome display	AGACCACAACGGTTTCCCTCTAGAAATAATTTTGTTTAACTTTAAGAAGGAG ATATATCCATGGCCCAGGTCCAGC
SDCAT-CG	Ribosome display	AGACCACAACGGTTTCCCTCTAGAAATAATTTTGTTTAACTTTAAGAAGGAG ATATATCCATGGCCCAGGTGCAGC
T8te	Ribosome display	CACCAGTAGCACCATTACCATTAGCAAGG
Pecseq1	Forward primer for VH and VL	GCAGGCTTGAGGTCTGGAC
P266	VH reverse	GCCCTTGACCAGGCATCCCAG
P156_CC	VL reverse	GGGACAGACAGAAAACAGCATGC
FSD001	Replacement GN by rspL/neoR cassette forward	GCCCCACTGTTTACCCCAGGCACTAGTACTGGCCTGTTCTCTGCATTGCATAC TGCTACCGGCCTGGTGATGATGGCGGGATCGT
FSD002	Replacement GN by rspL/neoR cassette reverse	CTTCTAGAAGATAGAGGGGCTTCCACATGGGCTGAGAGAAAGGCAAGCGAT GTCACTCTAGAAGAACTCGTCAAGAAGGCGATAG
FSD003	Replacement GN by Venus cassette forward	GCCCCACTGTTTACCCCAGGCACTAGTACTGGCCTGTTCTCTGCATTGCATAC TGCTACCATGGTGAGCAAGGGCGAGGAGCTGT
FSD004	Replacement GN by Venus cassette reverse	CTTCTAGAAGATAGAGGGGCTTCCACATGGGCTGAGAGAAAGGCAAGCGAT GTCACTCTACTTGTACAGCTCGTCCATGCCGAGA
FSD045	To sequence GN-Venus +-5000bp f1	CTCCAGGAGGAGGAAAAAGAG
FSD046	To sequence GN-Venus +-5000bp f2	CAGTGAGCTCCAGCTCACTG
FSD047	To sequence GN-Venus +-5000bp f3	CAAACCGTGCCACTTTATTTC
FSD048	To sequence GN-Venus +-5000bp f4	CTGGCTTGCCAGAAGATGATG
FSD049	To sequence GN-Venus +-5000bp f5	CAGCAGCCTCCACACTCGAG
FSD050	To sequence GN-Venus +-5000bp f6	CTTTGCACACATGCCTTTCAG
FSD051	To sequence GN-Venus +-5000bp f7	CTTCTTCATCGAGGGCTTCC
FSD052	To sequence GN-Venus +-5000bp f8	CAGCAGATGAGGCTGACAAG
FSD053	To sequence GN-Venus +-5000bp f9	CTCCTGGGGTCACTAACTTGC
FSD054	To sequence GN-Venus +-5000bp f10	CCTGATCTTCCACATCCTGTG
FSD055	To sequence GN-Venus +-5000bp f11	GGTACACAGCTTCCTCCCAG
FSD056	To sequence GN-Venus +-5000bp f12	CTGAAAGCTGTCTCAGCATGG
FSD057	To sequence GN-Venus +-5000bp f13	GACAACCCAGGAAGCATCAAG
FSD058	To sequence GN-Venus +-5000bp f14	GAACACTTGGTCCCAGTAGGTG
FSD059	To sequence GN-Venus +-5000bp f15	GGCAGAGAGTAGCTGGGTGTAG
FSD060	To sequence GN-Venus +-5000bp f16	GGACGTGTCACTCCCTGATTG
FSD061	To sequence GN-Venus +-5000bp r1	GTGTTGCTTCTTTGATTGGTCTG
FSD062	To sequence GN-Venus +-5000bp r2	CAATCAGGGAGTGACACGTCC
FSD063	To sequence GN-Venus +-5000bp r3	CTACACCCAGCTACTCTCTGCC
FSD064	To sequence GN-Venus +-5000bp r4	CACCTACTGGGACCAAGTGTTC
FSD065	To sequence GN-Venus +-5000bp r5	CTTGATGCTTCCTGGGTTGTC
FSD066	To sequence GN-Venus +-5000bp r6	CCATGCTGAGACAGCTTTCAG
FSD067	To sequence GN-Venus +-5000bp r7	CTGGGAGGAAGCTGTGTACC
FSD068	To sequence GN-Venus +-5000bp r8	CACAGGATGTGGAAGATCAGG
FSD069	To sequence GN-Venus +-5000bp r9	GCAAGTTAGTGACCCCAGGAG
FSD070	To sequence GN-Venus +-5000bp r10	CTTGTCAGCCTCATCTGCTG
FSD071	To sequence GN-Venus +-5000bp r11	GGAAGCCCTCGATGAAGAAG
FSD072	To sequence GN-Venus +-5000bp r12	CTGAAAGGCATGTGTGCAAAG
FSD073	To sequence GN-Venus +-5000bp r13	CTCGAGTGTGGAGGCTGCTG
FSD074	To sequence GN-Venus +-5000bp r14	CATCATCTTCTGGCAAGCCAG
FSD075	To sequence GN-Venus +-5000bp r15	GAAATAAAGTGGCACGGTTTG
FSD076	To sequence GN-Venus +-5000bp r16	CAGTGAGCTGGAGCTCACTG

Appendix 2: Table of primers.

Primer	Purpose	Sequence (5'-3')
FSD033	PCR Venus 5' for	CATATTTCCATAGAGACGTGCTCGACTACTTGTACAGCTCGTCCATGCCG
FSD034	PCR Venus 3' rev	GCAGGCAGGTGGACAGCAGAGGAAGCAGGAACCCAGAGGTGTGAGCTTGG AAGCGAGGCCATGGTGAGCAAGGGCGAGGAGC
FSD035	PCR RspLtet 5' for	ACAGGTTGGGCTGTGGGGAAAGTGTCCGGAGTGGTCTTAAGACCCAGAGTC ATTTCATCATCGAGATGGCGGACGCGATGGATAT
FSD036	PCR RspLtet 3' rev	CGGCATGGACGAGCTGTACAAGTAGTCGAGCACGTCTCTATGGAAATATG
FSD037	PCR RspLtet-Venus 5' for	ACAGGTTGGGCTGTGGGGAAAG
FSD038	PCR RspLtet-Venus 3' rev	GCAGGCAGGTGGACAGCAGAG
FSD039	Cloning removing RspL/tet Cassette	AATGGTGCCTAAGTATGGACAGGTTGGGCTGTGGGGAAAGTGTCCGGAGTG GTCTTAAGACCCAGAGTCATTTCATCACTTGTACAGCTCGTCCATGCCGAGA GTGATCCCGGCGGCGGTCACGAACTCCAGCAGGACCATGTGATCGC
FSD110	To sequence UGN-Venus +-3000bp f1	GAGCCTAATACCAAACTAGAGAGAG
FSD111	To sequence UGN-Venus +-3000bp f2	GATACACAAAGAGCACACATGC
FSD112	To sequence UGN-Venus +-3000bp f3	GGAGAGGAGAGATGAGGAGAAG
FSD113	To sequence UGN-Venus +-3000bp f4	GATTCCAGCAGTGGCATG
FSD114	To sequence UGN-Venus +-3000bp f5	GTAGCGACGACAACACAGTG
FSD115	To sequence UGN-Venus +-3000bp f6	CTTGTAACCAGCCTTTGCCTG
FSD116	To sequence UGN-Venus +-3000bp f7	GTCTCCGGTGAACTTTGGAG
FSD117	To sequence UGN-Venus +-3000bp f8	CTCTCCATGACATCTTCCCAG
FSD118	To sequence UGN-Venus +-3000bp f9	GTAGGTTTAGCTGCTCCTCTCC
FSD119	To sequence UGN-Venus +-3000bp r1	GCATTGAATTTGGCAAGTG
FSD120	To sequence UGN-Venus +-3000bp r2	CAGTGGCTGGAGAAAGGAGG
FSD121	to seq UGN-Venus +-3000bp r3	GACAGAATACCAGCCTGTTG
FSD122	To sequence UGN-Venus +-3000bp r4	GACTTGATGTGACACCCCAG
FSD123	To sequence UGN-Venus +-3000bp r5	GTCCAGTGACAGTCAGGAGAC
FSD124	To sequence UGN-Venus +-3000bp r6	GTACACAGACAGCCGAAAGACC
FSD125	To sequence UGN-Venus +-3000bp r7	CTTCTCCTCATCTCTCCTCTCC
FSD126	To sequence UGN-Venus +-3000bp r8	GCATGTGTGCTCTTTGTGTATC
FSD127	To sequence UGN-Venus +-3000bp f10	CTTCTCATCCAGCTCCTCGAG
GFPF1	mouse screening	GACGTAAACGGCCACAAGTT
GFPR1	mouse screening	GGATCTTGAAGTTCGCCTTG

Appendix 2: Table of primers (end).

Gene	Species	TaqMan™Gene Expression Assay Id
Guanylin (Guca2a)	mouse	Mm00433863_m1
Uroguanylin (Guca2b)	mouse	Mm01192051_m1
Beta actin (Actb)	mouse	Mm02619580_g1
Mucin 2 (Muc2)	mouse	Mm01276696_m1
Lysozyme (Lyz1)	mouse	Mm00657323_m1
SAM Pointed Domain Containing ETS Transcription Factor (Spdef gene)	mouse	Mm00600221_m1
SRY-Box 9 (Sox9)	mouse	Mm00448840_m1
Villin 1 (Vil1)	mouse	Mm00494146_m1
Glucagon (Gcg)	mouse	Mm01269055_m1
Gastric Inhibitory Polypeptide (Gip)	mouse	Mm00433601_m1
Peptide YY (Pyy)	mouse	Mm00520716_g1
Cholecystokinin (Cck)	mouse	Mm00446170_m1
Somatostatin (Sst)	mouse	Mm00436671_m1
Doublecortin Like Kinase 1 (Dclk1)	mouse	Mm00444950_m1
Transient Receptor Potential Cation Channel Subfamily M Member 5 (Trpm5)	mouse	Mm01129032_m1
Chemokine (C-C motif) ligand 9 (Ccl9)	mouse	Mm00441260_m1
Macrophage Myristoylated Alanine-Rich C Kinase Substrate (Marcksl1)	mouse	Mm00456784_m11
Leucine Rich Repeat Containing G Protein-Coupled Receptor 5 (Lgr5)	mouse	Mm00438890_m1
Guanylin (GUCA2A)	human	Hs00157859_m1
Uroguanylin (GUCA2B)	human	Hs00951189_m1
Beta actin (ACTB)	human	Hs01060665_g1
Venus (Yfp)	other	Mr03987581_mr

Appendix 3: Table of Taqman assays probes.

Use	Antibody target	Company and catalog number	Dilution
ELISA to control the proforms	Rabbit Polyclonal antibody against ProGuanylin	Abcam (Ab14427-50)	1/10
ELISA to control the proforms	Mouse Polyclonal antibody against ProUroguanylin	Abcam (Ab171982)	5µg/ml
ELISA to control the proforms	HRP labelled goat anti-rabbit IgG	Sigma (A2074)	1/5000
ELISA to control the proforms	HRP labelled goat anti-mouse HRP IgG	Jackson ImmunoResearch (115-035-164)	1/5000
For hybridoma	FITC labelled monoclonal antibody anti-mouse IgG	Jackson ImmunoResearch (115-095-1649)	10µg/ml
HTRF assay	AlexaFluor 647 labelled goat anti mouse Fc IgG	Jackson ImmunoResearch (115-605-164)	7.5nM
Phage ELISA	anti-M13-HRP	Amersham (27-9421-01)	1/5000
Cell sorting	anti-CD45-PE	Thermo Fisher (MA110233)	1/500
Immunohistochemistry	Donkey anti-mouse 647	Life technologies (A31571)	1/3000
Immunohistochemistry	Donkey anti-goat 488	Life technologies (A11055)	1/3000
Immunohistochemistry	Donkey anti-rabbit 555	Life technologies (A31572)	1/3000
Immunohistochemistry	Goat anti-GFP	Abcam (Ab5450)	1/1000
Immunohistochemistry	Rabbit anti-Lysozyme	Dako (A0099)	1/200
Immunohistochemistry	Rabbit anti-Muc2	Santa Cruz (sc15334)	1/200
Immunohistochemistry	Rabbit anti-ChgA	Santa Cruz (sc13090)	1/200
Immunohistochemistry	Mouse anti-E-cadherine	BD (BD610181)	1/200

Appendix 4: Table of antibodies and antisera used.

category	over-represented genes pvalue	under-represented genes pvalue	Number of differentially expressed genes in category	Number of genes in category	term
GO:0044421	8.95199E-12	1	144	3692	extracellular region part
GO:0005576	1.81137E-11	1	156	4218	extracellular region
GO:0031982	7.60489E-11	1	138	3500	vesicle
GO:0050830	1.41143E-10	1	15	83	defense response to Gram-positive bacterium
GO:0012505	4.21423E-10	1	138	3432	endomembrane system
GO:0042742	2.49716E-09	1	22	233	defense response to bacterium
GO:0031988	4.85984E-09	1	122	3183	membrane-bounded vesicle
GO:0098542	1.15643E-08	1	34	511	defense response to other organism
GO:0006952	2.01695E-08	1	63	1323	defense response
GO:0005509	3.7352E-08	1	39	586	calcium ion binding
GO:0043230	5.07504E-08	1	101	2613	extracellular organelle
GO:0043207	8.24897E-08	1	42	751	response to external biotic stimulus
GO:0051707	8.24897E-08	1	42	751	response to other organism
GO:0005794	1.10259E-07	1	63	1268	Golgi apparatus
GO:0009607	1.2408E-07	1	43	790	response to biotic stimulus
GO:0070062	2.16682E-07	1	98	2593	extracellular exosome
GO:1903561	2.88954E-07	1	98	2607	extracellular vesicle
GO:0009605	3.18102E-07	1	78	1849	response to external stimulus
GO:0006810	5.23917E-07	1	146	4133	transport
GO:0051234	9.86372E-07	0.9999996	150	4283	establishment of localization
GO:0031410	1.04803E-06	0.9999996	54	1105	cytoplasmic vesicle
GO:0097708	1.10872E-06	0.9999996	54	1107	intracellular vesicle
GO:0009617	1.26766E-06	0.9999996	28	452	response to bacterium
GO:0005615	3.69838E-06	0.9999983	57	1385	extracellular space
GO:0004653	4.46346E-06	0.9999998	6	17	polypeptide N-acetylgalactosaminyltransferase activity
GO:0032879	6.69064E-06	0.9999965	95	2432	regulation of localization
GO:0034341	6.74174E-06	0.9999991	10	78	response to interferon-gamma
GO:0008378	7.37446E-06	0.9999989	11	81	galactosyltransferase activity
GO:0050829	1.10079E-05	0.9999989	8	54	defense response to Gram-negative bacterium
GO:0006486	1.39591E-05	0.9999965	17	202	protein glycosylation
GO:0043413	1.39591E-05	0.9999965	17	202	macromolecule glycosylation
GO:0006950	1.80691E-05	0.9999894	109	3103	response to stress
GO:0051049	1.81094E-05	0.9999904	72	1754	regulation of transport
GO:0044444	1.91395E-05	0.9999877	201	6629	cytoplasmic part
GO:0016020	2.08217E-05	0.9999864	261	9136	membrane
GO:0099503	2.3421E-05	0.9999917	26	449	secretory vesicle
GO:1902578	2.40634E-05	0.9999861	97	2609	single-organism localization
GO:0070085	2.4284E-05	0.9999936	17	212	glycosylation
GO:0005795	3.8246E-05	0.9999946	9	64	Golgi stack
GO:0009100	4.15687E-05	0.9999866	21	308	glycoprotein metabolic process
GO:0071346	4.32005E-05	0.9999946	8	60	cellular response to interferon-gamma
GO:0044425	4.35207E-05	0.9999711	198	6727	membrane part
GO:0030141	4.42483E-05	0.9999861	20	318	secretory granule
GO:0008375	4.69602E-05	0.9999913	11	97	acetylglucosaminyltransferase activity
GO:0017137	4.75753E-05	0.9999895	13	126	Rab GTPase binding
GO:0020005	5.43291E-05	0.9999986	4	9	symbiont-containing vacuole membrane
GO:0016758	5.47412E-05	0.9999852	16	199	transferase activity, transferring hexosyl groups
GO:0044765	5.62671E-05	0.9999668	89	2395	single-organism transport
GO:0009101	5.66059E-05	0.9999826	19	269	glycoprotein biosynthetic process
GO:0051179	5.90572E-05	0.9999609	173	5398	localization
GO:0042470	6.35815E-05	0.9999949	6	29	melanosome
GO:0048770	6.35815E-05	0.9999949	6	29	pigment granule
GO:0016757	7.14531E-05	0.9999768	20	295	transferase activity, transferring glycosyl groups
GO:0045087	7.51368E-05	0.9999696	29	566	innate immune response
GO:0048471	7.5477E-05	0.9999685	31	574	perinuclear region of cytoplasm
GO:0020003	7.60942E-05	0.9999977	4	10	symbiont-containing vacuole
GO:0006811	8.33266E-05	0.9999562	55	1279	ion transport
GO:0031224	9.34658E-05	0.9999375	170	5728	intrinsic component of membrane
GO:0008047	0.000100654	0.9999617	25	422	enzyme activator activity
GO:0030968	0.000128321	0.9999813	8	63	endoplasmic reticulum unfolded protein response

Appendix 5: Gene Ontology of the functions enriched in *Guca2a*-expressing cells using GOseq in the 4 tissues.